
Electronic Thesis and Dissertation Repository

2-21-2019 2:00 PM

Investigation of radiation-hardened design of electronic systems with applications to post-accident monitoring for nuclear power plants

Qiang Huang
The University of Western Ontario

Supervisor
Jin Jiang
The University of Western Ontario

Graduate Program in Electrical and Computer Engineering
A thesis submitted in partial fulfillment of the requirements for the degree in Doctor of Philosophy
© Qiang Huang 2019

Follow this and additional works at: <https://ir.lib.uwo.ca/etd>



Part of the [Electrical and Electronics Commons](#), [Electronic Devices and Semiconductor Manufacturing Commons](#), [Systems and Communications Commons](#), and the [VLSI and Circuits, Embedded and Hardware Systems Commons](#)

Recommended Citation

Huang, Qiang, "Investigation of radiation-hardened design of electronic systems with applications to post-accident monitoring for nuclear power plants" (2019). *Electronic Thesis and Dissertation Repository*. 6025.
<https://ir.lib.uwo.ca/etd/6025>

This Dissertation/Thesis is brought to you for free and open access by Scholarship@Western. It has been accepted for inclusion in Electronic Thesis and Dissertation Repository by an authorized administrator of Scholarship@Western. For more information, please contact wlsadmin@uwo.ca.

Abstract

This research aims at improving the robustness of electronic systems used-in high level radiation environments by combining with radiation-hardened (rad-hardened) design and fault-tolerant techniques based on commercial off-the-shelf (COTS) components. A specific of the research is to use such systems for wireless post-accident monitoring in nuclear power plants (NPPs). More specifically, the following methods and systems are developed and investigated to accomplish expected research objectives: analysis of radiation responses, design of a radiation-tolerant system, implementation of a wireless post-accident monitoring system for NPPs, performance evaluation without repeat physical tests, and experimental validation in a radiation environment.

A method is developed to analyze ionizing radiation responses of COTS-based devices and circuits in various radiation conditions, which can be applied to design circuits robust to ionizing radiation effects without repeated destructive tests in a physical radiation environment. Some mathematical models of semiconductor devices for post-irradiation conditions are investigated, and their radiation responses are analyzed using Technology Computer Aided Design (TCAD) simulator. Those models are then used in the analysis of circuits and systems under radiation condition. Based on the simulation results, method of rapid power off may be effectively to protect electronic systems under ionizing radiation. It can be a potential solution to mitigate damages of electronic components caused by radiation.

With simulation studies of photocurrent responses of semiconductor devices, two methods are presented to mitigate the damages of total ionizing dose: component selection and radiation shielding protection. According to the investigation of radiation-tolerance of regular COTS components, most COTS-based semiconductor components may experience performance degradation and radiation damages when the total dose is greater than 20 K Rad (Si). A principle of component selection is given to obtain the suitable components, as well as a method is proposed to assess the component reliability under radiation environments, which uses radiation degradation factors, instead of the usual failure rate data in the reliability model. Radiation degradation factor is as the input to describe the radiation response of a component under a total radiation dose. In addition, a number of typical

semiconductor components are also selected as the candidate components for the application of wireless monitoring in nuclear power plants.

On the other hand, a multi-layer shielding protection is used to reduce the total dose to be less than 20 K Rad (Si) for a given radiation condition; the selected semiconductor devices can then survive in the radiation condition with the reduced total dose. The calculation method of required shielding thickness is also proposed to achieve the design objectives. Several shielding solutions are also developed and compared for applications in wireless monitoring system in nuclear power plants.

A radiation-tolerant architecture is proposed to allow COTS-based electronic systems to be used in high-level radiation environments without using rad-hardened components. Regular COTS components are used with some fault-tolerant techniques to mitigate damages of the system through redundancy, online fault detection, real-time preventive remedial actions, and rapid power off. The functions of measurement, processing, communication, and fault-tolerance are integrated locally within all channels without additional detection units. A hardware emulation bench with redundant channels is constructed to verify the effectiveness of the developed radiation-tolerant architecture. Experimental results have shown that the developed architecture works effectively and redundant channels can switch smoothly in 500 milliseconds or less when a single fault or multiple faults occur.

An online mechanism is also investigated to timely detect and diagnose radiation damages in the developed redundant architecture for its radiation tolerance enhancement. This is implemented by the built-in-test technique. A number of tests by using fault injection techniques have been carried out in the developed hardware emulation bench to validate the proposed detection mechanism. The test results have shown that faults and errors can be effectively detected and diagnosed. For the developed redundant wireless devices under given radiation dose (20 K Rad (Si)), the fault detection coverage is about 62.11%. This level of protection could be improved further by putting more resources (CPU consumption, etc.) into the function of fault detection, but the cost will increase.

To apply the above investigated techniques and systems, under a severe accident condition in a nuclear power plant, a prototype of wireless post-accident monitoring system (WPAMS) is designed and constructed. Specifically, the radiation-tolerant wireless device is implemented

with redundant and diversified channels. The developed system operates effectively to measure up-to-date information from a specific area/process and to transmit that information to remote monitoring station wirelessly. Hence, the correctness of the proposed architecture and approaches in this research has been successfully validated.

In the design phase, an assessment method without performing repeated destructive physical tests is investigated to evaluate the radiation-tolerance of electronic systems by combining the evaluation of radiation protection and the analysis of the system reliability under the given radiation conditions. The results of the assessment studies have shown that, under given radiation conditions, the reliability of the developed radiation-tolerant wireless system can be much higher than those of non-redundant channels; and it can work in high-level radiation environments with total dose up to 1 M Rad (Si).

Finally, a number of total dose tests are performed to investigate radiation effects induced by gamma radiation on distinct modern wireless monitoring devices. An experimental setup is developed to monitor the performance of signal measurement online and transmission of the developed distinct wireless electronic devices directly under gamma radiator at The Ohio State University Nuclear Reactor Lab (OSU-NRL). The gamma irradiator generates dose rates of 20 K Rad/h and 200 Rad/h on the samples, respectively. It was found that both measurement and transmission functions of distinct wireless measurement and transmission devices work well under gamma radiation conditions before the devices permanently damage. The experimental results have also shown that the developed radiation-tolerant design can be applied to effectively extend the lifespan of COTS-based electronic systems in the high-level radiation environment, as well as to improve the performance of wireless communication systems. According to testing results, the developed radiation-tolerant wireless device with a shielding protection can work at least 21 hours under the highest dose rate (20 K Rad/h).

In summary, this research has addressed important issues on the design of radiation-tolerant systems without using rad-hardened electronic components. The proposed methods and systems provide an effective and economical solution to implement monitoring systems for obtaining up-to-date information in high-level radiation environments. The reported contributions are of significance both academically and in practice.

Keywords

Rad-hardened, radiation hardened by design, commercial off-the-shelf, radiation-tolerant, radiation-tolerance assessment, fault-tolerant, triple module redundant, wireless post-accident monitoring system, nuclear power plant, severe accident, wireless sensor network, total dose test

Acknowledgments

I am grateful to my supervisor Dr. Jin Jiang for the opportunity to work on this exciting research, as well as his continuous guidance, inspiration, and patience throughout the entire duration of my Ph.D. studies. It would have been impossible without his support to complete this research.

Also thanks a lot to all members of the CIES research group for the help that took from many fields. The management skills of Dr. Xinhong Huang have made the research a much smoother process and she also gave many comments on the papers. Dr. Atual Bari gave many suggestions in the design and commissioning of the developed wireless monitoring system. Dr. Quan Wang has shared a lot of experiences with wireless sensor networks. Dr. Jianping Ma and Dr. Drew Rankin also gave many suggestions in this research. Mr. Yongqiang Deng gave many helps in the total dose test. Dr. Dongqing Wang, Mrs. Xirong Ning, Mr. Binggang Cui, Mr. Ning Pan, and Mr. Long Ding have always been ready to lend a hand over the years – both technical and nontechnical. The friendship of all members of CIES group will be cherished for the rest of my life.

The research has benefited from the generousities of many outside the research groups. The irradiation experimental test is set up in OSU-NRL by Dr. Lei R. Cao. I have also learned from many people in Canadian nuclear industries.

This research is financially supported by the Natural Sciences and Engineering Research Council of Canada (NSERC) and the University Network of Excellence in Nuclear Engineering (UNENE).

I would like to express great appreciate to my wife Ying Zhang, my daughter Yisi, my son Ian, and my whole family in China. They always give their everlasting love, understanding, encouragement, and support in past years. They will continue to fill up my heart with happiness and hope under each period and all conditions in my life.

Table of Contents

| | |
|---|-------|
| Abstract | i |
| Acknowledgments..... | v |
| Table of Contents | vi |
| List of Tables | xiv |
| List of Figures | xix |
| List of Appendices | xxvi |
| List of Symbols | xxvii |
| Nomenclature | xxxix |
| Chapter 1 | 1 |
| 1 Introduction | 1 |
| 1.1 Background | 1 |
| 1.2 Objectives | 5 |
| 1.3 Investigated Methods and Systems | 6 |
| 1.4 Research Scope | 9 |
| 1.5 Contributions..... | 11 |
| 1.6 Organization of the Thesis | 12 |
| Chapter 2 | 14 |
| 2 Literature Survey..... | 14 |
| 2.1 Background of Severe Accidents in NPPs..... | 14 |
| 2.1.1 Industry Standards for PAMS in NPPs..... | 14 |
| 2.1.2 Design Issues of Wireless Monitoring Systems for Severe Accidents in NPPs..... | 15 |
| 2.1.3 Radiation Environment under a Severe Accident..... | 16 |
| 2.2 Radiation Effects on Electronics..... | 17 |

| | | |
|-----------|--|----|
| 2.2.1 | Composition of Monitoring Systems in Post-Accident Applications..... | 17 |
| 2.2.2 | Mechanism of Radiation Interaction with Matters | 18 |
| 2.2.3 | Displacement Damage | 20 |
| 2.2.4 | Total Ionizing Dose..... | 21 |
| 2.2.5 | Single Event Effect | 24 |
| 2.2.6 | Radiation Effects on Semiconductor Devices..... | 27 |
| 2.3 | Rad-Hardened Design Techniques | 29 |
| 2.3.1 | Rad-Hardened by Device-Level Design | 30 |
| 2.3.2 | Rad-Hardened by Circuit-Level Design | 32 |
| 2.3.3 | Rad-Hardened by System-Level Design..... | 35 |
| 2.3.4 | Rad-Hardened by Shielding | 36 |
| 2.3.5 | Summary of Rad-Hardened Design Techniques..... | 37 |
| 2.4 | Modeling and Simulation Techniques | 39 |
| 2.4.1 | Simulation of Radiation Shielding..... | 39 |
| 2.4.2 | Simulations of Radiation Effects | 40 |
| 2.4.3 | Summary of Simulation Techniques..... | 42 |
| 2.5 | Concluding Remarks..... | 44 |
| Chapter 3 | | 45 |
| 3 | Analysis of Radiation Responses of Devices and Circuits | 45 |
| 3.1 | Introduction..... | 45 |
| 3.1.1 | Degradation Mechanism of Devices and Circuits | 45 |
| 3.1.2 | Photocurrent Modeling of a p-n Junction | 49 |
| 3.1.3 | Problem Statement..... | 55 |
| 3.1.4 | The Framework of the Proposed Analysis Method | 55 |
| 3.2 | Development of Device Models | 56 |
| 3.2.1 | Diode Model | 56 |

| | | |
|-----------|---|----|
| 3.2.2 | BJT Model | 58 |
| 3.3 | Case Study: Radiation-Induced Responses of an Ideal p-n Diode in TCAD | 61 |
| 3.3.1 | Simulation Parameters | 61 |
| 3.3.2 | Simulation Results | 62 |
| 3.3.3 | Discussion | 65 |
| 3.4 | Summary | 66 |
| Chapter 4 | | 67 |
| 4 | Design Part I: Component Selection | 67 |
| 4.1 | The Investigation of Radiation-Tolerance for COTS Components | 67 |
| 4.1.1 | Radiation Damages Thresholds on Electronics | 67 |
| 4.1.2 | The Definition of Total Dose Limit | 69 |
| 4.2 | The Method of Component Selection | 70 |
| 4.2.1 | The Principle of Component Selection | 70 |
| 4.2.2 | The Assessment Method of Component Selection | 71 |
| 4.3 | Selected Candidate Components..... | 73 |
| 4.4 | Summary | 75 |
| Chapter 5 | | 76 |
| 5 | Design Part II: Multi-Layer Radiation Shielding Protection | 76 |
| 5.1 | Introduction..... | 76 |
| 5.1.1 | Background..... | 76 |
| 5.1.2 | Problem Statement | 78 |
| 5.2 | The Design of Multi-Layer Radiation Protection | 79 |
| 5.3 | Calculation of Shielding Thickness in Multi-Layer Radiation Protection..... | 82 |
| 5.3.1 | Attenuation of Gamma Radiation | 82 |
| 5.3.2 | Calculation of the Shielding Thickness | 83 |

| | |
|--|-----|
| 5.4 Case Study: Design of Shielding Protection for Application to a Wireless Monitoring System in Nuclear Power Plants | 84 |
| 5.4.1 Development of Radiation Shielding Protection for the Proposed WPAMS | 84 |
| 5.4.2 Performance Evaluation..... | 86 |
| 5.5 Conclusions..... | 87 |
| Chapter 6..... | 89 |
| 6 Design Part III: Radiation-Tolerant Architecture | 89 |
| 6.1 Introduction..... | 89 |
| 6.1.1 Potential Solution Techniques | 89 |
| 6.1.2 Problem Statement | 90 |
| 6.2 Techniques for Preventing Single Event Effects | 91 |
| 6.2.1 Redundancy..... | 91 |
| 6.2.2 Hardware Switch..... | 92 |
| 6.2.3 Diversity Techniques | 94 |
| 6.2.4 Fault Detection and Diagnosis | 96 |
| 6.2.5 Prognostic for Lifespan of Components | 99 |
| 6.3 Resulting System Architecture | 100 |
| 6.3.1 Redundant-Tolerant Architecture | 100 |
| 6.3.2 Justification | 101 |
| 6.3.3 Analysis..... | 104 |
| 6.4 Performance Evaluation of the Developed System Architecture | 106 |
| 6.4.1 Emulation of Radiation Damages | 106 |
| 6.4.2 Actual Evaluation and Results | 108 |
| 6.5 Conclusions..... | 109 |
| Chapter 7..... | 110 |
| 7 Design Part IV: Online Fault Detection Mechanism | 110 |

| | | |
|-----------|--|-----|
| 7.1 | Problem Statement | 110 |
| 7.2 | The Framework of Detection Mechanism | 111 |
| 7.3 | Analysis of Radiation-Induced Damages..... | 112 |
| 7.3.1 | Analysis Model | 112 |
| 7.3.2 | Definition and Properties | 113 |
| 7.3.3 | Identification of Fault, Error, and Failure | 116 |
| 7.4 | Detection of Radiation Damages | 118 |
| 7.4.1 | Determination of $UFi(u)$ | 118 |
| 7.4.2 | Internal Detection..... | 119 |
| 7.4.3 | External Detection | 120 |
| 7.5 | Diagnosis of Radiation Damages..... | 121 |
| 7.5.1 | Fault Hypothesis | 121 |
| 7.5.2 | Detection Function..... | 121 |
| 7.5.3 | Diagnosis Mechanism..... | 121 |
| 7.6 | Experimental Validation | 123 |
| 7.6.1 | Experimental Results | 123 |
| 7.6.2 | Detection Coverage..... | 128 |
| 7.7 | Conclusions..... | 128 |
| Chapter 8 | | 130 |
| 8 | Implementation: an Application of Wireless Monitoring System for Radiation Environments in NPPs | 130 |
| 8.1 | Design Considerations | 130 |
| 8.2 | Development of Wireless Monitoring System..... | 133 |
| 8.2.1 | Measurement and Transmission Unit | 133 |
| 8.2.2 | Gateway | 138 |
| 8.2.3 | Remote Monitoring Station..... | 140 |

| | |
|---|-----|
| 8.3 Testing in a Normal Environment..... | 143 |
| 8.3.1 Accuracy of Parameters Measurement | 143 |
| 8.3.2 Wireless Communication Performance | 143 |
| 8.4 Summary | 144 |
| Chapter 9..... | 145 |
| 9 Evaluation: Radiation-Tolerance Assessment..... | 145 |
| 9.1 Problem Statement | 145 |
| 9.2 Evaluation of Radiation Shielding Protection..... | 146 |
| 9.3 Assessment of System Reliability..... | 146 |
| 9.3.1 Reliability Assessment Model | 146 |
| 9.3.2 Radiation Degradation Factor | 148 |
| 9.4 Radiation-Tolerance of the Developed Wireless Device..... | 149 |
| 9.5 Conclusions..... | 154 |
| Chapter 10..... | 155 |
| 10 Experimental Validation | 155 |
| 10.1 Overview | 156 |
| 10.1.1 Objectives of Experiments..... | 156 |
| 10.1.2 Experimental Approaches..... | 160 |
| 10.1.3 Radiation Level Considered in Experimental Validation | 161 |
| 10.1.4 Experimental Facility..... | 162 |
| 10.1.5 Experimental Schemes..... | 163 |
| 10.2 Part I: Investigation of Radiation Vulnerability with Diversified COTS Components | 165 |
| 10.2.1 Introduction of Irradiated Circuits | 165 |
| 10.2.2 Experimental Setup..... | 169 |
| 10.2.3 Experimental Results | 171 |

| | |
|--|-----|
| 10.2.4 Discussions | 184 |
| 10.2.5 Summary | 187 |
| 10.3Part II: Evaluation of Six Industrial Wireless Transceivers and Networks in a Radiation Environment | 188 |
| 10.3.1 Introduction of Selected Industrial Wireless Systems | 189 |
| 10.3.2 Experimental Setup | 198 |
| 10.3.3 Experimental Results | 200 |
| 10.3.4 Discussions | 205 |
| 10.3.5 Summary | 206 |
| 10.4Part III: Evaluation of Diversified Wireless Monitoring Devices in Radiation Environments at both High and Low Dose Rates | 207 |
| 10.4.1 Introduction of Irradiated Devices | 208 |
| 10.4.2 Experimental Setup | 209 |
| 10.4.3 Experimental Results | 213 |
| 10.4.4 Discussions | 223 |
| 10.4.5 Summary | 225 |
| 10.5Part IV: Evaluation of the Developed Radiation-Tolerant Wireless Device in a Radiation Environment | 227 |
| 10.5.1 Introduction of Irradiated Devices | 227 |
| 10.5.2 Experimental Setup | 230 |
| 10.5.3 Experimental Results | 232 |
| 10.5.4 Discussions | 237 |
| 10.5.5 Summary | 237 |
| 10.6Conclusions | 239 |
| Chapter 11 | 241 |
| 11 Summary, Conclusion, and Future Work | 241 |
| 11.1 Summary | 241 |

| | |
|------------------------|-----|
| 11.2Conclusions..... | 243 |
| 11.3Future Work..... | 246 |
| Bibliography | 248 |
| Appendix..... | 294 |
| Curriculum Vitae | 297 |

List of Tables

| | |
|--|----|
| Table 1-1: Radiation hardness assurance categories for space systems | 10 |
| Table 2-1: Energy-loss process as radiation interacting with matter | 19 |
| Table 2-2: Radiation effects on semiconductor devices | 20 |
| Table 2-3: Total ionizing dose effects on semiconductor technologies and devices | 23 |
| Table 2-4: Single event effects on modern electronics | 27 |
| Table 2-5: Summary of radiation effects on semiconductor devices (Homes-Siedle and Adams, 2002) | 28 |
| Table 2-6: Potential approaches to achieve rad-hardened design at different levels | 38 |
| Table 2-7: Potential approaches of modeling and computer simulations | 43 |
| Table 3-1: Definitions of constants and variables used for the simulation of ionizing radiation effects on semiconductor devices (Wirth & Rogers, 1964; Alexander, 2003) | 50 |
| Table 3-2: Simulation parameters of an ideal p-n diode | 61 |
| Table 3-3: Simulation results of photo-current response of an ideal p-n diode under forward bias | 63 |
| Table 3-4: Simulation results of photo-current response of an ideal p-n diode under reverse bias | 64 |
| Table 4-1: Radiation damages thresholds on electronics | 68 |
| Table 4-2: The summary of selected candidate components and radiation degradation factors | 74 |
| Table 5-1: Characteristics of particles and effective shielding layer | 78 |

| | |
|---|-----|
| Table 5-2: Summary of the Parameters of radiation shielding protection for different designs | 86 |
| Table 5-3: The performance evaluation for three shielding solutions (Sv/h) | 87 |
| Table 6-1: The provider of the signals for reconfigurator suggestions..... | 104 |
| Table 6-2: The analysis of faults and detection mechanism | 105 |
| Table 6-3: Summary of variables logic and experimental results in hardware emulation bench | 108 |
| Table 7-1: The summary of radiation-induced damages and emulation methods considered in this work..... | 124 |
| Table 7-2: The information of the developed radiation-tolerant wireless device | 127 |
| Table 8-1: Criteria variables and specifications considered in the design of wireless monitoring systems for nuclear power plants | 132 |
| Table 8-2: The implementation of radiation-tolerant wireless devices in this research | 137 |
| Table 8-3: The parameter measurement of the developed monitoring system in a normal environment | 143 |
| Table 8-4: The performance of wireless communication in a normal environment..... | 144 |
| Table 9-1: Radiation degradation factors of the developed wireless device | 151 |
| Table 10-1: Summary of experimental objectives and approaches in this total dose test | 161 |
| Table 10-2: Testing equipment using in the experiment | 164 |
| Table 10-3: The summary of the irradiated devices in Experiment Part I..... | 170 |
| Table 10-4: Radiation responses of analog signal processing circuits during 390 minutes under a high dose rate condition | 171 |
| Table 10-5: Status of the failed analog signal processing circuits..... | 173 |

| | |
|---|-----|
| Table 10-6: Measurement conversion outputs of analog-to-digital converters during 390 minutes under a high dose rate condition | 174 |
| Table 10-7: the drive capability of ADC's output port during 390 minutes under a high dose rate condition | 175 |
| Table 10-8: Output voltages of microcontroller's GPIOs during 390 minutes under a high dose rate condition | 176 |
| Table 10-9: Performance of the memory in microcontrollers during 390 minutes under a high dose rate condition | 177 |
| Table 10-10: Program performance of microcontroller during 390 minutes under a high dose rate condition | 178 |
| Table 10-11: PWM output of microcontrollers during 390 minutes under a high dose rate condition | 178 |
| Table 10-12: UART function of microcontrollers during 390 minutes under a high dose rate condition | 179 |
| Table 10-13: The status of typical functions in failed microcontroller circuits..... | 180 |
| Table 10-14: The output voltage of IO port of wireless transceivers during 390 minutes under a high dose rate condition | 181 |
| Table 10-15: Communication performance of wireless transceivers during 390 minutes under a high dose rate condition | 182 |
| Table 10-16: Radiation resistances of irradiated circuits under a high dose rate condition in Experiment Part I | 185 |
| Table 10-17: Selected wireless transceivers and networks to be irradiated in Experiment Part II..... | 190 |
| Table 10-18: Survival times and radiation resistances of irradiated wireless devices under a high dose rate condition in Experiment PART II | 200 |

| | |
|--|-----|
| Table 10-19: Experimental results of communication performance of ZigBee devices and network used in Experiment Part II | 202 |
| Table 10-20: Summary of communication performance of ISA100.11a devices and network used in Experiment Part II | 202 |
| Table 10-21: Experimental results of communication performance of WirelessHART devices and network used in Experiment Part I..... | 203 |
| Table 10-22: Experimental results of communication performance of LoRa devices and network used in Experiment Part II | 203 |
| Table 10-23: Summary of communication performance of 433MHz devices and network used in Experiment Part II. | 204 |
| Table 10-24: Experimental results of communication performances of 915MHz devices and network used in Experiment Part II. | 204 |
| Table 10-25: Summary of irradiated monitoring devices used in Experiment Part III | 209 |
| Table 10-26: Results of experimental evaluation of parameter measurement for non-redundant wireless devices under a normal condition | 214 |
| Table 10-27: Results of experimental evaluation of communication performance for non-redundant wireless devices under a normal condition | 215 |
| Table 10-28: Results of experimental evaluation of parameter measurement for non-redundant wireless devices under a high dose rate condition | 216 |
| Table 10-29: Results of experimental evaluation of communication performance for non-redundant wireless devices under a high dose rate condition | 217 |
| Table 10-30: Results of experimental evaluation of parameter measurement for non-redundant wireless devices under a low dose rate condition | 218 |
| Table 10-31: Results of experimental evaluation of communication performance for non-redundant wireless devices under a low dose rate condition | 219 |

| | |
|--|-----|
| Table 10-32: Survival times of non-redundant wireless monitoring devices under both high and low dose rate conditions | 223 |
| Table 10-33: Wireless devices used in Experiment Part IV | 228 |
| Table 10-34: Summary of semiconductor components used in irradiated devices in Experiment Part IV. | 228 |
| Table 10-35: Survival time and radiation hardness of the irradiated wireless devices..... | 232 |
| Table 10-36: The status of each channel in the developed redundant device after irradiated 21 hours under a high dose rate condition | 233 |
| Table 10-37: Comparison of wireless communication performance of Sample-1 under different exposure and radiation conditions..... | 233 |
| Table 10-38: Comparison of wireless communication performance of Sample-2 under different exposure and radiation conditions..... | 234 |
| Table 10-39: Comparison of wireless communication performance of Sample-3 under different exposure and radiation conditions..... | 235 |
| Table A-1: The implementation of the hardware emulation platform..... | 296 |

List of Figures

| | |
|---|----|
| Figure 1-1: A potential wireless monitoring system for high level radiation environments in a nuclear power plant..... | 2 |
| Figure 1-2: An overview of major aspects in this research | 6 |
| Figure 1-3: The framework of investigated methods and systems in this research | 7 |
| Figure 1-4: The investigated radiation-tolerant techniques in this research | 11 |
| Figure 2-1: Radiation effects on electronics devices. | 19 |
| Figure 2-2: The effects of ionizing radiation in SiO ₂ (Adell and Scheick, 2013; Srour and McGarrity, 1988)..... | 22 |
| Figure 2-3: The effect of ionizing radiation on the gate oxide in an n-channel <i>MOSFET</i> (Oldham and McLean, 2003)..... | 22 |
| Figure 2-4: The physical mechanism of single event effects (Baumann, 2005)..... | 24 |
| Figure 2-5: Abstraction levels of electronic system | 29 |
| Figure 2-6: Methods of rad-hardened design techniques..... | 30 |
| Figure 3-1: The layout of <i>p-n</i> geometry (Alexander, 2003) | 49 |
| Figure 3-2: Flow diagram of the developed analysis method..... | 56 |
| Figure 3-3: Companion model of diode for post-irradiation | 57 |
| Figure 3-4: Companion model of <i>NPN BJT</i> for post-irradiation | 59 |
| Figure 3-5: The simulation structure of the ideal p-n diode in TCAD | 62 |
| Figure 3-6: Photo-current response of an ideal p-n diode under forward bias in TCAD | 63 |
| Figure 3-7: Photo-current response of an ideal p-n diode under reverse bias in TCAD | 65 |

| | |
|--|-----|
| Figure 4-1: Radiation tolerance by a family of COTS components (Houssay, 2000)..... | 70 |
| Figure 4-2: Radiation degradation functions derived from Lauridsen, <i>et al.</i> , 1996b..... | 72 |
| Figure 5-1: Reduction of total radiation dose by shielding protection | 77 |
| Figure 5-2: Design framework for multi-layer radiation protection | 80 |
| Figure 5-3: The layout of the multi-layer shielding protection..... | 81 |
| Figure 5-4: An attenuation of gamma radiation under conditions of narrow geometry (Gollnick, 2011)..... | 82 |
| Figure 5-5: Gamma radiation attenuation under conditions of broad beam geometry (Gollnick, 2011)..... | 83 |
| Figure 6-1: The schematic of reconfigurator (a) power reconfigurator (b) bus reconfigurator | 93 |
| Figure 6-2: Hierarchical fault model for electronic systems | 96 |
| Figure 6-3: The proposed radiation-tolerant architecture | 100 |
| Figure 6-4: The flowchart of master selection mechanism..... | 101 |
| Figure 6-5: The block diagram of the decision making unit..... | 102 |
| Figure 6-6: The flowchart of the decision making in TMR _i | 103 |
| Figure 6-7: The architecture of the developed hardware emulation bench | 107 |
| Figure 7-1: The framework of the fault detection and diagnosis method..... | 112 |
| Figure 7-2: Hierarchical fault model for electronic systems | 112 |
| Figure 7-3: The block diagram of detection logical allocation..... | 119 |
| Figure 7-4: Voltage levels of a circuit block under the fault state..... | 119 |
| Figure 7-5: The flowchart of fault detection loop..... | 122 |

| | |
|--|-----|
| Figure 7-6: The flowchart of fault diagnosis function | 123 |
| Figure 8-1: A potential wireless monitoring system for high level radiation environments in a nuclear power plant..... | 133 |
| Figure 8-2: The framework of the developed radiation-tolerant wireless device | 134 |
| Figure 8-3: The TMR core of the proposed wireless communication system (Proakis and Salehi, 2008) | 135 |
| Figure 8-4: Picture of radiation-tolerant wireless device developed in this work | 136 |
| Figure 8-5: Picture of radiation shielding protection developed in this work | 136 |
| Figure 8-6: The block diagram of the gateway device developed in this research | 139 |
| Figure 8-7: Picture of gateway device developed in this research..... | 140 |
| Figure 8-8: Picture of the shielding for gateway device developed in this research | 140 |
| Figure 8-9: The overview of remote monitoring station developed in this research | 141 |
| Figure 8-10: Picture of the remote monitoring station used in this research | 141 |
| Figure 8-11: Picture of portable monitoring device used in this research | 142 |
| Figure 8-12: Picture of a monitoring software tool developed in this research..... | 142 |
| Figure 9-1: The comparison of the reliability of the developed redundant system and no-redundant channels under the given total doses (0, 10 K Rad (Si), 20 K Rad (Si), 50 K Rad (Si), and 100 K Rad (Si)) | 152 |
| Figure 9-2: Radiation assessment of the developed wireless device under various dose rates | 153 |
| Figure 10-1: Composition of a digital communication system (Proakis and Salehi, 2008) . | 157 |
| Figure 10-2: A block diagram of the implementation of a typical wireless transmission system | 157 |

| | |
|--|-----|
| Figure 10-3: An overview of the experimental validation in this research..... | 159 |
| Figure 10-4: The Co-60 gamma irradiator dose-rate curve (OSU-NRL, 2018) | 162 |
| Figure 10-5: Sample plate and shielding of ⁶⁰ Co gamma irradiator (OSU-NRL, 2018) | 163 |
| Figure 10-6: Schematic of the experimental setup inside ⁶⁰ Co irradiator..... | 164 |
| Figure 10-7: Irradiated circuits of analog signal processing in Experiment Part I | 166 |
| Figure 10-8: Pictures of electronic circuit boards for analog signal processing used in Experiment Part I | 167 |
| Figure 10-9: Pictures of electronic circuits for microcontroller modules used in Experiment PART I | 168 |
| Figure 10-10: Picture of electronic circuits for wireless transceiver modules using in Experiment Part I | 169 |
| Figure 10-11: Picture of experimental setup in Experiment Part I | 169 |
| Figure 10-12: Radiation responses of analog signal processing circuits during 390 minutes under a high dose rate condition | 172 |
| Figure 10-13: Radiation responses of analog-to-digital converter modules during 390 minutes under a high dose rate condition | 175 |
| Figure 10-14: Pictures of the developed devices to measure the performance of irradiated wireless transceivers using in Experiment Part I | 181 |
| Figure 10-15: Comparison of wireless signal performance of three wireless devices used in Experiment Part I | 183 |
| Figure 10-16: Estimated radiation resistances for irradiated samples testing used in Experiment Part I | 186 |
| Figure 10-18: Irradiated wireless devices used in Experiment Part II..... | 190 |

| | |
|---|-----|
| Figure 10-19: Typical Star topology of ZigBee network for industrial application (Wang and Jiang, 2016)..... | 191 |
| Figure 10-20: ZigBee devices used in Experiment Part II..... | 192 |
| Figure 10-21: WirelessHART network for industrial applications (Wang and Jiang, 2016) | 192 |
| Figure 10-22: WirelessHART devices used in Experiment PART II..... | 193 |
| Figure 10-23: Menu of displaying value of chosen sensor in HART Server..... | 194 |
| Figure 10-24: ISA100.11a network for industrial applications (Wang and Jiang, 2016)..... | 194 |
| Figure 10-25: Pictures of ISA100.11a devices used in Experiment PART II | 195 |
| Figure 10-26: Web application installed in ISA100.11a Gateway | 196 |
| Figure 10-27: Typical structure of LoRa network in industrial application (Centenaro <i>et al.</i> , 2016) | 196 |
| Figure 10-28: Pictures of gateway for LoRa, 433 MHz & 915MHz networks using in Experiment PART II | 197 |
| Figure 10-29: Typical structure of point-to-point network..... | 197 |
| Figure 10-29: Experimental setup for 2.4 GHz wireless networks used in Experiment Part II | 198 |
| Figure 10-30: Experimental setup for LoRa, 433MHz, and 915MHz wireless devices and networks used in Experiment Part II..... | 199 |
| Figure 10-31: The developed software tool to collect wireless messages and analyze the communication performance used in Experiment PART II | 200 |
| Figure 10-32: Radiation resistances of six industrial wireless transceivers and networks used in Experiment Part III | 201 |
| Figure 10-33: Block diagram of three diversified single-channel wireless monitoring units | 208 |

| | |
|--|-----|
| Figure 10-34: Picture of experimental setup used in Experimental Part III | 210 |
| Figure 10-35: An overview of experimental setup used in Experimental Part III..... | 210 |
| Figure 10-36: Picture of the developed wireless receiver used in Experiment Part III | 211 |
| Figure 10-37: Interface of the developed software tool to receive and to record wireless data used in Experiment Part III. | 212 |
| Figure 10-38: Pictures of the device before-irradiated and after-irradiated | 213 |
| Figure 10-39: Comparison of measurement accuracy of non-redundant wireless devices under three different radiation conditions..... | 220 |
| Figure 10-40: Comparison of communication performance of non-redundant wireless devices under three different radiation conditions..... | 221 |
| Figure 10-41: Comparison of wireless signal performance of non-redundant wireless devices under different radiation conditions..... | 222 |
| Figure 10-42: Top view of the shielding protection in Experiment Part IV | 229 |
| Figure 10-43: Irradiated samples used in experiment part IV | 230 |
| Figure 10-44: Experimental setup for the non-redundant wireless devices used in Experiment Part IV | 231 |
| Figure 10-45: Experimental setup for the redundant wireless device used in Experiment Part IV | 231 |
| Figure 10-46: Radiation resistances of irradiated wireless devices used in Experiment Part IV | 232 |
| Figure 10-47: Comparison of communication performance of Sample-1(S1) and Sample- 4(S4) under a high dose rate condition | 236 |
| Figure 10-48: Comparison of communication of Sample-2(S2) and Sample-4(S4) under a high dose rate condition | 236 |

| | |
|---|-----|
| Figure A-1: The architecture of the developed hardware emulation bench..... | 294 |
| Figure A-2: Picture of the developed hardware emulation bench | 295 |
| Figure A-3: Screen shot of the software tool in the control computer..... | 296 |

List of Appendices

| | |
|--|-----|
| Appendix A: Hardware Emulation Bench | 294 |
|--|-----|

List of Symbols

Chapter 3:

q : Electron charge = 1.602×10^{-19}

k : Boltzmann constant = 1.381×10^{-23}

g_0 : the uniform generation term = 4.3×10^{13}

u_n, u_p : electron and hole mobility

τ_n, τ_p : electron and hole lifetime

T : temperature

$\dot{\gamma}$: the ionizing dose rate

G : electron-hole generation rate $G = g_0 \dot{\gamma}$

E_{depl} : E field in the depletion region

E_n, E_p : E field in the n -side region and in the p -side region

D_n, D_p : the electron diffusion coefficient in n -side and the hole diffusion coefficient in p -side

U_n, U_p : recombination rate $U_n = \Delta n / \tau_n, U_p = \Delta p / \tau_p$

$\Delta n(x, t)$: electrons generated by ionization per unit volume = $n(x, t) - n(x, 0)$

$\Delta p(x, t)$: holes generated by ionization per unit volume = $p(x, t) - p(x, 0)$

W_{depl} : the depletion region width

L_n, L_p : the diffusion length in n -side silicon and p -side silicon

x_n, x_p : the length of n -side, p -side

Chapter 4:

Δ : radiation degradation factor under the total radiation dose D_t

P_0 : the value of a characteristic parameter before exposure

P_t : the value of the characteristic parameter after a total radiation dose D_t

P_f : the value of the characteristic parameter at failure with a total radiation dose D_f

Chapter 5:

u : the attenuation coefficient of shielding material

p : the density of shielding material

d : the shielding material thickness

I : the intensity of the radiation after passing the shielding thickness d

I_0 : the original intensity

B : the build-up factor, is greater than 1

E : the energy of the gamma radiation

Chapter 6:

A_i : the state of the i_{th} channel, corresponding to its powered (active) state and no power state (no active)

S_i : the state of the i_{th} spare channel, corresponding to its powered (active) state and no power state (no active)

F_{A_i} : the state of A_i channel

F_{S_i} : the state of S_i channel

R_{Si}, R_{Mi} : reconfigure suggestions

H : fault hypothesis

$E_n(H)$: detection function

P : prognostic hypothesis

$E_n(P)$: prognostic function

Chapter 7:

d_i : the state of the i_{th} component

c_j : the state of the j_{th} circuit block of the electronic equipment

s_k : the state of the k_{th} subsystem of the electronic equipment

R_{dc} : the relation from set D to set C

R_{cs} : the relation from set C to set S

X : the space of all inputs to an analog circuit

x : the input of an analog circuit, $x \in X$

$f(X)$: the output of an analog circuit

$F(X)$: design goal of the analog circuit

$E(X)$: error of the under-design circuit with the input x

N : the sample number

K : K_{th} run of the algorithm

X^N : the sample space of X

i : redundant circuit i

j : redundant circuit j

$Cor(i, j)$: the correlation between redundancy circuits i and j

Chapter 8:

$R(t)$: reliability of an item at time t

$R_{ij}(t)$: reliability of the j th layer in the channel i at time t

$R_{C_i}(t)$: reliability of the channel i at time t

$R_S(t)$: reliability of the proposed system at time t

$R'(t)$: reliability of an item at time t under total radiation dose D_t

$R'_{ij}(t)$: reliability of the j th layer in the channel i at time t under total radiation dose D_t

$R'_{C_i}(t)$: reliability of the channel i at time t under total radiation dose D_t

$R'_S(t)$: reliability of the proposed system at time t under total radiation dose D_t

m : the number of redundant channels in the system

λ : the failure rate of an item

λ_{ij} : the failure rate of the j th layer in channel i

λ_{ij_k} : the failure rate of k th component of the j th layer in channel i

Δ : radiation degradation factor under total radiation dose D_t

P_0 : the value of the characteristic parameter before exposure

P_t : the value of the characteristic parameter after a total radiation dose D_t

P_f : the value of the characteristic parameter at failure under total radiation dose D_f

Nomenclature

ADC: analog-to-digital converter

AMS: accident monitoring system

ANN: artificial neural network

ATREE: analog transient radiation effect on electronics

BCA: binary collision approximation

BIST: built-in self-test

BJT: bipolar junction transistor

CBR: case-based reasoning

CCD: charge-coupled device

CMOS: complementary metal-oxide-semiconductor

COTS: commercial off-the-shelf

DAC: digital-to-analog converter

DCC: differential charge cancellation

DD: displacement damage

DICE: dual interlocked storage cell

DMR: dual modular redundancy

EA: evolutionary algorithm

ECC: error correcting code

EDAC: error detection and correction

EHPS: electron-hole-pairs

EMI: electromagnetic interference

ENCF: evolutionary negative-correlation framework

EPRI: electric power research institute

ERD: evolutionary-robust-design

FDD: fault detection and diagnosis

FET: field-effect transistor

FH: fault hypothesis

FinFET: fin field-effect transistor

FIT: failure in time

FPGA: field-programmable gate array

GA: genetic algorithm

GEANT: geometry and tracking

GP: genetic programming

HBT: heterojunction bipolar transistor

HEMT: high electron mobility transistor

IC: integrated circuit

I&C: instrumentation and control

IEAE: international nuclear and radiological event scale

IEC: international electro-technical commission

IGBT: insulated-gate bipolar transistor

IRT: intel radiation tool

JFET: junction field-effect transistor

LET: linear energy transfer

ML: machine learning

MNA: modified nodal analysis

MOS: metal-oxide-semiconductor

MOSFET: metal-oxide-semiconductor field-effect transistor

MRAM: magnetic random access memory

MRED: Monte Carlo radiative energy deposition

MTJ: magnetic tunnel junction

MULASSIS: multi-layered shielding simulation software

MUSCA SEP³: multi-scale single event phenomena predictive platform

NIEL: nonionizing energy loss

NMOS: negative-channel metal-oxide semiconductor

NPP: nuclear power plant

NRC: nuclear regulatory commission

OLM: online monitoring system

PAMS: post-accident monitoring system

PHITS: particle and heavy ion transport code system

PMOS: positive-channel metal-oxide semiconductor

RAM: random access memory

RBR: rule-based reasoning

RFI: radio frequency interference

RHA: radiation-hardness assurance

RHBD: radiation-hardened by design

ROM: read-only memory

SAM: severe accident management

SDRAM: synchronous dynamic random-access memory

SEB: single event burnout

SEE: single event effect

SEFI: single event functional interrupt

SEGR: single event gate rupture

SEL: single event latchup

SES: single event snapback

SET: single event transient

SETTOFF: soft-error and timing-error-tolerant flip-flop

SEU: single event upset

SOI: silicon on insulator

SOS: silicon on sapphire

SRAM: static random access memory

SRH: Shockley-Reed-Hall

TCAD: technology computer aided design

TIARA: tool suite for radiation reliability assessment

TID: total ionizing dose

TILL: triple inter-locked latch

TMR: triple modular redundancy

SRIM: stopping and range of ions in matter

VHDL-AMS: VHSIC hardware description language

WPAMS: wireless post-accident monitoring system

Chapter 1

1 Introduction

1.1 Background

In 2011, Fukushima Daiichi nuclear disaster was triggered by a 9.0 magnitude earthquake and subsequent tsunami; and released a large quantity of radioactive substances to the environment because of multiple hydrogen explosions and fire damage to the containments of the facilities. One of the lessons learnt from the Fukushima disaster is the difficulty to obtain up-to-date information about the plant after the accident due to lack of monitoring systems, harsh radiation environment, and lose of on-site power. In the event of an accident in nuclear power plants (NPPs), essential information about the status of the plant is crucial to plant operators and emergency response teams to effectively manage and mitigate the effects of accident. The important variables of interests are temperature, humidity, hydrogen concentration, and radiation levels in the environment. It is also important to gather information about the conditions of protection systems, such as water level in a spent fuel pool, and coolant inventory, etc. However, it is very difficult and unsafe for plant operators to get such information manually since a high level of nuclear radiation can ionize molecules, interact with matter, and cause severe biological damage to humans. Moreover, conventional accident monitoring systems (AMSs) in nuclear power plants usually use wired networks, which may no longer be available after the accident, or require rewiring or reconfiguration. After Fukushima disaster, some military robots, such as PackBot, T-Hawk, and Moni-Robo, were eventually used to measure radiation levels, temperature, levels of radioactive material, and also to take some photographs to inspect the damage, but they cannot be for multipurpose use because of issues from radiation effects, mobility, and communication (Nagatani *et al.*, 2012). The damage from Fukushima disaster is so severe that the special equipment and new technologies have to be developed to deal with the harsh environment conditions during decommissioning processes of the plant.

As an integral part of Severe Accident Management (SAM) systems, nuclear power plant regulatory bodies now request NPPs to have some forms of Post-Accident Monitoring Systems (PAMSs) available on-site. Considering scenarios of potentially losing on-site power and other wired communication channels, during a severe accident, a potential approach to deal with similar situations is to use wireless technologies to implement post-accident monitoring system (PAMS), as shown in Figure 1-1, which can provide much needed information about the plant conditions, reactor integrity, and environment in the vicinity of the NPP without relying on likely damaged communication infrastructure. However, wireless systems are often made of semiconductor devices, which are particularly sensitive to high level ionizing radiation. A high level radiation can modify electrical parameters of a semiconductor device, and worsen its electrical characteristics, which may lead to functional failure and physical damage. Therefore, the operating environment has posed severe challenges for WPAMSs. Radiation-hardened (rad-hardened) techniques have to be used to design and to protect electronic devices inside WPAMSs to make them more resistant to high level of radiation.

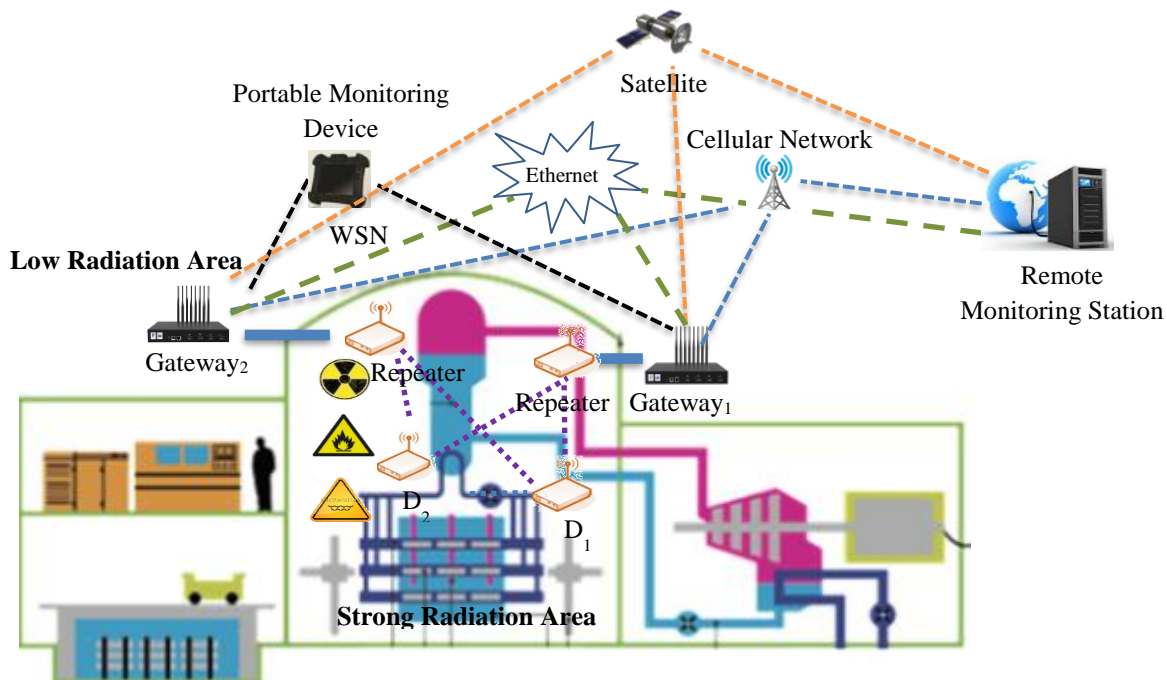


Figure 1-1: A potential wireless monitoring system for high level radiation environments in a nuclear power plant

One approach to alleviate such a problem is to employ rad-hardened components in such systems. Preliminary investigation reveals, however, that this approach can be prohibitively expensive due to special semiconductor materials used, complexity in manufacturing processes, and most of all, small size of the market supporting such devices. Furthermore, these rad-hardened devices may not be able to meet the modern requirements for high speed processing, large memory storage, and ultra-low power consumption. Another approach is to rely on regular commercial off-the-shelf (COTS) devices, but to utilize rad-hardened techniques to reduce the vulnerability of radiation effects on electronics and to prolong the life of the system during the mission of the deployment. Despite tremendous progress of rad-hardened design techniques in the past few decades, to implement an effective wireless monitoring systems for a severe accident in a NPP can still face several issues, such as:

- (1) Analysis of radiation responses of devices and circuits is important also necessary to design circuits to be robust to ionizing radiation effects and to accurately analyze their behavior under high level radiation fields. However, modeling techniques may suffer from accuracy issues in those applications with a wide range of ionizing radiation intensities. On the other hand, numerical modeling techniques is too complicated extremely time consuming, and requires a large amount of engineering works to obtain sufficient information of technological features.
- (2) With simulation studies of photocurrent responses of semiconductor devices under different levels of ionizing radiation, if the power on the junction can be removed quickly in an event of radiation exposure, a semiconductor device might not be damaged permanently by the accumulated photocurrent. Fault-tolerant techniques, combined with error detection, timely fault detection, and rapid recovery/repair, have been used to protect safety-critical systems and applied to a range of situations. However, existing fault-tolerant techniques and systems usually have three redundant modules and/or the duplication of important circuits and subsystems to realize majority voters, or use additional detectors to diagnose faults. These additional units and voters not only increase system complexity, but

are themselves usually non-redundant and subject to damage by ionizing radiation also. Hence they represent a major weakness in the system and as such should also be protected. A radiation-tolerant architecture with independent redundancy, online fault detection, real-time preventive remedial actions, and rapid power loss / recovery, as well as avoid the common-mode damage, is not only important, but also necessary for the design of COTS-based rad-hardened systems. Key issues to achieve this objective include:

- How to protect the device against potential damages as a result of total ionizing dose;
- How to achieve completely independent redundant architecture without additional detection units and/or hardware voters;
- How to avoid common-mode damages and/or multi-damages on redundant channels;
- How to implement mechanisms of online fault detection, real-time preventive remedial actions, and mechanisms of rapid power removal;
- How to detect radiation damages in redundant systems timely without addition measurement units and hardware voters;

(3) Radiation-tolerance assessment of the developed electronic system is a critical part in the design phase of rad-hardened electronic systems. In general, the performance of rad-hardened systems can be evaluated in two ways: physical tests and simulation with analysis. However, physical test is very precise but could be excessively complicated and expensive. On the other hand, limitations of simulation with analysis are that it is difficult to assess the radiation-tolerance of the whole system precisely.

Therefore, it is not only important but also necessary to investigate new rad-hardened analysis and design methodologies to achieve rad-hardened electronic systems by using regular COTS components. It is also beneficial to use these new approaches to design

self-powered and rad-hardened wireless monitoring systems for high level radiation environments after an accident in NPPs.

1.2 Objectives

The objectives of this research are listed as follows:

- (1) To investigate alternative ways to analyze, design, evaluate, and validate radiation-tolerant electronic systems by using commercial off-the-shelf components; and
- (2) To apply the proposed methodologies to design, implement, and validate a wireless monitoring system for high level of radiation environments in nuclear power plants after a severe accident.

An overview of major aspects dealt with in this research is given in Figure 1-2, which starts with top-level estimations of the radiation condition, and then after the considered radiation-level is defined, related defense techniques are proposed and designed, radiation-tolerance is assessed in order to validate the potential of the developed system.

the developed radiation-tolerant devices, and irradiation experimental validation. It can be seen in Figure 1-3 that the framework has covered the previously discussed issues.

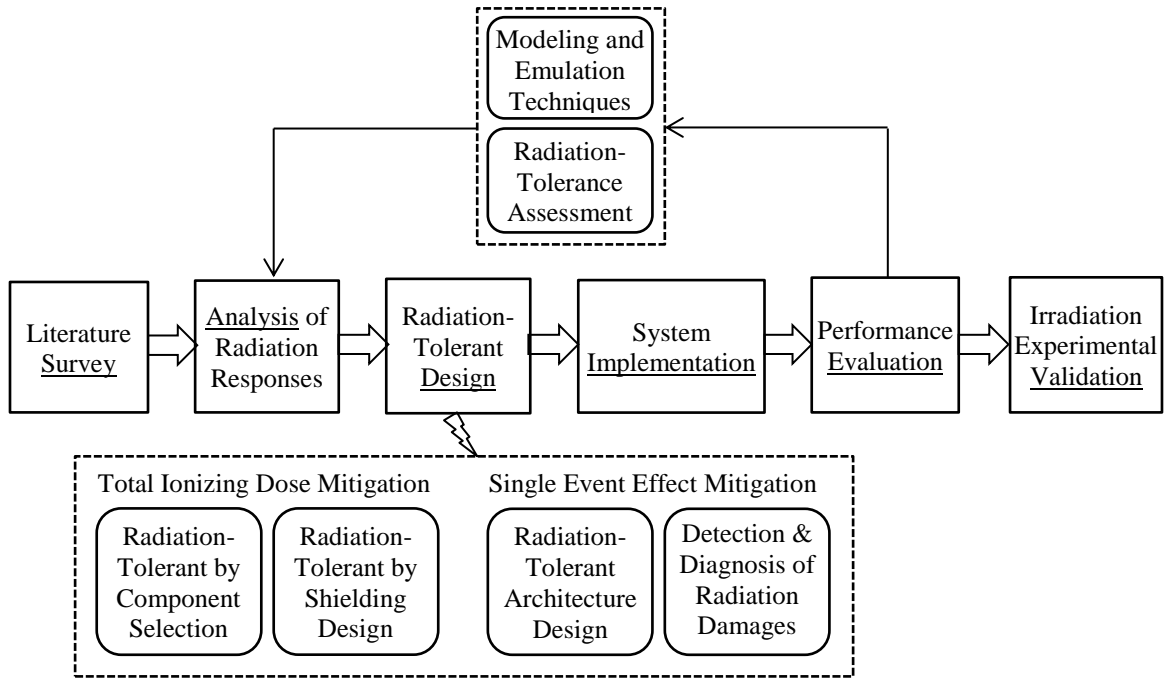


Figure 1-3: The framework of investigated methods and systems in this research

The following methods and systems are studied in this research to achieve the proposed objectives:

- (1) Survey: A great variety of radiation-hardened methods have been studied for a wide range of applications, such as in the aeronautics and space sectors, accident conditions in nuclear power plants, and military scenarios. Some techniques and methods related to this research have been investigated, which include radiation effects on electronics; rad-hardened design techniques from device-level, circuit-level, and system-level; as well as modeling techniques and computer simulation methods.
- (2) Analysis: combining a semi-empirical technique and a numerical technique, a method is investigated to analyze ionizing radiation responses of devices and circuits, which can be separated into three steps: models of semiconductor devices for post-irradiation are established; and then photocurrents of semiconductor

devices are calculated by using Technology Computer Aided Design (TCAD) simulator; radiation-induced circuit responses can be analyzed through the modified nodal analysis (MNA) circuit equations.

(3) Design: several defense techniques are investigated to protect against radiation effects and to prolong the lifespan of electronic systems in this research. They are:

- (Total ionizing dose hardening) A multi-layer protection and a method of component selection are designed to reduce the level of total dose and to allow regular commercial components to be used in high level radiation environments.
- (Single event effect hardening) A radiation-tolerant architecture is investigated to mitigate damages of single event effects and to allow COTS components to be used in high level radiation environments. Redundancy, radiation-tolerant design techniques, and diversify techniques are also investigated.
- (Single event effect hardening) An online detection mechanism is investigated to timely identify/locate radiation damages in redundant systems.

(4) Implementation: using the proposed defense techniques, a monitoring system for radiation conditions in a nuclear power plant is developed to obtain up-to-date environment information. The system includes radiation-tolerant wireless detectors, gateway device, portable monitoring device, and remote monitoring station.

(5) Evaluation: several emulation methods have been built to evaluate the correctness of the proposed radiation-tolerant methods and techniques through the techniques of fault injection. A hardware emulation test bench is developed to validate the proposed redundant architecture and the developed fault detection method through hardware- and software-implemented fault injection techniques. On the other hand, an assessment method is investigated to evaluate radiation-tolerance

of electronic systems without repeated physical tests. This can be separated to two parts: evaluation of radiation protection and reliability assessment. This method uses radiation degradation factors (Δ), instead of the usual failure rate data of an item in the reliability model, as input to describe the radiation response of this item under a total radiation dose D_t .

- (6) Validation: a number of total dose tests are performed to investigate the radiation resistance of the developed wireless devices and to evaluate the performance of the developed wireless monitoring systems with ^{60}Co gamma irradiator, as well as to validate the proposed radiation-tolerant design.

1.4 Research Scope

As previously mentioned, unlike other industrial accidents, accidents in a nuclear power plant can be associated with potential release of radioactive substances, which can cause severe damages to electronic devices at nearby site. One critical issue is therefore how to design wireless monitoring devices that can tolerate the strong radiation. In generally, a radioactive environment after a severe accident in a nuclear power plant can be characterized as follows:

- (1) Radiation environments: Alpha particles, Beta particles, Gamma rays, x-rays, and neutron particles (Adalja *et al.*, 2011; Sharp and Decretton, 1996);
- (2) Radiation effects on electronics: total ionizing dose, single event effects, and displacement damage.

The total dose is an important aspect consideration for electronic systems in radiation environments. Considering short-term radioactive release (less than 24 hours) in each stage of a nuclear accident (CODIRPA, 2012), it is assumed that the proposed WPAMS has to survive the first 24 hours of the accident. Taking the highest dose rate of radiation in the Fukushima accident (530 Sv/h) as the radiation rate (theguardian, 2017), the total radiation dose after the first 24 hours can be obtained as follows:

$$R = 530 \text{ Sv/h} \times 24 \text{ h} = 12720 \text{ Sv} = 1272.0 \text{ K Rad (Si)}.$$

In the field of radiation protection, Radiation Hardness Assurance (RHA) is often used to determinate the design specifications of electronics and materials of a space system, whose categories are presented on Table 1-1 (Hash *et al.*, 1997). The RHA is an important reference as radiation level considered, which is also used in the current research.

Table 1-1: Radiation hardness assurance categories for space systems

| RHA category | M | D | P | L | R | F | G | H |
|-----------------|---|----|----|----|-----|-----|-----|------|
| TID (K Rad(Si)) | 3 | 10 | 30 | 50 | 100 | 300 | 500 | 1000 |

Combing with the estimation total dose (1.272 M Rad (Si)) in 24 hours and RHA specification, total radiation dose (1 M Rad (Si)) – Class H is therefore considered as the upper limit of radiation in this work. Those cases whose total radiation doses are more than 1 M Rad (Si) are not considered in this work.

Investigations of rad-hardened design techniques in this research are limited within the following scopes:

- (1) This research only deals with damages by ionizing radiation, displacement damages are beyond of this research.
- (2) Total dose is limited as 1 M Rad (Si), those applications whose total doses are more than 1 M Rad (Si) are not considered.
- (3) This research focuses on rad-hardened by design by using regular COTS components. Using rad-hardened components (device-level) to achieve high radiation-tolerance is not considered.

With knowledge of damage mechanisms, the current approach combines techniques of rad-tolerant design, multi-layer shielding, and diversified component selection to achieve a radiation-tolerant design. The overall approaches are summarized in Figure 1-4.

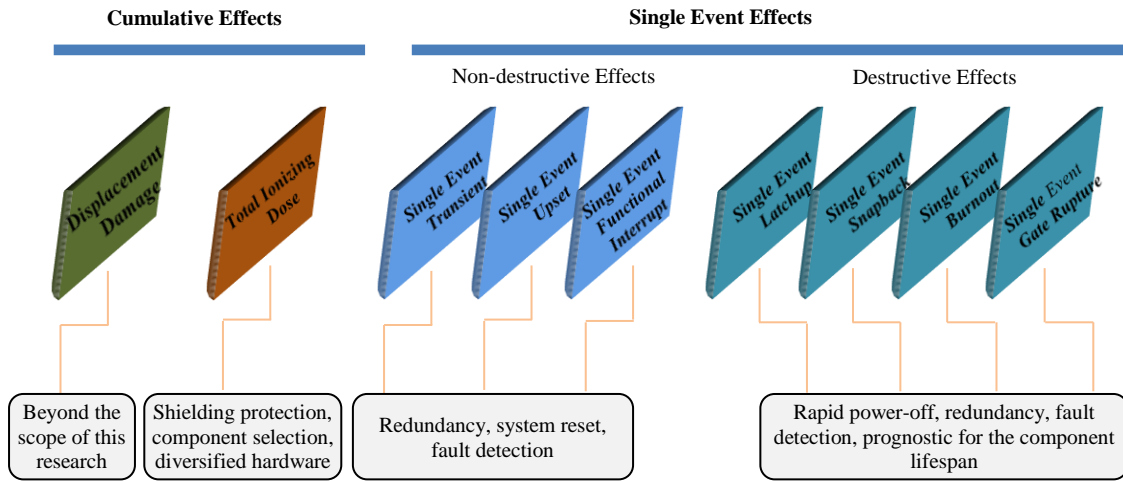


Figure 1-4: The investigated radiation-tolerant techniques in this research

1.5 Contributions

The contributions of this research can be summarized as follows:

- (1) Investigation of a method to analyze and to emulate responses of semiconductor devices and circuit in high level radiation fields.
- (2) Development of a multi-layer radiation protection technique, which can reduce the given total dose from 1 M Rad (Si) to be less than 20 K Rad (Si).
- (3) Development of a radiation-tolerant architecture, which can be used to mitigate single event effects on electronic systems through redundancy, online fault detection, real-time preventive remedial actions, and rapid power off.
- (4) Development of an online detection and diagnostic approach to identify/locate damages in redundant systems timely in radiation environments.
- (5) Proposed method to assess the radiation-tolerance of electronic systems without going through repeated destructive physical tests.
- (6) Design and commissioning of a wireless monitoring system to obtain up-to-date information from a simulated NPP environment under radiation environments.

- (7) Development of an irradiation test to validate the investigated radiation-tolerant methods and the designed systems.

1.6 Organization of the Thesis

The rest of the thesis is organized as follows:

- A literature survey on radiation effects on electronics, rad-hardened design techniques, and modeling and simulation techniques, is carried out in Chapter 2.
- The method to analyze and emulate radiation responses of semiconductor devices and circuits is presented in Chapter 3.
- The investigation of radiation-tolerance of regular COTS components and the principles of component selection used in this work are explained in Chapter 4.
- The developed multi-layer radiation protection is described in Chapter 5, which is to reduce the level of total dose and to avoid the common-mode damage in redundant systems.
- The proposed radiation-tolerant architecture is analyzed in Chapter 6 to mitigate damages of single event effects and to prolong the lifespan of the system.
- The online method to detect and to diagnose radiation damages in devices and circuits is investigated in Chapter 7.
- The implementation of a wireless monitoring system for radiation environments comparable to that of Fukushima accident is given in Chapter 8, which includes the development of wireless detectors, gateway device, portable monitoring device, remote monitoring station, and monitoring software.
- An analysis method to evaluate the radiation resistance of electronic systems without going through physical tests is provided in Chapter 9.

- A number of total dose tests to investigate radiation tolerance of the developed wireless monitoring devices are carried out in Chapter 10, as well as to validate the proposed radiation-tolerant methods.
- Conclusions are drawn in Chapter 11, along with some directions for future works.
- Details about the implementation of the hardware emulation bench are summarized in Appendix.

Chapter 2

2 Literature Survey

In the past several decades, a great variety of radiation-hardened methods have been studied for a wide range of applications, such as in aeronautics and deep space sector exploration, nuclear warfare, nuclear power plants in the event of an accident. Following the review of radiation-hardened methods and techniques, a survey of radiation effects on electronic devices is presented in this Chapter. Furthermore, rad-hardened design and analysis techniques are also discussed for enhancing in the survivability of electronic systems in strong radiation environments. More specifically, post-accident environments in nuclear power plants (NPPs) and industry standards and related regulatory guides for wireless post-accident monitoring system (PAMS) are also reviewed in this Chapter.

2.1 Background of Severe Accidents in NPPs

2.1.1 Industry Standards for PAMS in NPPs

After the Three Mile Island accident, the following three main standards for accident monitoring systems have been developed in the United States:

- (1) ANSI/ANS-4.5-1980 “Criteria for accident monitoring functions in light-water-cooled reactors”, which provides requirements on the selection and measurement variables (ANSI, 1980);
- (2) IEEE Std. 497-1981 “IEEE standard criteria for accident monitoring instrumentation for nuclear power generating stations”, which provides the design criteria for the relevant instrumentation (IEEE, 1981);
- and (3) Regulatory Guide 1.97 (rev. 3, May 1983) “Instrumentation for light-water-cooled nuclear power plants to assess plant and environs conditions during and following an accident”, which prescribes a detailed list of measurement variables and provides a comprehensive list of design and qualification criteria (NRC, 1983).

The integration of the above three standards is done in IEEE Std. 497-2002 with more functions and the criteria for variable selections (IEEE, 2002). Subsequently, variable selection, design, performance, and qualification and display criteria for accident monitoring instrumentation in NPPs are established in IEEE Std. 497-2010 (IEEE, 2010). IEEE Std. 497-2016 is considered to be the most recent standard and it provides more current guidance by enhancing existing standards and guidance (IEEE, 2016).

2.1.2 Design Issues of Wireless Monitoring Systems for Severe Accidents in NPPs

The mission of the wireless post-accident monitoring system is to obtain essential information about the status of the plant, which is crucial to plant operators and emergency response teams to effectively manage and mitigate the effects of accident. To achieve this mission, the following issues may need to be considered and investigated:

(1) EMI/RFI issues

Under a normal condition, applications of wireless technologies have been restricted in existing NPPs partially because of the vulnerability of existing I&C systems to electromagnetic interference and radio frequency interferences (EMI/RFI) emitted wireless devices (Ko and Lee, 2013). On the other hand, in the event of a severe accident, the plant is shut down; EMI/RFI is therefore no longer an issue.

(2) Radiation hardness

Unlike other industrial accidents, the levels of radiation after a severe accident can be high enough to cause severe damages to electronic devices. Therefore, the radiation-tolerance of such monitoring devices needs to be considered (Nagatani *et al.*, 2012).

(3) Communication issues

The reactor buildings constructed by concrete walls to shield radiation particles will also block wireless communication signals. Therefore, the quality of signal reception inside reactor buildings needs to be investigated and to ensure reliable communication (Nagatani *et al.*, 2012).

(4) Variables of Interests

The variables of interests under a severe accident are temperature, humidity, hydrogen concentration, and radiation levels of the environment, etc. It is also important to gather information about the conditions of protection systems, such as water level in a spent fuel pool, and coolant inventory, etc. Therefore, measurement variables need to be investigated according to IEEE 497 standard, as well as desirable locations of the related sensors (IEEE, 2016).

(5) Other issues

There are also several other crucial issues to considered in a harsh post-accident environment, such as high temperature, water damage, etc. Since this research mainly focuses on radiation-induced issues on electronic components used in wireless monitoring systems, their impacts will not be further explained.

2.1.3 Radiation Environment under a Severe Accident

In the event of a nuclear accident, a significant amount of radiation from the reactor core can be released due to failure of protection layers. Historically, there are three major nuclear accidents associated with nuclear power plants, Three Mile Island (1979), Chernobyl accident (1986) and Fukushima accident (2011). Luckily, there were no significant radioactive materials released to the environment in Three Mile Island accident, but the other two are very different. Chernobyl disaster exposed a significant fraction of core material into the environment. The total estimated release of radioactivity from the destroyed reactor is about 10^{18} Bq (Saenko *et al.*, 2011). The exposed reactor created γ -radiation and the highest dose level was about 300 Sv/h (Kortov and Ustyantsev, 2013). Similarly, Fukushima disaster also released a large amount of radioactive substances to the environment due to hydrogen explosions and fire damage to the containment structures (Takahashi, 2014). On June 6th, 2011, the radiation released to the atmosphere was estimated to be about 700,000 trillion Bq (Eisler, 2012). In March 2012, the level of radiation particles was estimated to be up to 73 Sv/h inside the containment of No.2 reactor (Eisler, 2012), and in Feb. 2017, it was up even further to

530 Sv/h (The Guardian, 2017). Under such post-accident conditions, electronic devices in the monitoring systems will not survive long time, if no special protection measures against radiation are taken. Radiation-hardened (rad-hardened) design methodologies, as well as rad-hardened analysis techniques in such cases are not luxury, but necessary, to ensure their reliable operation.

The principal types of radiation observed after a nuclear accident include alpha (α) particles, beta (β) particles, gamma (γ) rays, x-rays, and neutron particles (Adalja *et al.*, 2011; Sharp and Decretton, 1996). In general, neutrons are not a concern outside the reactor unless enough fissionable radioactive material is present to sustain a chain reaction. At Fukushima accident site, this has not happened and only alpha, beta, and gamma radiations have been detected outside the reactor (Adalja *et al.*, 2011).

2.2 Radiation Effects on Electronics

2.2.1 Composition of Monitoring Systems in Post-Accident Applications

Online monitoring systems (OLMs) have been used in nuclear power plants around the world to monitor several key plant conditions, such as detecting sensing-line blockages, testing the response time of pressure transmitters, monitoring the calibration of pressure transmitters, cross-calibrating temperature sensors in situ, assessing equipment condition, performing predictive maintenance of reactor internals, monitoring fluid flow, and extending the life of neutron detectors (Hashemian, 2011). The composition of those systems can be separated to several categories: sensors, electronic parts, other non-electronic components, etc. In general, semiconductor-based electronic parts are more sensitive to radiation than other components (Holmes-Siedle and Adams, 2002). The type of semiconductor electronic parts used in those systems varies widely, e.g., microcontrollers/microprocessors, memory chips (RAM/ROM), analog-to-digital converters (ADC), digital-to-analog converters (DAC), operational amplifiers, multiplexers, logic chips (TTL or CMOS), voltage references, transistors, diodes, etc. Moreover, these electronic components may be built with various different semiconductor technologies and different materials. Radiation effects on those

components and materials can be therefore different. The understanding of their responses to radiation is a significant part in the design of radiation-hardened system, which will be further discussed in the following Sections.

2.2.2 Mechanism of Radiation Interaction with Matters

The nature of interactions between radiation particles and target materials (semiconductors in this case) depends on properties of the particles (mass, charge, and kinetic energy) and the target (mass, charge, and density) (Srour, 1982). Radiation particles can be classified into three categories according to the way they interact with the materials: (1) photons, which interact through photoelectric effect, Compton scattering, or pair production; (2) charged particles, which interact through Rutherford scattering and nuclear interactions; and (3) neutrons, which interact through elastic scattering, inelastic scattering, and transmutation reactions (Srour, 1982; McLean and Oldham, 1987).

In general, radiation particles lose their energy through non-ionization processes (displacement) and/or ionization processes when they interact with semiconductor materials. Non-ionization processes are associated with neutrons, protons, alpha particles, heavy ions, and very high-energy photons. They can cause displacements in atoms in the target materials and/or change the arrangement of the crystal lattice's target atoms, resulting in adverse (often catastrophic) effects to electronic devices (Srour and McGarrity, 1988). On the other hand, ionization processes are primarily associated with charged particle interactions, such as electrons, protons, x -rays, and γ -rays (Gregory and Gwyn, 1974). They generate electron-hole pairs (ehps) when they pass through a semiconductor device. They usually cause glitches, abrupt changes, transient behavior, and soft errors (Gregory and Gwyn, 1974) in the device. Ionization processes can also result in permanent damages and destructive effects to devices if the accumulated dose or particle fluence has exceeded certain tolerance limits of particular device. Furthermore, all these two type of interactions can coexist. For example, a neutron can first collide with a nucleus to generate displacement damage, and then create secondary charged particles that can further impose ionization related damage (Makowski, 2006). The probability of component damage depends on radiation type, radiation energy, radiation

flux, and exposure duration. A list of existing publications on energy-loss processes as radiation interacting with matter is summarized in Table 2-1.

Table 2-1: Energy-loss process as radiation interacting with matter

| Energy-loss processes | References |
|--------------------------|--|
| Basic mechanisms | Barbottin and Vapaille, 1999; Srour, 1982; McLean and Oldham, 1987; Robinson, 1994 |
| Ionization processes | Foster, 2003; McLean and Oldham, 1987; Oldham, 2011; Srour and McGarrity, 1988 |
| Non-ionization processes | Foster, 2003; Gergory and Gwyn, 1974; McLean and Oldham, 1987; Oldham, 2011; Srour and McGarrity, 1988 |

Radiation effects on electronics can generally be categorized as: displacement damage (DD), total ionizing dose (TID), and single event effect (SEE) (Foster, 2003).

Displacement damage and total ionizing dose exposure are long term cumulative effects, while single event effect, as its name implies, is short-term one-time event. Those effects can be illustrated in Figure 2-1.

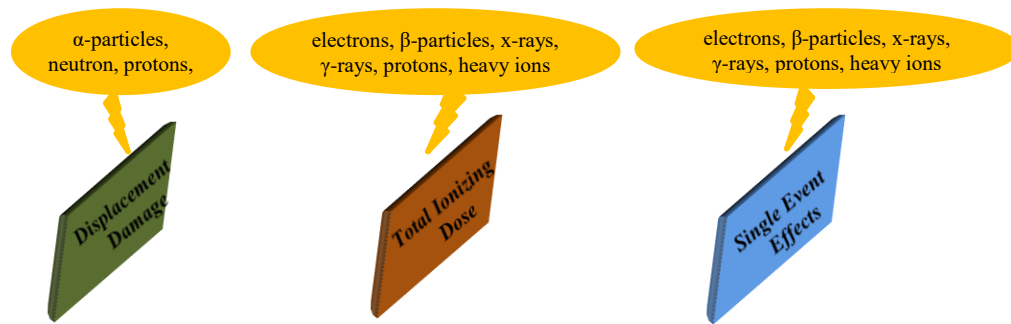


Figure 2-1: Radiation effects on electronics devices.

A list of representative publications above radiation effects on semiconductor devices is provided in Table 2-2. Details of different radiation effects are discussed further in Sections to follow.

Table 2-2: Radiation effects on semiconductor devices

| Radiation effects | References |
|---|--|
| Displacement damage | Arutt <i>et al.</i> , 2015; Barnaby <i>et al.</i> , 2017. Fernandez-Martinez <i>et al.</i> , 2013; Foster, 2003; George, 1992; Messenger and Spratt, 1958; Oldham, 2011; Srour <i>et al.</i> , 2003; Srour and Palko, 2013; Summers <i>et al.</i> , 1998; Wigner, 1946 |
| Total ionizing dose effect | Barnaby, 2006; Cellere and Paccagnella, 2004; Chen <i>et al.</i> , 2017; Fleetwood, 2013; Foster, 2003; Galloway and Schrimpf, 1990; Hughes and Benedetto, 2003; Johnston <i>et al.</i> , 1994; Nichols, 1980; Oldham, 2011; Oldham and McLean, 2003; Pease, 2003; Re <i>et al.</i> , 2006; Re <i>et al.</i> , 2008; Schwank, 1994 |
| Single event effects | Baumann, 2005; Buchner and McMorow, 2006; Cellere and Paccagnella, 2004; Dodd, 2005; Dodd <i>et al.</i> , 2007; Dodd and Massengill, 2003; Ferlet-Cavrois, 2013; Gadlage <i>et al.</i> , 2004; Koga <i>et al.</i> , 1997; Munteanu and Autran, 2008; Sexton, 2003; Soliman and Nichols, 1983; Titus, 2013; Troutman, 1986; Veronique <i>et al.</i> , 2013 |
| Displacement damage & Total ionizing dose effect & Single event effects | Adell and Scheick, 2013; Bagatin and Gerardin, 2015; Barbottin and Vapaille, 1999; Chen <i>et al.</i> , 2017; Claeys and Simoen, 2013; Cressler, 2013; Gregory and Gwyn, 1974; Gover, 1984; Holmes-Siedle and Adams, 2002; Hughes and Benedetto, 2003; Iniewski, 2010; Lv <i>et al.</i> , 2017; Makowshi, 2006; Messenger and Ash, 1986; Oldham, 2011; Pearton <i>et al.</i> , 2016; Polyakov <i>et al.</i> , 2013; Raoul, 2007; Schrimpf, 1994; Schrimpf and Fleetwood, 2004; Rathod <i>et al.</i> , 2011; Schwank <i>et al.</i> , 2008; Schwank <i>et al.</i> , 2013; Sexton, 1996; Simoen <i>et al.</i> , 2013; Srour and McGarrity, 1988 |

2.2.3 Displacement Damage

Displacement damage to an electronic device is caused by a long-term non-ionizing effect, and it occurs when an incident particle has enough energy to knock an atom free from its normal lattice site in the semiconductor and onto an interstitial site (Foster, 2003). As a result, it will change the properties of the electronic device due to minority carrier lifetime reduction, decreased carrier mobility, carrier transport, increased leakage current, and thermal charge generation (Srour *et al.*, 2003).

Ever since Wigner and his collaborators performed theoretical analysis and experimental verification of displacement damage in irradiated materials in the early 1940s (Wigner, 1946), numerous researchers have studied various aspects of displacement damage and its effects on various semiconductor devices and materials. A comprehensive review of displacement damage can be found in (Srouf and Palko, 2013), as well as several review papers, books, and short course notes about its various aspects and effects. Srouf and Palko also summarized the research history on investigation of displacement damage: (1) the first decade of the NSREC (1963-1972), focusing mainly on its effects in various semiconductor materials and devices; (2) the second decade (1973-1982), investigating its effects on more advanced devices and circuits, integrated-injection logic circuits, and charge-coupled devices (CCDs); (3) the third decade (1983-1992), concentrating on studies its effects on MOS devices and circuit technologies, as well as solar cells, GaAs devices, particle detectors, photodiodes, and bipolar transistors; (4) the fourth decade (1993-2002), addressing a broad variety of semiconductor devices and materials, as well as the nonionizing energy loss (NIEL), damage correlation, and synergistic effects; and (5) the most recent decade (2003-2012), continuously addressing the similar topics of previous decades and examining its effects in SDRAMs and memory devices, as well as conducting computational analysis of the process and the effects (Srouf and Palko, 2013).

2.2.4 Total Ionizing Dose

Total ionizing dose refers to the total amount of energy deposited by radiation particles passing through a semiconductor material. It is an important consideration for strong radiation environments, where the dose is typically in the range of 10^4 - 10^8 rad (Si) (Foster, 2003). When ionizing particles strike silicon oxide, interactions at the physical level can be described in four steps, as illustrated in Figure 2-2 (1) electron-hole-pairs (ehps) are formed by energy deposited in the semiconductor material and a fraction of the generated electron-hole-pairs recombine; (2) free carriers which escape the recombination are transported into the oxide; (3) hole trapping at the SiO_2/Si interface; and (4) the interface traps (or interface states) are produced at the SiO_2/Si interface (Adell and Scheick, 2013; Srouf and McGarrity, 1988). Considering an example of a MOSFET exposed to ionizing radiation, the positive charges are trapped at the Si/SiO_2 interface or

at the metal/SiO₂ interface, which is illustrated in Figure 2-3. As a result, a shift in the threshold voltage is generated and the device could not be turned off if this voltage shift is high enough for turn-off threshold value (Oldham and McLean, 2003).

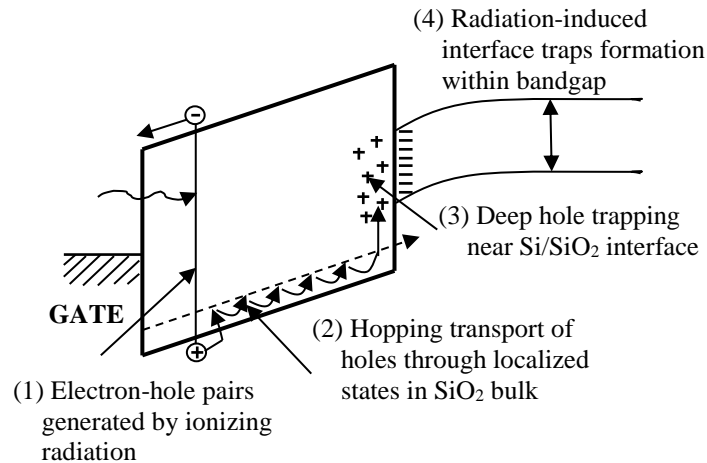


Figure 2-2: The effects of ionizing radiation in SiO₂ (Adell and Scheick, 2013; Srour and McGarrity, 1988)

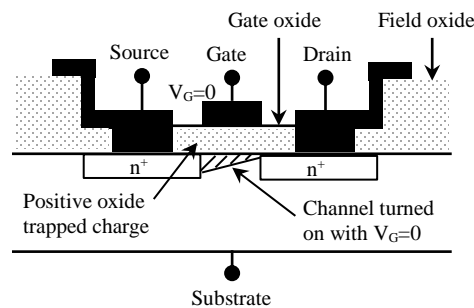


Figure 2-3: The effect of ionizing radiation on the gate oxide in an n-channel MOSFET (Oldham and McLean, 2003)

For MOS devices, such as transistors and integrated circuits (ICs), ionizing radiation will affect their functionalities and performance characteristics, which include threshold voltage shifts, mobility degradation, increased leakage currents, enlarged on-resistance, high-level of gate charge, and reduction in breakdown voltage (Adell and Scheick, 2013; Hughes and Benedetto, 2003). On the other hand, for bipolar devices, the recombination current will be increased and common-emitter current gain will be reduced due to

probably two reasons: increased density of interface traps at the surface of the extrinsic base region; and positive charge buildup (Johnston *et al.*, 1994). A list of publications for total ionizing dose effects on various semiconductor technologies and devices is provided in Table 2-3.

Table 2-3: Total ionizing dose effects on semiconductor technologies and devices

| Semiconductor technologies & Devices | References |
|--------------------------------------|--|
| <i>Semiconductor technologies</i> | |
| MOS | Adell and Scheick, 2013; Cardoso <i>et al.</i> , 2014; Hughes and Benedetto, 2003; Re <i>et al.</i> , 2006; Re <i>et al.</i> , 2008 |
| Bipolar | Adell <i>et al.</i> , 2012; Johnston <i>et al.</i> , 1994 |
| SOI | Alles <i>et al.</i> , 2015; Simoen <i>et al.</i> , 2004 |
| <i>Semiconductor devices</i> | |
| AD | Lee <i>et al.</i> , 1994; Pease <i>et al.</i> , 2007; Lee and Johnston, 1998 |
| HBT | Inanlou <i>et al.</i> , 2014; Praveen <i>et al.</i> , 2012; Sutton <i>et al.</i> , 2006; Zhang <i>et al.</i> , 2016 |
| HEMT | Hu <i>et al.</i> , 2004; Ives <i>et al.</i> , 2015; Kalavagunta <i>et al.</i> , 2008; O'Loughlin, 1987; Sun <i>et al.</i> , 2013 |
| BJT | Adell <i>et al.</i> , 2012; Kosier <i>et al.</i> , 1995; Schmidt <i>et al.</i> , 1995; Schmidt <i>et al.</i> , 1996 |
| FET | Cardoso <i>et al.</i> , 2013; Gaillardin <i>et al.</i> , 2006 |
| FinFET | Duan <i>et al.</i> , 2014; Zhang <i>et al.</i> , 2010; Zhang <i>et al.</i> , 2017 |
| JFET | Flament <i>et al.</i> , 1996; McGarrity <i>et al.</i> , 1992; Zuleeg <i>et al.</i> , 1977; Zuleeg and Lehovc, 1980 |
| NAND | Cellere <i>et al.</i> , 2007; Bagatin <i>et al.</i> , 2011; Kay <i>et al.</i> , 2012; Gerardin <i>et al.</i> , 2013; Nguyen <i>et al.</i> , 1999; Oldham <i>et al.</i> , 2006 |
| MOSFET | Hao <i>et al.</i> , 2017; Park <i>et al.</i> , 2008; Pizanoa <i>et al.</i> , 1998; Ren <i>et al.</i> , 2017; Schrimpf <i>et al.</i> , 1988; Simoen <i>et al.</i> , 2004; Zhang, <i>et al.</i> , 2013 |
| NOR | Cellere <i>et al.</i> , 2007; Gerardin <i>et al.</i> , 2013; Nguyen <i>et al.</i> , 1999 |
| RAM | Bernacki, <i>et al.</i> , 2000; Massengill <i>et al.</i> , 1986 |
| Voltage regulator | Adell <i>et al.</i> , 2004; Beaucour <i>et al.</i> , 1994; Kelly <i>et al.</i> , 2007; Pease <i>et al.</i> , 1998; Ramachandran <i>et al.</i> , 2006 |
| FPGA | Citterio <i>et al.</i> , 2016 |

2.2.5 Single Event Effect

The physical mechanisms of a single event effect can be divided into three steps, as illustrated in Figure 2-4. The first step involves two types of charge deposition: (1) direct ionization caused by inelastic interactions that transmit a large amount of energy to the struck atoms and generates electron-hole-pairs; and (2) indirect ionization caused by secondary particles between the incident particles and the atoms of materials that the microelectronic devices are made of. The second step is charge transport, where the released carriers are quickly transported and collected by elementary structures (e.g., p - n junctions). The third step is charge collection, where the parasitic current will create disturbances in the semiconductor devices and can cause permanent damage to the gate insulators or a latch-up of the device if the current is sufficiently high (Munteanu and Autran, 2008).

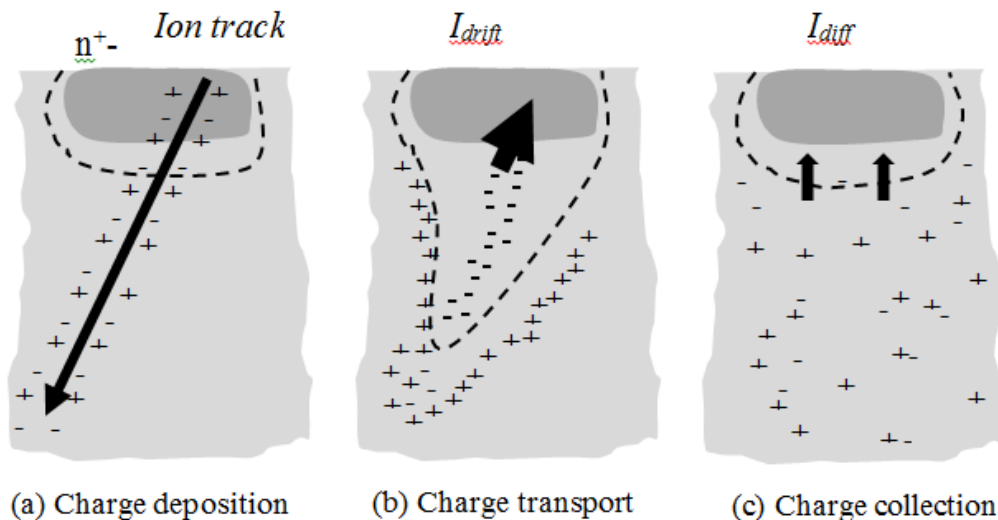


Figure 2-4: The physical mechanism of single event effects (Baumann, 2005)

Furthermore, depending on how the semiconductor reacts charge deposition leading to a failure, single event effects can further be separated into two types: non-destructive effect and destructive effect, which are explained in the following Sections.

➤ *Non-destructive effects*

If the semiconductor can be recovered from a failure caused by a single event effect through a system reset and/or data re-initialization, those effects are called non-destructive effects. They could include one of the following scenarios.

(1) Single Event Transient (SET)

A single event transient can be triggered by a short-term current caused by the generated electron-hole pairs, which may change the logic state of a circuit (Ferlet-Cavrois *et al.*, 2013). The short-term pulse can be eliminated if the deposited charges are removed by providing an alternative conducting path. The pulse may also propagate through subsequent circuit stages and induce a voltage transient (leading to reverse in logic states) (Ferlet-Cavrois *et al.*, 2013).

(2) Single Event Upset (SEU)

A single event upset can be triggered by the generated transient current and the charge collected at the struck electric node when a charged particle passes through a reverse-biased junction (Dodd and Massengill, 2003). Such effects on several circuits have been summarized (Dodd and Massengill, 2003). In case of a storage cell, this may lead to a cell upset. For an SRAM cell or a flip-flop, the state of the memory can be inverted. For a DRAM cell, the charge stored can be modified and interpreted as an invalid value. Furthermore, in logic circuits, SEUs can occur when a SET propagates through a combinational logic, and is then captured by a latch or a flip-flop.

(3) Single Event Functional Interrupt (SEFI)

A single event functional interrupt is a complex failure mode when a heavy ion particle strike triggers an abnormal mode, such as test mode, or reset mode, which can cause ICs to lose their intended functionalities temporarily (Koga *et al.*, 1997). Complex devices are more likely to exhibit SEFIs. For example, SDRAM has a built-in self-test (BIST) mode and a self-repairing boot sequence, which could be triggered inadvertently after a heavy ion strike leading to an unintended reset or idle state (Dodd and Massengill, 2003).

➤ *Destructive effects*

As the name implies, failures induced by destructive effects are catastrophic and the devices are permanently damaged. Such situations can be due to one of the following events.

(1) Single Event Latchup (SEL)

A single event latchup may be triggered in ICs by a *pnpn* four layer structure when any sources with excess carriers could turn on a thyristor-like device. A latchup creates a low resistance path between the power supply and the ground. Consequently, destructive current of a high magnitude may be produced in such a path, which can damage the device permanently (Sexton, 2003).

(2) Single Event Snapback (SES)

A single event snapback is caused by drain-to-source breakdown in NMOS transistors. Their effect is similar to SEL, but a *pnpn* four layer structure is not necessary. When heavy ions strike a semiconductor near the drain junction, the induced current can be high enough to cause an avalanche multiplication. If this condition stays long enough, a sufficiently high amplitude current pulse will be produced and the transistor will be turned ON inadvertently. The resulting high amplitude current can cause permanent damage to the device (Sexton, 2003).

(3) Single Event Burnout (SEB)

A single event burnout may occur if the drain-to-source voltage is higher than the second breakdown voltage due to high current caused by large volume of ionizing particles passing through a bipolar power transistor or an MOSFET. The device will suffer from overheat locally, and failure can occur if the current is not removed quickly (Sexton, 2003).

(4) Single Event Gate Rupture (SEGR)

A single event gate rupture is usually caused by SEB in power MOSFETs when heavy ions hit the gate region simultaneously. A SEGR can cause a short circuit between the

drain and the gate, which results in local overheating and causes irreversible damage in the gate region (Sexton, 2003).

A list of available publications for single event effects on semiconductor devices is provided in Table 2-4.

Table 2-4: Single event effects on modern electronics

| Single event effects | References |
|-----------------------------------|---|
| <i>Non-destructive effects</i> | |
| Single event transient | Buchner and McMorow, 2006; Dodd <i>et al.</i> , 2004; Ferlet-Cavrois <i>et al.</i> , 2013; Gadlage <i>et al.</i> , 2004; Wang, 2011; Wirth <i>et al.</i> , 2008 |
| Single event upset | Dodd and Massengill, 2003; Dodd <i>et al.</i> , 2007; Karnik <i>et al.</i> , 2004 |
| Single event functional interrupt | Dodd and Massengill, 2003; Koga <i>et al.</i> , 1997; Koga <i>et al.</i> , 2001 |
| <i>Destructive effects</i> | |
| Single event latchup | Becher <i>et al.</i> , 2002; Gregory and Shafer, 1973; Johnston <i>et al.</i> , 1990; Johnston <i>et al.</i> , 1997; Kolasinsky <i>et al.</i> , 1979; Leavy and Poll, 1969; Sexton, 2003; Soliman and Nichols, 1983; Troutman, 1986 |
| Single event snapback | Dodd <i>et al.</i> , 2000; Koga and Kolasinski, 1989; Ochoa <i>et al.</i> , 1984; Sexton, 2003; Stassinopoulos <i>et al.</i> , 1992 |
| Single event burnout | Hohl and Galloway, 1987; Hohl and Johnson, 1989; Johnson <i>et al.</i> , 1992; Kuboyama <i>et al.</i> , 1992; Liu <i>et al.</i> , 2006; Oberg and Wert, 1987; Sexton, 2003; Titus, 2013; Titus <i>et al.</i> , 1991 |
| Single event gate rupture | Allenspach <i>et al.</i> , 1996; Brews <i>et al.</i> , 1993; Borulta <i>et al.</i> , 2001; Johnson <i>et al.</i> , 1998; Sexton, 2003; Sexton <i>et al.</i> , 1998; Sexton <i>et al.</i> , 1997; Titus, 2013 |

2.2.6 Radiation Effects on Semiconductor Devices

Radiation effects on modern semiconductor devices are briefly described in Table 2-5 (Holmes-Siedle and Adams, 2002).

Table 2-5: Summary of radiation effects on semiconductor devices (Homes-Siedle and Adams, 2002)

| Device types | | Radiation effects |
|--|--|--|
| Diodes | Low-power rectifier diodes | The mean reverse leakage current will be increased by small radiation-induced alterations in the surface charge. |
| | High-power rectifier | Serious degradation in the forward voltage drop. |
| | Zener diodes | Zener breakdown voltages do not change much, the transient current is reduced. |
| | Microwave diodes | Inherently 'hard' to both total dose and neutron irradiation. |
| Opto-electronics | Phototransistors | The output current degrades. |
| | LEDs and lasers | Neutron damage reduces the minority-carrier lifetime in the active regions; particles produce new defects to reduce the light output efficiency. |
| | Opto-couplers | The degradation of component parts, such as the current transfer ratio. |
| | Charge-coupled devices (CCDs) | Threshold voltage shift on CCD gates due to TID effects, displacement damage reduces the CTE, increases the dark current, produces dark current nonuniformities and generates random telegraph noise in individual pixels. |
| Solar cells | Solar cells | Cell efficiency can be seriously affected by radiation-induced defects by degradation of diffusion length. |
| Power semiconductors | Bipolar power transistors | A low doping level for the collector and a high base width which can lead to high sensitivity to neutron irradiation. |
| | Thyristors | Triggering parameters degrade suddenly as the neutron dose is increased; can suffer from single-event effects. |
| | Power MOSFETs | Parameter changes under radiation: threshold voltage shift, transconductance degradation, reduction in breakdown voltage, burn-out induced by transients. |
| | Insulated-gate bipolar transistor (IGBT) | BiMOS power switching device with high input impedance and low drive requirements; can suffer from the low total-dose tolerance of the MOSEFT portion and heavy ion. |
| Junction field-effect and heterojunction transistors | Field-effect transistor (FET) | Be tolerant of the effects of heavy ionization and bulk damage, special silicon JFET devices are even more tolerant to neutrons. |
| | Heterojunction bipolar transistor (HBT) | High degree of inherent radiation hardness. |
| Miscellaneous electronic components | Capacitors | The electrical effects of total-dose do not have any effects until a dose about 10^7 rad. |
| | Resistors and conductors | Discrete resistors have been irradiated at very high radiation environments with no problems; conduction in metals is not affected by radiation particles. |
| | Quartz crystals | Permanent shifts in frequency and changes the responsivity; 'swept' quartz is less susceptible to radiation. |
| | Vacuum tubes | More desirable to use in very high neutron/gamma environments. |
| | Semiconductor microwave devices | Reduction in majority-carrier concentration by bulk displacement damage; transient increase in majority carriers generated by a burst of radiation. |
| Miscellaneous hardware | Connectors, cables, gaskets, O-rings, switches | Depend on the properties of the component materials, the mechanical properties of plastics show the onset of damage in the range 10^7 to 10^9 rad. |

As can be seen, radiation effects on semiconductor devices can be a complex process. The outcomes depend on many factors. These include materials used, structures chosen, manufacturing processes, domain of usages, and the surrounding environment conditions. All these factors should be considered when selecting devices in the design and construction of monitoring systems for severe accident monitoring systems for nuclear power so that higher tolerance to radiation can be achieved.

2.3 Rad-Hardened Design Techniques

From a pure physical composition point of view, any electronic systems can be decomposed bottom up in several levels: device-, circuit-, and system-levels. During system design, both hardware design and software development, rad-hardened techniques should be adopted at each level to minimize the impacts of potential radiation effects. This concept can briefly be illustrated in Figure 2-5. Rad-hardened design techniques at different levels are summarized in Figure 2-6, which will be further described in subsequent Sections.

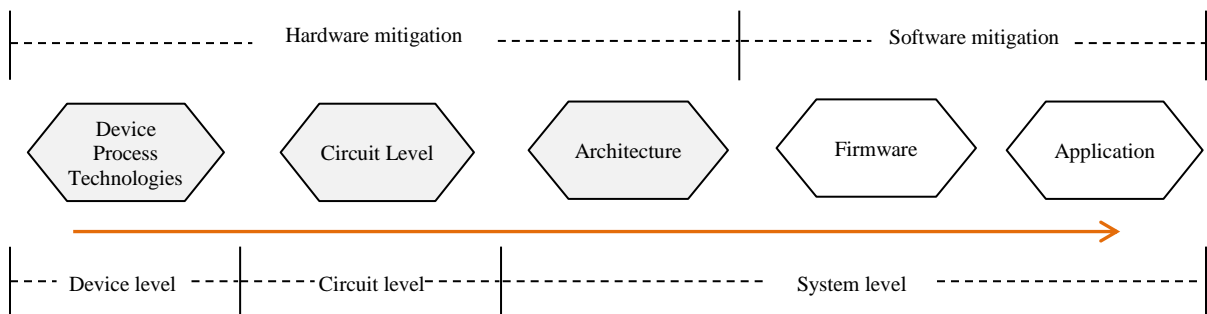


Figure 2-5: Abstraction levels of electronic system

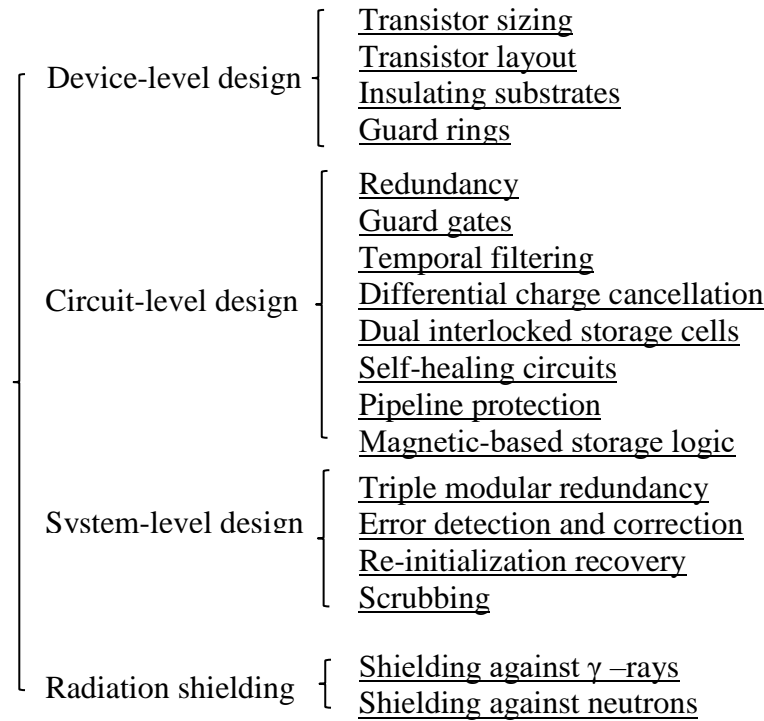


Figure 2-6: Methods of rad-hardened design techniques

2.3.1 Rad-Hardened by Device-Level Design

Rad-hardened techniques at device-level typically focus on increasing the radiation resistance of a design by fundamentally changing and improving the fabrication processes (Garg *et al.*, 2009). In general, the devices which have undergone such special process are often known as rad-hardened components, which indeed have higher resistance to ionizing radiation. However, because of the special process involved, as well as the small volume production to feed the small market demand, these devices turn to be excessively expensive. Nevertheless, the techniques used can be summarized as follows:

(1) Rad-hardened by sizing

Rad-hardening by increasing the aspect ratio (W/L) of the transistor to improve the radiation tolerance, as a larger gate area has higher current carrying capability and higher node capacitance than a smaller area. Moreover, increasing the size of the transistor can

effectively lower the magnitude and shorten the duration of the transient voltage pulse. If the transistor size is sufficiently large, such transient voltage pulse can even be eliminated (Zhou and Mohanram, 2004).

(2) Special layout design for transistor

One can also improve the radiation tolerance of transistors through special layout design. For example, in annular transistors, one can enclose the source or the drain in transistors to prevent charge buildup in isolation oxides (Wallden, 2014). It has been noted that the lifespan of annular MOSFET with reduced drain electric field is three times more than that of a conventional device with the same technology under radiation conditions (Mayer *et al.*, 2004). Using H-gate and ringed-source layouts can also increase drain leakage current and make the threshold voltage higher, which can enhance the radiation tolerance capability of the transistors (Liu *et al.*, 2010).

(3) Silicon on insulator (SOI) / Silicon on sapphire (SOS)

Insulating substrates can also be used to reduce the sensitivity of bulk devices to ionizing radiation. This can be accomplished by using an insulator layer to separate the active region and the inactive substrate, which is named Silicon on Insulator (SOI). This approach results in lower parasitic capacitance and increases resistance to latchup. Silicon on Sapphire (SOS) is a hetero-epitaxial technique of the SOI family for IC manufacturing, which consists of a silicon film grown on a sapphire (Al_2O_3) substrate. It has been found that the space grade SOI/SOS IC chips are many orders greater than those of ordinary commercial grade IC chips (Yu *et al.*, 2011) as far as radiation-tolerance is concerned. For example, their sensitive volume for dose rate effects is typically two orders of magnitude lower than that of bulk-silicon devices (Schwank *et al.*, 2003).

(4) Guard rings

Guard rings can be designed around p-wells and n-wells to prevent SEL and to reduce inter-device leakage. p⁺ diffusion or n⁻ diffusion ring surrounding adjacent NMOS and/or PMOS devices will generate a higher voltage threshold and prevent leakage between them (Camplani *et al.*, 2014; Irani *et al.*, 2017).

2.3.2 Rad-Hardened by Circuit-Level Design

Special circuit design techniques can also be used at the circuit-level to improve fault avoidance capabilities and to reduce the vulnerability to radiation damage (Garg *et al.*, 2009). These techniques as well as the associated references can be summarized as follows:

(1) Critical circuits redundancy

Within the overall system design, critical circuits in the system should be duplicated using redundancies to enhance the reliability and fault-tolerance (Aydos and Fey, 2017; Li *et al.*, 2014; Lu *et al.*, 2014; Rajaei *et al.*, 2015; and Smith and Mostert, 2007). Furthermore, the concepts of local space and time redundancy can be effective to prevent soft-error latches (Nicolaidis and Zorian, 1998; Mavis and Eaton, 2002; and Hazucha *et al.*, 2004). As an example, a triple inter-locked latch (TILL) is presented in (Li *et al.*, 2014), where the irradiation tests have shown that the TILL has a SEU threshold of LET over 42 MeV-cm²/mg, which is much higher than that of conventional latches. Furthermore, the cross section of the TILL is at least one order of magnitude lower than that of a conventional latches.

(2) Guard gate

Guard gate can be used to prevent SETs from a latch. An example is presented in (Balasubramanian *et al.*, 2005), where a buffer circuit with two inputs and one output has been considered. Both inputs are connected to the output of a combinational logic block; however, one input has been delayed. If the output of the combinational logic block encounters a SET pulse, the delayed signal will not change the logic status immediately and will become different from the other input. Hence, the guard gate output will become float and will maintain the previous voltage value to prevent SETs from happening.

(3) Temporal filtering

Temporal filtering is a technique that generates multiple versions of the same signal, but separates them by delayed elements. These elements are then put through a majority voter

to produce the desired output. For example, a SET-hardened latch with temporal filtering is described in (Lacoe, 2008), where the data input is connected to three separate edge-triggered D-flip-flops in parallel. If a transient signal is induced at the input, it will arrive at all the flip-flops at the same time, but the clock signals will not arrive at the same moment because two clock signals are delayed by Δt and $2\Delta t$ at the flip-flops separately. Therefore, only one clock signal will arrive with the transient, and the other two inputs will produce the correct signal (Mavis and Eaton, 2002).

(4) Differential charge cancellation (DCC) layout

Differential charge cancellation layout leverages the inherent common-mode rejection of differential circuits to mitigate voltage transients induced by heavy ion strikes. One experimental verification of a circuit hardened through DCC layout technique has been given in (Blaine *et al.*, 2012). It has been shown that DCC layout can provide more than an order of magnitude reduction in sensitive area across all tested energies with two-photon absorption (TPA) laser facility (Blaine *et al.*, 2012). Another TPA testing is also presented in (Atkinson *et al.*, 2013) to demonstrate the effectiveness in the mitigation SETs through DCC layout. The conclusion is that the DCC layout can significantly mitigate SETs at low levels of charge deposition, as well as diminish charge sharing in the baseline layout (Atkinson *et al.*, 2013).

(5) Dual interlocked storage cells (DICE)

Dual interlocked storage cell uses a four node redundant structure to mitigate SEUs (Blum and Delgado-Frias, 2006; Zhao, 2015). DICE can be applied to replace latches and flip-flops distributed within logic blocks in CMOS devices and also used to implement SEU-hardened SRAMs. Some solutions of DICE can be found in (Calin *et al.*, 1996; Lacoe, 2008; Gorbunov *et al.*, 2014; Wang *et al.*, 2015; and Hui *et al.*, 2015). A comparison of different radiation-hardened by design techniques for SRAM blocks manufacture of two IC chips with similar functionalities is given in (Gorbunov *et al.*, 2014). It demonstrates that DICE cells can achieve about 2-3 orders of magnitude lower than cross-sections for 6T-cells.

(6) Self-healing circuits

Self-healing circuits make use of other circuit blocks to monitor the behaviors of the main circuit. In a simple team, it contains some feedback to tune circuit parameters in a closed-loop fashion to detect any change in the main circuit (Howard *et al.*, 2012; Inanlou *et al.*, 2013; and Rajaei *et al.*, 2013). For example, a method using chopper stabilization is presented to improve the precision of voltage references in ionizing radiation environments (Shetler *et al.*, 2015). The tests have shown that adoption of the chopper stabilization can lead to 96% reduction in radiation-induced shift. A rad-hardened sensing circuit is also proposed to reduce the radiation-induced currents for protecting the Magnetic Tunnel Junction (MTJ) in conventional magnetic random access memory MRAMs (Chabi *et al.*, 2014). The simulation results have shown that the SEU probability can be reduced to as low as 0.01% for more than 50 fC of the injected charge.

(7) Pipeline protection

Pipeline protection techniques use self-checking register architecture to combat both SEUs inside a register and SETs captured by the register (Das *et al.*, 2009; Lin *et al.*, 2016). For example, a radiation-hardened pipeline is proposed in (Lin *et al.*, 2016) by incorporating soft-error- and timing-error-tolerant flip-flop (SETTOFF)-based self-checking cells into the sequential cells in the pipeline. The gate-level injection results have shown that a SETTOFF-based self-checking technique requires more than 30% less area and 80% less power overhead than the triple modular redundancy does.

(8) Magnetic-based storage logic

Static random access memory (SRAM) is very susceptible to radiation-induced soft errors (Rajaei *et al.*, 2015). Due to its inherent characteristics, magnetic tunnel junction (MTJ) will have relatively higher resistance to radiation-induced soft errors, some radiation-hardened magnetic random access memory (MRAM)-based field-programmable gate arrays (FPGAs) are proposed in (Goncalves *et al.*, 2013; Rajaei 2016; and Rajaei and Mamaghani, 2017) to achieve advantages of non-volatility, low power consumption, high performance, and high tolerance to soft errors.

2.3.3 Rad-Hardened by System-Level Design

Rad-hardening techniques at the system-level typically use fault detection approaches and tolerance mechanisms to enhance the radiation resistance of the system (Garg *et al.*, 2009). Some of these techniques can be summarized as follows:

(1) Redundant element

Redundant elements can take one of the four forms: hardware redundancy (Mahmood and McCluskey, 1988; Mukherjee *et al.*, 2002), information redundancy (Samson *et al.*, 2001), time redundancy (Nicolaidis, 1999), and software redundancy (Lindoso *et al.*, 2012; Rebaudengo *et al.*, 2004). Hardware redundancy relies on duplication of subsystems to detect and to correct single error, and to achieve fault tolerance to single event effects, such as dual modular redundancy (DMR), triple modular redundancy (TMR) (Brinkley *et al.*, 2000; Clark *et al.*, 2011; and Li *et al.*, 2000). Information redundancy uses error correcting codes (ECC) techniques, and error detection and correction (EDAC) methods by re-assigning corrected values to avoid error accumulation (Shirvani *et al.*, 2000). Examples of this techniques include parity checking (Tiwari and Tomko, 2005), rectangular codes (Patel and Hong, 1974), hamming codes (Morelos-Zaragoza, 2002; Shooman, 2003), and reed-Solomon codes (Neuberger *et al.*, 2005). Time redundancy uses slack-time in the system schedule to improve transient-fault tolerance capability by performing recovery executions whenever fault occurs (Ejali *et al.*, 2000). Finally, software redundancy relies on multiple versions of independently developed software to tolerant faults in software operational environments (Eckhardt *et al.*, 1991), such as N-version programming (Avizienis, 1985), and recovery blocks (Randell, 1975).

(2) Re-initialization recovery

Re-initialization recovery utilizes an external timer circuit, acting as a watchdog, to perform a forced reset for the system when other rad-hardening methods deemed ineffective (Yu *et al.*, 2011). The watchdog timer can be implemented in hardware or software or through a combination of both at several levels, such as subsystem-to-

subsystem, box-to-box, board-to-board, and device-to-device (LaBel and Gates, 1996). The multiple watchdog time-out solution is demonstrated in (LaBel *et al.*, 1992) and the developed system has successfully been tested for SEL for BNL (LaBel and Gates, 1996).

(3) Scrubbing

Scrubbing can be used to avoid accumulation of errors and to reduce the probability of multiple errors (Nidhin *et al.*, 2017). There are two different types scrubbing algorithms: preventive and corrective. A preventive algorithm will perform scrubbing periodically regardless whether this is an error. On the other hand, a corrective scrubbing will read back configuration memory periodically and trigger scrubbing only when the algorithm has detected an error (Herrera and Lopez-Vallejo, 2013).

2.3.4 Rad-Hardened by Shielding

Radiation shielding is an effective way to mitigate radiation effects and to increase the reliability and prolong the life of electronic systems. The shielding can be applied to package and/or relevant IC chips. The effectiveness of shielding depends on the properties of shielding materials, and radiation type, and radiation tolerance level of semiconductor (Shultis and Faw, 2005). The type and required thickness and mass of the shielding material, uniformity of shielding capability, permanence and availability of shielding depends on radiation levels to be attenuated, resilience of the devices to radiation exposure (Shultis and Faw, 2005). Shielding characteristics can be determined numerically based on a linear attenuation coefficient, the total mass attenuation coefficient for γ -rays, and the effectiveness in removal of cross-section for fast neutrons (Yilmaz *et al.*, 2011).

Shielding properties of many materials have been investigated and reported in the literature. For example, these include concrete (Gencel *et al.*, 2011; Kharita *et al.*, 2008; Korkut *et al.*, 2010; and Yilmaz *et al.*, 2011), concrete mixed with mineral additives (Akkurt *et al.*, 2010; Damla *et al.*, 2010; Kharita *et al.*, 2008; Kharita *et al.*, 2011; and Kurudirek *et al.*, 2009), alloys (Abdao, 2002), aluminum and tungsten (Mangeret *et al.*, 1996), fly-ash brick materials (Singh and Badiger, 2014), conlemanite and epoxy resin

(Okuno, 2005), and a reusable shielding material with high density of desired nuclei (iron, hydrogen, and boron) (Calzada *et al.*, 2011). Even though concrete and concrete related materials might not be suitable for protecting electronic systems directly, the information is still very relevant when determining the plant locations for installation for such systems. For completeness, the relevant references are also included herein. A comparative study of radiation shielding for some shielding concretes and glass systems can be found in (Kurudirek, 2014). Because electronic components have different susceptibility to radiation, shielding materials have also been used directly on components level. e.g., a depleted boron is studied in (Kern and Smeltzer, 1986) to protect the integrated circuits directly.

2.3.5 Summary of Rad-Hardened Design Techniques

Existing rad-hardened design techniques for mitigation radiation effects are summarized in Table 2-6 together with a list of available literature for radiation hardening design techniques.

Table 2-6: Potential approaches to achieve rad-hardened design at different levels

| Potential approaches | Effects mitigation | References |
|---|--------------------|---|
| <i>Device-level design</i> | | |
| Transistor sizing | TID, SEE | Zhou and Mohanram, 2004; Zhou and Mohanram, 2006 |
| Transistor layout | TID, SEE | Liu <i>et al.</i> , 2010; Mayer <i>et al.</i> , 2004; Seixas <i>et al.</i> , 2017 |
| Insulating substrates | TID, SEE | Schwank <i>et al.</i> , 2003; Vizkelethy <i>et al.</i> , 2005 |
| Guard rings | SEL | Camplani <i>et al.</i> , 2014; Irani <i>et al.</i> , 2017 |
| <i>Circuit-level design</i> | | |
| Redundancy | SEE | Aydos and Fey, 2017; Li <i>et al.</i> , 2014; Lu <i>et al.</i> , 2014; Rajaei <i>et al.</i> , 2015; Smith and Mostert, 2007; Yan <i>et al.</i> , 2017 |
| Guard gates | SET | Balasubramanian <i>et al.</i> , 2005; Qi <i>et al.</i> , 2015 |
| Temporal filtering | SET | Lacoe, 2008 |
| Differential charge cancellation | SET | Atkinson <i>et al.</i> , 2013; Blaine <i>et al.</i> , 2012 |
| Dual interlocked storage cells | SEU | Calin <i>et al.</i> , 1996; Hui <i>et al.</i> , 2015; Lacoe, 2008; Gorbunov <i>et al.</i> , 2014; Wang <i>et al.</i> , 2015 |
| Self-healing circuits | TID, SEE | Adell <i>et al.</i> , 2018; Chabi <i>et al.</i> , 2014; Howard <i>et al.</i> , 2012; Inanlou <i>et al.</i> , 2013; Rajaei <i>et al.</i> , 2013; Shetler <i>et al.</i> , 2015 |
| Pipeline protection | SEU, SET | Das <i>et al.</i> , 2009; Lin <i>et al.</i> , 2016 |
| Magnetic-based storage logic | SEE | Goncalves <i>et al.</i> , 2013; Rajaei 2016; Rajaei and Mamaghani, 2017; Wang <i>et al.</i> , 2018 |
| <i>System-level design</i> | | |
| Redundant elements & Co-design approach | SEE | Brinkley <i>et al.</i> , 2000; Ciani <i>et al.</i> , 2014; Clark <i>et al.</i> , 2011; Clark <i>et al.</i> , 2015; Cuenca-Asensi <i>et al.</i> , 2011; Eftaxiopoulos <i>et al.</i> , 2016; Huang <i>et al.</i> , 2015; Li <i>et al.</i> , 2000; Siegle <i>et al.</i> , 2015; Sterpone <i>et al.</i> , 2013 |
| Error detection and correction | SEU, SET | Morelos-Zaragoza, 2002; Neuberger <i>et al.</i> , 2005; Patel and Hong, 1974; Shirvani <i>et al.</i> , 2000; Tiwari and Tomko, 2005; Shooman, 2003 |
| Re-initialization recovery | SEU, SET | Lopez-Morillo <i>et al.</i> , 2018; Makowski, 2006 |
| Scrubbing | TID, SEE | Herrera and Lopez-Vallejo, 2013; Nidhin <i>et al.</i> , 2017 |
| <i>Radiation shielding</i> | | |
| Shielding against γ -rays | TID | Abdao, 2002; Akkurt <i>et al.</i> , 2010; Calzada <i>et al.</i> , 2011; Damla <i>et al.</i> , 2010; Gencel <i>et al.</i> , 2011; Kern and Smeltzer, 1986; Kharita <i>et al.</i> , 2008; Kharita <i>et al.</i> , 2011; Korkut <i>et al.</i> , 2010; Kurudirek <i>et al.</i> , 2009; Kurudirek, 2014; Mangeret <i>et al.</i> , 1996; Okuno, 2005; Shultis and Faw, 2005; Singh and Badiger, 2014; Yilmaz <i>et al.</i> , 2011 |
| Shielding against neutrons | DD | |

In a specific circuit design, multiple of these techniques can be used concurrently to provide greater protection for the designed system. However, one does have to consider the complexity of the resulting design and other practical constraints, such as size, weight, and cost.

2.4 Modeling and Simulation Techniques

At the system design phase, it is important to develop different techniques to evaluate various rad-hardened techniques. Of course, the most reliable technique is known as radiation-hardness assurance (RHA) which is a physical test using radiation source. RHA evaluate whether a system, a subsystem, or a component can operate correctly in the given radiation environment. The radiation environment is created by using external perturbation sources to perform natural or accelerated particle radiation, laser beam, etc. (Quinn *et al.*, 2013; Uznanski *et al.*, 2014; Shaneyfelt *et al.*, 2008). The results from these tests are very precise, but the procedure/process can be very complicated and expensive (Gorbunov *et al.*, 2011). To achieve relatively quick feedback in the design iteration, evaluation of the radiation protection can also be accomplished using modeling and computer simulations. Modeling techniques for radiation shielding and simulation of radiation effects (TID, DD, and SEEs) are reviewed in following Sections.

2.4.1 Simulation of Radiation Shielding

Several modeling and simulation packages have been developed to study radiation transport problems by using the Monte Carlo method (Shultis and Faw, 2005), such as FLUKA (Ballarini *et al.*, 2007; Fasso *et al.*, 2005; Fasso *et al.*, 2003; Korkut *et al.*, 2012; Yue *et al.*, 2009), GEANT4 (Allison, 2006; BAK *et al.*, 2010; Santina *et al.*, 2003; Titt and Newhaser, 2005; Zeynali *et al.*, 2012), PHITS (Iwase *et al.*, 2002), SHIELD (Dementyev and Sobolevsky, 1999), and MULASSIS (Lei *et al.*, 2002). The solutions from some of these packages have been validated with experimental data (Beskrovnaia *et al.*, 2008; Fernandez-Hernando *et al.*, 2006; Tessa *et al.*, 2009). There has been a good match in the estimates of energy deposition for various materials between the Monte Carlo predictions and measurements. In general, all the above packages are potential tools for shielding simulation ((Beskrovnaia *et al.*, 2008; Tessa *et al.*, 2009). However,

the verification results in (Beskrovnaia *et al.*, 2008) show that the Monte Carlo calculations with FLUKA can be used to estimate the beam stopper thickness in the beam direction, GEANT4 code is better for the design of the nuclotron upper shielding, shielding of beam transport channel and the transverse size of the beam stopper, and SHIELD code is good for both areas but it needs the long period of calculation.

2.4.2 Simulations of Radiation Effects

1) Displacement damage simulation

Accurate prediction of displacement damage is an important step towards the prediction of radiation effects. Several special modeling and computation methods have been developed (Carter *et al.*, 1975; Chang *et al.*, 2013; Deng *et al.*, 2003; Gittus, 1978; Norgett *et al.*, 1975; Marcelot *et al.*, 2015). On the other hand, some solutions have been developed by using simulator tools, such as SPECTER and SRIM (Lee and Farnum, 1995; Ziegler, 2004), the Monte Carlo modeling (Khorsandi, 2007), Monte Carlo Radiative Energy Deposition (MRED) code (Reed *et al.*, 2015), ATREE (Roig *et al.*, 2014b), Technology Computer Aided Design (TCAD) (Wang *et al.*, 2015), and GEANT4 (Weller *et al.*, 2004). Those solutions are all potential candidates for displacement damage simulation.

A summary of displacement damage simulation is presented in (Srour and Palko, 2015), the simulation elements mainly include: particle transport, energy deposition of damage, and material response. With respect to these simulation elements, Monte-Carlo techniques can be used in the calculation of particle transport and energy deposition, while BCA codes work wells for light particles and for heavier particles with energies above a few keV; Molecular dynamics approaches are the most suitable to study the production of damage in displacement cascades; but there have two difficulties to analyze device responses: complex damage structures to the result change in electronic properties of the semiconductor material, and the determination of changes in defect structures within short time (Srour and Palko, 2015).

2) Total ionizing dose simulation

Several simulations and models for total ionizing dose effects on different devices and systems are investigated in (Aguirre and Wirth, 2013; Esqueda, 2007; Esqueda *et al.*, 2015; Huang *et al.*, 2014; Mikkola, 2008; Schlenvogt *et al.*, 2013; Zebrev and Gorbunov, 2009; Zebrev *et al.*, 2014; Nasr-Storey *et al.*, 2015; Ding *et al.*, 2014; Marcelot *et al.*, 2015). Software packages are also proposed to analyze and calculate TID effects, such as 3D_SPACE software (Specialized Electronic Systems) (Akhmetov *et al.*, 2014), TCAD techniques (Passei *et al.*, 2015; Patrick *et al.*, 2015; Petrosjanc *et al.*, 2009; Turowsky *et al.*, 2004; Wang *et al.*, 2015), Analog Transient Radiation Effects on Electronics (ATREE) (Roig *et al.*, 2014a), Monte Carlo Radiative Energy Deposition (MRED) code (Reed *et al.*, 2015), and ECORCE (Etude du COmportement sous Radiation des Composants Electroniques) (Michez *et al.*, 2013, and Michez *et al.*, 2015).

These computer tools are very useful. However, to get accurate results, the simulation tools require sufficient information about technological features of the devices and system configurations (Gorbunov *et al.*, 2011). Moreover, it is generally difficult to integrate physical models to a circuit-level simulation. Several solutions of transferring parameters between physical-level and circuit-level are presented with help of behavioral modeling using VHSIC hardware description language (VHDL-AMS) or other Analog-HDL (Cock *et al.*, 2009; Gorbunov *et al.*, 2011; Jagannathan *et al.*, 2010; Mikkola *et al.*, 2007a; Mikkola *et al.*, 2007b). All those simulations are more than hundred times faster than conventional SPICE-based method and still can achieve a good simulation accuracy.

3) Single event effects simulation

Several papers (Dodd, 1996, 2005; Dodd and Massengill, 2003; Reed *et al.*, 2013) have provided complete descriptions of the modeling and simulation of single event effects and reviewed its history and the evolution. Significant amount of research has been focused on the simulation of SEUs and SETs (Aguirre *et al.*, 2007; Artola *et al.*, 2015a; Inguibert and Duzellier, 2004; Tang and Cannon, 2004; Truscott *et al.*, 2004; Warren *et al.*, 2008; Reed *et al.*, 2015). Several models are presented for device-level and circuit-level simulations (Munteanu and Autran, 2008; Song *et al.*, 1988), and different tools are applied to calculate and simulate SEEs, such as, the multi-scale single event phenomena

predictive platform (MUSCA SEP³) from a system level down to a semiconductor target (Artola *et al.*, 2015b; Hubert *et al.*, 2011; Hubert *et al.*, 2014; Velazco *et al.*, 2014), TIARA transport tool (Roche *et al.*, 2014), Intel Radiation Tool (IRT) (Seifert, 2015), Monte Carlo Radiative Energy Deposition (MRED) code (Weller *et al.*, 2010) and TCAD (Huang *et al.*, 2017; Jung *et al.*, 2014; Michez *et al.*, 2015; Rezzak and Wang, 2015; Song *et al.*, 2014). In addition, an approach named “mixed-mode” or “mixed-level” simulation combines physical-level and circuit-level models to predict the ionizing responses is also developed (Davinci, 2003). On the other hand, some approaches through software fault injections have also been applied to study, simulate, and analyze SEEs (Ruano *et al.*, 2007; Sterpone *et al.*, 2006, Tsiliogiannis *et al.*, 2014).

Those simulation methods can be separated to several levels for the analysis of the interaction of ionizing particles with matter: physical-based device models, multidimensional device simulations, circuit simulations, and mixed device/circuit simulations (Dodd and Massengill, 2003). Physical device simulators focus on the prediction of the response of devices to incident radiation, circuit simulators concern the modeling of circuit response to a single event, and codes consider the error rate (Dodd and Massengill, 2003).

2.4.3 Summary of Simulation Techniques

The software tools and modeling techniques to simulate radiation shielding and radiation effects on electronics are summarized in Table 2-7, as well as a list of existing publications based on modeling and simulation techniques.

Table 2-7: Potential approaches of modeling and computer simulations

| Potential approaches | References |
|--|--|
| <i>Radiation shielding simulation</i> | |
| Monte Carlo method | Shultis and Faw, 2005 |
| FLUKA | Ballarini <i>et al.</i> , 2007; Fasso <i>et al.</i> , 2005; Fasso <i>et al.</i> , 2003; Korkut <i>et al.</i> , 2012; Yue <i>et al.</i> , 2009 |
| GEANT4 | Allison, 2006; BAK <i>et al.</i> , 2010; Santina <i>et al.</i> , 2003; Titt and Newhaser, 2005; Truscott <i>et al.</i> , 2000; Zeynali <i>et al.</i> , 2012 |
| PHITS | Iwase <i>et al.</i> , 2002 |
| SHIELD | Dementyev and Sobolevsky, 1999 |
| MULASSIS | Lei <i>et al.</i> , 2002 |
| <i>Simulation of displacement damage</i> | |
| Modeling and computation methods | Chang <i>et al.</i> , 2013; Deng <i>et al.</i> , 2003; Gittus, 1978; Norgett <i>et al.</i> , 1975; Marcelot <i>et al.</i> , 2015 |
| SPECTER & SRIM | Lee and Farnum, 1995; Ziegler, 2004 |
| MRED | Reed <i>et al.</i> , 2015 |
| ATREE | Roig <i>et al.</i> , 2014b |
| TCAD | Wang <i>et al.</i> , 2015 |
| GEANT4 | Weller <i>et al.</i> , 2004 |
| <i>Simulation of total ionizing dose effects</i> | |
| Modeling and computation methods | Aguirre and Wirth, 2013; Esqueda, 2007; Esqueda <i>et al.</i> , 2015; Huang <i>et al.</i> , 2014; Mikkola, 2008; Schlenvogt <i>et al.</i> , 2013; Zebrev and Gorbunov, 2009; Zebrev <i>et al.</i> , 2014; Nasr-Storey <i>et al.</i> , 2015; Ding <i>et al.</i> , 2014; Marcelot <i>et al.</i> , 2015 |
| 3D_SPACE | Akhmetov <i>et al.</i> , 2014 |
| TCAD | Passeri <i>et al.</i> , 2015; Patrick <i>et al.</i> , 2015; Petrosjanc <i>et al.</i> , 2009; Turowsky <i>et al.</i> , 2004; Wang <i>et al.</i> , 2015 |
| ATREE | Roig <i>et al.</i> , 2014a |
| MRED | Reed <i>et al.</i> , 2015 |
| ECORCE | Michez <i>et al.</i> , 2013, and Michez <i>et al.</i> , 2015 |
| Multi-level simulation | Cock <i>et al.</i> , 2009; Gorbunov <i>et al.</i> , 2011; Jagannathan <i>et al.</i> , 2010; Mikkola <i>et al.</i> , 2007a; Mikkola <i>et al.</i> , 2007b |
| <i>Simulation of single event effects</i> | |
| Modeling and computation methods | Artola <i>et al.</i> , 2015a; Baumann, 2005; Dodd, 1996, 2005; Dodd and Massengill, 2003; Reed <i>et al.</i> , 2013 |
| MUSCA SEP ³ | Artola <i>et al.</i> , 2015b; Hubert <i>et al.</i> , 2011; Hubert <i>et al.</i> , 2014; Velazco <i>et al.</i> , 2014 |
| TIARA | Roche <i>et al.</i> , 2014 |
| IRT | Seifert, 2015 |
| TCAD | Huang <i>et al.</i> , 2017; Jung <i>et al.</i> , 2014; Michez <i>et al.</i> , 2015; Rezzak and Wang, 2015; Song <i>et al.</i> , 2014 |
| Mixed-level simulation | Davinci, 2003 |
| Fault injection simulation | Ruano <i>et al.</i> , 2007; Sterpone <i>et al.</i> , 2006, Tsiligiannis <i>et al.</i> , 2014 |

Even those simulation results have a good agreement with results from physical test. However, it is important to mention that those modeling and simulation methods and techniques cannot replace physical tests all-together. It should be viewed as a complementary to physical tests. In addition, it can also be used to select electronic components and to evaluate radiation-tolerance in the design phase of the system.

2.5 Concluding Remarks

In this Chapter, the background of a potential wireless post-accident monitoring system in nuclear power plants is briefly discussed. A technical review of radiation effects on electronics is presented and existing rad-hardened design techniques are surveyed. In addition, Simulation techniques to investigate radiation effects and rad-hardened designs are also explained.

The conventional approach to design electronic equipment with high radiation tolerance is based on radiation-hardened components, which has high resistance to ionizing radiation but could be excessively expensive. They are only applied in those applications where the cost is not a primary concern, such as space exploration, military applications, etc. Using ordinary commercial off-the-shelf (COTS) components but utilizing rad-hardened design techniques can also achieve high level of radiation tolerance. Furthermore, many new designs have the higher design requirements on speed, storage, functions, which are only available through using COTS components.

Based on those studies, using COTS components combining with rad-hardened design techniques and fault-tolerant techniques may provide an effective and economical solution to design and to implement the potential wireless monitoring systems for nuclear power plants under a severe accident condition.

Chapter 3

3 Analysis of Radiation Responses of Devices and Circuits

To design circuit robust ionizing radiation damages and to accurately analyze their behavior under radiation conditions are not only important, but also necessary in the design of rad-hardened systems. Unfortunately, conventional electronic simulators, such as SPICE, do not consider radiation effects on electronic components so they have no capability to simulate radiation responses of devices and circuits. On the other hand, physical radiation tests need real radiation environments and are also extremely expensive.

This Chapter starts with the understanding of the mechanism of radiation-induced damages on semiconductor devices and circuits, a method is presented to analyze and to model responses of semiconductor devices and circuits in strong radiation environments by combining with the semi-empirical technique and the numerical technique. It can be applied to design circuits and electronic systems against radiation effects in the design phase and to evaluate the effectiveness of those circuits and systems without repeated destructive tests. Some device models are also described for the post-irradiation condition. Finally, a simulation of radiation-induced responses on an ideal p - n junction is given as a case study by using Sentaurus Technology Computer-Aided Design (TCAD) simulator.

3.1 Introduction

3.1.1 Degradation Mechanism of Devices and Circuits

The type of semiconductor electronic components in an electronic system varies widely, e.g., microcontroller/microprocessor, memory (RAM/ROM), transceiver, analog-to-digital converter (ADC), digital-to-analog converter (DAC), operation amplifier, multiplexer, logic chips (TTL or CMOS), voltage reference, transistor, diode, etc. Moreover, these electronic components may be made by various semiconductor technologies, such as Metal-oxide-semiconductor (MOS), bipolar technology, or other

technologies. The understanding of the mechanism of radiation effects on various devices and circuits are a critical part in the radiation-hardened design. Degradation mechanism and radiation effects on MOS/Bipolar devices and circuits are summarized as follows.

1) MOS devices and circuits

Due to charges are trapped between the interface and oxide when ionizing radiation interacts with semiconductor material of the device, major degradation of MOS device and circuit characteristics can be summarized as: (1) threshold voltage shift in MOS transistor, then loss of on/off control; (2) mobility degradation; (3) increase in leakage currents; and (4) reduction of breakdown voltage (Galloway and Schrimpf, 1990; Michez, *et al.*, 2013).

(1) Threshold voltage shift

Taken MOSFET device as an example, it usually uses a field oxide to isolate transistor channel regions and electrically isolate adjacent transistors. As a result, MOSFET device is sensitive to ionizing radiation due to charge buildup in the field oxide regions. The primary effect is a large threshold voltage shift due to radiation-induced positive charge (Witczak *et al.*, 2005; Wahle *et al.*, 1990). The shift of N-MOSFETs is usually negative due to the buildup of positive trapped charge in the gate oxide, which can be partially compensated by the buildup of negative interface trapped charge; and the charge in interface traps of P-MOSFETs is predominantly positive (Galloway and Schrimpf, 1990).

(2) Mobility degradation

When radiation-induced charges scatter in interface traps, except the shift of the threshold voltage, it also significantly degrades the channel mobility in MOSFETs, and mobility degradation can result in the significant reduction in transconductance and current-drive capability. Then a loss of drive capability can be encountered due to increasing the threshold voltage and/or reducing the mobility (Galloway and Schrimpf, 1990).

(3) Leakage currents

Radiation-induced charge also has significant effects on the subthreshold characteristics due to it decreases the sensitivity of surface potential to gate voltage and results in the change in the gate voltage. This degradation leads to that subthreshold current increases at a given gate voltage below threshold (Galloway and Schrimpf, 1990). For N-MOSFETs, the subthreshold leakage current increases at a given gate voltage meanwhile the threshold voltage reduces. In addition, the surface recombination velocity at SiO₂-Si interface increases, it also leads to the increasing of the junction leakage current (Galloway and Schrimpf, 1990).

(4) Breakdown voltage

For power DMOS devices, in general, ionizing radiation leads to the reduction of its breakdown voltage. The change of high voltage DMOS devices is much more than that of low voltage device (Galloway and Schrimpf, 1990).

Major effects on MOS integrated circuits can be summarized as: (1) the increasing of the static power supply current because of the increasing of the leakage current; (2) the generation of leakage paths between circuit nodes due to the change of the surface potential; (3) the issue of the power supply because of the increase in leakage current; and (4) propagation delay and/or the change of circuit timing parameter which depend on the mobility of the charge carriers and the threshold voltage (Galloway and Schrimpf, 1990).

2) Bipolar devices and circuits

When ionizing radiations pass through bipolar device, due to an increase in the density of interface traps at the surface of the extrinsic base region and positive charge buildup, the degradation of bipolar transistor include two aspects: the increase of recombination current, and the reducing the common-emitter current gain (Johnston *et al.*, 1994).

As a result, when a device includes *p-n* junctions, photocurrent will be generated due to the transport of generated carriers within the oxide when it is exposed to ionizing radiation. The total photocurrent (J_{total}) is the sum of the prompt photocurrent from the depletion region (J_{depl}), the diffusion photocurrent from n region (J_p), and the diffusion

photocurrent from p region (J_n). The prompt photocurrent is caused by electron-hole-pairs generated in the depletion region, which are immediately swept out and appear a photocurrent flowed from n -side to p -side (Alexandr, 2003). The amplitude is determined by the electron charge times (q), the generation coefficient (g_0), the dose rate ($\dot{\gamma}$), and the volume of the depletion region (Wirth and Rogers, 1964; Alexandr, 2003). On the other hand, the diffusion photocurrent is caused by excess minority carriers reached the edge of the depletion region, which are swept across the p - n junction and generate a photocurrent under the steady state condition. If carriers are further away than the diffusion length (L_n and L_p), they do not contribute to the photocurrent (Alexandr, 2003).

Taking a diode as an example, major radiation-induced effects are the increase of the reverse current and the changes of the forward voltage (Aguirre and Wirth, 2013). The radiation response is represented a linear current source (I_p) in the model of diode.

Semiconductor materials, three dimensional structures, and radiation dose rate can affect this current source.

The physical construction of *BJTs* consists of a pair of p - n junctions close together. When they are exposed to ionizing radiation, the density of interface traps increases at the surface of the extrinsic base region; and positive charges build up in the emitter-base depletion region (Schlenvogt *et al.*, 2013). The typical response is a large increase of base current (I_b) and a slight change of the collector current (I_c). As a result, the primary ionizing response of *BJTs* is the degradation of the current gain β (I_c/I_b), particularly at the low dose-rates (Gorbunov *et al.*, 2009; Jagannathan *et al.*, 2010). Generally, *NPN BJTs* are more sensitive than *PNP BJTs* because *NPN BJTs* have a much lower doping level in p-doped base region than the p-emitter region of *PNP BJTs*, which easily leads to the inversion (Ruano *et al.*, 2007). The photocurrents of ionizing radiation responses are represented by two linear current sources in parallel with base/emitter and base/collector in the *NPN BJT* model.

Due to total dose damage in bipolar devices is not self-scaling, it depends on the perimeter-to-area ratio, and oxide properties and current density, there are therefore no

simple parameters that can be used to characterize the general behavior of bipolar devices with widely differing designs and geometries (Johnston *et al.*, 1994).

3.1.2 Photocurrent Modeling of a p-n Junction

1) Overview

When a silicon device consists of one or more *p-n* junctions, whose geometry is illustrated in Figure 3-1 (Alexander, 2003), photocurrents are generated due to the transport of generated carriers in device depletion regions and/or within diffusion regions, which are named the prompt photocurrent and the diffusion photocurrent.

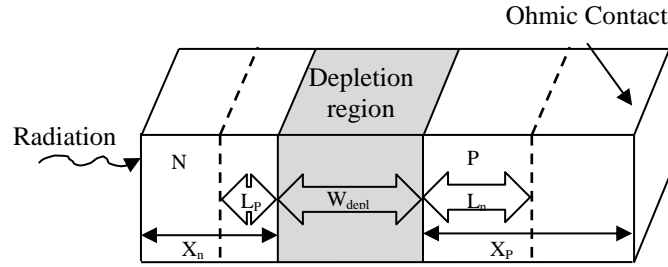


Figure 3-1: The layout of *p-n* geometry (Alexander, 2003)

For *p-n* junctions, the total photocurrent (J_{total}) is the sum of the prompt photocurrent from the depletion region (J_{depl}), the diffusion photocurrent from *n* region (J_p), and the diffusion photocurrent from *p* region (J_n), which is indicated in Eq. (3-1) (Wirth & Rogers, 1964).

$$J_{total} = J_{depl} + J_p + J_n . \quad (3-1)$$

The analytical and experimental solutions of photocurrents in semiconductor devices have been developed since mid-1960s in (Gleason *et al.*, 2013; Wirth & Rogers, 1964; Wunsch & Axness, 1992; Dierking, 1969; Raymond & Willis, 1965; Enlow & Alexander, 1988; Ishaque, *et al.*, 1991; Alexander, 2003; Ishaque, 1989; Fjeldly *et al.*, 2001; Kerr *et al.*, 2012; Gwyn *et al.*, 1967). This section provides a summary of those solutions and all variables used in this section are summarized in Table 3-1.

The prompt photocurrent is caused by electron-hole-pairs generated in the depletion region, which are immediately swept out and appear a photocurrent flowed from n -side to p -side (Alexander, 2003). The amplitude is determined by the electron charge times (q), the generation coefficient (g_0), the dose rate ($\dot{\gamma}$), and the volume of the depletion region (Wirth & Rogers, 1964; Alexander, 2003). Assuming a carrier starts at a distance x_0 from the depletion edge, the velocity is a constant and can be expressed as (Wunsh & Axness, 1992).

Table 3-1: Definitions of constants and variables used for the simulation of ionizing radiation effects on semiconductor devices (Wirth & Rogers, 1964; Alexander, 2003)

| Symbol | Definition | Unit |
|------------------|---|------------------------|
| q | electron charge = 1.602×10^{-19} | C |
| k | Boltzmann constant = 1.381×10^{-23} | J/K |
| g_0 | the uniform generation term = 4.3×10^{13} | $1/cm^3 \cdot rad(Si)$ |
| u_n, u_p | electron and hole mobility | $cm^2/V \cdot s$ |
| τ_n, τ_p | electron and hole lifetime | s |
| T | temperature | K |
| $\dot{\gamma}$ | the ionizing dose rate | $rad(Si)/s$ |
| G | electron-hole generation rate $G = g_0 \dot{\gamma}$ | $1/s \cdot cm^3$ |
| E_{depl} | E field in the depletion region | v/cm |
| E_n, E_p | E field in the p -side region and in the n -side region | v/cm |
| D_n, D_p | the electron diffusion coefficient in p -side and the hole diffusion coefficient in n -side | $(kT/q)u_n$ |
| U_n, U_p | recombination rate $U_n = \Delta n/\tau_n, U_p = \Delta p/\tau_p$ | $1/s \cdot cm^3$ |
| $\Delta n(x, t)$ | electrons generated by ionization per unit volume = $n(x, t) - n(x, 0)$ | cm^{-3} |
| $\Delta p(x, t)$ | holes generated by ionization per unit volume = $p(x, t) - p(x, 0)$ | cm^{-3} |
| W_{depl} | the depletion region width | cm |
| L_n, L_p | the diffusion length in p -side silicon and n -side silicon | cm |
| x_n, x_p | the length of n -side, p -side | cm |

$$v = \frac{d_x}{d_t} = -uE_{depl} \quad (3-2)$$

where

u : the minority carrier mobility

x : the carrier position at time t , $x = -uE_{depl}t + x_0$

t : the time for the carrier to reach the junction, $t = x_0/uE_{depl}$

Thus

$$J_{depl} = \begin{cases} qGuE_{depl}t & t < W_{depl}/uE_{depl} \\ qGW_{depl} & t \geq W_{depl}/uE_{depl} \end{cases} \quad (3-3)$$

On the other hand, the diffusion photocurrent is caused by excess minority carriers reached the edge of the depletion region, which are swept across the p - n junction and generate a photocurrent under the steady state condition. If carriers are further away than the diffusion length (L_n and L_p), they do not contribute to the photocurrent (Alexander, 2003). According to the current flow equations, the diffusion photocurrent includes both a drift term and a diffusion term, which are indicated in Eq. (3-4) and Eq. (3-5) (Alexander, 2003).

$$J_n = qD_n \frac{\partial \Delta n}{\partial x} + qu_n \Delta n E_n \quad (3-4)$$

$$J_p = -qD_p \frac{\partial \Delta p}{\partial x} + qu_p \Delta p E_p \quad (3-5)$$

According to electron and hole continuity equations, the time rate of changed excess carriers is depended on the generated carriers, the recombined carriers, and the divergence of the carrier flow within the volume, which are indicated in Eq. (3-6) and Eq. (3-7) (Alexander, 2003).

$$\frac{\partial \Delta n}{\partial t} = G - U_n + \frac{1}{q} \frac{\partial J_n}{\partial x} \quad (3-6)$$

$$\frac{\partial \Delta p}{\partial t} = G - U_p - \frac{1}{q} \frac{\partial J_p}{\partial x} \quad (3-7)$$

Combining Eq. (3-4) to Eq. (3-7), the behavior of excess electrons and holes generated by transient ionizing radiation in p -side and n -side are indicated in Eq. (3-8) and Eq. (3-9) (Alexander, 2003).

$$\frac{\partial \Delta n}{\partial t} = g_0 \dot{\gamma}(t) - \frac{\Delta n}{\tau_n} + u_n \Delta n \frac{\partial E_n}{\partial x} + u_n E_n \frac{\partial \Delta n}{\partial x} + D_n \frac{\partial^2 \Delta n}{\partial x^2}. \quad (3-8)$$

$$\frac{\partial \Delta p}{\partial t} = g_0 \dot{\gamma}(t) - \frac{\Delta p}{\tau_p} + u_p \Delta p \frac{\partial E_p}{\partial x} + u_p E_p \frac{\partial \Delta p}{\partial x} - D_p \frac{\partial^2 \Delta p}{\partial x^2}. \quad (3-9)$$

According to the number of excess carriers generated by radiation particles, applications can be separated into two categories conditions: low injection level and high injection level. At low injection level, the number of carriers is much less than the doping concentration. On the other hand, as the dose rate increases or in heavily doped p - n junctions, the density of excess generated carriers may approach or surpass the density of majority carriers in p -side and/or n -side. The analysis results of photocurrent modeling may therefore not accurate. (Alexander, 2003; Fjeldly *et al.*, 2001).

2) Low injection level

At low injection level, the diffusion length (L_n, L_p) depends on the minority carrier diffusion coefficient (D_n, D_p) and minority carrier lifetime (τ_n, τ_p), which are indicated in Eq. (3-10) and Eq. (3-11). The minority carrier lifetime is a constant, which can be obtained from Shockley-Reed-Hall (SRH) recombination statistics for semiconductors. The minority carrier diffusion coefficient is determined by the minority carrier mobility (u_n, u_p) and kT/q .

$$L_n = \sqrt{D_n \tau_n}. \quad (3-10)$$

$$L_p = \sqrt{D_p \tau_p}. \quad (3-11)$$

Wirth-Rogers provided a solution for infinite p - n junctions with negligible electric fields based on several assumptions of one-dimensional geometry, uniformly doping, and constant across voltage (Wirth & Rogers, 1964). For example, for a pulse function with

magnitude G and duration T , the solution of Wirth-Rogers for the n -side region is indicated in Eq. (3-12) (Wirth & Rogers, 1964).

$$J_{total}(t) = \begin{cases} qG \left[W_{depl} + \sqrt{D_n \tau_n} \operatorname{erf} \left(\sqrt{t/\tau_n} \right) + \sqrt{D_p \tau_p} \operatorname{erf} \left(\sqrt{t/\tau_p} \right) \right] \\ qG \left\{ \sqrt{D_n \tau_n} \left[\operatorname{erf} \left(\sqrt{t/\tau_n} \right) - \operatorname{erf} \left(\sqrt{(t-T)/\tau_n} \right) \right] + \sqrt{D_p \tau_p} \left[\operatorname{erf} \left(\sqrt{t/\tau_p} \right) - \operatorname{erf} \left(\sqrt{(t-T)/\tau_p} \right) \right] \right\} \end{cases} \quad (3-12)$$

Enlow-Alexander presented an approximate solution in (Gleason *et al.*, 2013), which use Laplace transform techniques for a lightly doped p - n diode with a constant E -field. However, it is inaccurate if ohmic fields are greater than about 10 V/cm (Wunsch & Axness, 1992). Wunsch-Axness also provided a time domain solution for the lightly doped p - n diode, which is appropriate for many modern device structures, whose solution for the n -side region is indicated in Eq. (3-13) (Wunsch & Axness, 1992). The steady state solution is indicated in Eq. (3-14) (Wunsch & Axness, 1992).

$$J_p(t) = J(\infty) - qGL_p \left\{ \sqrt{1 + \beta_p^2} \operatorname{erf} \left(\sqrt{1 + \beta_p^2} \sqrt{t/\tau_p} \right) + \beta_p e^{-t/\tau_p} \operatorname{erf} \left(\beta_p \sqrt{t/\tau_p} \right) - \sum_{m=0}^{\infty} \left(\frac{\beta_p^2}{1 + \beta_p^2} \right) \times \frac{\gamma[m + 0.5(1 + \beta_p^2)t/\tau_p]}{\Gamma(m + 0.5)} - \frac{2}{\zeta_p} \sum_{m=1}^{\infty} \frac{e^{-c_m t/\tau_p} [1 - (-1)^m e^{\zeta_p \beta_p}]}{c_m} \times \left[\frac{(m\pi)^2}{(m\pi)^2 + (\zeta_p \beta_p)^2} \right] \right\} \quad (3-13)$$

$$J_p(\infty) = qGL_p \sqrt{1 + \beta_p^2} \times \left\{ \frac{\cosh \left(\zeta_p \sqrt{1 + \beta_p^2} \right) - e^{\zeta_p \beta_p}}{\sinh \left(\zeta_p \sqrt{1 + \beta_p^2} \right)} - \frac{\beta_p}{\sqrt{1 + \beta_p^2}} \right\} \quad (3-14)$$

where

Γ : the gamma function

γ : the incomplete gamma function

$$c_m = (m\pi L_p/x_n)^2 + \beta_p + 1$$

$$\beta_p = \frac{u_p E_p L_p}{2D_p}$$

$$\zeta_p = x_n / L_p$$

3) High injection level

At high injection level, the concept of the depletion region loses validity and boundary conditions are difficult to define. The following assumptions in the condition of low level injection are inappropriate for the high injection level (Alexander, 2003):

- (1) As the dose rate increases, the excess carrier density increases until the traps saturate, and the lifetime reaches the saturated Shockley-Reed-Hall (SRH) lifetime. For the very high ionizing dose rates, the recombination process changes from trap assisted to direct band-to-band and the lifetime decreases significantly (Alexander, 2003).
- (2) When the density of excess carriers approaches the density of majority carriers, electrons and holes do not move respectively, the movement generates an imbalance in charge and an internal electric field (Alexander, 2003).
- (3) The diffusion coefficient and mobility of minority carriers may approach the ambipolar diffusion coefficient and mobility if the density of excess carriers is high enough (Alexander, 2003).
- (4) The effective diffusion length will be increased due to the effect of the ambipolar diffusion (Alexander, 2003).

In consequence, the complete transport equations for the high injection level are very difficult to solve analytically (Ishaque *et al.*, 1989; Fjeldly *et al.*, 2001). Gleason-Schlenvogt developed a transient physics and equivalent circuit model for the high injection level, which was examined with TCAD simulations and the experimental data of physical radiation test (Gleason *et al.*, 2013). The limitation is that the steady-state current is determined by analytical solutions, which are also limited to the scope of their

assumptions. Fjeldly-Ytterdal presented the stationary and dynamic model to simulate the photocurrents of semiconductor devices for a wide range of ionizing radiation intensities (Fjeldly *et al.*, 2001), whose transient photocurrent (I_G) is indicated in Eq. (3-15).

$$J_{total} = q(GW_{depl} + G_p L_{pd} + G_n L_{nd}). \quad (3-15)$$

Effective e-h generation rates (G_p, G_n) are related to the dynamic voltages V_{Gp} and V_{Gn} , which are represented by RC equivalent delay circuits (Fjeldly *et al.*, 2001). However, this solution is depended on the choice of parameters and delay times are difficulty to determine.

3.1.3 Problem Statement

In general, the purpose of modeling photocurrent is to predict the ionizing responses of semiconductor devices and to analysis the response of a circuit or a system. As previously discussed, accurate predictions of photocurrent must consider 3-D structures and the appropriate formulations for different radiation dose rates (Alexander, 2003). However, it is very complicated and also difficult to resolve to those equations for general applications due to it depends on the selection of boundary conditions and assumptions for different radiation dose rates and/or different doped silicones. As a result, the major issue is the determination of photocurrents in different applications, particularly those applications in the high injection level.

On the other hand, existing solutions is usually implemented with Gummel-Poon transistor models. The appropriate current sources are inserted into devices models to simulate the responses of photocurrents. However, Gummel-Poon transistor models are non-linear and needs high computational costs. Hence, they are usually only used in circuit simulators, *e.g.* SPICE, and not suitable for low-cost online algorithm.

3.1.4 The Framework of the Proposed Analysis Method

This work combines the semi-empirical technique and the numerical technique to investigate a method for the analysis of ionizing radiation responses of devices and circuits, whose flow diagram is show in Figure 3-2.

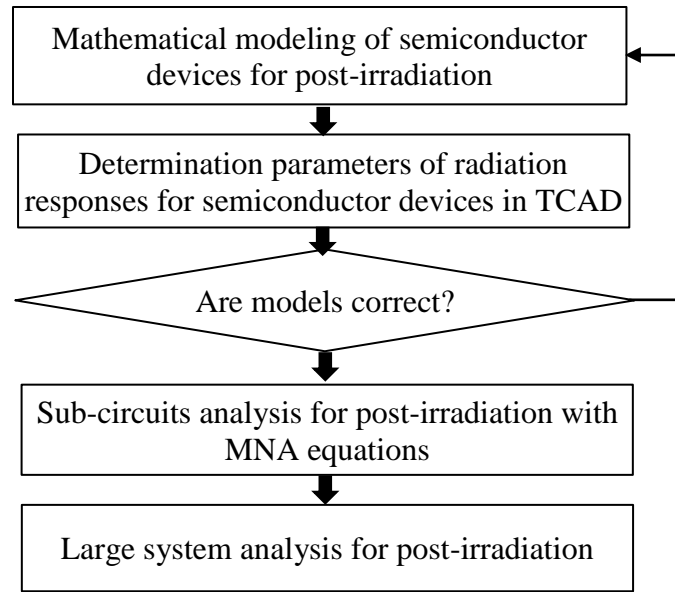


Figure 3-2: Flow diagram of the developed analysis method

Photocurrents of semiconductor devices can be calculated in TCAD. Then, the results are integrated into the modified nodal analysis (MNA) circuit equations to analyze radiation-induced responses of circuits.

- (1) Device modeling for post-irradiation: linear mathematical models of semiconductor devices can be established for post-irradiation based on radiation responses, which can be calculated in TCAD.
- (2) Sub-circuit analysis: based on device models, the proprieties of sub-circuit for post-irradiation can be calculated by the using of MNA equation.
- (3) Large system analysis: a whole system can be separated into a number of sub-circuit blocks, whose radiation responses can be obtained through Step 2. Then, radiation response of the whole system can be analyzed by the integration of all sub-circuit blocks.

3.2 Development of Device Models

3.2.1 Diode Model

1) Diode response

As previously discussed, photocurrent will be generated due to the transport of generated carriers within the oxide when diodes are exposed to ionizing radiation. Major radiation-induced effects in diodes are a general increase of the reverse current and the changes of the forward voltage (Snow *et al.*, 1967). The Companion model of diode for post-irradiation in this work is illustrated in Figure 3-3. The radiation response is represented as a linear current source (I_p) in the model of diode, which is determined by semiconductor materials, three dimensional structures, and radiation dose rate.

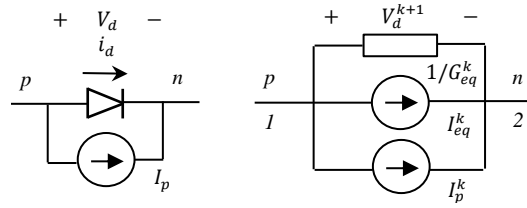


Figure 3-3: Companion model of diode for post-irradiation

2) Diode modeling

The element equation of diode for before-irradiation is expressed in Eq. (3-20) (Najm, 2010):

$$i_d = g(v_d) = I_{sat} \left(e^{\frac{v_d}{\eta V_T}} - 1 \right). \quad (3-20)$$

where

I_{sat} is the reverse saturation current,

v_d is the applied bias,

$V_T \triangleq kT/q$ is the thermal voltage,

$\eta \approx 1$ is the ideality factor

Assuming the diode is biased at v_d^k and i_d^k . The diode element stamp for before- and post-irradiation can be expressed in Eq. (3-21).

$$\begin{bmatrix} G_{eq}^k & -G_{eq}^k \\ -G_{eq}^k & G_{eq}^k \end{bmatrix} \begin{bmatrix} v_1^{k+1} \\ v_2^{k+1} \end{bmatrix} = \begin{bmatrix} -I_{eq}^k \\ I_{eq}^k \end{bmatrix}. \quad (3-21)$$

where

$$G_{eq}^k \triangleq \frac{d i_d}{d v_d} = \frac{I_{sat}}{\eta V_T} e^{\frac{v_1^k - v_2^k}{\eta V_T}}$$

I_{eq}^k for before-irradiation is:

$$I_{eq}^k = i_d^k - G_{eq}^k (v_1^k - v_2^k)$$

I_{eq}^k for post-irradiation is:

$$I_{eq}^k = i_d^k - G_{eq}^k (v_1^k - v_2^k) + I_p^k$$

3.2.2 BJT Model

1) BJT response

The physical construction of *BJTs* consists of a pair of *p-n* junctions closed together. When they are exposed to ionizing radiation, the density of interface traps increases at the surface of the extrinsic base region; and positive charges build up in the emitter-base depletion region (Johnston *et al.*, 1994). The typical response is a large increase of base current (I_b) and a slight change of the collector current (I_c). As a result, the primary ionizing response of *BJTs* is the degradation of the current gain β (I_c/I_b), particularly at the low dose-rates (Zhao *et al.*, 2015; Montagner *et al.*, 1998). Generally, *NPN BJTs* are more sensitive than *PNP BJTs* because *NPN BJTs* have a much lower doping level in p-doped base region than the p-emitter region of *PNP BJTs*, which easily leads to the inversion (Johnston *et al.*, 1994). Some models for ionizing radiation responses of *BJTs* have been developed in (Fjeldly *et al.*, 2001; Zhao *et al.*, 2015; Montagner *et al.*, 1998; Kleiner and Messenger, 1982). In those models, photocurrents are represented as linear current sources to insert into each junction in *BJT* devices.

The Companion model of the *NPN BJT* for post-irradiation in this work is illustrated in Figure 3-4. The photocurrents of ionizing radiation responses are represented by two linear current sources (I_{peb} and I_{pcb}) in parallel with base/emitter and base/collector in the *NPN BJT* model. Different responses may be generated when *BJTs* are the part in different circuits. To accurately model the radiation response of *BJTs*, both the forward and inverse parameters have to involve into the model (Alexander, 2003).

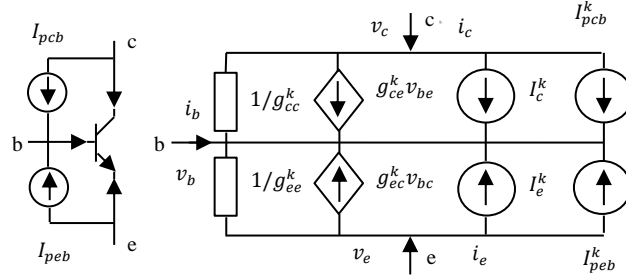


Figure 3-4: Companion model of *NPN BJT* for post-irradiation

2) BJT modeling

The element equations of the *NPN BJT* with Ebers-Moll model for before-irradiation are indicated in Eqn.22 to Eqn. 3-24 (Najm, 2010).

$$i_e = -I_{es} \left(e^{\frac{v_{be}}{V_{Te}}} - 1 \right) + a_R I_{cs} \left(e^{\frac{v_{bc}}{V_{Tc}}} - 1 \right). \quad (3-22)$$

$$i_c = a_F I_{es} \left(e^{\frac{v_{be}}{V_{Te}}} - 1 \right) - I_{cs} \left(e^{\frac{v_{bc}}{V_{Tc}}} - 1 \right). \quad (3-23)$$

$$i_b = -(i_e + i_c). \quad (3-24)$$

where

I_{es} is the emitter junction saturation current, I_{cs} is the collector junction saturation current,

β_f, β_r are the ideal maximum forward and reverse current gains,

$a_F = \frac{\beta_f}{\beta_f + 1}$ is typically in the range 0.98 and 0.99 for the forward active region,

$a_R = \frac{\beta_r}{\beta_r + 1}$ is typically in the range 0.1 and 0.5 for the reverse active region.

The element stamp of *NPN BJT* for before- and post-irradiation is expressed in Eq. 3-25.

$$\begin{array}{ccccccc}
 & e & c & b & & RHS & \\
 & \vdots & \vdots & \vdots & & \vdots & \\
 e \cdots & g_{ee}^k & -g_{ec}^k & (g_{ec}^k - g_{ee}^k) & \vdots & -I_e^{\cdot k} & \\
 c \cdots & -g_{ce}^k & g_{cc}^k & (g_{ce}^k - g_{cc}^k) & & -I_c^{\cdot k} & \\
 b \cdots & (g_{ce}^k - g_{ee}^k) & (g_{ec}^k - g_{cc}^k) & (g_{cc}^k + g_{ee}^k) & & I_e^{\cdot k} + I_c^{\cdot k} & \\
 & & & -g_{ce}^k - g_{ec}^k & & &
 \end{array} \quad (3-25)$$

where

$$g_{ee} \triangleq \frac{I_{es}}{V_{Te}} e^{v_{be}/V_{Te}}, g_{ec} \triangleq a_R \frac{I_{cs}}{V_{Tc}} e^{v_{bc}/V_{Tc}}$$

$$g_{ce} \triangleq a_F \frac{I_{es}}{V_{Te}} e^{v_{be}/V_{Te}}, g_{cc} \triangleq \frac{I_{cs}}{V_{Tc}} e^{v_{bc}/V_{Tc}}$$

and

$$i_e^k = -I_{es} \left(e^{\frac{v_{be}^k}{V_{Te}}} - 1 \right) + a_R I_{cs} \left(e^{\frac{v_{bc}^k}{V_{Tc}}} - 1 \right)$$

$$i_c^k = a_F I_{es} \left(e^{\frac{v_{be}^k}{V_{Te}}} - 1 \right) - I_{cs} \left(e^{\frac{v_{bc}^k}{V_{Tc}}} - 1 \right)$$

$I_e^{\cdot k}$ and $I_c^{\cdot k}$ for before-irradiation are:

$$I_e^{\cdot k} = I_e^k = i_e^k + g_{ee}^k v_{be}^k - g_{ec}^k v_{bc}^k$$

$$I_c^{\cdot k} = I_c^k = i_c^k - g_{ce}^k v_{be}^k + g_{cc}^k v_{bc}^k$$

$I_e^{\cdot k}$ and $I_c^{\cdot k}$ for post-irradiation are:

$$I_e^{\cdot k} = I_e^k + I_{peb}^k = i_e^k + g_{ee}^k v_{be}^k - g_{ec}^k v_{bc}^k + i_{peb}^k$$

$$I_c^k = I_c^k + I_{pcb}^k = i_c^k - g_{ce}^k v_{be}^k + g_{cc}^k v_{bc}^k + i_{pcb}^k$$

Thus

$$\beta_{post}^k = \frac{I_c^k}{I_e^k} = \frac{i_c^k + i_{pcb}^k}{i_e^k + i_{peb}^k}. \quad (3-26)$$

3.3 Case Study: Radiation-Induced Responses of an Ideal p-n Diode in TCAD

3.3.1 Simulation Parameters

The radiation-induced responses of an ideal diode with constant doping are performed in TCAD. For simplicity, only one-dimensional geometry is considered in the calculation and simulation. Simulation parameters of the ideal diode are summarized in Table 3-2, which are taken from the references (Fjeldly *et al.*, 2001; Kerr *et al.*, 2012).

Table 3-2: Simulation parameters of an ideal p-n diode

| Parameter | Value | |
|------------------|---------------------------|--------------|
| Radiation source | | |
| Pulse width | 5e-8s | |
| Pulse dose-rate | 0, 2, 1E4, 1E9 Rad (Si)/s | |
| p-n junction | n-side | p-side |
| W_n, W_p | 2.8875e-6m | 2.8875e-6m |
| D_n, D_p | 1.036e-3 m²/s | 2.59e-3 m²/s |
| τ_p | 2e-5 s | 2e-5 s |
| Doping | 1e16 m-3 | 1e16 m-3 |
| Depletion region | | |
| W_{depl} | 1.225e-6 m | |

The simulation structure of the ideal diode in TCAD is shown in Figure 3-5.

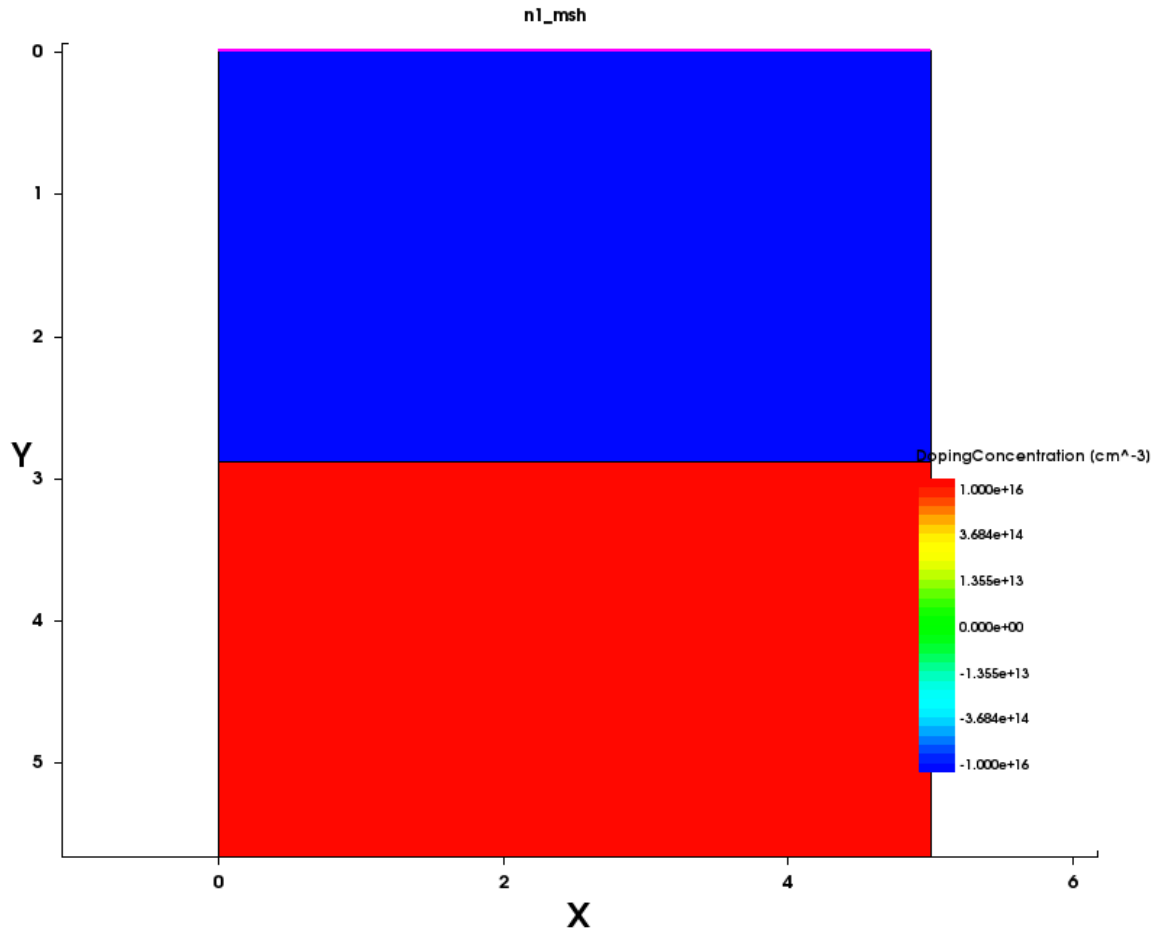


Figure 3-5: The simulation structure of the ideal p-n diode in TCAD

3.3.2 Simulation Results

Two cases with different biases are considered in this simulation. One is to obtain photo-current with forward bias and another one is reverse bias.

1) Photo-current with forward bias

Under various voltages, simulation results of photo-current response of an ideal p - n under forward bias are listed in Table 3-3 and shown in Figure 3-6.

Table 3-3: Simulation results of photo-current response of an ideal p-n diode under forward bias

| Time | Total rate | | | | Voltage |
|------|-------------------|-------------------|---------------|----------|---------|
| | 1.0E9 Rad (Si) /s | 1.0E9 Rad (Si) /s | 2 Rad (Si) /s | 0 | |
| 0 | -9.97777 | -14.9778 | -18.5881 | -19.3842 | 0.00 |
| 1 | -10.2184 | -11.5074 | -11.5073 | -11.5073 | 0.30 |
| 2 | -6.49530 | -6.49528 | -6.49528 | -6.49528 | 0.60 |
| 3 | -3.91851 | -3.91851 | -3.91851 | -3.91851 | 0.90 |
| 4 | -3.40214 | -3.40214 | -3.40214 | -3.40214 | 1.20 |
| 5 | -3.17658 | -3.17658 | -3.17658 | -3.17658 | 1.50 |
| 6 | -3.17658 | -3.17658 | -3.17658 | -3.17658 | 1.50 |
| 7 | -3.17658 | -3.17658 | -3.17658 | -3.17658 | 1.50 |
| 8 | -9.97775 | -14.2648 | -14.3579 | -14.3579 | 0.00 |
| 9 | -9.97777 | -14.9778 | -18.6548 | -20.0148 | 0.00 |
| 10 | -9.97777 | -14.9778 | -18.6487 | -20.0454 | 0.00 |

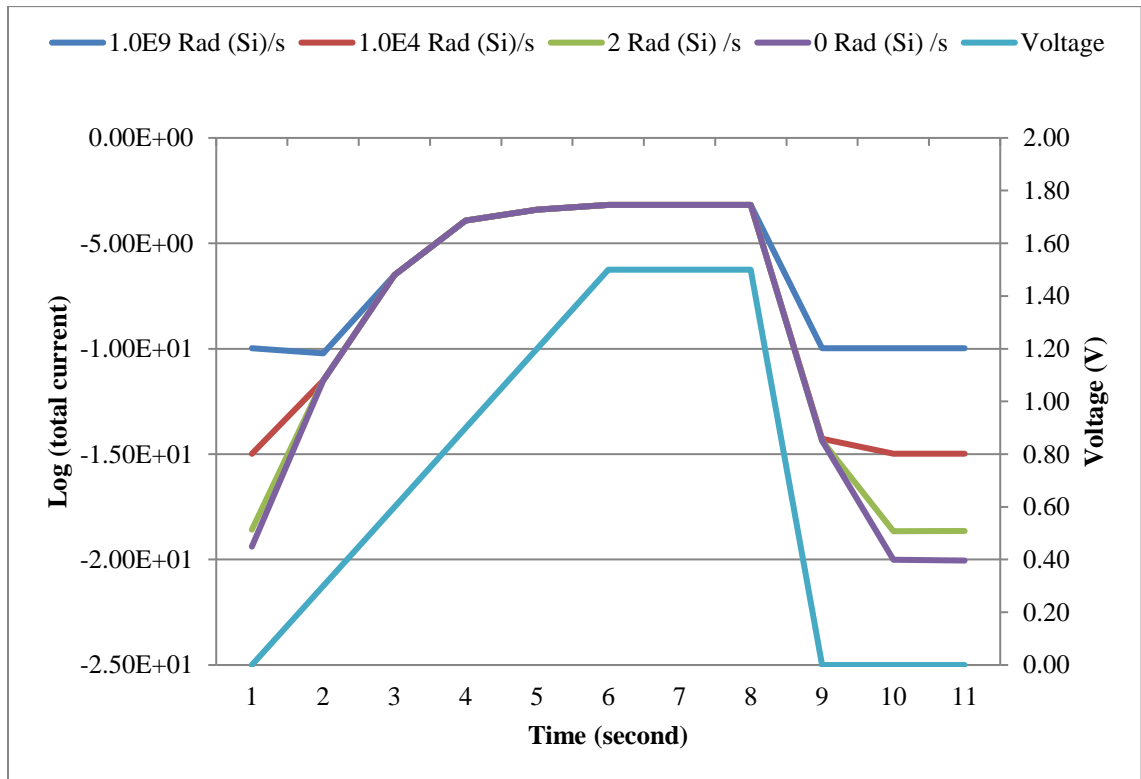


Figure 3-6: Photo-current response of an ideal p-n diode under forward bias in TCAD

2) Photo-current with reverse bias

Under various voltages, simulation results of photo-current response of an ideal $p-n$ under reverse bias are listed in Table 3-4 and shown in Figure 3-7.

Table 3-4: Simulation results of photo-current response of an ideal p-n diode under reverse bias

| Time | Total rate | | | | Voltage |
|------|-------------------|-------------------|---------------|----------|---------|
| | 1.0E9 Rad (Si) /s | 1.0E9 Rad (Si) /s | 2 Rad (Si) /s | 0 | |
| 0 | -9.97777 | -14.9777 | -18.7234 | -19.7953 | 0.00 |
| 1 | -9.83609 | -14.6456 | -15.0951 | -15.0953 | 0.30 |
| 2 | -9.73038 | -14.5716 | -15.0854 | -15.0855 | 0.60 |
| 3 | -9.64705 | -14.5141 | -15.0927 | -15.0930 | 0.90 |
| 4 | -9.57802 | -14.4502 | -15.0436 | -15.0439 | 1.20 |
| 5 | -9.51878 | -14.3934 | -14.9939 | -14.9943 | 1.50 |
| 6 | -9.51878 | -14.4415 | -15.2293 | -15.2296 | 1.50 |
| 7 | -9.51878 | -14.4415 | -15.2293 | -15.2296 | 1.50 |
| 8 | -9.97779 | -14.5096 | -14.3825 | -14.3824 | 0.00 |
| 9 | -9.97777 | -14.9778 | -18.7234 | -19.5144 | 0.00 |
| 10 | -9.97777 | -14.9778 | -18.7234 | -19.5144 | 0.00 |

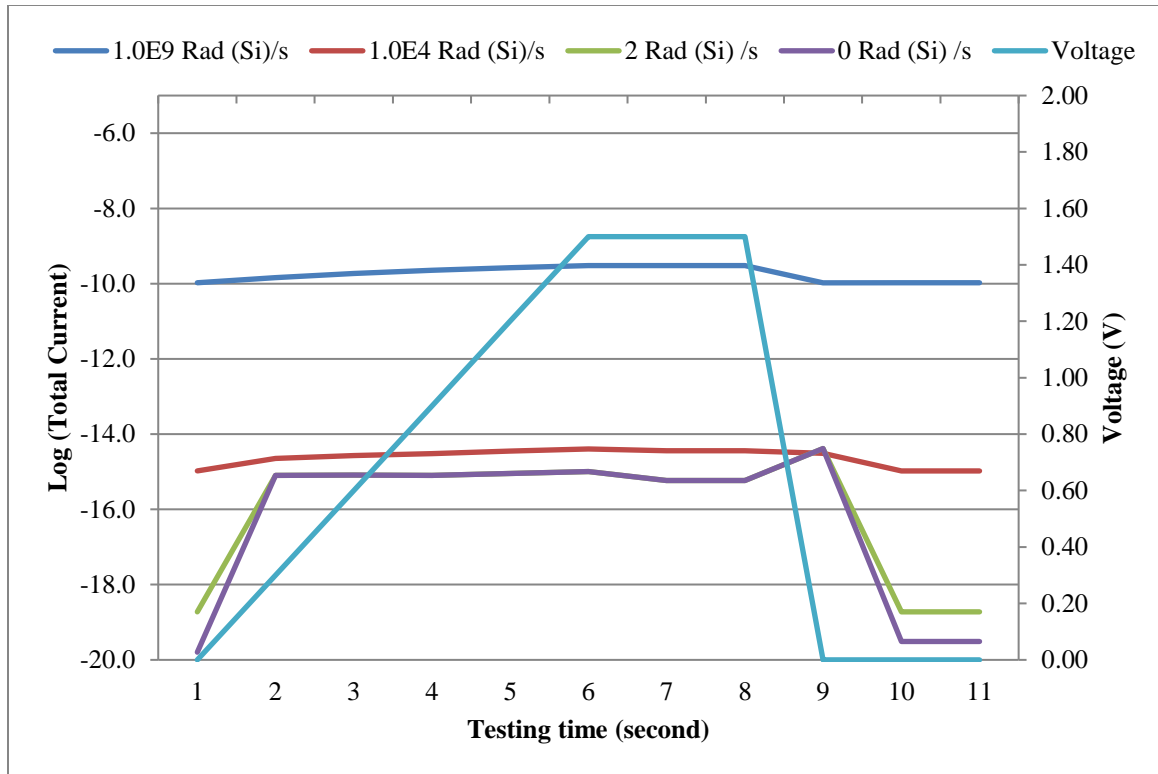


Figure 3-7: Photo-current response of an ideal p-n diode under reverse bias in TCAD

3.3.3 Discussion

Based on simulation results and studies in this work, the following discussions apply to this simulation results:

- Under the condition of both forward bias and reverse bias, simulation results have shown that photo-current increases when total dose rate increases under both forward bias and reverse bias. However, it is more intense than that of reverse bias.
- Under the condition of the variable voltage, the results have shown that photo-currents under different conditions, such as forward or reverse biases, or low/high dose rates, will decrease significantly if the bias voltage is reduced to zero.

3.4 Summary

In this Chapter, a method is proposed to analyze radiation responses of MOS/Bipolar devices and circuits, as well as two device models are investigated for the post-irradiation condition. Some simulations in TCAD have been also performed to obtain radiation-induced responses of an ideal p-n diode. The simulation results show that photo-current under different radiation conditions decreases significantly if the bias voltage is reduced to zero. Therefore, the damage to the semiconductor device by the accumulated photo-current may be averted if the device is de-energized quickly.

In fact, destructive single event effects, such as SEL, SES, SEB, and SEGR, are all caused by accumulated current and their effects can be mitigated if the current is quickly removed. Moreover, non-destructive single event effects, such as SET, SEU, and SEFI, can be recovered by using data re-initialization and/or system recovery, which can also be accomplished by rapid power off. Methods of rapid power off are therefore highly effectively in protecting electronic systems under ionizing radiation. It can be a potential solution to mitigate the damages of single event effects.

Chapter 4

4 Design Part I: Component Selection

As mentioned in Chapter 2, an electronic system built with regular commercial off-the-shelf components will definitely be damaged when cumulative total dose is 1 M Rad (Si) (Messenger and Ash, 1991). Radiation effects on various devices, circuits and systems are different, depending on their unique materials, structure, manufacturing technologies, and applications, where the dose range is typically in the range of 10^4 - 10^8 rad (Si) (Foster, 2003). Therefore, some techniques have to be used to reduce total dose then to make electronic device more resistant to the effects of total ionizing dose. Two approaches are involved in this research to mitigate damages of total ionizing dose: (1) component selection, which is to select regular commercial components with high radiation resistance for the give total dose limit; and (2) radiation shielding protection, which is to use shielding materials for the reduction of total dose to be less than the given level. The former is discussed in this Chapter and the latter will be explained in the next Chapter.

Component selection is a significant step in the design phase of COTS-based radiation-tolerant systems. This Chapter starts with the investigation of radiation-tolerances of various regular COTS components are investigated. Based on the result of the investigation, the total dose limit in this work is defined as 20 K Rad (Si) in this work. Subsequently, the principle of component selection is given. Then, a method is proposed to assess radiation resistance through using a radiation degradation factor. Finally, a number of component candidates for the implementation of the proposed wireless monitoring system are given.

4.1 The Investigation of Radiation-Tolerance for COTS Components

4.1.1 Radiation Damages Thresholds on Electronics

Selecting COTS components with high radiation resistances is the significant step to achieve a radiation-tolerant system. Therefore, the understanding of radiation effects on

these devices and technologies and the investigation of their radiation-tolerances are vital in the design of the radiation-tolerant system. Radiation damages thresholds on electronics are summarized in Table 4-1 (Houssay, 2000).

Table 4-1: Radiation damages thresholds on electronics

| Device | Type/Comments | Threshold level (Gy) |
|----------------|--|----------------------|
| Digital IC | Bipolar logic | $100-10^6$ |
| | JFET, MESFET logic | 10^5 |
| | MOSFET logic | 50-500 |
| | Microprocessor | 10-500 |
| | Memory | $50-5 \cdot 10^3$ |
| | EPROM | 10-200 |
| Analog IC | Bipolar linear circuit | $10-10^4$ |
| | MOS linear circuit | 10-100 |
| | Operational amplifiers and comparators | $50-10^6$ |
| | Voltage regulator | 10^3-10^6 |
| | Analog-to-digital converter | $100-10^4$ |
| | Sample and hold | 10^3 |
| | Multiplexer | $50-10^3$ |
| | Timer | 100 |
| Diode | Rectifying diode | 10^3 |
| | Switching diode | 10^5 |
| | Zener and avalanche diode | 10^5-10^6 |
| | Schottky diode | 10^6 |
| | Microwave diode | 10^6 |
| | Varactor diode | 10^5 |
| Transistor | Junction field effect transistor | 10^6 |
| | MESFET | 10^6 |
| | MOSFET | 100 |
| Optoelectronic | Photodiode | 10^6 |
| | Phototransistor | $10-10^4$ |
| | Light emitting diode | 10^6 |
| | Opto-coupler | 10^3-10^6 |
| | Laser diode | $100-10^4$ |
| Vacuum tube | | 10^6 |

Table 4-1 Continued

| Device | Type/Comments | Threshold level (Gy) |
|-----------|---|----------------------|
| Crystal | Synthetic quartz crystal | 10^4 |
| | Natural quartz | 100 |
| Resistors | Precision wire-wound ceramic bobbin | 10^6 - 10^{10} |
| | Metal film | 10^5 - 10^9 |
| | Precision wire-wound epoxy bobbin, carbon film | 10^4 - 10^7 |
| | Other film | 10^4 - 10^7 |
| | Composition | 10^3 - 10^5 |
| | Oxide film | 10 - 10^4 |
| Capacitor | Glass | 10^5 - 10^8 |
| | Paper | 10^5 |
| | Mica | 10^4 - 10^7 |
| | Ceramic | 10^4 - 10^8 |
| | Tantalum | 10^3 - 10^5 |
| | Polyester | 10^3 - 10^7 |
| | Polycarbonate | 10^2 |
| | Electrolyte | 10^2 |
| Insulator | Depends on the hardness of the former and the insulator materials | 10 - 10^6 |
| Cables | | at least 10^6 |
| Connector | Polystyrene – dose to produce 25% damage | 6×10^7 |
| | Polyethylene – dose to produce 25% damage | 9×10^5 |
| | Duroc ceramic – dose to produce 25% damage | 3×10^6 |
| | Melamine plastic | 3×10^6 |
| Relay | Switch based, asbestos filled phenolformald | 1×10^7 |
| | Switch based, unfilled phenolformald | 1×10^5 |

4.1.2 The Definition of Total Dose Limit

According to radiation damage thresholds on electronics summarized in Table 4-1, semiconductor devices are more sensitive to ionizing radiation than other electronic devices. Radiation-tolerance by a family of regular commercial semiconductor components is shown in Figure 4-1, which can also be used as a reference in the component selection.

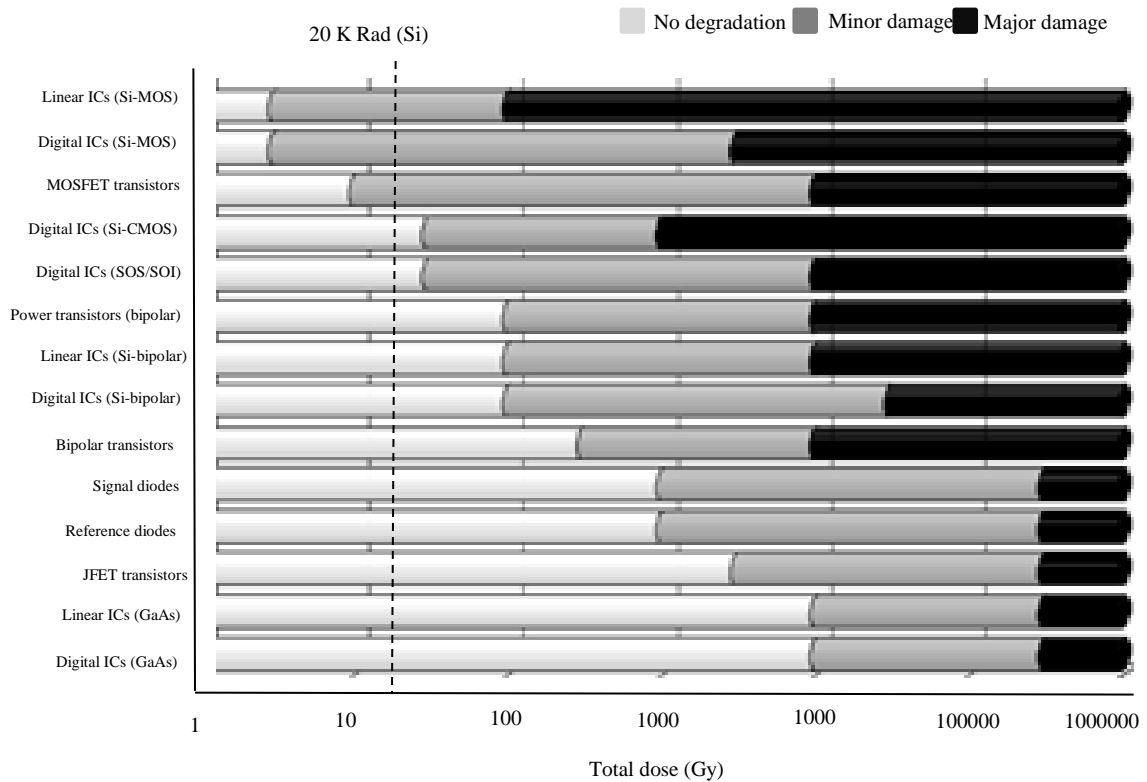


Figure 4-1: Radiation tolerance by a family of COTS components (Houssay, 2000)

According to radiation damages thresholds in Table 4-1 and radiation tolerance in Figure 4-1, as well as radiation test data in the literature (Boutte *et al.*, 2013; Cochran *et al.*, 2008; Cochran *et al.*, 2006), most semiconductor components will experience device degradation and radiation damages when the total dose is more than 20 K Rad (Si) (1 Gy = 100 Rad (Si)) (Messenger and Ash, 1991). Therefore, the total dose limit is defined as 20 K Rad (Si) in this work. The radiation-resistances of selected candidate components should be more than this total dose limit.

4.2 The Method of Component Selection

4.2.1 The Principle of Component Selection

Referring to radiation test data from the NASA Goddard Space Flight Center, the principles of component selection in this work are listed as follows:

- To implement redundant channels and their spares with diversity semiconductor technologies, *e.g.*, One channel uses bipolar components, second channel uses CMOS components, and third channel uses hybrid components;
- To select semiconductor component with higher radiation resistance by the calculation of its radiation degradation factor based on radiation test data, the selected component should work normally under the condition of total dose 20 K Rad (Si);
- To improve the radiation resistance of each channel by the assessment of reliability under the given radiation conditions.

4.2.2 The Assessment Method of Component Selection

To take radiation effects in consideration in system reliability analysis, a new method for electronic systems has been developed (Lauridsen *et al.*, 1996a; Lauridsen *et al.*, 1996b). This method uses radiation degradation factors(Δ), instead of the usual failure rate data of an item in the reliability model, as input to describe the radiation response of this item under a total radiation dose D_t , which will lie in the interval $[0, 1]$ and can be defined as follows:

$$\Delta = \min \left\{ \left| (P_0 - P_t) / (P_0 - P_f) \right|, 1 \right\}. \quad (4-1)$$

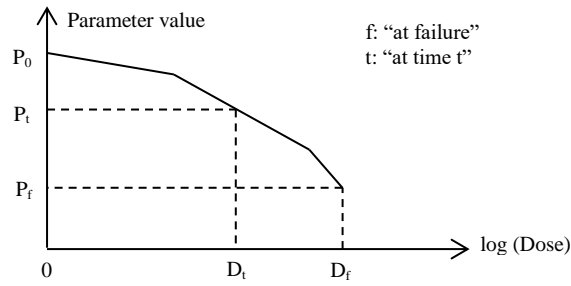
A detailed description of the radiation degradation factor can be found in Lauridsen *et al.*, 1996b.

$$\Delta = \begin{cases} (P_0 - P_t) / (P_0 - P_f) & \text{for } P_0 \geq P_t > P_f \text{ or } P_0 \leq P_t < P_f \\ 0 & \text{for } P_t > P_0 > P_f \text{ or } P_t < P_0 < P_f \\ 1 & \text{for } P_0 > P_f > P_t \text{ or } P_0 < P_f < P_t \end{cases} \quad (4-2)$$

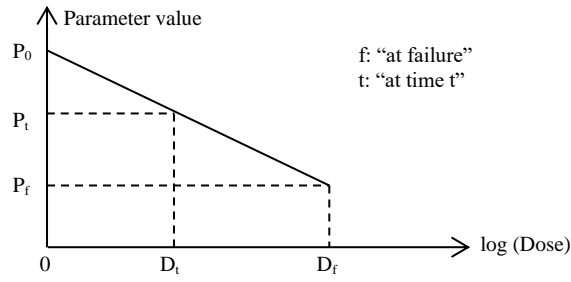
Previous research (Lauridsen, *et al.*, 1996a; Lauridsen, *et al.*, 1996b) has derived the parameter values of radiation degradation from real radiation test data; with radiation degradation functions which are used to describe how the material and/or components change their properties under given radiation conditions. Radiation degradation functions

are separated into three categories in (Lauridsen, *et al.*, 1996b), as shown in Figure 4-2 (Lauridsen, *et al.*, 1996b).

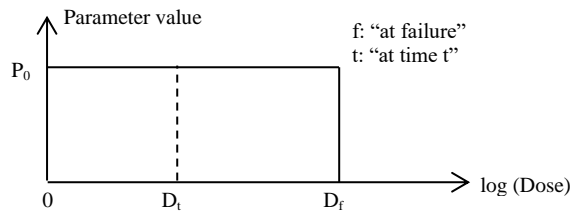
- (1) Piece-wise linear radiation degradation function, with logarithmic dose values and linear parameter values;
- (2) Linear radiation degradation function in the entire range of exposure; and
- (3) Constant radiation degradation function. The value 1 is up to D_f , and the value 0 is assumed to fail abruptly at the threshold dose.



(a) Piece-wise linear radiation degradation function



(b) Linear curve in the entire range of exposure



(c) Simple radiation degradation function

Figure 4-2: Radiation degradation functions derived from Lauridsen, *et al.*, 1996b

Due to the fact that semiconductor components may have a number (n_p) of critical parameters, in this study, the radiation degradation factor is defined as the mean value of those degradation factors of all critical parameters, which can be described as follows.

$$\Delta = \frac{\sum_{i=1}^{n_p} \min \left\{ \left| \frac{(P_{i_0} - P_{i_i})}{(P_{i_0} - P_{i_f})} \right|, 1 \right\}}{n_p}. \quad (4-3)$$

4.3 Selected Candidate Components

The difficulty of the assessment lies in determining the degradation factors for semiconductor devices. Most of radiation degradation factors under different radiation doses in this study come from NASA Goddard Space Flight Center radiation test data, which are available from online resources; others are derived from the existing literature (Messenger and Ash, 1991; Houssay, 2000; Kulkarni and Agarwal, 2003). Specifically, P_f of some components are not easy to obtain from the NASA database and literature, and are instead derived from specification limits of electronic parameters. Selected candidate components for the proposed wireless monitoring system and their radiation degradation factors for various total doses are summarized in Table 4-2.

Table 4-2: The summary of selected candidate components and radiation degradation factors

| Device Type | Device | Δ_{10K} | Δ_{20K} | Δ_{50K} | Δ_{100K} |
|-----------------------------|----------|----------------|----------------|----------------|-----------------|
| BJT | 2N2222 | 0.1940 | 0.3201 | 0.4267 | 0.4591 |
| Voltage reference | LT1021 | 0.0774 | 0.1010 | 0.2104 | 0.3432 |
| | LT1009 | 0.0642 | 0.1099 | 0.5158 | 0.5786 |
| | MP5010 | 0.0000 | 0.0000 | 0.0000 | 0.0000 |
| | AD580 | 0.1510 | 0.0181 | 0.0087 | 0.0094 |
| | REF-10 | 0.1408 | 0.3371 | 0.3204 | 0.3846 |
| | AD780 | 0.0039 | 0.0229 | 0.0246 | 0.0209 |
| | TL431 | 0.0055 | 0.0269 | 0.0238 | 0.0646 |
| | LM117HVK | 0.1639 | 0.2916 | 0.2933 | 0.2464 |
| | LP2951 | 0.1226 | 0.1737 | 0.3277 | 0.5699 |
| | UDS2983 | 0.3607 | 0.2557 | 0.2472 | 0.2541 |
| OP amplifier | CLC502 | 0.0208 | 0.0365 | 0.0383 | 0.0365 |
| | PA51M | 0.0409 | 0.0770 | 0.2989 | 0.2168 |
| | LM108 | 0.2377 | 0.3964 | 0.6620 | 0.6537 |
| | LM136 | 0.0098 | 0.0186 | 0.2431 | 0.2593 |
| | MC35181 | 0.0689 | 0.1551 | 0.3673 | 0.5151 |
| | LM317 | 0.2970 | 0.4120 | 0.5294 | 0.5568 |
| | PA07M | 0.1360 | 0.0764 | 0.1757 | 0.2717 |
| | OP43 | 0.1409 | 0.3128 | 0.4047 | 0.4182 |
| | AD544 | 0.1331 | 0.3963 | 0.4759 | 0.5132 |
| | AD713 | 0.3271 | 0.6739 | 0.8221 | 0.7451 |
| | MP3518 | 0.0689 | 0.1551 | 0.3673 | 0.5151 |
| | TL074 | 0.2402 | 0.3267 | 0.3742 | 0.3250 |
| | AD574 | 0.0178 | 0.0486 | 0.0633 | 0.0649 |
| Analog-to-digital converter | AD674 | 0.1735 | 0.1503 | 0.2741 | 0.3345 |
| | AD7885 | 0.0181 | 0.0229 | 0.0246 | 0.0209 |
| | AD713 | 0.2265 | 0.3899 | 0.4286 | 0.3926 |
| | AD713 | 0.2265 | 0.3899 | 0.4286 | 0.3926 |
| E ² PROM | 28C010 | 0.0187 | 0.0465 | 0.1001 | 0.1179 |
| FPGA | A1280 | 0.0023 | 0.0244 | 0.1341 | 0.1326 |
| Microcontroller | 82C59 | 0.0638 | 0.0654 | 0.0985 | 0.1190 |
| Logic gate | 54AC02 | 0.0469 | 0.0494 | 0.0480 | 0.0724 |
| | 54AC08 | 0.0133 | 0.0244 | 0.1850 | 0.2432 |

4.4 Summary

In this Chapter, radiation resistances of regular COTS components have been investigated. The results have shown that semiconductor-based electronic devices are more sensitive to ionizing radiation than that of other components. According to radiation damage threshold on electronic and radiation test data in literature, the total dose limit is defined as 20 K Rad (Si) in this work.

On the other hand, the principle of component selection is also given in this Chapter, as well as the assessment method of radiation tolerance in the selecting of semiconductor devices. Based on radiation test data in literature, a number of selected candidate components and their radiation degradation factors are also presented. Many radiation tests for simpler semiconductor devices have been performed in literature, such as BJT, operator amplifier, analog-to-digital converter, voltage reference, logic gate, etc. However, there have a limit number of test data for more complicate modern devices, such as microcontroller, microprocessor, wireless transceiver, etc. More investigations of radiation test for those modern devices need be investigated in the future.

Chapter 5

5 Design Part II: Multi-Layer Radiation Shielding Protection

As mentioned in Chapter 4, it is necessary and also important to find a way to reduce the cumulative total dose to be less than 20 K Rad (Si). Otherwise, COTS-based electronic systems cannot survive for a period of long time when the cumulative total dose is 1 M Rad (Si). As studied in the literature, shielding protection is an effective solution to mitigate radiation damages, and to increase the reliability and the lifespan of electronic systems. It is therefore considered as a solution to reduce the total dose in this work.

This Chapter starts with potential shielding materials to mitigate damages of total dose and related problem statement. Then, the design of a multi-layer shielding protection is presented in detail. A method to calculate the required shielding thickness according to the given radiation condition is also covered. Finally, a multi-layer radiation shielding protection is designed with several different solutions for the application of wireless monitoring in nuclear power plants.

5.1 Introduction

5.1.1 Background

As previously mentioned in Section 4.1.2, the objective of a radiation shielding protection is to decrease the cumulative total dose to be less than 20 K Rad (Si) from the given cumulative dose (1 M Rad (Si)), so as to avoid common-mode damages for redundant systems. Therefore, the cumulative total dose measured after the shielding protection must be less than 20 K Rad (Si). Because the selected electronic devices in the design can work in when the cumulative total dose is from 0 K Rad (Si) to 20 K Rad (Si), presented in Figure 5-1.

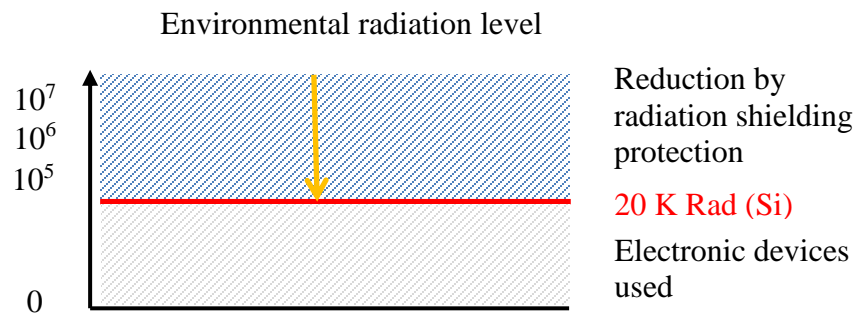


Figure 5-1: Reduction of total radiation dose by shielding protection

There are several factors that can influence the selection and the use of shielding materials, such as attenuation effectiveness, strength, resistance to damage, thermal properties, and cost, etc. The primary factors include:

- Energy level of the radiation source;
- Maximum allowable dose rate;
- Geometrical relationships between the radiation source and the position of the device;
- Distance from the source to the device;

Characteristics of different shielding materials and particle types are summarized in Table 5-1.

Table 5-1: Characteristics of particles and effective shielding layer

| Radiation particles | Characterizes | Comments |
|---------------------|--|---|
| Alpha and Beta | Material density is the important parameter to block alpha and beta, and thickness is less of concern. | A half-inch plastic can shield against alpha particles, but lead is ineffective to block alpha. |
| Gamma and x-ray | High-density materials are more effective to reduce intensity of radiation. | Lead is particularly effective to block gamma and x-ray. |
| Neutron | Neutron shielding should be incorporated both high and low atomic number elements. | Lead is ineffective to block neutron. |

A great variety of materials have been investigated for radiation shielding purpose to protect electronics in the literature, such as alloys, concrete, aluminum, copper, lead, and tungsten, iron, hydrogen, and boron, etc. (Gencel *et al.*, 2011; Kharita *et al.*, 2008; Korkut *et al.*, 2010; Yilmaz *et al.*, 2011, Akkurt *et al.*, 2010; Damla *et al.*, 2010; Kharita *et al.*, 2008; Kharita *et al.*, 2011; Kurudirek *et al.*, 2009, Abdao, 2002, Mangeret *et al.*, 1996, Singh and Badiger, 2014, Okuno, 2005, Calzada *et al.*, 2011, Kurudirek, 2014; Zeynali *et al.*, 2012). Since the shielding characteristics of those materials are different. A parameter known as Half-value thickness (HVT) is used to express the thickness of the material at which the intensity of radiation is reduced by one half as compared to the entry surface (Yilmaz *et al.*, 2011).

5.1.2 Problem Statement

For a complicated radiation environment (alpha particles, beta particles, gamma rays, x-rays, and neutron particles) after a severe accident in a nuclear power plant, the objective of shielding protection cannot be achieved by using only one shielding material. Hence, a radiation shielding protection with different materials has to be used to protect common-mode damages of COTS-based electronic components are used in the radiation-tolerant systems. On the other hand, for the portability of the wireless system, the size and weight of the shielding protection are also limited.

Key issues to deal with radiation shielding protection for COTS-based systems can be summarized as follows:

- (1) To design a shielding protection to reduce the intensity of Alpha, Beta, and Gamma radiation simultaneously;
- (2) To minimize common-mode damages in redundant systems; and
- (3) To evaluate the effectiveness of the proposed multi-layer shielding protection under different radiation environments.

5.2 The Design of Multi-Layer Radiation Protection

In this work, the framework of shielding design is shown in Figure 5-2. Firstly, design specifications are obtained according to the considered radiation conditions and the design objectives of radiation-tolerance. Subsequently, the architecture of the multi-layer protection is presented. Then, the materials are selected based on the design objectives. The size and thickness are then calculated. Finally, simulations are carried out to validate the effectiveness of the design for radiation particles at different energy levels.

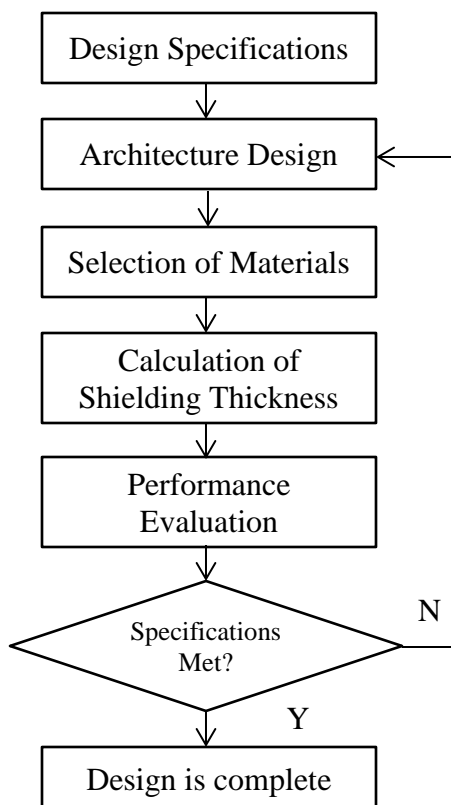


Figure 5-2: Design framework for multi-layer radiation protection

To enhance the radiation tolerance, the proposed architecture for electronic systems includes triple module redundant channels with spare units. The entire system is further protected by a multi-layer of radiation shielding as illustrated in Figure 5-3 to increase the radiation tolerance while avoiding the common-mode damage. The physical circuit board configuration is shown in Figure 5-3 (a). The three layers of shielding protection are illustrated in Figure 5-3 (a) (b) and (c), respectively. The first layer tightly encloses the circuit boards, while the second layer allows the circuit boards to be embedded in a lead-block. Finally, third layers encapsulate the entire system. Different materials used in each layer are determined by the type and the radiation degradation factors of semiconductor devices on these circuit boards.

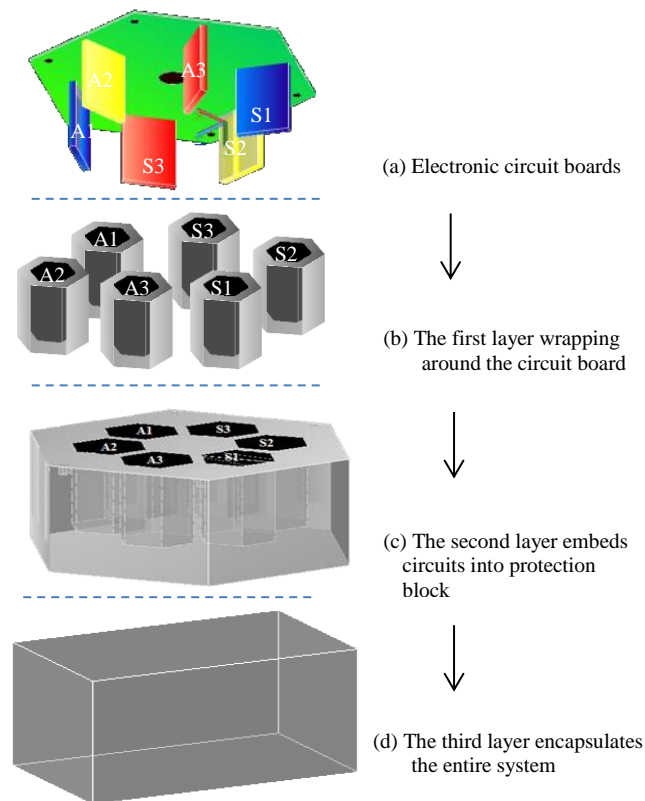


Figure 5-3: The layout of the multi-layer shielding protection.

This radiation shielding has several unique advantages:

- It is able to reduce the total dose to a tolerable level that the circuit components can safely operate under the given radiation condition;
- It reduces the likelihood of common-mode damages because different shielding materials, shielding thickness, positioning angle, and placement locations are used. These approaches will have different effects on the radiation exposure to the electronic systems in six different irradiation directions (See installation of the circuit boards with different angles in Figure 5-3 (a));
- It allows one to select different shielding materials for different radiation particles;

- It is possible to custom design by selecting specific shielding materials for the first layer with consideration of the characteristics of the semiconductor materials in a specific channel.

5.3 Calculation of Shielding Thickness in Multi-Layer Radiation Protection

Considering gamma (γ) ray is more difficult to block than alpha (α) and beta (β) particles. As a worst case scenario, only gamma radiation is considered as the radiation source in the evaluation of the shielding protection.

5.3.1 Attenuation of Gamma Radiation

When a gamma ray passes through a material under conditions of a narrow geometry, as shown in Figure 5-4 (Gollnick, 2011), no photons are scattered. This is idealistic and without collimation or at a longer distance. Under this condition, a straight-line relationship between the logarithm of the intensity and the thickness of the shielding can be established as follows (Gollnick, 2011).

$$I = I_0 e^{-ud}. \quad (5-1)$$

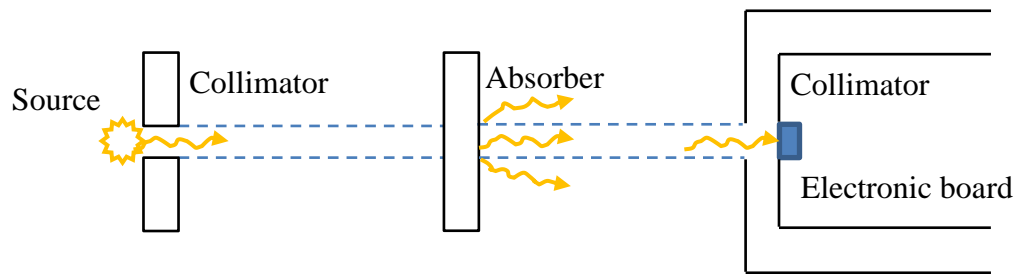


Figure 5-4: An attenuation of gamma radiation under conditions of narrow geometry (Gollnick, 2011)

The linear attenuation coefficient (u) is the probability per unit thickness that particles interact with the material. This value is dependent upon the atomic number Z of the material and its density (p). This relation can also be described through a linear attenuation coefficient as follows (Yilmaz *et al.*, 2011).

$$I = I_0 e^{-(u/p)(pd)}. \quad (5-2)$$

However, under a broad geometry condition, as shown in Figure 5-5 (Gollnick, 2011), all scattered photons are assumed to reach the detector (or circuits in our case). This is also unrealistic. The first method under a narrow geometry condition underestimates the dose rate, while the second method under a broad geometry condition overestimates it (Gollnick, 2011). To obtain a dose rate closer to reality, the shielding thickness can be estimated by the use of a build-up factor (B), which is defined as the ratio of the intensity of the radiation at any point in a beam to the intensity of the primary radiation only at that point. It is a function of the total attenuation coefficient, the thickness of the shielding material, and the energy of the gamma radiation (Yilmaz *et al.*, 2011; Suteau and Chiron, 2005). Under this condition, only some of the scattered photons can reach the device, which is closer to a real situation, Eq. (5-2) can, therefore, be estimated by Eq. (5-3) (Gollnick, 2011).

$$I = B(ud, E) \cdot I_0 \cdot e^{-(u_t/p)(pd)}. \quad (5-3)$$

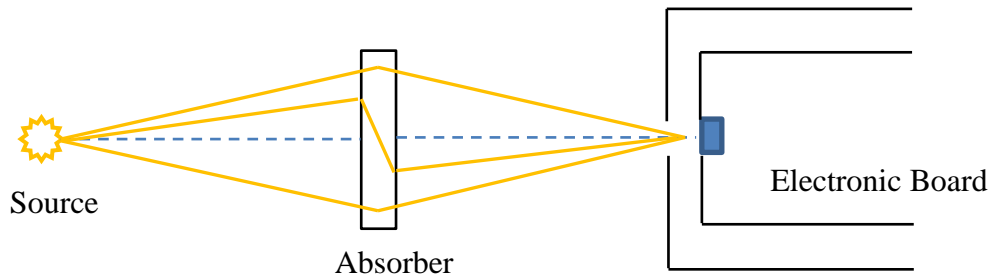


Figure 5-5: Gamma radiation attenuation under conditions of broad beam geometry (Gollnick, 2011)

Build-up factors have been calculated for different levels of gamma energies and for various shielding materials, which can be found in (ANSI/ANS, 1991).

5.3.2 Calculation of the Shielding Thickness

As previously discussed, for a given radiation source, a given radiation dose rate, and a known shielding material, based on Eq. (5-1) to Eq. (5-3), the required shielding thickness under a broad geometry can be calculated as follows:

$$d = \ln \left(B \cdot \frac{I_0}{I} \right) / u. \quad (5-4)$$

According to Eq. (5-4), various shielding materials can be selected and their performance compared, the designed shielding thickness can also be evaluated to achieve the design objective, of reducing the total dose to a level less than 20 K Rad (Si).

5.4 Case Study: Design of Shielding Protection for Application to a Wireless Monitoring System in Nuclear Power Plants

5.4.1 Development of Radiation Shielding Protection for the Proposed WPAMS

As illustrated in Figure 5-3, with different shielding materials used in different layers, shielding thickness, radiation angle, and installation locations, all have different effects on the radiation exposure experienced by electronic devices in the six identified areas, as shown in Figure 5-3(a) ($A_1 - A_3, S_1 - S_3$). Taking Co-60 as a gamma radiation source, and considering radiation rates in Fukushima accident, the objectives of the shielding protections can be summarized as follows:

- Under the condition with dose rate 70 Sv/h, for a 24h period, the highest total dose in six areas should be less than 2.6 K Rad (Si).
- Under the condition with dose rate 530 Sv/h, for a 24h period, the highest total dose in six areas should be less than 20 K Rad (Si);
- Under the condition with dose rate 1350 Sv/h, for a 24h period, the highest total dose in six areas should be less than 50 K Rad (Si);
- Under the condition with dose rate 2700 Sv/h, for a 24h period, the highest total dose in six areas should be less than 100 K Rad (Si);

Theoretically, all materials can be used for radiation shielding if thick enough. The choice of the shielding material is dependent on many factors: desired attenuated radiation levels, effectiveness of heat dissipation, resistance to radiation damage, required thickness and weight, multiple use considerations, uniformity of shielding capability, permanence of shielding and availability (Yilmaz *et al.*, 2011). According to the design

specifications and radiation given in Eq. (5-1) to Eq. (5-4), those designs for the proposed multi-layer radiation shielding have been investigated. The details are described in the next following Sections.

Design #1 is to use copper, lead, and tungsten. Its detailed parameters can be determined as follows theory calculation:

- The material in the first shielding layer is tungsten, with the diameter being 4cm, and the thickness is chosen to be 1cm.
- The material in the second shielding layer is lead, with the size being 24cm X 24cm X 18cm, and the thickness is chosen to be 6cm; and
- The material in the third shielding layer is copper, with the size being 26cm X 26cm X 20cm, and the thickness is chosen to be 1cm;

Design #2 is constructed with aluminum, iron, and lead. The detailed parameters can be determined as follows theory calculation:

- The material in the first shielding is lead, with the diameter being 4.2cm, and the thickness is chosen to be 1.2cm.
- The material in the second shielding layer is Iron, with the size being 38.6cm X 38.6cm X 18cm, and the thickness is chosen to be 13cm; and
- The material in the third shielding layer is aluminum, with the size being 42.2cm X 42.2cm X 21.6cm, and the thickness is chosen to be 1.8cm;

Design #3 is constructed with lead glass, lead, and tungsten. Its detailed parameters can be determined as follows theory calculation:

- The material in the first shielding layer is lead, with the size diameter being 4cm, and the thickness is chosen to be 1cm.
- The material in the second shielding layer is iron, with the size being 24cm X 24cm X 18cm, and the thickness is chosen to be 6cm; and
- The material in the third shielding layer is aluminum, with the size being 25.4cm X 25.4cm X 19.4cm, and the thickness is chosen to be 0.7cm;

The parameters of these three designs are summarized in Table 4-4. Their performance evaluations are given in next Section.

Table 5-2: Summary of the Parameters of radiation shielding protection for different designs

| Design Solutions | Layers | Material | Size | Thickness |
|------------------|--------------|------------|-----------------------------|-----------|
| Design #1 | First layer | Tungsten | 4 cm | 1 cm |
| | Second layer | Lead | 24 cm X 24 cm X 18 cm | 6 cm |
| | Third layer | Copper | 26 cm X 26 cm X 20 cm | 1 cm |
| Design #2 | First layer | Lead | 4.2 cm | 1.2 cm |
| | Second layer | Iron | 38.6 cm X 38.6 cm X 18 cm | 13 cm |
| | Third layer | Aluminum | 42.6 cm X 42.6 cm X 19.6 cm | 1.8 cm |
| Design #3 | First layer | Tungsten | 4 cm | 1 cm |
| | Second layer | Lead | 24 cm X 24 cm X 18 cm | 6 cm |
| | Third layer | Lead glass | 25.4 cm X 25.4 cm X 19.4cm | 0.7 cm |

5.4.2 Performance Evaluation

The shielding performance of the above three designs has been evaluated by a program RadPro Calculator (Rad Pro Calculator, 2018). RadPro Calculator provides an effective tool for calculating the radiation dose rate and layers of protections. This program has been widely used among radiation safety officers, health physics technicians (HP) and other professionals in radiation physics and radiological engineering. Many researches have also used RadPro Calculator for various academic and engineering applications (Brugger *et al.*, 2014; Prelas *et al.*, 2016). With regard to various dose rates, the performance evaluation is performed in RadPro Calculator. The results are summarized in Table 5-3.

Table 5-3: The performance evaluation for three shielding solutions (Sv/h)

| Design Solutions | Initial dose rate | Layer 1 | Layer 2 | Layer 3 |
|------------------|-------------------|---------|---------|---------|
| Design #1 | 72 | 45 | 2 | 1.1 |
| | 530 | 345 | 14.5 | 8 |
| | 1350 | 900 | 38 | 21 |
| | 2700 | 1800 | 75 | 41.5 |
| Design #2 | 72 | 55.5 | 1.8 | 1.1 |
| | 530 | 410 | 13 | 8 |
| | 1350 | 1040 | 33 | 20 |
| | 2700 | 2090 | 65 | 40 |
| Design #3 | 72 | 46 | 2 | 1.1 |
| | 530 | 340 | 14.5 | 8 |
| | 1350 | 900 | 38 | 21 |
| | 2700 | 1800 | 75 | 41.5 |

Considering the highest dose rate in the Fukushima accident, being 530 Sv/h, the dose rates within the shielded area are reduced to 8 Sv/h. Since the survival lifespan is 24 hours, the total dose after three shielding layer are 194 Sv (19.4 K Rad(Si)). Therefore, all three designs satisfy the design specifications. On the other hand, the size of design #3 is the smallest form factor and design #2 is the biggest. However, the cost of design #3 is the highest. Moreover, lead glass has the similar shielding characterize with lead. Therefore, design #2 is selected as the shielding protection configuration in this work.

5.5 Conclusions

In this Chapter, based on the characteristics of various shielding materials, a multi-layer shielding protection is proposed to reduce the total dose to a safe level for electronics. A method to calculate the required shielding thickness is also presented. Three solutions have been considered to achieve the design requirements in this work. Based on the results of simulation, all three can be reduce the total dose to be less than 20 K Rad (Si) from the given radiation condition (1 M Rad (Si)). Considering the size, the weight, the

cost, and the shielding performance, the design #2 (Copper + Lead + Tungsten) is the best one and it is therefore selected in this work.

It is important to point out that this work just focuses on the performance analysis for blocking the total dose, for other types of radiations with various energy levels, more solutions are needed.

Chapter 6

6 Design Part III: Radiation-Tolerant Architecture

In Chapter 3, simulation studies of photocurrent responses have indicated that the photocurrents of the ideal p - n diode under different levels of ionizing radiations can be reduced dramatically if the bias voltage on the junction can be promptly reduced to zero. Hence, if the power on the junction can be removed quickly in an event of radiation exposure, a semiconductor device might not be damaged permanently by the accumulated photocurrent. This observation leads to the development of a new radiation-tolerant architecture and associated protection strategies.

This Chapter starts with the potential solution techniques and related problem statement. Subsequently, some defense techniques are proposed for single event effects mitigation. Then, a radiation-tolerant architecture by using fault-tolerant techniques is developed to perform those functions and techniques. Based on this architecture, system-level design and analysis have been carried out. Detailed radiation protection techniques and diversity against the common-mode failure, online fault diagnosis scheme and prognostic algorithm to detect, identify, and prognosticate potential radiation-induced faults, have been presented. Finally, to validate the correctness of the architecture and the system logic, a number of injection experiments are performed in a developed hardware emulation bench.

6.1 Introduction

6.1.1 Potential Solution Techniques

To mitigate damages caused by single event effects, some existing designs utilize three redundant duplicates for critical circuits and subsystems followed by a majority voter to select the most desirable output. Others rely on extra added circuits to detect faults. These techniques have been used in a range of situations, from low-level structures, to complex circuits, hardware modules, and even multi-core architecture (Gao *et al.*, 2015; Fenton *et al.*, 2001; Kim *et al.*, 2010; Cuenca-Asensi *et al.*, 2011; Sterpone *et al.*, 2013; Voilante *et al.*, 2011; Straka *et al.*, 2013; Abate *et al.*, 2008; Wang *et al.*, 2011). A drawback of those

techniques is that additional measurement/test units and/or majority voters have to be employed to detect and diagnose faults caused by radiation. The fact of the matter is that these additional circuits themselves are also subject to the same radiation damage.

Moreover, most of existing fault detection and diagnosis (FDD) methods for electronic systems mainly focus on common hardware or software faults in redundant systems, not on cross-board radiation damages. For example, a fault tolerant platform able to function in harsh space environments is developed in (Sterpone *et al.*, 2013) for using in satellite payload processing. Its main weakness is that the inter-module communication and control buses are not independent of each other. The whole system will thus encounter failure when just one module has faults on the buses. In the architecture proposed in (Violante *et al.*, 2011), the problem is the control logic unit which is also sensitive to radiation particles.

It is important to point out that, unlike random hardware failures, radiation-induced damages can affect multiple redundant channels causing functional failure of the whole system. Special techniques have to be developed to deal with such unique situation regarding common-mode failures.

6.1.2 Problem Statement

As discussed in the previous Sections, to design and build a rad-hardened system using only COTS components, it is imperative to adopt radiation-tolerant architectures with independent and diversified redundancies, online fault-detection and prognostic scheme, equipped with proactive rapid power-off for recovery, as well as command-mode damage avoidance. Within this framework, the following specific goals are investigated:

- (1) To design completely independent redundant architecture without additional detection units and/or hardware voters.
- (2) To avoid common-mode damage in redundant channels.
- (3) To design the mechanisms of online fault detection, real time preventive remedial actions, and rapid power loss.

In order to address these issues, this work develops a radiation-tolerant architecture with a decision-making unit to achieve a high level of radiation tolerance and to prolong the lifespan of COTS-based systems in high level radiation environments.

6.2 Techniques for Preventing Single Event Effects

6.2.1 Redundancy

One way to ensure continued operation of the system in the event of potential radiation damages, the proposed system makes use of redundancy to ensure that not all channels fail at the same time. It should have the capacity to detect and to prognosticate faults and errors in a timely manner, and then locate faults and errors in order to make a reconfiguration decision to deal with device power loss. Furthermore, in the proposed redundant architecture, each redundant channel has to be completely independent and there must have no additional measurement/test units or hardware majority voters.

In general, a sender in a modern digital communication system includes several subsystems: input transducer, source encoder, channel encoder, modulator, and transmitter. In this work, a function of decision making is inserted to perform the self-diagnostic function, which is integrated in existing hardware and therefore does not need any additional hardware. Each redundant channel can be divided into three layers: the input layer, the decision layer, and the output layer. The input layer's job is to collect the information coming from input sensors, source encoders, and channel encoders. Subsequently, fault detection, fault diagnosis, prognostic assessment, and reconfiguration suggestions, are accomplished in the decision layer. The output layer then transmits and/or receives data with the outsider, which consists of a digital modulator and transceiver. All functions of the parameter measurement and the self-diagnostic are accomplished inside each redundant channel, which does not need additional measurement units to detect and diagnose faults.

To achieve these requirements, the proposed redundant system totally has six channels to build an active triple modular redundant (TMR) system with their spares to replace the active one in case of fault or failure. For the sake of analysis, the following definitions are used to describe various channel states:

Definition 1: the system consists of three active channels and three respective spaces.

$$A = \{A_1, A_2, A_3\} \quad (1 \leq i \leq 3).$$

where A_i represents the state of the i_{th} channel with $A_i = 1$ and 0, respectively, corresponding to its powered (active) state and non-power state (inactive).

$$S = \{S_1, S_2, S_3\} \quad (1 \leq i \leq 3).$$

where S_i represents the state of the i_{th} spare channel with $S_i = 1$ and 0, respectively, corresponding to its powered (active) state and non-power state (inactive).

Definition 2: for channel A_i and S_i , their working conditions can be represented in the following sets:

$$F_{A_i} = \{F_{A_1}, F_{A_2}, F_{A_3}\}.$$

where F_{A_i} describes the state of A_i channel. If A_i is completely broken, then $F_{A_i} = 1$, otherwise $F_{A_i} = 0$.

$$F_{S_i} = \{F_{S_1}, F_{S_2}, F_{S_3}\}.$$

where F_{S_i} describes the state of S_i channel. If S_i is completely broken, then $F_{S_i} = 1$, otherwise $F_{S_i} = 0$.

6.2.2 Hardware Switch

With regard to the reconfigurator unit, its radiation resistance has to be higher than that of all redundant channels. Otherwise, it will be a major weakness of the whole system. In this work, two configurator are applied to control the power supply of each channel (the power reconfigurator), as well as the location of internal buses (the bus reconfigurator), which are determined by the reconfigure suggestions (R_{Si} & R_{Mi}). The power reconfigurator is to guarantee that the system only ever has three channels working simultaneously, which is critical for the whole system (see Figure 6-1 (a)). The bus reconfigurator, illustrated in Figure 6-1 (b), serves as the independent communication

mechanism. This way, the bus will not affect other channels when one channel fails. In addition, V_{in_1} , V_{in_2} , V_{in_3} , and V_{in_r} are the power inputs to the redundant channels and relays, and V_{Ai} , V_{Si} are the power supplies for the redundant (TMR) core (A_i) and spare units (S_i), which are controlled by the reconfigure commands (R_{Si} & R_{Mi}). In addition, the system has independent and diversified buses: internal bus (*Combus*), to exchange information with other channels; and *IO bus* (*IObus*), to accomplish the selection of primary channels.

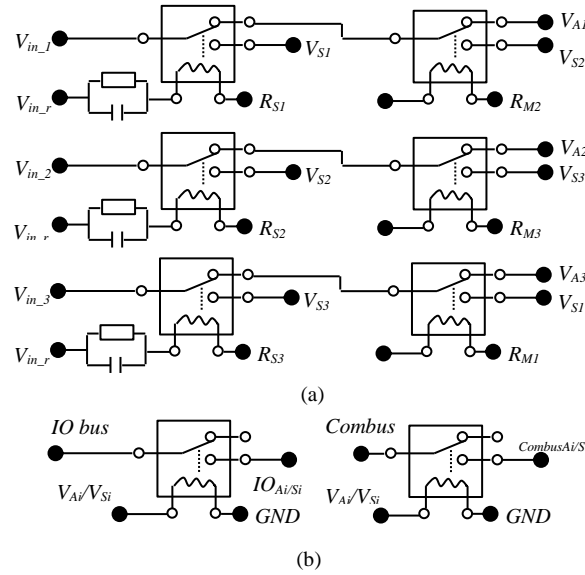


Figure 6-1: The schematic of reconfigurator (a) power reconfigurator (b) bus reconfigurator

To ensure reliable operation, both Bus Reconfigurator and Power Reconfigurator units should have higher level of radiation resistance than the rest of electronic components in the system. For this reason, both units are designed using passive devices only, such as resistors (tolerant up to 10^4 - 10^{10} Gy), capacitors (tolerant up to 10^4 - 10^8 Gy), and non-electronic relays (tolerant up to 10^5 - 10^7 Gy) (Houssay, 2000; Boutte, *et al.*, 2013; Cochran, *et al.*, 2008; Cochran, *et al.*, 2006). The reconfigurator therefore can at least withstand a high level of radiation (10^4 Gy).

6.2.3 Diversity Techniques

One of the weaknesses for redundant systems is their vulnerabilities with respect to common-mode failures. To ensure that the system is well protected, the following diversification strategies are chosen:

1) Radiation protection

Radiation shielding is an effective solution to mitigate the effects of radiation, and to increase the reliability and lifespan of the electronic system. The efficiency and functional quality of a particular electronic system are determined by: the type of radiation it is exposed to, the radiation resistance of its semiconductors, and the unique properties of the shielding materials (Shultis and Faw, 2005). Many different solutions for obtaining high levels of radiation resistance in radiation shielding have been applied for the package and/or chips (Abdao, 2002; Mangeret *et al.*, 1996; Calzada *et al.*, 2011). This work combines the proposed radiation-tolerant architecture with a structure of radiation protection (illustrated in Figure 4-5) whose design increases the radiation tolerance while avoiding common-mode damage. As illustrated in Figure 4-5, differences in shielding material, shielding thickness, radiation angle, and radiation locations, all have different effects on the radiation exposure experienced by electronic systems in the six identified areas ($A_1 - A_3, S_1 - S_3$). The proposed architecture therefore offers the possibility of reducing instances of common-mode damage. On the other hand, another objective of this radiation protection is to ensure that the total radiation doses experienced by all six areas should be less than a pre-specified level. Parameters of radiation protection are also dependent on the given radiation condition.

2) Enforcing differences

Enforced differences are also considered for preventing common-mode failures in the proposed architecture. Approaches used can be described as follows:

- Use diversified semiconductor technologies (E_1): Considering the following facts: Bipolar devices can withstand a higher total dose; but they are particularly sensitive to lower dose rates. On the other hand, MOS devices are sensitive to

higher total doses and can also be robust to lower dose rates. Devices are chosen to complement these unique properties to cover perceivable conditions.

- Rely on diversified, but functionally equivalent, components (E_2): Among different channels, devices (mainly CPUs) rely on different technologies to implement identical functions. In this case, a microcontroller, FPGA, and/or a microprocessor are used, as they offer different tolerance to radiation.
- Select the same component, but from different manufacturers (E_3): Because different manufacturing processes, such as semiconductor materials, component size, etc., can realize the same functionalities for certain electronic components, but with different level of radiation tolerance, it is beneficial to select components of the same functionalities made by different manufacturers.
- Use different tools for implementing different software and algorithms for the same functionalities (E_4): Due to memory utilization and storage locations, a same software module developed using different programming languages and environment may have different responses to radiation effects. In this case, different programming environments have been used to develop modules for different channels.

In summary, A_i and A_j ($i = 1, 2, 3; j = 1, 2, 3; \text{ and } i \neq j$) are built with diversified hardware, diversified software, as well as different shielding protection. However, A_i and S_i ($i = 1, 2, 3$) are built with the same hardware, but different software logics to achieve the same functionalities. Different shielding protection is used in second layer also. Thus, the protection measures used in different channels can be summarized as follows:

$$\begin{cases} A_i \& A_j (i \neq j): & E_1, E_2, E_3, E_4 \\ A_i \& S_j (i \neq j): & E_1, E_2, E_3, E_4 \\ A_i \& S_i: & E_4 \end{cases}$$

6.2.4 Fault Detection and Diagnosis

Even though all possible measures have been taken at the system design and component selection processes, there is still no guarantee that the system will function trouble-free. To further improve the reliability of the system, real-time fault detection and diagnosis schemes are developed so that some remedial actions can be taken during the operation to restore system performance, for example by a rapid power reset.

A hierarchical fault model, drawn according to electronic system abstraction levels, is illustrated in Figure 6-2. Radiation disturbances and/or other disturbances will directly affect the device level, after which the disturbances will be transmitted to the circuit and system level (subsystem). Faults at the device level (L_1) correspond to sensors and semiconductor components; faults at the circuit level (L_2) correspond to analog circuits, digital circuits, and mix circuits; and faults at the system level (L_3) correspond to subsystems or functional modules.

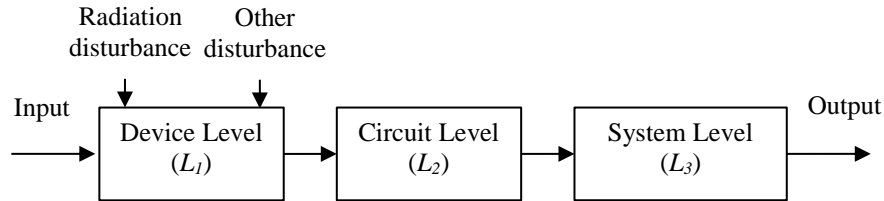


Figure 6-2: Hierarchical fault model for electronic systems

As previously discussed, the system should have the capacity to detect and prognosticate faults and errors in a timely manner, and then locate faults and errors in order to make a reconfiguration decision to deal with device power loss. The objective of fault detection is to detect abnormal operating conditions of those levels under radioactive environments, and to estimate the nature and extent of the damages. Three definitions are given below to describe various states at device, circuit and subsystem levels:

Definition 3 (Device): An electronic system consists of a number (n_d) of components.

$$D = \{d_1, \dots, d_i, \dots, d_{n_d}\} \quad (1 \leq i \leq n_d).$$

where d_i represents the state of the i_{th} component with $d_i = 0$ being operational and 1 being fault states, respectively.

Definition 4 (Circuit): An electronic system consists of a number (n_c) of circuit modules. Each module consists of a number of components.

$$C = \{c_1, \dots, c_j, \dots, c_{n_c}\} \quad (1 \leq j \leq n_c) \quad .$$

where c_j represents the j_{th} circuit modules in the electronic system. Similar representations are used to represent the operational and fault modes as in **Definition 5** in all subsequent definitions.

Definition 5 (Subsystem): An electronic system can be decomposed into a number (n_s) of subsystems. Each subsystem consists of several circuit modules.

$$S = \{s_1, \dots, s_k, \dots, s_{n_s}\} \quad \forall s_k (1 \leq k \leq n_s) .$$

where s_k represents the k_{th} subsystem.

Definition 6 (Functional State): For each circuit module and subsystem, two states can be defined:

X_C, X_S represent the state that temporary fault or recovered failure in the circuit blocks and subsystems, with $x = 0$ for operational and 1 for temporary fault or recovered failure, respectively.

Y_C, Y_S represent the state that permanently fails in the circuit blocks and subsystems, with $y = 0$ for no failure and 1 for permanent failure, respectively.

For each circuit module, the following conditions can be defined for the operational state:

$$X_c = \{x_{c_1}, \dots, x_{c_{n_c}}\} \quad \forall x_{c_j} (1 \leq j \leq n_c) .$$

If c_j operates incorrectly, $x_{c_j} = 1$, otherwise $x_{c_j} = 0$.

$$Y_c = \{y_{c_1}, \dots, y_{c_{n_c}}\} \quad \forall y_{c_j} (1 \leq j \leq n_c).$$

If c_j is completely failed, $y_{c_j} = 1$, otherwise $y_{c_j} = 0$.

For each subsystem, the following state can be defined:

$$X_s = \{x_{s_1}, \dots, x_{s_{n_s}}\} \quad \forall x_{s_k} (1 \leq k \leq n_s).$$

If s_k operates incorrectly, $x_{s_k} = 1$, otherwise $x_{s_k} = 0$.

$$Y_s = \{y_{s_1}, \dots, y_{s_{n_s}}\} \quad \forall y_{s_k} (1 \leq k \leq n_s).$$

If s_k is completely failed, $y_{s_k} = 1$, otherwise $y_{s_k} = 0$.

Based on the above definitions, a fault hypothesis for malfunctions of circuit blocks and subsystems can be formed in Eq. (6-1), where the goal is to integrate states of circuit blocks and subsystems.

$$H = [X, Y]. \quad (6-1)$$

where X is the summary of X_c and X_s , as well as Y is the summary of Y_c and Y_s .

A detection function reflects the credibility of H as defined in Eq. (6-2). A smaller $E(H)$ suggests a higher credibility of H . If the detection function is equal or greater than unity, a reconfigure command should be issued.

$$E(H) = \sum_j^{n_c} (w_{xc_j} x_{c_j} + w_{yc_j} y_{c_j}) + \sum_k^{n_s} (w_{xs_k} x_{s_k} + w_{ys_k} y_{s_k}). \quad (6-2)$$

where w_{xc_j} , w_{yc_j} , w_{xs_k} , and w_{ys_k} are the weights of the discrepancy index. The range of the weights is from 0.1 to 1. If $w_1 \gg w_2$, it means that the discrepancy index w_1 is much more important than w_2 . The values of these weights are determined according to the significance of circuit blocks and subsystems in electronic systems.

6.2.5 Prognostic for Lifespan of Components

The objectives of prognosis protection are: (1) to predict the behavior of a circuit based on the present measurements, and hence to estimate whether a module or a subsystem can remain functional before complete failure occurs; and (2) to select the most appropriate channels for the radiation environment and corresponding characteristics of the diversified hardware. A hypothesis to predict malfunction of a device and a circuit block can be defined as follows:

$$P = [p_d, p_c]. \quad (6-3)$$

where $p_d = \{p_{d_1}, \dots, p_{d_{n_d}}\}$ represents the state of the i_{th} device with $p_{d_i} = 0$ and 1, respectively, based on the prediction of its operational and fault states, and $p_c = \{p_{c_1}, \dots, p_{c_{n_c}}\}$ represents the prediction of incorrect circuit operation. If c_j is predicted to operate incorrectly, then $p_{c_j} = 1$, otherwise $p_{c_j} = 0$.

A prognostic function can be formed to reflect the prediction state of the credibility of P , which can be defined in Eq. (6-4). A smaller $E_n(P)$ suggests a higher credibility of P .

$$E_n(P) = \sum_i^{n_d} w_{d_i} p_{d_i} + \sum_j^{n_c} w_{c_j} p_{c_j} \quad (n = 1, 2, 3). \quad (6-4)$$

where w_{d_i} and w_{c_j} are the weights of the discrepancy index of devices and circuit blocks.

A function can also be used to reflect whether a particular semiconductor technology for a specific channel can work correctly in a given radiation environment.

$$R_n = f(s, d) \quad (n = 1, 2, 3). \quad (6-5)$$

where s is the information about the radiation environment; d is the information on the semiconductor technologies; and R_n is the predicted channel selection. If channel n is estimated to have no capacity to operate in the given environment for a specific semiconductor technologies, $R_n = 1$, otherwise $R_n = 0$.

Using the fault prognostic function, if $E_n(P)$ is equal or greater than 1 or $R_n = 1$, the reconfiguration command should be issued by the decision-making unit.

6.3 Resulting System Architecture

6.3.1 Redundant-Tolerant Architecture

Based on previous studies on radiation damages to COTS components and potential prevention techniques, a radiation-tolerant architecture with independent redundancy, online fault-detection, real-time prognostic protection, rapid power off/ recovery, as well as command-mode damage avoidance, is proposed as shown in Figure 6-3. The architecture consists of an active triple modular redundancy (TMR) core (A_1, A_2, A_3), with spare units (S_1, S_2, S_3), and a bus, as well as a power reconfigurator. In an event that an active channel has malfunctioned, its corresponding spares will be reconfigured to replace the failed channel or channels automatically. This architecture can prolong the life for both devices and systems through independent built-in redundant channels, online fault detection, real-time prognostic protection, and rapid power off/on recovery, as well as reduction of modes for common-mode damages.

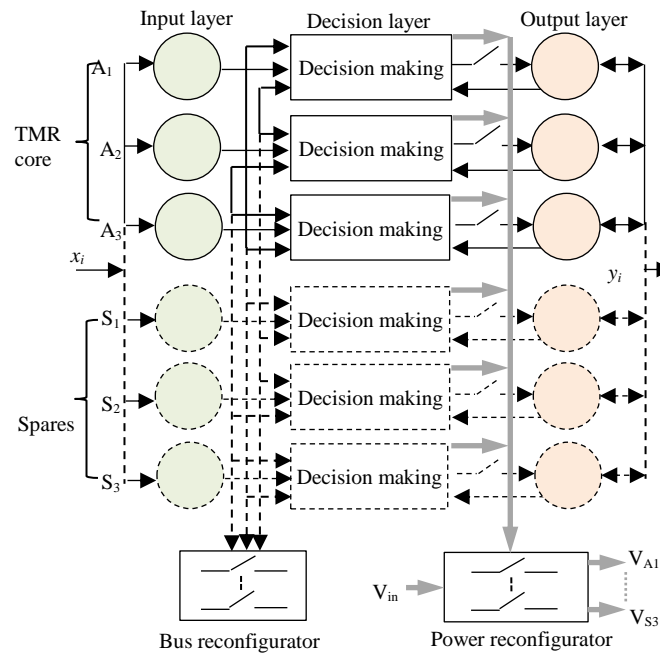


Figure 6-3: The proposed radiation-tolerant architecture

signal R_{Mi} is registered. This channel will be permanently removed from the system. As mentioned early, diversity in components selection has been extensively used to avoid simultaneous failures of all three channels in this system.

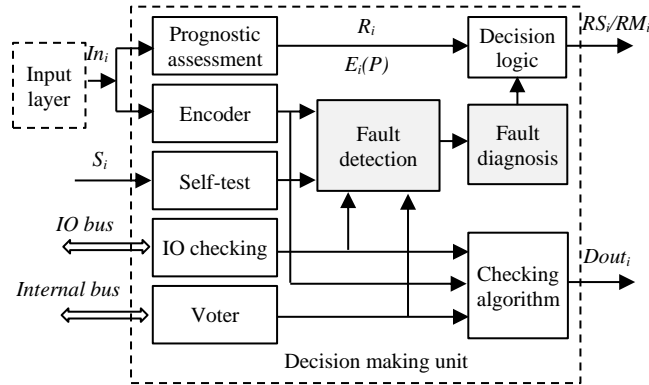


Figure 6-5: The block diagram of the decision making unit

In particularly, R_{Mi} are only provided by the primary channel under two cases: both a channel and its spare are in a state of failure; or neither are suitable to work at a given radiation level. In addition, it is assumed that cases of all three channels simultaneously encountering either faults or failure can be avoided by using a diversity of techniques. As such, this scenario is not considered in this work.

The operating principle of the proposed system works as follows: when one channel fails to operate, which will be detected by the self-diagnosis and/or the function external-diagnosis units, the decision-making units in another channel will generate some reconfiguration recommendations to cut off the power in a timely manner and its spare channel will be powered up to form a new TMR core.

2) Functionalities and operation of the decision logic unit

The objective of the decision logic unit is to integrate the functions of fault diagnosis and component life-span prognostics to generate potential reconfiguration signals (R_{Si} and R_{Mi}). A flowchart for this unit is illustrated in Figure 6-6. Specifically, all channels have the ability to detect, diagnose, and configure other channels in the TMR core until all channels have failed.

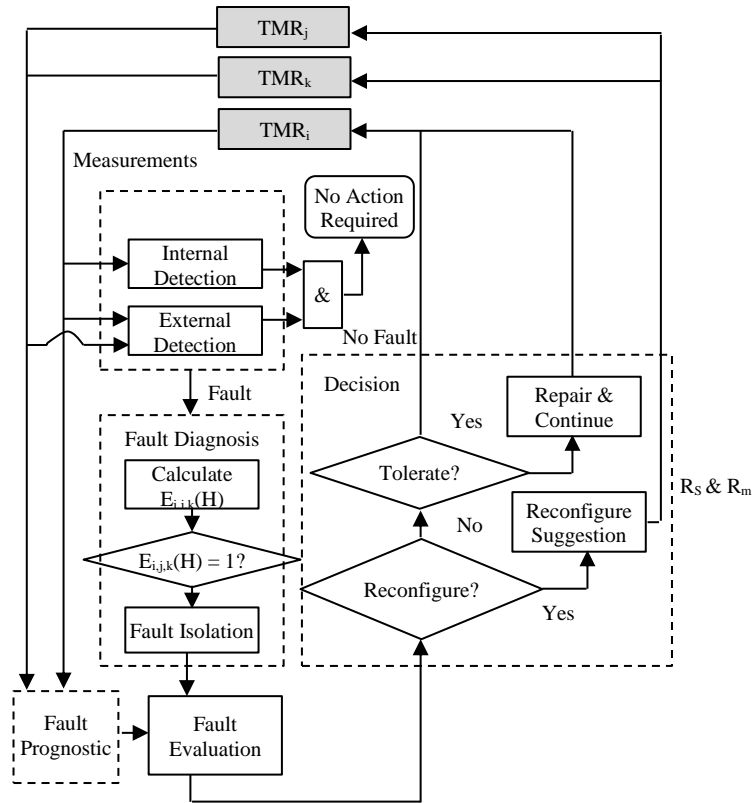


Figure 6-6: The flowchart of the decision making in TMR_i

If the semiconductor technology used in one channel (A_i) has no capacity to operate correctly in the given radiation environment ($R_i = 0$), or a channel (A_i) and its spare (S_i) are both failed, this channel and its spare will be power-off. Otherwise, only one of them is power-on. The active state of all channels (A_i and S_i) can be described in Eq. (6-6).

$$\begin{cases} S_i = 0 \& A_i = 0, & \text{if } F_{A_i} = 1 \& F_{S_i} = 1, \text{ or } R_i = 1 \\ S_i = \bar{A}_i, & \text{otherwise} \end{cases} \quad (6-6)$$

The detailed logics of the reconfiguration commands are determined by the outputs of the fault diagnosis and prognosis schemes, which are illustrated in Eq. (6-7) and Eq. (6-8).

The signal R_S is used to switch the power supply between the active channel and its spare; and the signal R_M is used to remove the power supply of one active channel and that of its spare. If one of the detection function ($E_i(H)$), prognostic function ($E_i(P)$), and the predicted channel (R_i) selection is set, reconfiguration commands will be issued.

$$R_{Si} = \bar{R}_{Si} \quad \text{if } E_i(H) \geq 1 \text{ or } E_i(P) \geq 1 \& R_i = 0 \quad (1 \leq i \leq 3). \quad (6-7)$$

$$\begin{cases} R_{Mi} = 0 & \text{if } R_j = 1 \text{ or } R_k = 1 \quad (1 \leq i, j, k \leq 3, i \neq j \neq k) \\ R_{Mi} = 0 & \text{if } F_{Aj} = 1 \text{ and } F_{Sj} = 1 \quad (1 \leq i, j \leq 3, i \neq j) \\ R_{Mi} = 1 & \text{otherwise} \end{cases} \quad (6-8)$$

Signals for the reconfigurator suggestions are generated as a result of the decision-making unit in other channels, as illustrated in Table 6-1.

Table 6-1: The provider of the signals for reconfigurator suggestions

| Reconfigurator signal | A ₁ & S ₁ | A ₂ & S ₂ | A ₃ & S ₃ | Primary |
|---|---------------------------------|---------------------------------|---------------------------------|---------|
| R _{S1} | | ✓ | ✓ | |
| R _{S2} | ✓ | | ✓ | |
| R _{S3} | ✓ | ✓ | | |
| R _{M1} &R _{M2} &R _{M3} | | | | ✓ |

6.3.3 Analysis

In general, it is difficult to online detect radiation response of each semiconductor device in an electronic system without additional measurement/testing units. In the developed redundant system, the detection focuses on the detection from circuit- and system-level. All circuit blocks and subsystems are monitored by external channel and/or itself to rapid remove its power when it encounters radiation damage. Then, according to the output of circuit blocks and subsystems, the damage of component can be analyzed. In a typical digital communication system, a sender is usually conducted by variety semiconductor component, which is listed in Column 2 of Table 6-2. The detailed radiation response of each component in this work and related damage result on the subsystem is listed in Column 3, 4, and 5 of Table 6-2, and its detection method is illustrated in Column 6.

Table 6-2: The analysis of faults and detection mechanism

| Function | Component | Radiation effects | Radiation responses of component | Damage response | Detection mechanism |
|--|-------------------------|-----------------------------------|---|---|---------------------|
| <i>Input Source</i> | Voltage reference | TID | The degradation of V_z , within specification for high dose rate | The output voltage decreases, OPs work nonfunctional. | External detection |
| | | SEU, SEL | Short only for SEU, increasing with a latchup current. | | |
| | Bipolar OP | TID | The degradation is depending on both the manufacturer and the circuit configuration. | OPs work nonfunctional. The output of the function of input source will be incorrect. | External detection |
| | | SEL | The degradation in current during irradiation. | | |
| | | SET | To be susceptible to SET, positive SETs are expected for positive supply voltage, both input and supply voltages affect amplitude and duration | | |
| | NPN BJT | TID | The primary ionizing response of <i>BJTs</i> is the degradation of the current gain $\beta (I_c/I_b)$, particularly at the low dose-rates. | The output of the function of input source will be incorrect. | External detection |
| <i>Source Encoder</i> | Voltage reference diode | TID | Increase of the reverse current and the changes of the forward voltage. | The AD's reference voltage will be incorrect. | External detection |
| | A/D converter | TID | Electronic parameters are higher under high radiation dose, the part experiences functional failure at high irradiation levels. | The output of the functions of source encoder will be incorrect. | External detection |
| | | SEU | A number of least significant bits (LSBs) are masked out with the condition of positive analog input; the LET threshold for the negative input is significantly higher. | | |
| | | SEL | The LET threshold for SEL is higher, no SEL was observed in some radiation tests. | | |
| | | SEFI | To cause every conversion to be in error until they were reset by cycling power to the device. | | |
| <i>Channel Encoder & Decision Making & Digital Modulator</i> | Micro-controller (CPU) | TID | Parameters exceed the maximum specification limit when the dose is more than 10 K Rad (Si). | Microcontroller will be nonfunctional. | External detection |
| | | SEU, SEL, SEFI on SRAM | A logic gate switch, voltage transients, alteration of stored information, and destructive effects. | SRAM will be nonfunctional. | Internal detection |
| | | SET, SEL, SEU, SEFI, TID on Flash | SETs are high current transients, possibly upset producing events; memory's contents are altered during the transient events. | Flash will be nonfunctional. | Internal detection |
| | | SEE on GPIO | The logical switch on GPIO ports. | The output of GPIO port will be nonfunctional. | External detection |
| | Logic gate | TID | The degradation of electronical parameters during high irradiation level; the part is functional and stays within the specification limit. | Microcontroller will be nonfunctional | External detection |
| | | SEU,SEL | A logic gate switch, destructive effects occur. | | |
| <i>Transceiver</i> | Voltage reference diode | TID | Increase of the reverse current and the changes of the forward voltage. | Wireless transmitter will not work. | Internal detection |
| | Varactor | TID | Increase of the reverse current not of a serious degree, and the forward-voltage drop not essentially change. | Wireless transmitter will not work. | Internal detection |
| | Wireless transmitter | TDI | The failure of functions. | Wireless transmitter will be nonfunctional. | External detection |

As illustrated in Table 6-2, when radiation effects on semiconductor components happen, the function of related circuit block and/or subsystem may not work or be nonfunctional. Then, through the external detection and/or the internal detection of the nonfunctional of

subsystems, semiconductor component can be online monitored. Subsequently, the decision-making unit generates reconfiguration suggestions to rapid remove the power of its channel and to power on its spares. The whole system will not work when all redundant channel are damaged.

6.4 Performance Evaluation of the Developed System Architecture

6.4.1 Emulation of Radiation Damages

1) Radiation-induced damages considered in this work

As previously discussed, the emulation of radiation-induced failure is also a critical element to evaluate the effectiveness and correctness of the design. This work combines with two emulation methods to mimic radiation responses of semiconductor component: circuit emulation, which is based on hardware-implemented fault injection, using external circuits to mimic circuit responses under radioactive conditions; and logic emulation, which is based on software-implemented fault injection, and uses injection commands to forcibly control and/or stop system functions. According to the analysis listed in Table 6-2, the radiation failure modes concerned in this work are listed as follows.

- (1) Total dose effects on bipolar devices and circuits, such as diode, BJT, OP Amplifier;
- (2) Total dose effects on MOS devices and circuits, such as MOSFET, A/D converter, microcontroller, transceiver;
- (3) Single event effects on *MOSFET* devices, such as SEB, SEGR;
- (4) Single event effects on integrated circuits (ICs) (microcontroller, SRAM, Flash, wireless transceiver, etc.), such as SEU, SET, SEL, SEFI.

2) Hardware emulation bench

In the design phase of electronic systems for high level radiation environments, evaluating the system's weaknesses and effectiveness is necessary but also difficult.

Generally, the evaluation can be accomplished by a physical radiation test, which uses external perturbation sources, such as natural and accelerated particle radiation, laser beams, pin forcing, etc.; such tests are very precise (Quinn et al., 2013). However, physical radiation tests are not always suitable in the design phase due to their excessive complexity and expense. Evaluation can also be accomplished by testing via a simulated environment, which usually uses logic resources of the circuit or system to access internal elements and insert the effect of a fault, according to the fault model (Quinn et al., 2013).

In this work, a hardware emulation bench is developed to evaluate the correctness of the proposed architecture. The bench uses fault injection techniques to mimic radiation damages on semiconductor devices. It combines with two emulation methods: logic emulation (LE), which is based on software-implemented fault injection, and uses injection commands to forcibly control and/or stop system functions; and circuit emulation (CE), which is based on hardware-implemented fault injection, using external circuits to mimic circuit responses under radioactive conditions. The architecture of this emulation bench is illustrated in Figure 6-7.

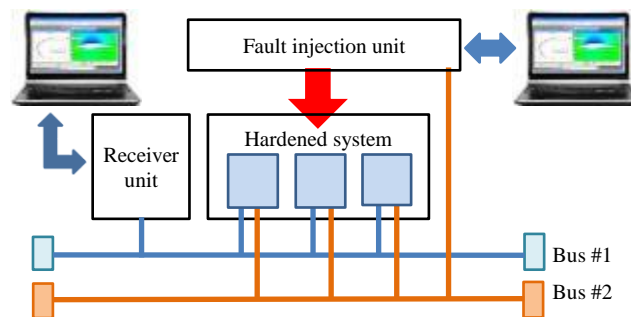


Figure 6-7: The architecture of the developed hardware emulation bench

The developed hardware emulation bench includes four parts: a redundant wireless device, a wireless gateway, emulation circuits, and a control tool. The emulation bench is built with two communication buses: bus #1 (915MHz network) is used to transmit/receive the normal communication data; and bus #2 (RS485) is used to transmit/receive commands/reports for fault injection. This emulation bench is illustrated in Appendices A.

6.4.2 Actual Evaluation and Results

Variables ($R_i, E_i(P), E_i(H)$) under several different cases and related experimental results (A_i, S_i) on the hardware emulation platform are listed in Table 6-3. Specifically, other cases are not listed in the table due to their similarity to the listed cases. The experimental results show that wireless channels can switch smoothly in several hundred milliseconds when single faults and multi-faults are inserted; reconfiguration suggestions are also correctly generated in the architecture's decision-making unit. Therefore, the proposed architecture can clearly be shown to work smoothly and the logics of fault diagnosis, fault prognostic, and the logic of decision unit are correct and effective.

Table 6-3: Summary of variables logic and experimental results in hardware emulation bench

| Variables | | | | | | | | | Previous State | | | | | | Experimental results | | | | | |
|-----------|-----|-----|--------|--------|--------|--------|--------|--------|----------------|----------------|----------------|----------------|----------------|----------------|----------------------|----------------|----------------|----------------|----------------|----------------|
| R-1 | R-2 | R-3 | E(P)-1 | E(P)-2 | E(P)-3 | E(H)-1 | E(H)-2 | E(H)-3 | A ₁ | A ₂ | A ₃ | S ₁ | S ₂ | S ₃ | A ₁ | A ₂ | A ₃ | S ₁ | S ₂ | S ₃ |
| 0 | 0 | 1 | 0 | 0 | x | 0 | 0 | x | 1 | 1 | 1 | 0 | 0 | 0 | 1 | 1 | 0 | 1 | 0 | 0 |
| 0 | 0 | 1 | 1 | 0 | x | 0 | 0 | x | 1 | 1 | 1 | 0 | 0 | 0 | 0 | 1 | 0 | 1 | 1 | 0 |
| 0 | 0 | 1 | 0 | 0 | x | 0 | 1 | x | 1 | 1 | 1 | 0 | 0 | 0 | 1 | 0 | 0 | 1 | 1 | 0 |
| 0 | 1 | 0 | 0 | x | 0 | 0 | x | 0 | 1 | 1 | 1 | 0 | 0 | 0 | 1 | 0 | 1 | 1 | 0 | 0 |
| 0 | 1 | 0 | 1 | x | 0 | 0 | x | 0 | 1 | 1 | 1 | 0 | 0 | 0 | 0 | 0 | 1 | 1 | 1 | 0 |
| 0 | 1 | 0 | 0 | x | 0 | 1 | x | 0 | 1 | 1 | 1 | 0 | 0 | 0 | 0 | 0 | 1 | 1 | 1 | 0 |
| 1 | 0 | 0 | x | 0 | 0 | x | 0 | 0 | 1 | 1 | 1 | 0 | 0 | 0 | 0 | 1 | 1 | 0 | 1 | 0 |
| 1 | 0 | 0 | x | 1 | 0 | x | 0 | 0 | 1 | 1 | 1 | 0 | 0 | 0 | 0 | 0 | 1 | 0 | 1 | 1 |
| 1 | 0 | 0 | x | 0 | 0 | x | 1 | 0 | 1 | 1 | 1 | 0 | 0 | 0 | 0 | 0 | 1 | 0 | 1 | 1 |
| 0 | 0 | 0 | 1 | 0 | 0 | 0 | 0 | 0 | 1 | 1 | 1 | 0 | 0 | 0 | 0 | 1 | 1 | 1 | 0 | 0 |
| 0 | 0 | 0 | 0 | 0 | 0 | 1 | 0 | 0 | 1 | 1 | 1 | 0 | 0 | 0 | 0 | 1 | 1 | 1 | 0 | 0 |
| 0 | 0 | 0 | 1 | 1 | 0 | 0 | 0 | 0 | 1 | 1 | 1 | 0 | 0 | 0 | 0 | 0 | 1 | 0 | 1 | 1 |
| 0 | 0 | 0 | 0 | 0 | 0 | 1 | 1 | 0 | 1 | 1 | 1 | 0 | 0 | 0 | 0 | 0 | 1 | 0 | 1 | 1 |
| 0 | 0 | 0 | 1 | 0 | 0 | 1 | 0 | 0 | 1 | 1 | 1 | 0 | 0 | 0 | 0 | 1 | 1 | 1 | 0 | 0 |
| 0 | 0 | 0 | 1 | 0 | 0 | 0 | 1 | 0 | 1 | 1 | 1 | 0 | 0 | 0 | 0 | 0 | 1 | 1 | 1 | 0 |
| 0 | 0 | 0 | 1 | 1 | 0 | 0 | 0 | 0 | 1 | 1 | 1 | 0 | 0 | 0 | 0 | 0 | 1 | 1 | 1 | 0 |
| 0 | 0 | 0 | 0 | 0 | 0 | 1 | 1 | 0 | 1 | 1 | 1 | 0 | 0 | 0 | 0 | 0 | 1 | 1 | 1 | 0 |
| 0 | 0 | 0 | 1 | 0 | 0 | 1 | 0 | 0 | 1 | 1 | 1 | 0 | 0 | 0 | 0 | 1 | 1 | 1 | 0 | 0 |
| 0 | 0 | 0 | 1 | 0 | 0 | 0 | 1 | 0 | 1 | 1 | 1 | 0 | 0 | 0 | 0 | 0 | 1 | 1 | 0 | 0 |
| 0 | 0 | 0 | 1 | 0 | 0 | 0 | 1 | 0 | 1 | 1 | 1 | 0 | 0 | 0 | 0 | 0 | 1 | 1 | 1 | 0 |
| 0 | 0 | 0 | 1 | 0 | 0 | 0 | 1 | 0 | 1 | 1 | 1 | 0 | 0 | 0 | 0 | 0 | 1 | 1 | 1 | 0 |

Notes: Results of many cases are omitted from the table due to their similarities with those given cases. 'x' stands for 0 or 1.

The experimental results have shown that wireless channels can switch smoothly in several hundred milliseconds (less than 500ms) when single- and multi-faults are inserted; reconfiguration suggestions are also correctly generated in the architecture's decision-making unit. Therefore, the proposed architecture can clearly be shown to work smoothly and the logics of fault diagnosis, fault prognostic, and decision unit are correct and effective.

6.5 Conclusions

In this Chapter, a radiation-tolerant architecture with a decision making unit is presented to allow COTS-based electronic systems for highly radioactive environments through independent redundancy, online fault detection, real-time preventive remedial actions, and rapid power loss/recovery. To evaluate the proposed architecture, a wireless communication system with redundant and diversified channels is implemented as a case study; and a simulated fault injection experiment has been performed on a hardware bench. The experimental results have shown, the developed radiation-tolerant architecture was verified to effectively work, and wireless channels were shown to switch smoothly in several hundred milliseconds (less than 500ms) when single- and multi-faults are inserted. The logics of fault diagnosis, fault prognostic, and decision unit work correctly.

Therefore, the developed radiation-tolerant architecture can be used to design COTS-based systems to achieve the independence, diversified, and redundancy without additional detection units and/or hardware voters. The function of fault detection and diagnosis, the algorithm of fault prognosis, the assessment method of radiation-tolerance, and the results of the physical radiation test will all be explained in the following Chapters.

Chapter 7

7 Design Part IV: Online Fault Detection Mechanism

As previously discussed, methods of rapid power off are therefore highly effectively in protecting electronic systems under ionizing radiation, the key step is to timely detect the fault and the damage. Fault diagnosis techniques, such as case-based reasoning (CBR), rule-based reasoning (RBR), model-based approaches, machine learning (ML) approaches, artificial neural networks (ANN), etc., have been applied to isolate the nature and the location of the failures; and the correct diagnosis information is then used to reconfigure the unit to recover the functionality of the system (Fenton *et al.*, 2001). In fact, an effective method of fault detection and diagnosis (FDD) plays an important role in some radiation-hardened electronic systems.

This Chapter starts with the analysis of radiation damages in electronic systems. Subsequently, the online detection mechanism of radiation damages is illustrated, as well as the real-time diagnosis algorithm is discussed. Finally, some experimental tests are used to validate the effectiveness and correctness of the developed detection mechanism. As well as the detection coverage under the given radiation condition (20 K Rad (Si)) is given.

7.1 Problem Statement

Most existing fault detection and diagnosis (FDD) methods for electronic systems mainly focus on common hardware faults in redundant systems, not on cross-board radiation damages (Fenton *et al.*, 2001; Gao *et al.*, 2015). Some model-based FDD methods have been considered, but it is not a trivial task to develop accurate models to deal with potential failure modes caused by radiation (Fenton *et al.*, 2001; Gao *et al.*, 2015). Moreover, those methods usually detect and diagnose fault occurrences by using additional measurement/test units or majority voters, which are also affected and damaged by radiation. Therefore, it represents a major weakness in the whole system and as such should also be protected.

As previously discussed, the difficulty to diagnose radiation damages in electronic systems is the lack of the self-diagnosis architecture and the online diagnosis method of post-irradiation responses. Key issues to deal with the detection and diagnosis of radiation damages are listed as follows:

- (1) The analysis and identification of fault, error, and failure of devices and circuits under the given radiation condition.
- (2) An online logic to detect radiation damages and a real-time algorithm to diagnose and to locate radiation damages.
- (3) The validation of the developed detection method without physical radiation test in the design phase.

To address these issues, in this Chapter, combining with the radiation-tolerant architecture developed in Chapter 6, an online detection and diagnostic approach is developed to timely identify/locate radiation damage in the system for prolonging its life, which are significant for the proposed radiation-tolerant architecture.

7.2 The Framework of Detection Mechanism

The functional organization and data flow of the fault detection and diagnosis unit can be illustrated in Figure 7-1. This unit consists of two parts: (a) database creation and (b) real-time fault detection and prognosis for decision-making. In the first part, data specifications of the electronic components, boundaries of faults, errors, and failure are obtained to create an alarm database. Such information is used to create a fault detection hypothesis test framework. During online operation, measurements are then used to test the hypothesis, subsequently, to generate appropriate decisions in the decision-making unit for the reconfigurator.

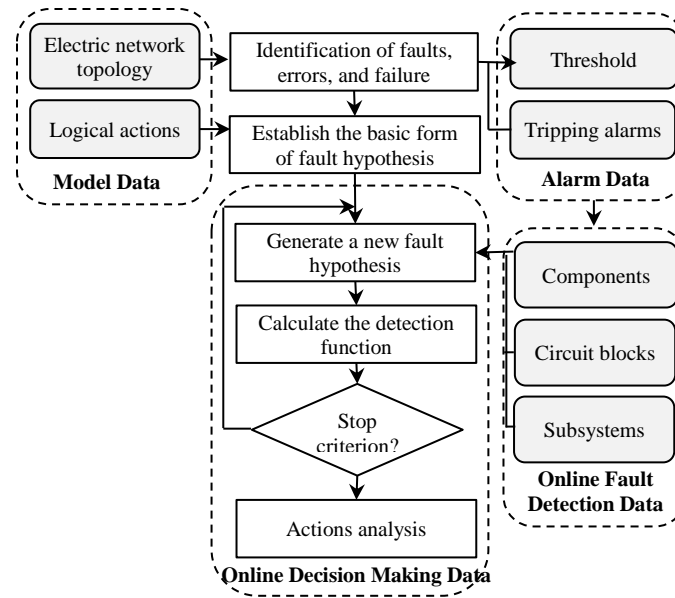


Figure 7-1: The framework of the fault detection and diagnosis method

7.3 Analysis of Radiation-Induced Damages

7.3.1 Analysis Model

According to abstraction levels of electronic systems, a hierarchical fault model is illustrated in Figure 7-2. Radiation disturbances and/or other disturbances will affect device level directly, and then the disturbance will be transmitted to circuit level and system level (subsystem). Faults at device level (L_1) correspond to sensor and semiconductor components, faults at circuit level (L_2) correspond to analog circuits and digital circuits, and faults at system level (L_3) correspond subsystems or functional modules.

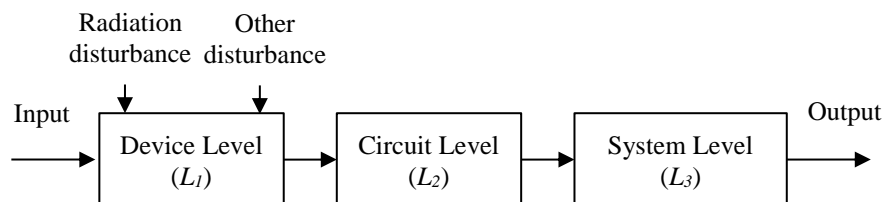


Figure 7-2: Hierarchical fault model for electronic systems

The state of each level is defined as x_i ($i = 1, 2, 3$). The model can be described as follows:

$$\begin{cases} x_1(k+1) = (A + \Delta A)x(k) + (B + \Delta B)u(k) + B_r n_r(k) + B_o n_o(k) \\ x_2(k+1) = (C + \Delta C)(x_1(k) + \Delta x_1) \\ x_3(k+1) = y(k+1) = (D + \Delta D)(x_2(k) + \Delta x_2) \end{cases} \quad (7-1)$$

where

$x_\varphi(k) \in R^n$, $u(k) \in R^m$, $y(k) \in R^p$, $n_r(k) \in R^{l_r}$, $n_o(k) \in R^{l_o}$ is the state of the different levels, the input, radiation fault, and the component/parameter fault, respectively. A, B, C, D are known parameter matrices; and $\Delta A, \Delta B, \Delta C, \Delta D, \Delta x_1, \Delta x_2$ are unknown fault and errors.

As previously discussed, the system should detect and diagnose faults and errors ($\Delta A, \Delta B, \Delta C, \Delta D, \Delta x_1, \Delta x_2$) in a timely manner. A number of assumptions for faults concern in this work are listed as follows:

- (1) Each component is either functioning, fault and failure;
- (2) Each circuit block is functional, operating incorrectly, and failure;
- (3) Each subsystem is functional, operating incorrectly, and failure;
- (4) All components are functional at initial moment.

7.3.2 Definition and Properties

Definition 1 (Device): An electronic system consists of a number (n_d) of components.

$$D = \{d_1, \dots, d_i, \dots, d_{n_d}\} \quad (1 \leq i \leq n_d).$$

where d_i represents the state of the i_{th} component with $d_i = 0$ and 1, respectively, corresponding to its functional and fault state.

Definition 2 (Circuit): An electronic system consists of a number (n_c) of circuit blocks. Each module consists of a number of components.

$$C = \{c_1, \dots, c_j, \dots, c_{n_c}\} \quad (1 \leq j \leq n_c) \quad .$$

where c_j represents the j_{th} circuit of the electronic system.

Similar representations are used to represent the operational and fault modes at

Definition 2 in all subsequent definitions.

Definition 2 (Subsystem): An electronic system can be decomposed into a number (n_s) of subsystems. Each subsystem consists of several circuit modules.

$$S = \{s_1, \dots, s_k, \dots, s_{n_s}\} \quad (1 \leq k \leq n_s) \quad .$$

Definition 3 (Functional State): For each circuit module and subsystem, two states can be defined.

X_C, X_S represent the state that temporary fault or recovered failure in the circuit blocks and subsystems, with $x = 0$ for operational and 1 for temporary fault or recovered failure, respectively.

Y_C, Y_S represent the state that permanently fails in the circuit blocks and subsystems, with $y = 0$ for no failure and 1 for permanent failure, respectively.

For each circuit module, the following conditions can be defined for the operational state.

$$X_c = \{x_{c_1}, \dots, x_{c_j}, \dots, x_{c_{n_c}}\} \quad (1 \leq j \leq n_c) \quad .$$

If c_j operates incorrectly, $x_{c_j} = 1$, otherwise $x_{c_j} = 0$.

$$Y_c = \{y_{c_1}, \dots, y_{c_j}, \dots, y_{c_{n_c}}\} \quad (1 \leq j \leq n_c) \quad .$$

If c_j is completely failed, $y_{c_j} = 1$, otherwise $y_{c_j} = 0$.

For each subsystem, the following state can be defined:

$$X_s = \{x_{s_1}, \dots, x_{s_k}, \dots, x_{s_{n_s}}\} \quad (1 \leq k \leq n_s).$$

If s_k operates incorrectly, $x_{s_k} = 1$, otherwise $x_{s_k} = 0$.

$$Y_s = \{y_{s_1}, \dots, y_{s_k}, \dots, y_{s_{n_s}}\} \quad (1 \leq k \leq n_s).$$

If s_k is completely failed, $y_{s_k} = 1$, otherwise $y_{s_k} = 0$.

Definition 4 (Logic Action): R_{dc} is the relation from set D to set C , and R_{cs} is the relation from set C to set S . The entries of R_{dc} and R_{cs} are defined by:

$$M_{dc_{i,j}} = \begin{cases} 1, & (d_i, c_j) \in R_{dc} \\ 0, & (d_i, c_j) \notin R_{dc} \end{cases}.$$

and

$$M_{cs_{j,k}} = \begin{cases} 1, & (c_j, s_k) \in R_{cs} \\ 0, & (c_j, s_k) \notin R_{cs} \end{cases}.$$

Thus, the relation from set D to set S can be expressed by:

$$M_{ds_{i,k}} = M_{dc_{i,j}} \times M_{cs_{j,k}}.$$

Definition 5 (Fault Set): for the circuit block c_j , the fault set is

$$Fc_j = \{Fc_{j_1}, \dots, Fc_{j_{n_d}}\}.$$

Fc_{j_i} describes that ionizing radiation effects of i_{th} component d_i to the circuit block c_j .

Fc_{j_0} denotes the functional state of the circuit block c_j , which considers components tolerance effect.

$$Fc_{j_i} = 0 \quad \text{if } M_{i,j} = 0.$$

For the subsystem s_k , the fault set is

$$FS_k = \{FS_{k_1}, \dots, FS_{k_{n_c}}\}.$$

FS_{k_j} describes that ionizing radiation effects of j_{th} circuit block c_j to the sub-system s_k .

FS_{k_0} denotes the functional state of the subsystem s_k .

$$FS_{k_j} = 0 \quad \text{if } M_{j,k} = 0.$$

7.3.3 Identification of Fault, Error, and Failure

The identification focuses on analog and mixed circuit blocks with certain input. Suppose that u is the measured voltage of the output of one circuit block (c_j). An ambiguity region of the output of the circuit block (c_j) for all components d_i can be created in time domain.

$$u^{d_i}(t) = \{u^{d_1}(t), u^{d_2}(t), \dots, u^{d_{n_d}}(t)\}.$$

with

$$u^{d_i}(t) = 0 \quad \text{if } M_{i,j} = 0 (1 \leq i \leq n_d, 1 \leq j \leq n_c).$$

In general the element value with component tolerance is changed from Y to $Y + \Delta Y$. The upper and lower envelopes of the output of the circuit block (c_j) for all components responses are:

$$u_{upper}^d(t) = \{\max(u^{d_1}(t), \max(u^{d_2}(t)), \dots, \max(u^{d_{n_d}}(t)))\}.$$

and

$$u_{lower}^d(t) = \{\min(u^{d_1}(t), \min(u^{d_2}(t)), \dots, \min(u^{d_{n_d}}(t)))\}.$$

Thus, the response for the functional state of the circuit block (c_j) is:

$$u_{lower}^d(t) \leq u(t) \leq u_{upper}^d(t).$$

On the other hand, for the output of the circuit block (c_j) of each component d_i under the condition of the fault, error, and failure ($u_{fault}^{d_i}$, $u_{err}^{d_i}$, and $u_{fail}^{d_i}$), the upper and lower envelopes of the circuit c_j output for sensitive component d_i under the fault state are:

$$u_{fault}^{d_i}(t) \leq u(t) \leq u_{err}^{d_i}(t). \quad (7-2)$$

$$u_{err}^{d_j}(t) \leq u(t) \leq u_{fail}^{d_j}(t). \quad (7-3)$$

The fault, error, and failure of the circuit block (c_j) response $u_{fault}^{c_j}$, $u_{err}^{c_j}$, and $u_{fail}^{c_j}$ can also be obtained. The upper and lower envelopes of the fault state of the circuit c_j response are:

$$u_{fault}^{c_j}(t) \leq u(t) \leq u_{err}^{c_j}(t). \quad (7-4)$$

The upper and lower envelopes of the broken state of the circuit block (c_j) response are:

$$u_{err}^{c_j}(t) \leq u(t) \leq u_{fail}^{c_j}(t). \quad (7-5)$$

According to Eq. (7-2) to Eq. (7-5), malfunction of components and circuit blocks in analog and mixed circuits can be classified into several types:

- (1) Component operates incorrectly, the output of related circuit block should be range from $u_{fault}^{d_i}$ to $u_{err}^{d_i}$;
- (2) Component fails, the output of related circuit block should be range from $u_{err}^{d_i}$ to $u_{fail}^{d_i}$;
- (3) Circuit block operates incorrectly, the output of circuit block should be range from $u_{fault}^{c_j}$ to $u_{err}^{c_j}$;
- (4) Circuit block is broken; the output of circuit block should be range from $u_{err}^{c_j}$ to $u_{fail}^{c_j}$.

Fault diagnosis of analog and mixed circuits is to identify the current state of the circuit block according to the measured value u . If u is within the neighborhood of the nominal value under fault F_i , the similarity between the current state and fault F_i is high. On the other hand, if u is out of the neighborhood, the similarity will be low. $U_{F_i}(u)$ is used to express the similarity between the current state and fault F_i state. According to the maximum degree of criterion, if fault F_i satisfies

$$U_{F_i}(u) = \max \{U_{F_0}(u), U_{F_1}(u), U_{F_2}(u), \dots, U_{F_{nd}}(u)\}. \quad (7-6)$$

Then we can deem that u is subordinate to F_i , and the current state is more similar with fault F_i state.

7.4 Detection of Radiation Damages

7.4.1 Determination of $U_{F_i}(u)$

According to the characteristics of different circuit blocks and/or subsystems, the method of the determination of $U_{F_i}(u)$ can be separated into internal detection and external detection. Even though Figure 7-1 illustrates a general framework for fault detection and diagnosis schemes, the current design includes three distinctive levels: devices, circuits, and subsystems. Damage to the device propagates to circuit and subsystem. According to the characteristics of circuit modules and subsystems, detection of fault state can be carried out within its own channel or by using the data from other channels. For circuit modules, such as power related circuits, self-test circuits, faults can be detected within the channel. However, other circuit modules, particularly with uncertain inputs, such as sensor inputs, sub-functional blocks, it would be difficult to validate their functionalities within the channel. The fault detection is often accomplished by comparing with the measurements from other channels. These two approaches can be shown in Figure 7-3.

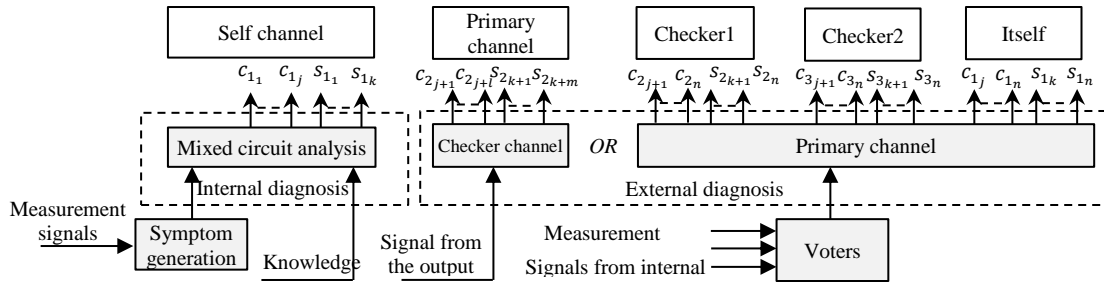


Figure 7-3: The block diagram of detection logical allocation

7.4.2 Internal Detection

For analog and mixed circuits with certain input, the determinate $U_{F_i}(u)$ is accomplished by the comparison of the measured voltage with the voltage distribution under the fault state. The voltage distribution under the fault state can be obtained from the calculation result of the identification of fault, error, and failure. For example, suppose the voltage distribution of a circuit block (c_j) under the fault state is presented as Figure 7-4.

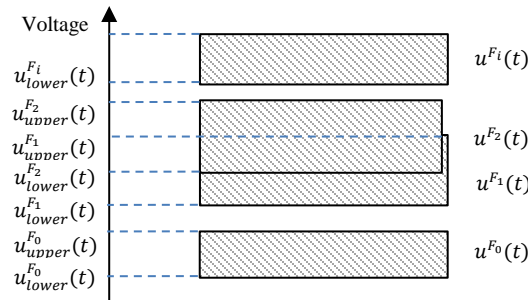


Figure 7-4: Voltage levels of a circuit block under the fault state

When there has free space between $u^{F_0}(t)$ and $u^{F_i}(t)$, if the measured voltage u is located at the region of $u^{F_0}(t)$ or $u^{F_i}(t)$, then

$$U_{F_0}(u) = 1 \quad \text{or} \quad U_{F_i}(u) = 1.$$

When there has no free space between $u^{F_1}(t)$ and $u^{F_2}(t)$. If u is located at the overlap region of $u^{F_1}(t)$ and $u^{F_2}(t)$, the similarity between the current state and fault F_1 , F_2 state can be determined by sensitivity analysis for d_1 and d_2 .

7.4.3 External Detection

For those circuit blocks with uncertain input, the determinate $U_{F_i}(u)$ is accomplished by combining with the error detection code and the voter mechanism. The information of circuit blocks and subsystems can be encoded and transmitted to the primary channel through the internal bus. Then, the primary channel accomplishes the function of detection damages among all three channels. As previously mentioned, due to the inputs of those circuits are unknown, moreover, in high level radiation fields, radiation damages may occur in one or two even three of the triplication simultaneously. The detection of radiation damages in those circuits is difficult by only using majority voters and/or additional test/detection units. A filter function is therefore used to detect radiation damages in three channels according to past and present measurements, which is expressed in Eq. (7-7). The detection function will output the states of those circuit blocks.

$$[X_{1_j}, X_{2_j}, X_{3_j}, Y_{1_j}, Y_{2_j}, Y_{3_j}] = f(m_{1_j}, m_{2_j}, m_{3_j}, p_{1_j}, p_{2_j}, p_{3_j}). \quad (7-7)$$

where

m_{l_j} is the present measurement of the circuit block j in the channel l ;

p_{l_j} is the past measurement of the circuit block j in the channel l ;

X_{l_j}, Y_{l_j} is the state of the circuit block j in the channel l .

7.5 Diagnosis of Radiation Damages

7.5.1 Fault Hypothesis

Based on the above definitions, a fault hypothesis for malfunctions of circuit blocks and subsystems can be formed in Eq. (7-8), where the goal is to integrate states of circuit blocks and subsystems.

$$H = [X, Y]. \quad (7-8)$$

where X is the summary of X_C and X_S , as well as Y is the summary of Y_C and Y_S .

7.5.2 Detection Function

A detection function reflects the credibility of H as defined in Eq. (7-8). A smaller $E(H)$ suggests a higher credibility of H . If the detection function is equal or greater than unity, a reconfigure command should be issued.

$$E(H) = \sum_j^{n_c} (w_{xc_j} x_{c_j} + w_{yc_j} y_{c_j}) + \sum_k^{n_s} (w_{xs_k} x_{s_k} + w_{ys_k} y_{s_k}). \quad (7-9)$$

where w_{xc_j} , w_{yc_j} , w_{xs_k} , and w_{ys_k} are the weights of the discrepancy index. The range of the weights is from 0.1 to 1. If $w_1 \gg w_2$, it means that the discrepancy index w_1 is much more important than w_2 . The values of these weights are determined according to the significance of circuit blocks and subsystems in electronic systems.

7.5.3 Diagnosis Mechanism

The flowchart of fault detection loop in each channel is illustrated in Figure 7-5. The states of fault hypothesis (H_1, H_2, H_3) will be timely updated for the calculation of detection functions ($E(H_1), E(H_2), E(H_3)$) in each channel for all three channels. The results of fault detection are transmitted to the diagnosis loop for the calculation of objective function, then the decision making unit generates diagnosis results and reconfigure suggestions.

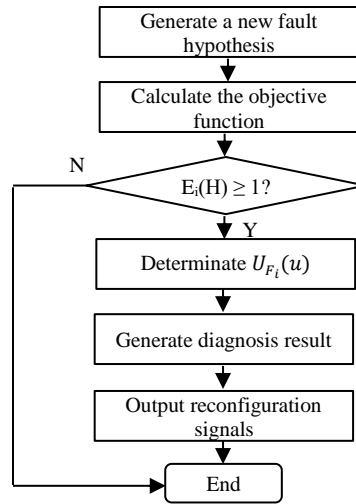


Figure 7-6: The flowchart of fault diagnosis function

7.6 Experimental Validation

7.6.1 Experimental Results

The proposed method of fault detection and diagnosis are validated in the developed hardware emulation bench which is described in Appendices A. Detailed information are listed in Table 7-1. Radiation effects and their responses of selected semiconductor devices are described in Column (5) and Column (6) of Table 7-1. The radiation damages concerned in this work are listed as follows:

- (1) Total dose effects on bipolar devices and circuits, such as diode, BJT, OP Amplifier;
- (2) Total dose effects on MOS devices and circuits, such as MOSFET, A/D converter, transceiver;
- (3) Single event effects on MOSFET devices, such as SEB, SEGR;
- (4) Single event effects on ICs (microcontroller, SRAM, Flash, etc.), such as SEU, SET, SEL, SEFI.

Above radiation-induced failure, several simple failures can be emulated through external circuits. However, most failures are very sophisticated due to the significant architecture

and fabrication technology of complicated circuits. They are therefore only performed through the method of software-implemented fault injection. All emulation approaches and related radiation-induced damages are summarized in Table 7-1.

Table 7-1: The summary of radiation-induced damages and emulation methods considered in this work

| Component | Fault number | Radiation-induced damage | Emulation method |
|-----------------------------|--------------|---|--|
| Diode | F1 | Gain degradation | (HW) Adding a current source to mimic gain degradation |
| | F2 | Loss of the function | (HW) Removing the component |
| BJT | F3 | The gain degradation at collector-emitter voltage | (HW) Adding a current source to mimic gain degradation |
| | F4 | The gain degradation at base-emitter voltage | (HW) Adding a current source to mimic gain degradation |
| | F5 | Loss of the function | (HW) Removing the component |
| OPs | F6 | The change of circuit parameters/ gain degradation | (HW) Adjusting resistor values to change amplify gain |
| | F7 | Loss of the function | (HW) Removing the component |
| MOSFET | F8 | Large threshold voltage shift, loss of on/off control | (HW) Injecting a voltage to change the ON/OFF state |
| | F9 | Destructive effects | (HW) A short circuit between the drain and the gate |
| | F10 | Loss of the function | (HW) Removing the component |
| Analog-to-digital converter | F11 | Loss of drive capability | (HW) Disconnect the output control signal |
| | F12 | Propagation delay and/or the change of circuit timing | (HW) Disconnect control/data signals |
| | F13 | Inaccurate conversion | (HW) Adjusting the input of the measurement signal |
| | F14 | Temporarily lose the functionality | (SW) Temporarily disable the function of transceiver |
| | F15 | Loss of the function / out of the control | (HW) Removing the component |
| Logic gate | F16 | The change of the voltage level | (HW) Inverting the voltage level |
| | F17 | Loss of drive capability | (HW) Disconnect the output signal |
| | F18 | Loss of the function | (HW) Removing the component |
| Voltage reference | F19 | Loss of drive capability | (HW) Adjusting the configure circuit |
| | F20 | Loss of the function | (HW) Removing the component |
| MCU | F21 | Loss of drive capability on GPIO | (HW) Disconnect the GPIO signal |
| | F22 | The invert of the voltage level | (HW) Inverting the voltage level of GPIO output |
| | F23 | The change of circuit timing parameter (inaccurate frequency) | (SW) Changing the timer period |

(Continued Table 7-1)

| Component | Fault number | Radiation-induced damage | Emulation method |
|--|--------------|--|--|
| | F24 | The change of circuit parameter (data / address bus) | (SW) Injecting a wrong value on data/address bus |
| | F25 | Temporarily lose the functionality (SEFI) | (HW) Hardware restart |
| | F26 | Loss of the function / out of the control | (HW) Removing the component/module |
| SRAM | F27 | Loss of drive capability on bus | (SW) Injection a wrong value on a unit of SRAM |
| | F28 | The invert of the voltage level of memory unit (SEU) | (SW) Injection a wrong value on a unit of SRAM |
| | F29 | Temporarily lose the functionality (SEFI) | (SW) Temporarily disable the function of SRAM |
| | F30 | Loss of the function / out of the control | (SW) Disable the function of SRAM |
| FLASH | F31 | Loss of drive capability on bus | (SW) Injection a wrong value on a unit of flash |
| | F32 | The change of the voltage level of memory unit | (SW) Injection a wrong value on a unit of flash |
| | F33 | Temporarily lose the functionality | (SW) Temporarily disable the function of flash |
| | F34 | Loss of the function / out of the control | (SW) Disable the function of flash |
| Transceiver | F35 | A loss of drive capability on control signal | (HW) Disconnect the control signal |
| | F36 | Non-function of receiving data | (HW) Disconnect the receiving circuit |
| | F37 | Receiving incorrect data | (SW) Injection a wrong data in receiving buffer |
| | F38 | Non-function of sending data | (HW) Disconnect the sending circuit |
| | F39 | Sending incorrect data | (SW) Injection a wrong data in sending buffer |
| | F40 | Incorrect frequency | (SW) Modifying the configuration of frequency |
| | F41 | Temporarily lose the functionality | (SW) Temporarily disable the function of transceiver |
| | F42 | Loss of the function | (SW) Disable the function of transceiver |
| HW: hardware-based emulation; SW: software-based emulation | | | |

As mentioned in Chapter 6, a hardware emulation bench, illustrated in Appendices A, is developed to evaluate the correctness of the proposed detection method. The bench uses a combination of fault injection techniques, which combined with two emulation methods, mimic radiation effects on semiconductor devices; logic emulation (LE), which is based on software-implemented fault injection, and uses injection commands to forcibly control and/or stop system functions; and circuit emulation (CE), which is based on hardware-

implemented fault injection, using external circuits to mimic circuit responses under radioactive conditions. With respect to each fault, related emulation method is listed in Column (4) of Table 7-1.

The hardware emulation platform includes an implementation of a wireless monitoring system as a case study of the proposed radiation-tolerant architecture. In this work, for simplicity, all channels are considered with the same hardware to validate the developed architecture and fault detection mechanism; and the system considers two uncertain input signals: 4~20mA and 0~100 Ω . The detailed information of the implementation of the wireless channel is given in Table 7-2. Specifically, those components with the high radiation resistances, such as resistance, capacitance, etc., are not listed in the table due to they have the capacity to survive in the given radiation condition. Each wireless channel consists of 13 semiconductor components (component-level), which are listed in the Column (2) of Table 7-2; 9 circuit blocks (circuit-level): 2 voltage reference circuit, 2 analog signal processing circuits, A/D convert circuit, memory circuit, controller circuit, wireless sending circuit, wireless receiving circuit; also includes 6 modules (system-level): signal input, source encoder, channel encoder, decision making, digital modulator, and transceiver.

Table 7-2: The information of the developed radiation-tolerant wireless device

| Comp. | Q. | FIT | Fault cases | Radiation response analysis | Detection Mechanism | Detection Period | Fault coverage |
|-----------------------|----|------|-------------|---|---------------------|------------------|----------------|
| Voltage reference | 1 | 3.30 | F19, F20 | The output voltage decreases, OPs work nonfunctional | External | 200 ms | 1/2 |
| OPs | 4 | 1.85 | F6, F7 | OPs work nonfunctional. The output of the function of input source will be incorrect. | External | 200 ms | 2/2 |
| NPN BJT | 1 | 2.45 | F3-F5 | The output of the function of input source will be incorrect. | External | 200 ms | 1/3 |
| Voltage reference | 1 | 3.30 | F19, F20 | The AD's reference voltage will be incorrect. | External | 200 ms | 2/2 |
| AD converter | 1 | 0.20 | F11-F12 | Out of control | External | 200 ms | 2/2 |
| | | | F13 | The output (10bits) of the functions of source encoder will be incorrect. | | | 7/10 |
| | | | F14-F15 | Loss of the functionality | | | 2/2 |
| Microcontroller (CPU) | 1 | 5.60 | F24 | Microcontroller will be nonfunctional. | External | 300 ms | 1/1 |
| | | | F23 | Timer period is incorrect. | Internal | 100 ms | 1/1 |
| | | | F27-F30 | SRAM (256 bytes) will be nonfunctional | Internal | 500 ms | 16/256 |
| | | | F31-F34 | Flash (4K bytes) will be nonfunctional | Internal | 300 ms | 256/4096 |
| | | | F21-F22 | The output of GPIO (32 bits) will be nonfunctional. | External | 500 ms | 24/32 |
| | | | F25, F26 | Microcontroller will not work. | External | 300 ms | 2/2 |
| Logic gate | 1 | 0.50 | F16-F18 | Microcontroller will be nonfunctional. | External | 300 ms | 3/3 |
| Diode | 1 | 3.30 | F1-F2 | Wireless transmitter may be nonfunctional | Internal | 500 ms | 1/2 |
| Varactor | 1 | 3.30 | F1-F2 | Wireless transmitter may be nonfunctional | Internal | 500 ms | 1/2 |
| Wireless transmitter | 1 | 1.90 | F35 | Out of control | Internal | 500 ms | 1/1 |
| | | | F36-F40 | Communication will be nonfunctional | External | 500 ms | 5/5 |
| | | | F41-F42 | Wireless transmitter will not work | External | 500 ms | 2/2 |

7.6.2 Detection Coverage

One way to quantify the effectiveness of the fault tolerance capability is by fault coverage measure C . This figure of merit is defined as the number of faults dealt with successfully over the total number of faults considered (Kim *et al.*, 2006).

$$C = P(\text{fault processed correctly} / \text{fault existence}). \quad (7-13)$$

Considering a system in a radiation environment, for a given time Δt , the fault detection coverage of a system C_{system} can be calculated by:

$$C_{system} = \frac{\sum_{i=1}^N C_{i,d} \cdot \lambda_i \Delta t}{\sum_{i=1}^N \lambda_i \Delta t} = \frac{\sum_{i=1}^N C_{i,d} \cdot \lambda_i}{\sum_{i=1}^N \lambda_i}. \quad (7-14)$$

where

$C_{i,d}$ is the detected faults in component i ; and λ_i is the failure rate of component i ($i = 1, 2, \dots, n_d$).

In the current validation process, for the chosen fault rates in Column 4 in Table 7-2 and experimental results, the detection coverage is calculated to be 62.11%. This means that 62.11% of perceivable radiation induced fault scenarios can be successfully dealt with.

7.7 Conclusions

In this Chapter, a method of fault detection and diagnosis within a radiation-tolerant architecture is developed to enhance the radiation tolerance and to prolong the life of electronic systems. To evaluate the proposed method, a number of simulated experiments through fault injection are performed on a developed hardware emulation bench. The experimental results have shown that the radiation-tolerant wireless device was verified to effectively work and the developed detection and diagnosis logic was also verified to timely detect the abnormal condition. The detection coverages of the developed method for the redundant wireless device is 62.11%. Moreover, the detection coverages can be improved if putting more resources into the function of fault detection but need more cost.

Based on the experiment results in this work, the developed detection and diagnosis method can timely detect and diagnose most of radiation damages in the radiation-tolerant architecture. It can therefore be applied to design redundant systems without rad-hardened devices for high level radiation fields. System validation through the physical radiation test will be presented in the following Chapters.

Chapter 8

8 Implementation: an Application of Wireless Monitoring System for Radiation Environments in NPPs

Considering various potential scenarios, e.g., the high level of radiation, the lack of power, and the damaged communication infrastructure, during a severe accident in nuclear power plants, a self-powered wireless monitoring system (WPAMS) is extremely useful in surveying the plant even when there is no functioning communication infrastructure during a severe post-accident situation, as well as those high level radiation fields in nuclear power plants. Key issue is to protect wireless devices for surviving in high level radiation environments. As previously mentioned, a number of radiation-hardened design techniques and methods are investigated in this research, which can be applied to implement the proposed wireless monitoring system. On the other side, this wireless monitoring system can be also used to validate the correctness and effectiveness of the investigated techniques and methods.

This Chapter starts with design considerations of the proposed wireless monitoring system for high level radiation environments in nuclear power plants. Subsequently, the developments of all devices in the system are described in detail, which include radiation-tolerant wireless device, gateway device, portable monitoring device, and remote monitoring station. Then, the developed system is tested in the normal condition, as well as related test results are presented.

8.1 Design Considerations

1) Design Requirements

The mission of a wireless monitoring system is to obtain essential information about the status of the plant even when there is no communication infrastructure, which is crucial to plant operators and emergency response teams to effectively manage and to mitigate the effects of the accident. In this mission, the issues listed in Chapter 2.1.2 may need to be considered and investigated.

As explained in Chapter 1.2, the highest radiation level considered in this research is 1 M Rad (Si). Those cases whose total radiation doses are more than 1 M Rad (Si) are not considered in this research.

2) Criteria Variables

The monitoring variables should refer the selection criteria of IEEE Std.-2016. The variable types include type A, B, C, D, and E.

- Type A: planned manually controlled actions for accomplishment of safety functions for which there is no automatic control.
- Type B: assess the process of accomplishing or maintaining plant safety functions
- Type C: indicate an actual breach of fission product barriers.
- Type D: indicate performance of safety systems, indicate the performance of required auxiliary support features, indicate the performance of other systems necessary to achieve and maintain a safe shutdown condition, verify safety system status.
- Type E: monitor the magnitude of releases of radioactive materials through identified pathways, monitor the environmental conditions used to determine the impact of release of radioactive materials through identified pathways, monitor radiation levels and radioactivity in the plant environs, monitor radiation and radioactivity levels in the control room and selected plant areas where access may be required for plant recovery.

Also Regulatory Guide 1.97 (rev 3) provides a graded method to requirements according to the importance of variables. Three separate categories are listed as follows.

- Category 1: provides the most stringent requirements and is intended for key variables.
- Category 2: provides less stringent requirements and generally applies to instrumentation designated for indicating system operating status.

- Category 3: is intended to provide requirements that will ensure that high-quality off-the-shelf instrumentation is obtained and applies to backup and diagnostic instrumentation.

One of the lessons we learned from the Fukushima accident is that the equipment should be for multi-purpose use under post-accident circumstances, such as radiation detecting, hydrogen monitoring, thermal imaging, pressure, temperature, gas, and humidity sensing. Considering those factors, the criteria variables and specifications for WPAMS are shown in Table 8-1. Furthermore, conditions of protection systems, such as water level in a spent fuel pool, coolant inventory, containment pressure, etc., also need to be monitored. The system should reserve some channels which used for monitoring those condition parameters. Moreover, those channels have flexible voltage range and can be reconfiguration according to sensors signals, e.g., 0.5v to 5v voltage signal, 4~20 mA current signal, etc.

Table 8-1: Criteria variables and specifications considered in the design of wireless monitoring systems for nuclear power plants

| Parameter | Type | Category R.G 1.97 | Measurement range |
|------------------------------------|--------|----------------------|----------------------|
| Neutron flux | Type B | 1 | 10^{-6} % to 100 % |
| Containment Hydrogen concentration | Type C | 1 | 0 to 30 vol-% |
| Containment area radiation | Type C | 1 | 1 to 10^7 R/hr |
| Containment atmosphere humidity | Type D | | 0% to 100% |
| Containment atmosphere temperature | Type D | 2 | 40 °F to 400 °F |

3) Potential Solution

Considering potential scenarios and issues during a severe accident, a wireless monitoring system, illustrated in Figure 8-1, is proposed in this work to obtain up-to-date information of the plant after a severe accident. The proposed monitoring system includes four types of devices: radiation-tolerant wireless devices (strong radiation field), gateway

device (low radiation field), portable monitoring device, and remote monitoring station. The detailed implementations of those devices are described in the follow.

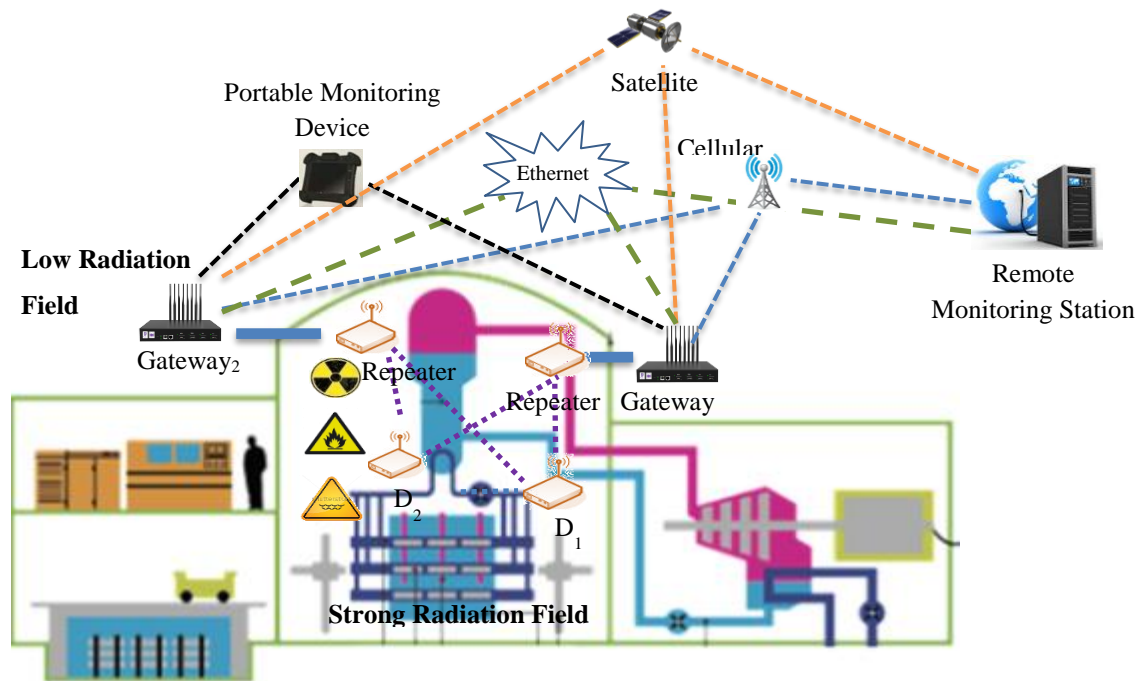


Figure 8-1: A potential wireless monitoring system for high level radiation environments in a nuclear power plant

8.2 Development of Wireless Monitoring System

8.2.1 Measurement and Transmission Unit

In the proposed monitoring system, wireless devices will be installed in high level radiation environments and are used to collect up-to-date environment parameters, such as temperature, humidity, gamma dose, neutron level, hydrogen level, water level, etc., and to transmit that information to the gateway which is installed out of the containment. Therefore they have to have high radiation resistance to survive in those environments. The previously investigated techniques will be used in the implementation of those wireless devices. The framework of the developed radiation-tolerant wireless device is illustrated in Figure 8-2.

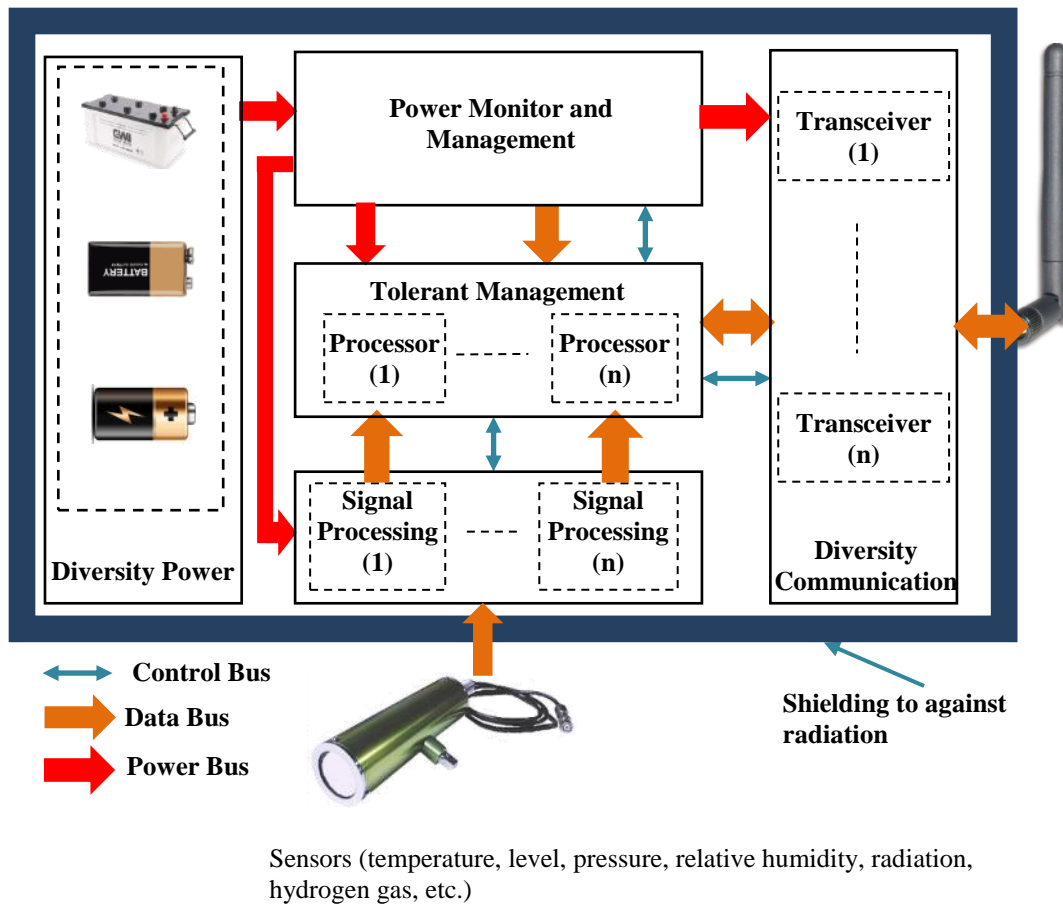


Figure 8-2: The framework of the developed radiation-tolerant wireless device

As illustrated in Figure 8-3, the tolerant management of the developed radiation-tolerant wireless device includes an active triple modular redundant core. Each modular consists of an input layer, a decision layer, and an output layer. Specially, the input layer consists of input sources, a source encoder, and a channel encoder; the decision layer consists of the decision-making unit; and the output layer consists of a digital modulator and transceiver. For simplicity's sake, only temperature sensor and water level sensor are taken as the input signal in this Chapter. In addition, all channels are constructed with diversified semiconductor technologies.

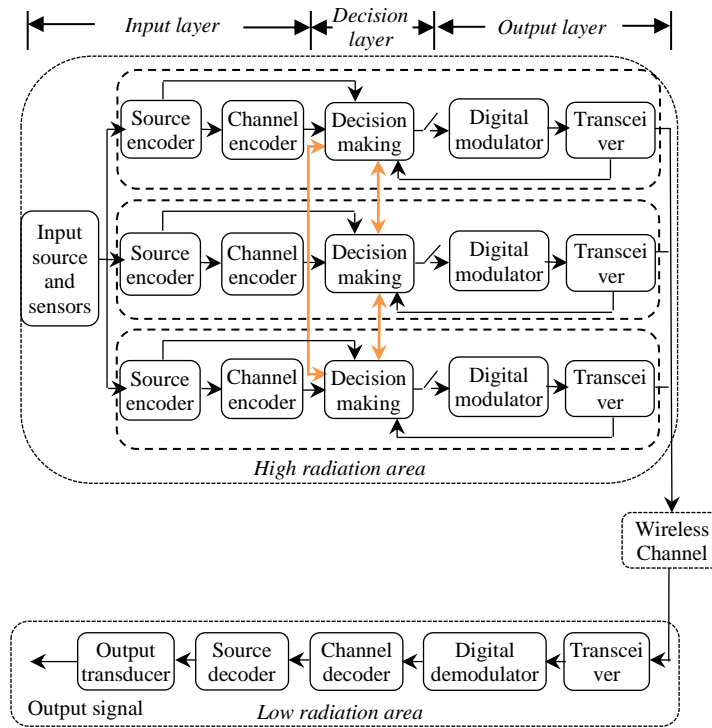


Figure 8-3: The TMR core of the proposed wireless communication system (Proakis and Salehi, 2008)

On the other hand, component selection is a significant step to implement radiation-tolerant system. Radiation hardness of different semiconductor technologies and COTS components are different. In this work, referring to radiation test data from the NASA Goddard Space Flight Center, all wireless channels and their spares are implemented with diversified devices. Picture of the developed wireless device is shown in Figure 8-4, as well as picture of the radiation shielding protection is illustrated in Figure 8-5.

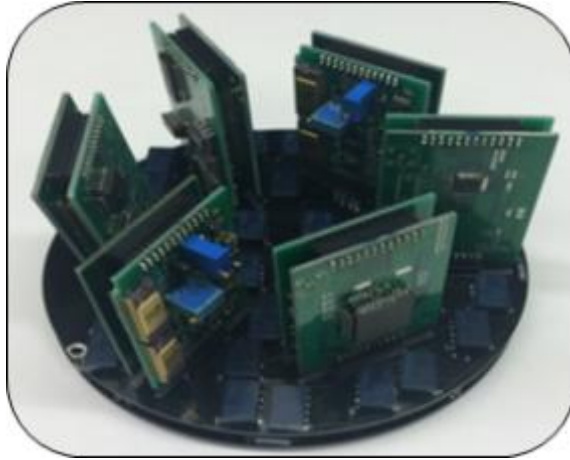


Figure 8-4: Picture of radiation-tolerant wireless device developed in this work

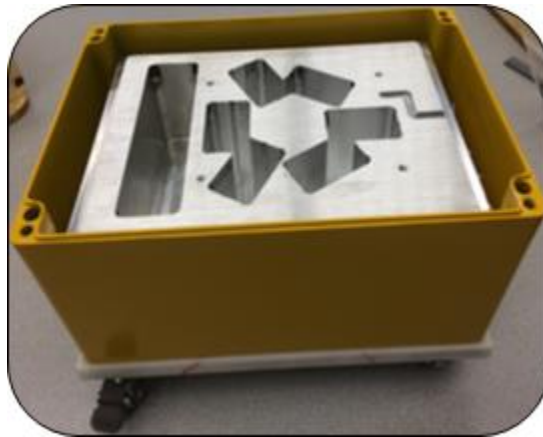


Figure 8-5: Picture of radiation shielding protection developed in this work

The detailed implementation of wireless monitoring device and related information are listed in Table 8-2. Specifically, those components, such as resistance, capacitor, relay, etc., are not listed in the table due to their robustness to radiation.

Table 8-2: The implementation of radiation-tolerant wireless devices in this research

| Channel | Function | Type | Quan. | Technology | Manufacture |
|--------------------------------|------------------------------|---------------------|-------|---------------------|----------------|
| A ₁ &S ₁ | Source encoder | NPN BJT | 1 | Bipolar | Semicoa |
| | | Voltage reference | 1 | Bipolar | Ti |
| | | OP amp | 3 | Bipolar | National Semi. |
| | Channel encoder | Voltage reference | 1 | Bipolar | Ti |
| | | AD | 1 | Bipolar | Analog Devices |
| | Decision & Digital | E ² PROM | 1 | CMOS | Atmel |
| | | Microcontroller | 1 | CMOS | Microchip |
| | Transceiver | Voltage reference | 1 | Bipolar | Linear |
| | | Diode | 1 | Bipolar | Toshiba |
| | | 433 MHz RF | 1 | Bipolar | RFMD |
| A ₂ &S ₂ | Source encoder | Voltage reference | 1 | BiCMOS | Ti |
| | | OP amp | 3 | CMOS | Analog Devices |
| | Channel encoder | OP amp | 1 | CMOS | Analog Devices |
| | | Voltage reference | 1 | CMOS | Ti |
| | | AD | 1 | BiCMOS | Analog Devices |
| | Decision & Digital modulator | Microcontroller | 1 | CMOS | Atmel |
| | | Logic gate | 1 | CMOS | Ti |
| | Transceiver | 433MHz RF | 1 | CMOS | Freescall Semi |
| A ₃ &S ₃ | Source encoder | Voltage reference | 1 | HSCMOS | Allegro |
| | | OP amp | 3 | BiFET | Ti |
| | Channel encoder | Voltage reference | 1 | CMOS | Analog Devices |
| | | AD | 1 | LC ² MOS | Analog Devices |
| | | OP amp | 2 | Hybrid | Motorola |
| | Decision & Digital modulator | Microcontroller | 1 | TTL Logic | Silicon |
| | | Logic gate | 1 | TTL Logic | Ti |
| | Transceiver | 433 MHz RF | 1 | TTL Logic | Silicon |
| | | Voltage reference | 1 | BiMOS | Ti |

Specially, as previously mentioned, the important variables of interests are temperature, humidity, hydrogen concentration, and radiation levels of the environment. It is also important to gather information about the conditions of protection systems, such as water level in a spent fuel pool, and coolant inventory etc. However, to be simple, only two different sensor signals are involved in this work, they are:

- 4~20 mA current source (water level sensor);
- 0~100 Ω resistance (temperature sensor).

More work about sensors, such as gamma detector, neutron detector, etc., will be investigated in other works.

8.2.2 Gateway

The objective of a gateway device is to collect the up-to-date information from wireless devices, to transmit that information to remote emergency monitoring station and/or the portable monitoring device, and also to integrate and to preserve that information. The device works in the low level radiation fields and consists of diversified communication interfaces, such as diversified wireless networks, Ethernet network, satellite communication interface, cellular network, etc. It therefore needs a powerful processor to hand all communication threads and data processing tasks.

In this work, the gateway device is constructed by Freescale i.mx6 microprocessor, which is a feature- and performance-scalable multicore platform based on the ARM Cortex architecture and run up to 1.2 GHz with various communication interfaces. The gateway device includes several local hardware interfaces, such as USB, SD card, HDMI, LCD, etc. They are used to debug, to setup working parameters, and to save the history data. The overview of the developed gateway device is illustrated in Figure 8-6.

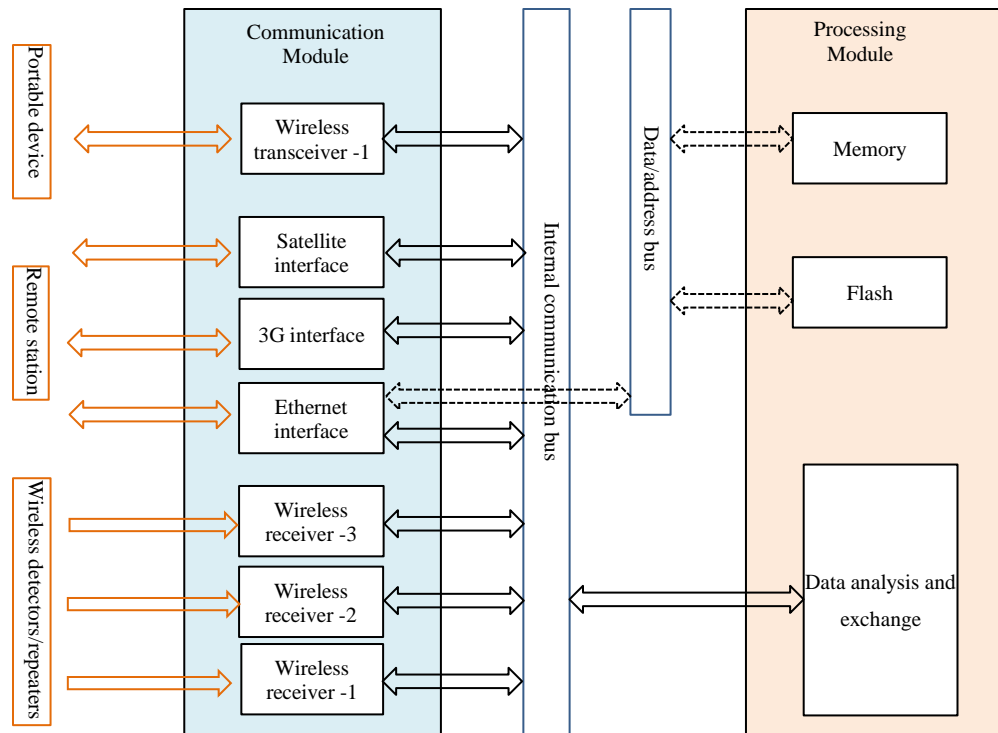


Figure 8-6: The block diagram of the gateway device developed in this research

In addition, the gateway device uses a Linux operating system to manage its resources, which include several threads to accomplish all functions, such as WSN communication thread. On the other hand, due to the gateway device is installed in the low level of radiation fields, a copper shielding (1cm thickness) is used to mitigate radiation effects on the electronics. The picture of the developed gateway device is shown in Figure 8-7, as well as the developed shielding for gateway device is illustrated in Figure 8-8.



Figure 8-7: Picture of gateway device developed in this research



Figure 8-8: Picture of the shielding for gateway device developed in this research

8.2.3 Remote Monitoring Station

1) Remote monitoring station

The objective of remote monitoring station is to collect the up-to-date information from the gateway devices, to manage and to analyze environment parameters of high radiation fields, as well as to display those parameters. A software tool is therefore developed to control, to collect, and to display the information of environment parameters, as well as to analyze the node performance of wireless network.

In this work, a rugged laptop is used as the remote monitoring station to accomplish all functions, such as message transceive function, data collecting management, data

processing, database management, and GUI function. The overview of this software tool is illustrated in Figure 8-9.

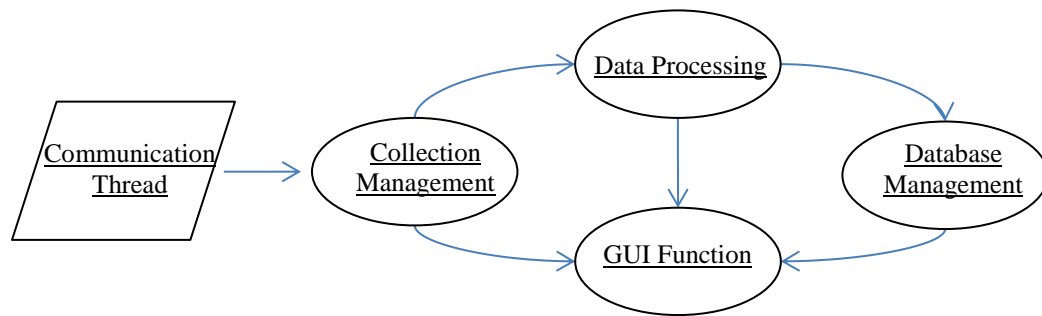


Figure 8-9: The overview of remote monitoring station developed in this research

Picture of the remote monitoring station used in this research is shown in Figure 8-10.



Figure 8-10: Picture of the remote monitoring station used in this research

2) Portable monitoring device

In addition, a portable monitoring device is also implemented in this work by using the DLI8800 rugged tablet, which also includes several hardware interfaces, such as USB ports, user-programmable key, and multiple radio communication interfaces. Operating system uses Windows Embedded 7. Picture of portable monitoring device is shown in Figure 8-11.



Figure 8-11: Picture of portable monitoring device used in this research

3) Monitoring Tool

A software tool has been developed to collect, to display, and to handle the data in the remote monitoring device and portable monitoring device. It is developed by using C++ in Microsoft Visual Studio. Picture of the software tool is shown in Figure 8-12.



Figure 8-12: Picture of a monitoring software tool developed in this research

8.3 Testing in a Normal Environment

8.3.1 Accuracy of Parameters Measurement

Taking water level as an example, the measurement results during 24 hours, listed in Table 8-3, demonstrate the reliable and accurate monitoring performance of the developed system under a normal condition.

Table 8-3: The parameter measurement of the developed monitoring system in a normal environment

| Parameter | Actual value | Duration (hour) | Max measurement value | Deviation (%) | Min measurement value | Deviation (%) |
|-------------|--------------|-----------------|-----------------------|---------------|-----------------------|---------------|
| Water Level | 2 inch | 1 | 2 | 0% | 2 | 0% |
| | 10 inch | 1 | 10.2 | 2% | 9.8 | 2% |
| | 20 inch | 1 | 20.3 | 1.5% | 19.8 | 1% |
| | 40 inch | 1 | 40.4 | 1% | 39.6 | 1% |

8.3.2 Wireless Communication Performance

In the test, wireless device sends one message packet to the gateway at a period of two seconds. Packet loss rate can be calculated by:

$$PacketLossRate = PacketLoss / PacketSent \quad (8-1)$$

And packet error rate can be calculated by:

$$PacketErrorRate = PacketError / ReceivedTotalPacket \quad (8-2)$$

The test results of communication performance under a normal condition are given in Table 8-4. The test results have shown that the real-time transmission from wireless detectors to the remote monitoring station is stable and reliable. The remote station receives the data and adequately displays the up-to-date information.

Table 8-4: The performance of wireless communication in a normal environment

| During Time (hours) | Received Total Packets | Packet Loss | Loss Rate (%) | Packet Error | Error Rate (%) |
|------------------------|------------------------------|-------------|------------------|--------------|-------------------|
| 24 | 43153 | 47 | 0.054% | 55 | 0.127% |

8.4 Summary

In this Chapter, based on design considerations, the implementation of the proposed wireless monitoring application for radiation environment in a nuclear power plant is presented in detail. The system includes four type devices: radiation-tolerant wireless device, gateway device, portable monitoring device, and remote monitoring device. In a normal environment, the developed system can work smoothly. Experimental results have shown that environment parameters can be correctly measured and its deviation is less than 2%. In addition, the performance of wireless communication satisfies the design requirement; its packet loss rate and packet error rate are 0.054% and 0.127%, respectively.

Experiment results have shown that the proposed redundant architecture is correct and the developed wireless monitoring system can be used to effectively obtain up-to-date information from a specified environment. The radiation-tolerance assessment for the developed redundant wireless device will be explained in Chapter 9. As well as the experimental validation in a real radiation environment will be presented in Chapter 10.

Chapter 9

9 Evaluation: Radiation-Tolerance Assessment

In the design of a radiation-tolerant system, the assessment of its radiation-tolerance is a critical step. The physical test is very precise but could be excessively complicated and expensive. As well as simulation method is difficult to assess the radiation-tolerance of the whole system. A method is developed in this Chapter to assess the radiation-tolerance in the design phase without repeated physical test.

This Chapter starts with the problem about radiation-tolerance assessment in the design of electronic systems for high radiation level fields. Subsequently, reliability assessment models are established for before- and post-irradiation. Then, radiation degradation factor are used to describe the radiation response of the component, the subsystem, and the system under a total radiation dose. Finally, the reliability assessment for the developed wireless device is given in detail.

9.1 Problem Statement

In general, the performance of rad-hardened systems can be evaluated in two ways: (1) physical tests: which use external perturbation sources (natural and accelerated particle radiation, laser beam, pin forcing, etc.) to create a similar radiation environment to evaluate the performance of the design. This approach is very precise but could be excessively complicated and expensive; and (2) simulation with analysis: which uses logic relationships of the circuits and systems to access internal elements and insert the effect of a radiation induced fault according to the fault model. However, a limitation of this approach is that it is difficult to assess the radiation-tolerance of the whole system.

To address these issues, an approach by combining with reliability analysis and radiation degradation factor is developed. Key issues to deal with the assessment of radiation-tolerance without physical tests are listed as follows:

- (1) To establish reliability assessment model for post-irradiation.

- (2) To obtain radiation degradation factors for semiconductor components.

9.2 Evaluation of Radiation Shielding Protection

Taking radiation levels (7.3 K Rad/h and 53 K Rad/h) in Fukushima nuclear accident, as illustrated in Chapter 5, using Co-60 as a radiation source for gamma radiation, the ability of the developed protections can be evaluated with the aid of RadPro Calculator (Rad Pro Calculator, 2018).

- Under the condition with dose rate 70 Sv/h (7 K Rad/h), for a 24h period, the highest total dose in six areas should be less than 2.6 K Rad (Si).
- Under the condition with dose rate 530 Sv/h (53 K Rad/h), for a 24h period, the highest total dose in six areas should be less than 20 K Rad (Si);
- Under the condition with dose rate 1350 Sv/h (130 K Rad/h), for a 24h period, the highest total dose in six areas should be less than 50 K Rad (Si);
- Under the condition with dose rate 2700 Sv/h (270 K Rad/h), for a 24h period, the highest total dose in six areas should be less than 100 K Rad (Si);

9.3 Assessment of System Reliability

9.3.1 Reliability Assessment Model

The reliability function $R(t)$ represents the probability that an item (component, subsystem, or system) will perform the designed functions over a given time interval $[0, t]$ under specific operating environment and conditions (Song and Wang, 2013). Conventional analysis methods for system reliability are dependent on probabilistic approaches, which incorporate all failure events as random events. These methods are based on two fundamental assumptions: (1) binary state assumptions, where the system can only be in either of the two states (fully functioning or completely failed); and (2) probability assumptions, where the system failure behavior is fully characterized by the probability measures (Ravi *et al.*, 2000). However, there are many uncertainties when a device or a system is operating in a harsh environment, which may include strong level of radiation, extremely high temperature, and high humidity, etc.; those uncertainties challenge the assumptions made in the “conventional” reliability analysis of the

components, and lead to an increase in the probability of failure for the item (component, subsystem, and/or system) (Lauridsen *et al.*, 1996). Therefore, the analysis employed by the conventional methods may not represent a realistic situation in a harsh environment. Radiation effects should be considered in the reliability analysis.

The current work establishes the assessment model for non-radiation conditions first through failure rates to obtain the reliability of the proposed architecture under radiation conditions. The failure rate $\lambda(t)$ of an item expresses the “possibility to failure” of the item after time t has passed (Song and Wang, 2013). It is estimated from the mean number of failures per unit time, which can be expressed by failure in time (*FIT*) as follows:

$$1 \text{ FIT} = 10^{-9} \text{ failure / hour.}$$

The reliability $R(t)$ of the item can then be determined from the failure rate $\lambda(t)$ with the consideration of $R(0) = 1$ as follows from (Song and Wang, 2013):

$$R(t) = e^{-\int_0^t \lambda(\tau) d\tau}. \quad (9-1)$$

Assuming that the failure rate is independent of time (t), then $\lambda(t) = \lambda$, Eq. (9-1) can be simplified to (Song and Wang, 2013)

$$R(t) = e^{-\lambda t}. \quad (9-2)$$

Considering that the proposed architecture consists of an input layer, a decision layer, and an output layer; and the reliability of diversified channels are all different, the reliability of the j th layer in the channel i , which consists of n_l components, can be evaluated using the formula.

$$R_{ij}(t) = e^{-\lambda_{ij}t} = \prod_{k=1}^{n_l} e^{-\lambda_k t} = e^{-\sum_{k=1}^{n_l} \lambda_{ijk} t} \quad (i = 1, \dots, m; j = 1, 2, 3). \quad (9-3)$$

The reliability of the channel i can be described as follows:

$$R_{C_i}(t) = e^{-\lambda_{C_i}t} = \prod_{j=1}^3 e^{-\lambda_{ij}t} = e^{-\sum_{j=1}^3 \lambda_{ij}t} \quad (i = 1, \dots, m). \quad (9-4)$$

According to Eq. (9-3), $R_{i1}(t)$, $R_{i2}(t)$, and $R_{i3}(t)$ can be obtained. Subsequently, the reliability model of the proposed architecture under non-radiation conditions can be derived as follows:

$$R_s(t) = \left(1 - \prod_{i=1}^m (1 - R_{i1}(t))\right) \times \left(1 - \prod_{i=1}^m (1 - (R_{i2}(t) \times R_{i3}(t)))\right). \quad (9-5)$$

Specifically, as previously discussed, cases of all three channels encountering failures simultaneously are not considered in this work, common-mode failure is therefore not considered.

9.3.2 Radiation Degradation Factor

To take radiation effects in consideration in the system reliability analysis, a new analysis method for electronic systems has been developed in (Lauridsen *et al.*, 1996a; Lauridsen *et al.*, 1996b). This method uses radiation degradation factors (Δ), instead of the usual failure rate data, of an item in the reliability model, to describe the radiation response of this item under a total radiation dose D_t , which will lie in the interval $[0, 1]$ and can be defined as follows:

$$\Delta = \min \left\{ \left| (P_0 - P_t) / (P_0 - P_f) \right|, 1 \right\}. \quad (9-6)$$

A detailed description of the radiation degradation factor can be found in (Lauridsen *et al.*, 1996b).

$$\Delta = \begin{cases} (P_0 - P_t) / (P_0 - P_f) & \text{for } P_0 \geq P_t > P_f \text{ or } P_0 \leq P_t < P_f \\ 0 & \text{for } P_t > P_0 > P_f \text{ or } P_t < P_0 < P_f \\ 1 & \text{for } P_0 > P_f > P_t \text{ or } P_0 < P_f < P_t \end{cases}. \quad (9-7)$$

Some previous studies (Lauridsen, *et al.*, 1996a; Lauridsen, *et al.*, 1996b) have derived the parameter values of radiation degradation based on actual radiation test data; with radiation degradation function which are used to describe how the properties of the materials and/or components change under various radiation conditions.

Since semiconductor components may have a number (n_p) of critical parameters, in this study, the radiation degradation factor is chosen as the mean value of the degradation factors across all critical parameters as follows:

$$\Delta = \frac{\sum_{i=1}^{n_p} \min \left\{ \left| \frac{(P_{i_0} - P_{i_i})}{(P_{i_0} - P_{i_f})} \right|, 1 \right\}}{n_p}. \quad (9-8)$$

The reliability ($R'(t)$) of an item under the total radiation dose D_t can then be expressed in Eq. (9-9).

$$R'(t) = (1 - \Delta) \cdot R(t) = (1 - \Delta) \cdot e^{-\lambda t}. \quad (9-9)$$

The reliability of the j th layer in the channel i under the total radiation dose D_t can be evaluated in Eq. (9-10).

$$R'_{ij}(t) = \prod_{k=1}^{n_j} (1 - \Delta_k) e^{-\lambda_k t} \quad (i = 1, \dots, m; j = 1, 2, 3). \quad (9-10)$$

Assuming that the channel i consists of n_c components, the reliability of the channel i under the total radiation dose D_t can be evaluated by using Eq. (9-11).

$$R'_{c_i}(t) = \prod_{k=1}^{n_c} (1 - \Delta_k) e^{-\lambda_k t} \quad (i = 1, \dots, m). \quad (9-11)$$

Using Eq. (9-10), the reliabilities $R'_{i1}(t)$, $R'_{i2}(t)$, and $R'_{i3}(t)$ can be evaluated. The reliability model of the redundant architecture mentioned in Figure 6-3 under the total radiation dose D_t can be derived as Eq. (9-12).

$$R'_s(t) = \left(1 - \prod_{i=1}^m (1 - R'_{i1}(t)) \right) \times \left(1 - \prod_{i=1}^m (1 - (R'_{i2}(t) \times R'_{i3}(t))) \right). \quad (9-12)$$

9.4 Radiation-Tolerance of the Developed Wireless Device

In the assessment of system reliability using Eq. (9-12), only the total radiation dose has been considered. One difficulty in the assessment is proper determination of the degradation factors for semiconductor devices used. Most of radiation degradation factors

under different radiation doses in this study come from NASA Goddard Space Flight Center radiation test database, which are publicly available on-line; others are derived from the existing literature (Messenger and Ash, 1991; Houssay, 2000; Kulkarni and Agarwal, 2003).

In this work, the failure rates of semiconductor components listed in Column (5) of Table 9-1 come from the online resources of their manufacturers, while those radiation degradation factors listed in Column (7) to (10) of Table 9-1. For some components, their P_f are not available in NASA database and literature. Under these circumstances, they are derived from the limits of respective parameters in the specifications. According to the sources used, they can be categorized into three types:

- Most radiation degradation factors (83.34%) for different radiation doses are derived from the test data;
- Several radiation degradation factors (8.33%) are derived from the test data of similar components of same function and same semiconductor technologies;
- Other radiation degradation factors (8.33%) are derived from the mean value of the test data of different components with the same semiconductor technologies.

Table 9-1: Radiation degradation factors of the developed wireless device

| Channel | Function | Type | Q. | FIT | R. D.F | Δ | Δ | Δ | Δ |
|--------------------------------|------------------------------|---------------------|----|------|-----------|----------|----------|----------|----------|
| | | | | | | 10K | 20K | 50K | 100K |
| A1&S1 | Source encoder | NPN BJT | 1 | 2.45 | A | 0.194 | 0.3201 | 0.4267 | 0.4591 |
| | | Voltage ref. | 1 | 3.30 | A | 0.0774 | 0.1010 | 0.2104 | 0.3432 |
| | | OP Amp | 3 | 1.85 | A | 0.0208 | 0.0365 | 0.0383 | 0.0365 |
| | Channel encoder | Voltage ref. | 1 | 3.30 | A | 0.0642 | 0.1099 | 0.5158 | 0.5786 |
| | | AD | 1 | 0.20 | A | 0.0178 | 0.0486 | 0.0633 | 0.0649 |
| | Decision & digital modulator | E ² PROM | 1 | 2.20 | A | 0.0023 | 0.0244 | 0.1341 | 0.1326 |
| | | FPGA | 1 | 3.30 | A | 0.0187 | 0.0465 | 0.1001 | 0.1179 |
| | Transceiver | Voltage ref. | 1 | 3.30 | C | 0.0000 | 0.0000 | 0.0000 | 0.0000 |
| | | Varactor | 1 | 3.30 | A | 0.0000 | 0.0577 | 0.0145 | 0.0769 |
| | | 915 MHz RF | 1 | 1.90 | A | 0.0395 | 0.0745 | 0.1503 | 0.1810 |
| A ₂ &S ₂ | Source encoder | Voltage ref. | 1 | 3.30 | A | 0.1510 | 0.0181 | 0.0087 | 0.0094 |
| | | OP amp | 3 | 0.28 | A | 0.0409 | 0.0770 | 0.2989 | 0.2168 |
| | Channel encoder | OP amp | 1 | 0.28 | A | 0.2377 | 0.3964 | 0.6620 | 0.6537 |
| | | Voltage ref. | 1 | 3.30 | A | 0.1408 | 0.3371 | 0.3204 | 0.3846 |
| | | AD | 1 | 0.25 | A | 0.1735 | 0.1503 | 0.2741 | 0.3345 |
| | Decision& digital modulator | Controller | 1 | 5.60 | A | 0.0638 | 0.0654 | 0.0985 | 0.1190 |
| | | Logic gate | 1 | 0.50 | A | 0.1330 | 0.0244 | 0.1850 | 0.2432 |
| | Transceiver | 915 MHz RF | 1 | 2.0 | A | 0.1026 | 0.1336 | 0.2310 | 0.2451 |
| A ₃ &S ₃ | Source encoder | Voltage ref. | 1 | 3.30 | A | 0.1408 | 0.3371 | 0.3204 | 0.3846 |
| | | OP amp | 3 | 0.20 | A | 0.0689 | 0.1551 | 0.3673 | 0.5151 |
| | Channel encoder | Voltage ref. | 1 | 3.30 | A | 0.0039 | 0.0216 | 0.0223 | 0.0644 |
| | | AD | 1 | 1.60 | A | 0.0181 | 0.0229 | 0.0246 | 0.0209 |
| | | OP amp | 2 | 0.20 | A | 0.1360 | 0.0764 | 0.1757 | 0.2717 |
| | Decision& digital modulator | Controller | 1 | 2.26 | A | 0.0109 | 0.0134 | 0.0149 | 0.0168 |
| | | Logic gate | 1 | 3.30 | A | 0.0469 | 0.0494 | 0.0480 | 0.0724 |
| | Transceiver | 915 MHz RF | 1 | 1.90 | A | 0.0479 | 0.0781 | 0.1108 | 0.1567 |
| | | Voltage ref. | 1 | 3.30 | A | 0.0055 | 0.0269 | 0.0238 | 0.0646 |

According to Eq. (9-12), under four total radiation dose levels (10 K Rad (Si), 20 K Rad (Si), 50 K Rad (Si), 100 K Rad (Si)), the reliabilities of the developed wireless devices are shown in Figure 9-1. It can be seen that the reliability decreases significantly as the total radiation dose increases. Moreover, through the comparison, the reliabilities in

single channel (A_1/S_1 , A_2/S_2 , A_3/S_3), the system with triple channels (FT ($m=3$)), and the system with six redundant channels (FT ($m=6$)), also shown in Figure 9-1. It is evident that the reliabilities (98.4%, 94.9%, 61.5%, 44.2%) of the system with redundant architectures are much higher than those (60.3%, 37.5%, 11.9%, 7.2%; 33.6%, 20.7%, 3.2%, 3.4%; and 35.2%, 36.8%, 16.0%, 6.2%) of non-redundant channels under the same radiation conditions.

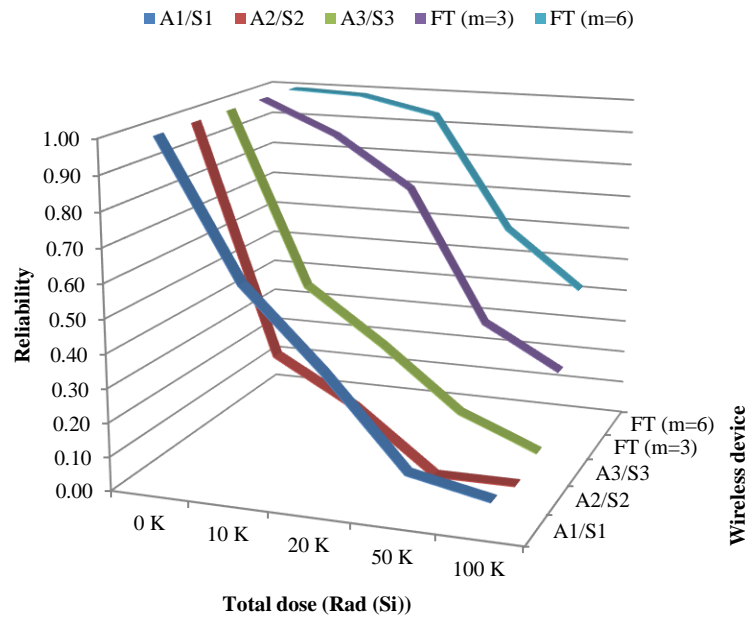


Figure 9-1: The comparison of the reliability of the developed redundant system and non-redundant channels under the given total doses (0, 10 K Rad (Si), 20 K Rad (Si), 50 K Rad (Si), and 100 K Rad (Si))

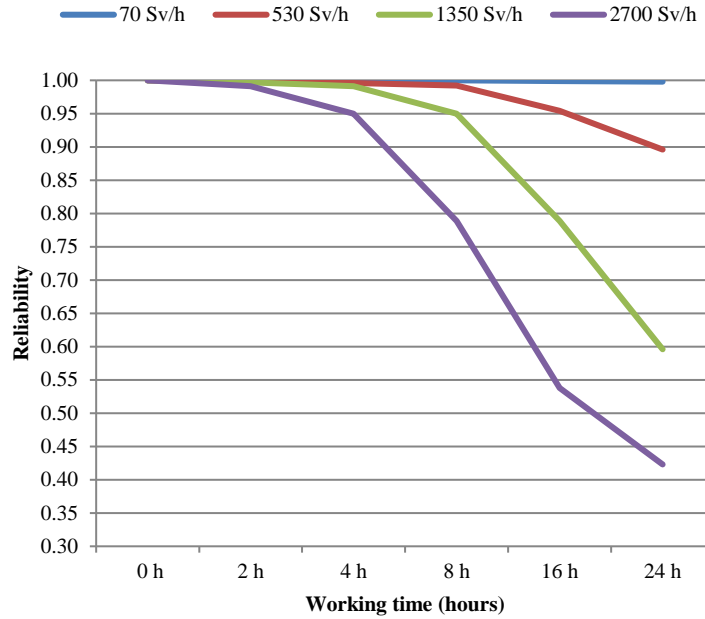


Figure 9-2: Radiation assessment of the developed wireless device under various dose rates

In a summary, combining with the developed radiation protection in Chapter 5, the radiation assessment of the developed system under various dose rates for (24h) duration is illustrated in Figure 9-2. It can be seen that the reliability of the developed device under a dose rate of 530Sv/h for 24 h is about 89.6%. This means that the device can therefore work reliably in those high level radiation environments. Cumulative dose can be calculated by:

$$Dose = Dose\ Rate \times Irradiated\ Time. \quad (9-12)$$

According to Eq. (9-12), using the levels of Fukushima disaster as a guideline, before March 2012, the highest dose rate recorded is about 73 Sv/h, that means the developed system can survive for at least 7 days. In Feb. 2017, the highest recorded dose rate is 530 Sv/h, the system can survive for at least 24 hours.

On the other hand, based on the calculation, as the radiation level increases, the radiation degradation factors of the semiconductor components increase significantly as well, which results in decreases of the reliability of these components. Moreover, under

different levels of the total doses, the reliability (60.3%, 37.5%, 11.9%, 7.2%) of A_1/S_1 channel (bipolar semiconductor technologies) is higher than that (35.2%, 36.8%, 16.0%, 6.2%) of A_3/S_3 channel (Hybrid semiconductor technologies) and much higher than that (33.6%, 20.7%, 3.2%, 3.4%) of A_2/S_2 channel (CMOS semiconductor technologies).

These results agree with the known knowledge in the domain of radiation assurance.

Hence, this assessment technique can be used to select components and to evaluate the radiation-tolerance of the entire whole system in the design phase. It is also an effective tool to aid in design of tests in a physical radiation environment.

9.5 Conclusions

In this Chapter, an assessment method of the radiation-tolerance of a wireless monitoring device is presented for radiation conditions, which is developed by using radiation protection and radiation-tolerant techniques. The study results show that total dose can be effectively decreased by radiation protections. The analytical results conclude that, under given radiation conditions (10 K Rad (Si), 20 K Rad (Si), 50 K Rad (Si), 100 K Rad (Si)), the reliability of the developed architecture (98.4%, 94.9%, 61.5%, 44.2%) is much higher than those of non-redundant channels (60.3%, 37.5%, 11.9%, 7.2%; 33.6%, 20.7%, 3.2%, 3.4%; and 35.2%, 36.8%, 16.0%, 6.2%). The system reliability can further be improved by selecting components with higher radiation resistance and/or by increasing the protection capability of radiation shielding.

According to assessment studies, the developed system can work in high level radiation fields with a total dose up to 1 M Rad (Si). It provides an economical and effective solution to obtain up-to-date information in the event of a severe accident in a nuclear power plant without resorting to use of expensive rad-hardened electronics components. However, it is important to mention that the proposed radiation-tolerance assessment method should not replace physical tests. It can be used to design physical tests and be treated as complementary tool. Their value cannot be underestimated at the design phase of the system to select suitable electronic components and to evaluate their radiation-tolerance.

Chapter 10

10 Experimental Validation

In the design of a radiation-hardened electronic system, the investigation of the correctness and effectiveness of the proposed radiation-hardened design techniques and the evaluation of the radiation hardness of the developed electronic devices are the critical parts. They are usually performed by exposing the device and/or system to a radiation environment and measuring the performance parameters. Over the years, a lot of research works has been done to obtain radiation data. In general, a radiation test has three distinct objectives: (1) to investigate the mechanisms of the interaction of radiation particles with semiconductor materials and to understand how a device fails caused by these effects; (2) to investigate radiation responses of specific devices and technologies for the component selection in the system design; and (3) to investigate the radiation hardness of the product to determine its acceptability (Ronald *et al.*, 1988). The first type of tests is fundamental for the understanding of radiation effects and damages on electronics. The second focuses on radiation responses of devices and technologies. The third focuses on the system-level to investigate the radiation hardness of the product. However, investigation of radiation responses of modern wireless communication devices is limited in the literature. Such information is not only significant but also necessary for design of systems operating in high level radiation environment.

In this Chapter, to investigate the radiation hardness of the developed wireless systems, as well as to validate the investigated methods, four different experiments with several distinct wireless devices built with diversified commercial off-the-shelf (COTS) components have been performed under radiation conditions with both high dose rate (20 K Rad (Si)/h) condition and low dose rate (200 Rad (Si)/h) condition by using ^{60}Co gamma irradiator in Nuclear Reactor Laboratory of the Ohio State University (OSU-NRL). The goals are: (1) the investigation of radiation vulnerabilities of the wireless monitoring system with diversified commercial off-the-shelf components under a high dose rate condition; (2) performance evaluation of popular wireless transceivers and networks under a radiation environment; (3) evaluation of diversified non-redundant

wireless monitoring devices under radiation conditions with high and low dose rate; (4) evaluation of the radiation hardness of the developed radiation-tolerant wireless devices under a high dose rate condition.

This Chapter starts with the objectives of the total dose test. Test facility is then described and experimental approaches are also explained. Subsequently, experimental schemes, experimental results, and related technical discussions for four tests are presented in detail. Finally, based on experiment results, conclusions are given.

10.1 Overview

10.1.1 Objectives of Experiments

To obtain up-to-date information, modern digital communication technologies are often applied to specifically deal with digital data and digitally pre-processed signals and also to transmit that information. The composition of a digital communication system is illustrated in Figure 10-1. The basic elements of a transmitter in a digital communication system include: (1) input transducer, which converts the output of a practical sensor into an electrical signal; (2) source encoder, which converts the output of either an analog or a digital source into a sequence of binary digits; (3) channel encoder, which introduces, in a controlled manner, some redundancy in the binary information sequence used at the receiver to overcome the effects of noise and interference encountered in the transmission of the signal through the channel; (4) digital modulator, which serves as the interface to map the binary information sequence into the signal waveforms (Proakis and Salehi, 2008). At a receiver end, the basic elements are: (1) digital demodulator, which processes channel-corrupted transmitted waveforms and reduces each of them to a single number that represents an estimate the transmitted data symbol; (2) channel decoder, which reconstructs the original information sequence from the knowledge of the code used in the channel encoder; (3) source decoder, which reconstructs the original signal from the source; and (4) output transducer, which converts the electrical signals into a form that is understandable to the user (Proakis and Salehi, 2008).

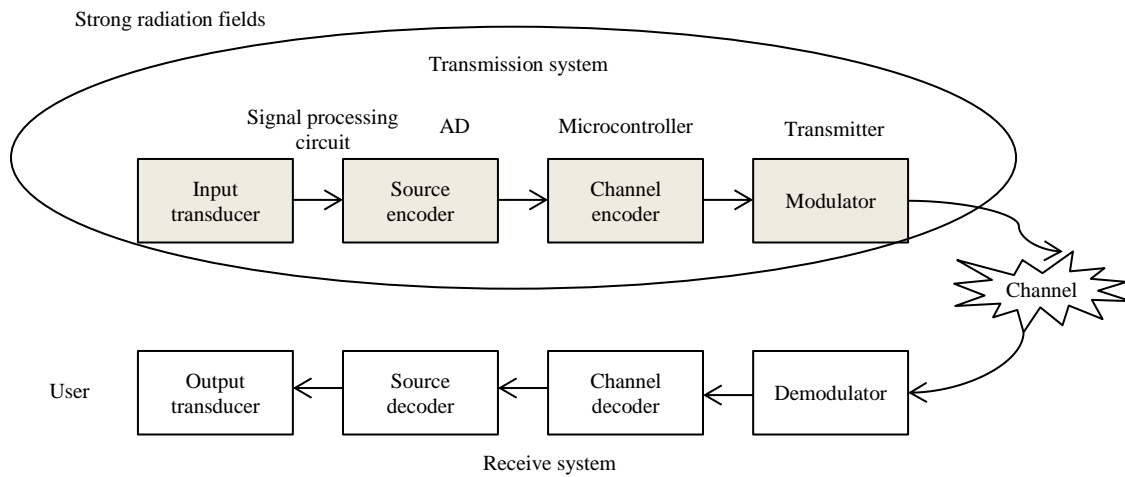


Figure 10-1: Composition of a digital communication system (Proakis and Salehi, 2008)

As illustrated in Figure 10-1, various modern semiconductor components and circuits have to be used for implementing the functions in wireless senders, such as signal processing circuit, analog-to-digit converter, microcontroller/microprocessor, and transceiver, etc. The block diagram of a typical transmission system is illustrated in Figure 10-2.

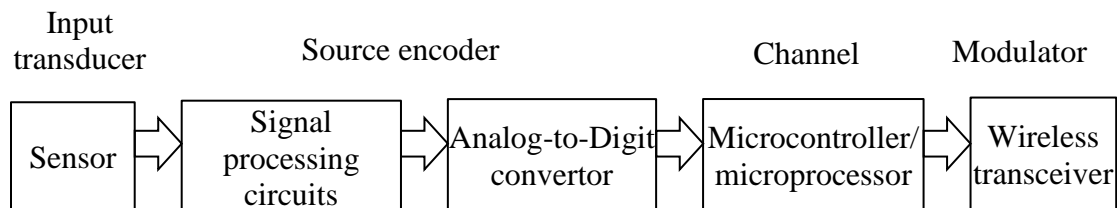


Figure 10-2: A block diagram of the implementation of a typical wireless transmission system

When a transmission system works in a strong radiation environment, semiconductor-based electronic components and circuits could be damaged due to radiation particles through either non-ionization processes (displacement damage) and/or ionization processes (total ionizing dose and single event effect) (Srouf and McGarrity, 1988;

Gregory and Gwyn, 1974). In order to ensure that a device can complete its mission in a radiation environment, investigation of radiation responses at component-level, circuit-level, and system-level becomes significant and necessary. As explained in Chapter 2, many research works have been carried out to investigate radiation effects on components. However, for a digital communication system, investigation of radiation effects on circuit-level and system-level is still limited. There have a number of questions need to be investigated, such as:

- (a) Which module is most sensitive to high level radiation?
- (b) Which wireless transceivers and networks are suitable to be used in a high level radiation environment?
- (c) How different wireless measurement and communication devices can be built with diversified hardware to survive under different radiation environments? and
- (d) What is the radiation hardness of the developed redundant wireless device in a high level radiation environment?

Hence, the experiments in this research focus on circuit- and system-level rather than component-level to determine answers to the above questions through measuring radiation responses of the developed wireless devices, as well as to validate the developed radiation-hardened methods. The overview of the experimental validations is illustrated in Figure 10-3.

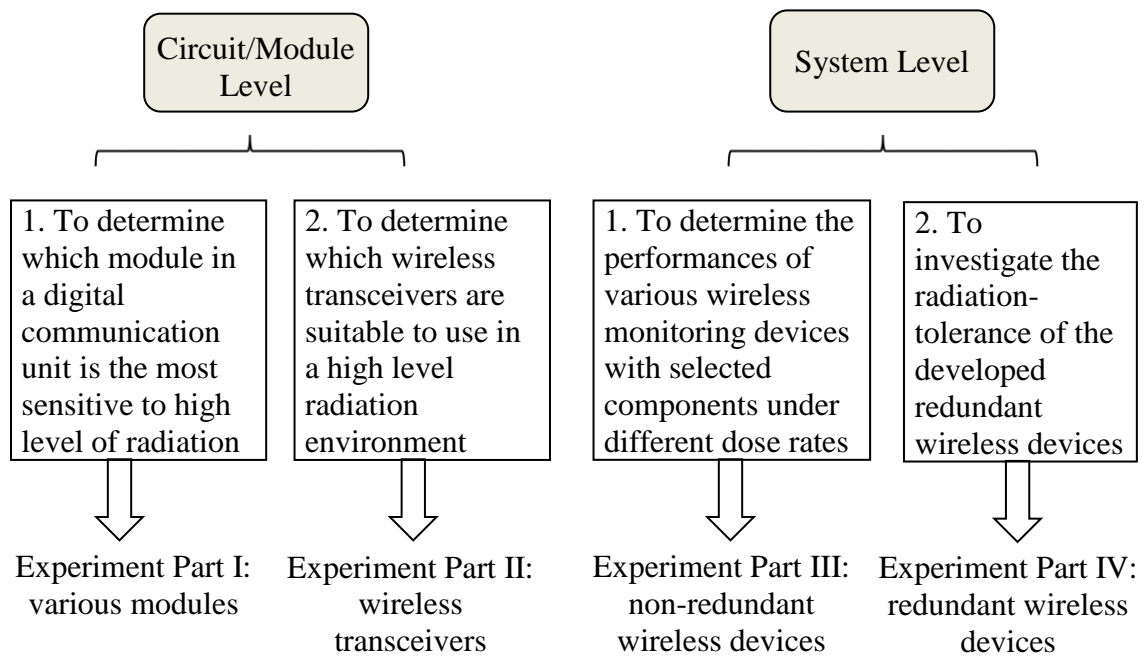


Figure 10-3: An overview of the experimental validation in this research

The objectives of the irradiation test are as follows:

- (1) Experiment Part I: to investigate radiation vulnerability in wireless measurement and transmission devices with diversified COTS components in a radiation environment with a high dose rate;
- (2) Experiment Part II: to evaluate the performance of popular wireless transceivers and networks, such as ZigBee, Wireless-Hart, ISA100.11a, LoRa, 433MHz network, and 915MHz network, in a radiation environment with a high dose rate;
- (3) Experiment Part III: to evaluate the performance of non-redundant wireless devices implemented with different semiconductor technologies, e.g., CMOS, Bipolar, and Hybrid, etc., under radiation conditions with both low and high dose rate conditions.
- (4) Experiment Part IV: to evaluate the performance of the developed redundant wireless devices under a radiation condition with a high dose rate, such as lifespan, and the performance of wireless communication, etc.

10.1.2 Experimental Approaches

One typical approach of a system and part level hardness assurance is to irradiate the system and/or the part by a selected radiation source (such as γ source) for fixed period of time and then test hardware for potential errors and/or degradations (Ronald *et al.*, 1988). According to characterizations of the radiation source, it can be also separated into three types: (1) displacement damage test, which is performed by exposing a device to a fixed particle fluence (electron, proton, or neutron) and characterizing its parameter degradation; (2) total dose test, which is performed by exposing a device to an ionizing radiation environment and measuring the electrical performance under various operating conditions; and (3) single particle effects test, which is performed by continually measuring the device responses under a high-energy particle accelerator while the device is operating (Ronald *et al.*, 1988).

Furthermore, there are two other tests to characterize the responses: (1) step-stress test, which is performed by first measuring the electrical performance of the device, subsequently, exposing it to a fixed dose of ionizing radiation for a certain duration of time, then re-measuring those parameters to obtain their responses; and (2) in-flux test, which the device response is continually measured while it is being irradiated (Ronald *et al.*, 1988).

According to the previously mentioned objectives, the current work focuses on total dose test at the circuit-level and the system-level. All test samples will be exposed to an ionizing radiation environment first. Afterwards the electrical performance and wireless communication performance are measured. In Experimental Part I, using the method of step-stress test, irradiated samples are exposed to radiation for a fixed period of time, and then their electrical parameters are re-measured until most modules fail. Other experiments are performed using online method to continually measure the device response until it fails.

Three type parameters are monitored to reflect behaviors of tested samples under radiation environments: (1) the lifespan defined that the unit has a functional failure under the condition of dose rate; (2) the accuracy of parameter measurement, e.g., 4~20

mA current signal; and (3) the performance of wireless communication, e.g., packet error rate, packet loss rate, frequency, and received signal strength indicator (RSSI). The amount of radiation dose can be calculated how much radiation the device has accumulated over time, which is illustrated in the following equation.

$$Dose = Dose\ Rate \times Irradiated\ Time.$$

Hence, radiation resistance of the irradiated sample can be calculated by:

$$Radiation\ Resistance = Dose\ Rate \times Survival\ Time. \quad (10-1)$$

Experimental objectives and approaches of each test are summarized in Table 10-1.

Table 10-1: Summary of experimental objectives and approaches in this total dose test

| Experiments | Objectives | Dose rates | Approaches |
|-------------|---|------------------------|------------|
| Part I | To investigate radiation vulnerability in a wireless measurement and transmission device | 20 K Rad/h | Off -line |
| Part II | To evaluate the performance of six industrial wireless transceivers and networks under a radiation environment | 20 K Rad/h | Online |
| Part III | To evaluate the performances of non-redundant wireless devices implemented with varies semiconductor technologies under radiation conditions with both low and high dose rate | 20 K Rad/h & 200 Rad/h | Online |
| Part IV | To investigate radiation hardness of the developed redundant wireless device with a shielding protection | 20 K Rad/h | Online |

10.1.3 Radiation Level Considered in Experimental Validation

As mentioned in Chapter 2.1.3, in March 2012, the level of radiation particles was estimated to be up to 73 Sv/h (7.3 K Rad/h) inside the containment of No.2 reactor in Fukushima plant (Eisler, 2012), and in Feb. 2017, it was up even further to 530 Sv/h (53

K Rad/h) (The Guardian, 2017). Therefore, taking that information as a reference, radiation level in this experimental validation is therefore considered in the range of 10 K Rad/h \sim 100 K Rad/h. The selected highest dose rate in this test is 20 K Rad/h, which is within ballpark of 530 Sv/h.

10.1.4 Experimental Facility

In this work, all tested devices are irradiated in a 6"-diameter dry tube in the Cobalt-60 underwater irradiator in Nuclear Reactor Laboratory of the Ohio State University. The irradiation chamber is a dry, air-filled, 6 inches tube that is open to atmosphere (OSU-NRL, 2018). For samples, a shielded elevator is used to move them into the irradiation position. The approximate dose rate at the peak location is 20 K Rad (Si)/h and the lowest dose rate is 200 Rad (Si)/h (2018-10-08) (OSU-NRL, 2018). The Cobalt-60 gamma irradiator dose-rate curve in 6" tube is shown in Figure 10-4.

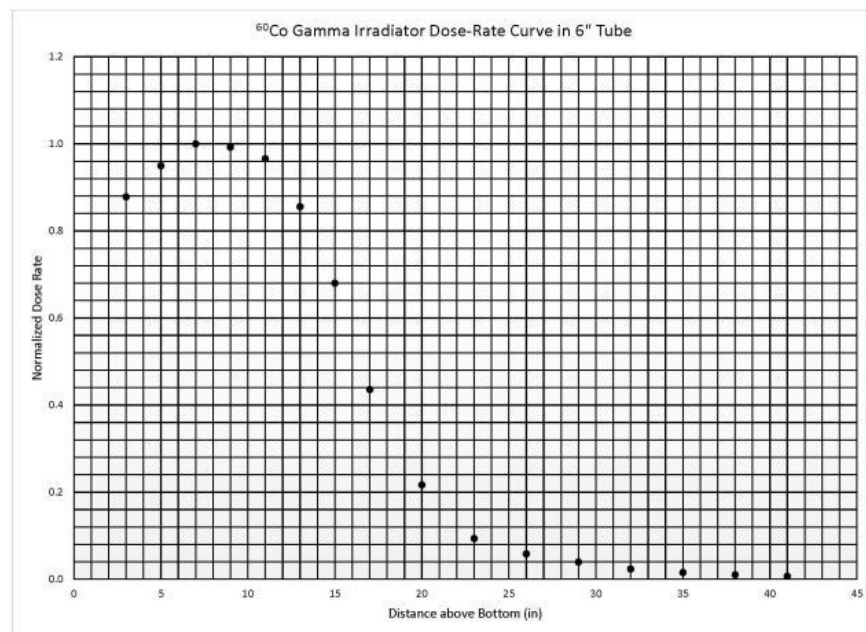


Figure 10-4: The Co-60 gamma irradiator dose-rate curve (OSU-NRL, 2018)

The distance above the bottom of the highest dose rate (20 K Rad/h) is 8 inch and that of the lowest dose rate (200 Rad/h) is 20 inch. The sample plate and the shielding of the Co-60 gamma irradiator are shown in Figure 10-5.

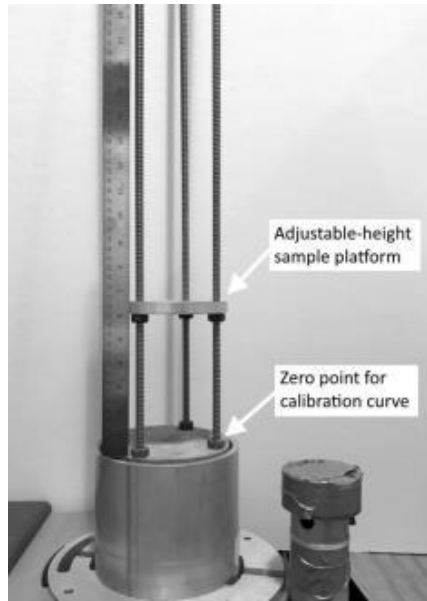


Figure 10-5: Sample plate and shielding of ^{60}Co gamma irradiator (OSU-NRL, 2018)

10.1.5 Experimental Schemes

Due to the highest dose rate in ^{60}Co gamma irradiator is located at the bottom and the length of dry tube is about 45 inch, it is therefore difficult to use the online method for directly measuring signals from the devices under test. Moreover, the measurement equipment cannot be directly exposed to the radiation source. There are several issues need to be resolved if the tests are performed through continually measuring the device responses while it is being irradiated. These issues are: (1) signal issues, where the signal will be attenuated if transmitted by using long cables; (2) power supply issue, where the power will be reduced if passing through a long cable, and (3) the location of the measurement equipment, which cannot be working in strong radiation environments.

An experimental setup is developed to obtain responses of irradiated devices under a high dose rate (20 K Rad/h) condition. An illustration diagram for a high dose rate condition is shown in Figure 10-6.

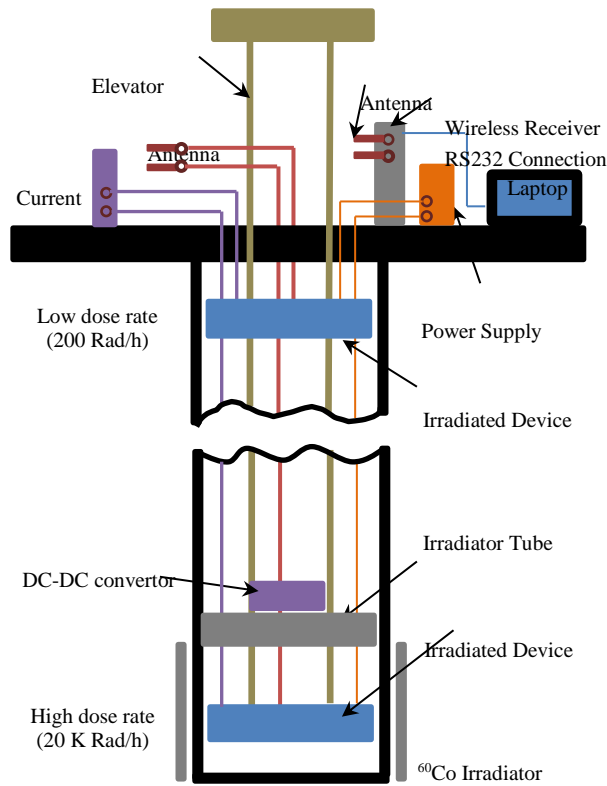


Figure 10-6: Schematic of the experimental setup inside ^{60}Co irradiator

Some equipment and devices are used to measure electrical parameters and obtain behaviors of the device while the samples are irradiated. A list is provided in Table 10-2.

Table 10-2: Testing equipment using in the experiment

| Equipment | Type | Manufacture | Function |
|-------------|----------------------------|-------------|---|
| 34410 A | Digital multi-meter | AGiLENT | To measure 4~20 mA signal as a reference |
| 1672 D | Precision DC power supply | BK | DC power supply for irradiated samples |
| TDS2024B | Oscilloscope | TEKTRONIX | To measure electrical parameters of an irradiated sample |
| RF Explorer | Handheld spectrum analyzer | Seed Studio | To measure frequency and RSSI of wireless transceivers |
| T430 | Laptop | Lenovo | To receive, record, and analyze wireless communication data |

10.2 Part I: Investigation of Radiation Vulnerability with Diversified COTS Components

In this Section, a total dose test for various modules in a typical wireless measurement and transmission unit is performed under a high dose rate (20 K Rad/h) condition by using ^{60}Co gamma irradiator. The irradiated modules are implemented with selected diversified commercial off-the-shelf components as indicated in Chapter 4, which include the module of analog signal processing, the module of analog-to-digital converter, the module of microcontroller, and the module of wireless transceiver. The results of this test will provide a guideline at the design phase for wireless monitoring systems to be used in high level radiation environments.

This Section starts with the experimental background, which includes test circuits and related experimental approaches. Subsequently, experimental setup is described in detail. Then, experimental results for each module are presented, which include the output of the analog signal processing circuits, the response of the analog-to-digital converters, the performance of microcontroller units, and the performance of wireless transceivers. Finally, several technical discussions and limitation of this test are presented.

10.2.1 Introduction of Irradiated Circuits

(1) Analog Signal Processing Circuits

When ionizing radiation passes through a bipolar device, due to an increase in the density of interface traps at the surface of the extrinsic base region and positive charge buildup, the degradation of a bipolar transistor can include two aspects: the increase of recombination current, and the reduction in the common-emitter current gain (Johnston *et al.*, 1994). For many linear bipolar technologies, the degradation at a given total dose depends on the dose rate and it is more prominent at the low dose rate, which is called Enhanced Low Dose Rate Sensitivity (ELDRS) (Boch *et al.*, 2004). Several critical parameters of operational amplifiers under different dose rates have been investigated in (Boch *et al.*, 2004; Pease *et al.*, 1997; Pease *et al.*, 1998), such as the input bias current, supply current, input offset voltage, and output voltage, etc. As previously mentioned,

this test focuses on circuit responses, instead of component responses. Therefore, the output voltage of the entire circuit is the only parameter considered in this test.

Many variables in a nuclear power plant are measured by sensors whose output is a current source (4~20 mA). The processing circuit for 4~20 mA signal is illustrated in Figure 10-7. Experiment Part I is performed under the condition of high dose rate for three different operational amplifiers: CLC502, LM108, and UA741, which are manufactured by National Semiconductor, Texas Instruments, and STMicroelectronics, respectively. The main purpose is to evaluate radiation-induced damage in different operational amplifiers, as well as to determine the radiation hardness of different amplifier circuits. Due to the selected operational amplifiers need a -5V signal as the power source and the input of the power supply is +5 V, several voltage regulators are used to generate -5 V signal: LT1611, MAX660, and LM2662, which are manufactured by Linear Technology, and Texas Instruments, respectively.

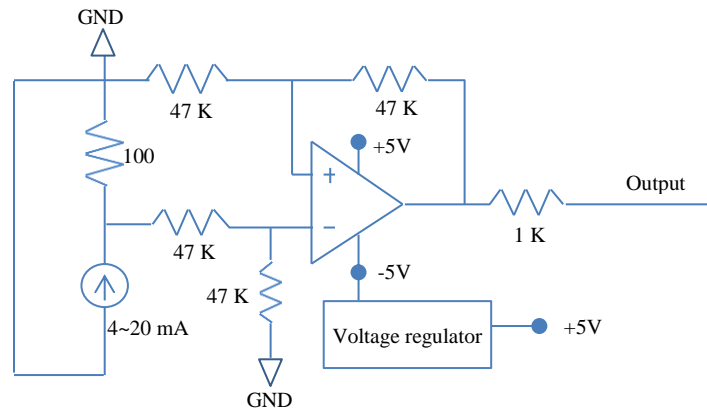


Figure 10-7: Irradiated circuits of analog signal processing in Experiment Part I

Pictures of electronic circuits for analog signal processing used in Experiment Part I are shown in Figure 10-8.

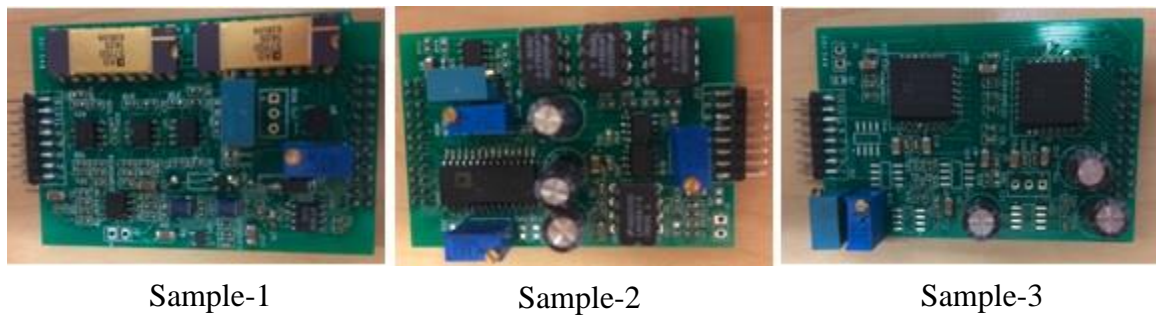


Figure 10-8: Pictures of electronic circuit boards for analog signal processing used in Experiment Part I

(2) Analog-to-Digital Converter

Analog-to-digital converter (ADC) is analog- and mix-signal circuit in a digital communication system, which can become non-functional due to performance degradation, loss of calibration, transient output errors, and latchup caused when it works in strong ionizing radiation environments (Sternberg *et al.*, 2006). Several critical parameters of various ADCs amplifiers under different dose rates have been investigated in (Sternberg *et al.*, 2006; Kalshnikov *et al.*, 1998; Lee and Johnston, 1998; Lee *et al.*, 1994), which include conversion time, degraded conversion function, power supply current, output voltage degradation, reference voltage degradation, and current noise, etc.

In this work, the test is performed under the radiation condition with high dose rate for three circuits with different ADCs: AD571, AD674, and AD1671, which are all manufactured by Analog Devices. Several parameters are involved to reflect radiation responses of those circuits: the output voltage of ADC' IO port and the output of analog-to-digital conversion. The analog-to-digital circuits and analog signal circuits are integrated in a same circuit board, which is shown in Figure 10-8.

(3) Microcontroller Module

For the measurement and transmission unit, many functions of calculation and control are carried out inside the microcontroller module, which is the most important part in a

digital communication system. Ionizing radiation may affect many aspects of the microcontroller, such as degradation of general-purpose input/output (GPIO)'s drive capability, non-function of memory units, inaccuracy of clock frequency, etc. In this work, tests for three type microcontrollers are performed under the radiation condition with a high dose rate: P89V51RC2, PIC16F77, and C8051F581, which are manufactured by NXP, Microchip, and Silicon Labs, respectively. Several test parameters are involved in this part: output voltage of GPIO, performance of memory unit (SRAM and EEPROM/FLASH), accuracy of clock frequency (PWM). Pictures of irradiated circuit boards of microcontroller modules are shown Figure 10-9.

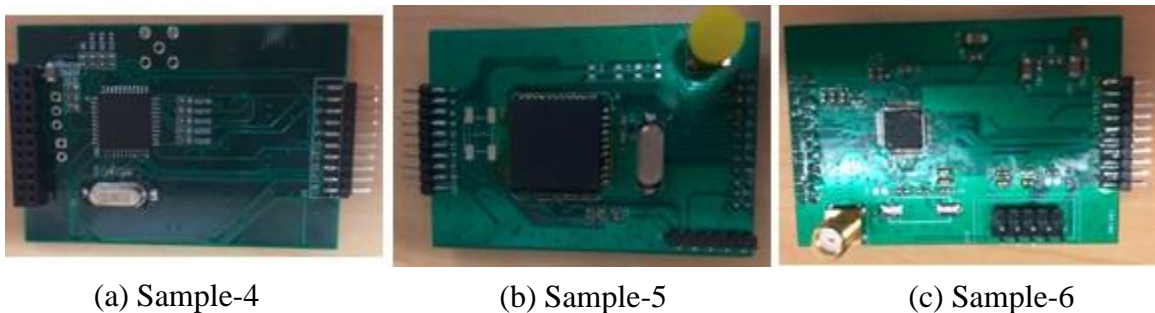


Figure 10-9: Pictures of electronic circuits for microcontroller modules used in Experiment PART I

(4) Wireless Transceiver Module

Irradiation may affect many aspects of wireless transceiver from system-level, such as degradation of IO's drive capability, inaccuracy of frequency, degradation of communication performance, received signal strength indicator (RSSI), etc. In this work, tests for three type wireless transceivers (433 MHz & 915 MHz) have been performed under the radiation condition with a high dose rate: RF2905, SI4463, and SX1278, which are manufactured by RF Micro Devices, Silicon Labs, and Semtech, respectively. Several test parameters are involved to obtain the degradation of wireless transceivers: output voltage of IO port, packet loss rate, packet error rate, frequency, and RSSI.

Pictures of irradiated circuit boards of wireless transceiver modules in Experiment Part I are shown in Figure 10-10.

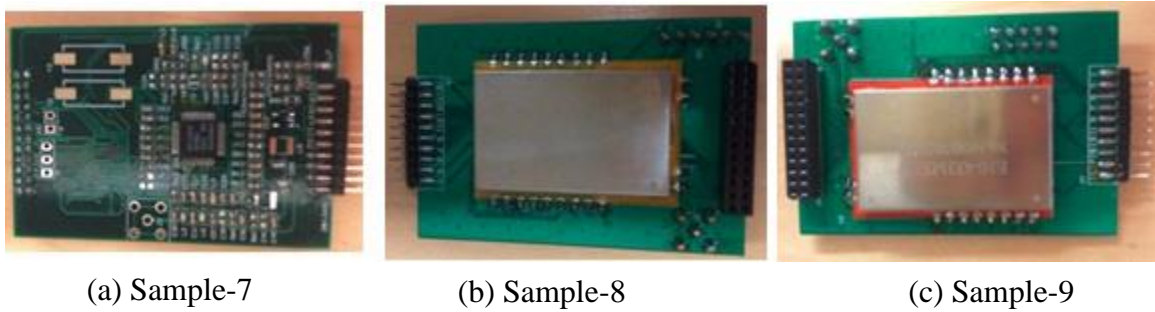


Figure 10-10: Picture of electronic circuits for wireless transceiver modules using in Experiment Part I

10.2.2 Experimental Setup

In this test, samples are placed in the 6-inch diameter Co-60 irradiator tube. The gamma irradiator generates the dose rate of 20 K Rad/h on the samples. A voltage source located outside the irradiator is connected to wireless measurement and transmission units as power supply with 30 ft wires. A DC-DC converter is installed at the top of the elevator as power supplies for all irradiated samples. A lead shielding is used to mitigate radiation damages on the DC-DC converter. Picture of this experimental setup is shown in Figure 10-11.

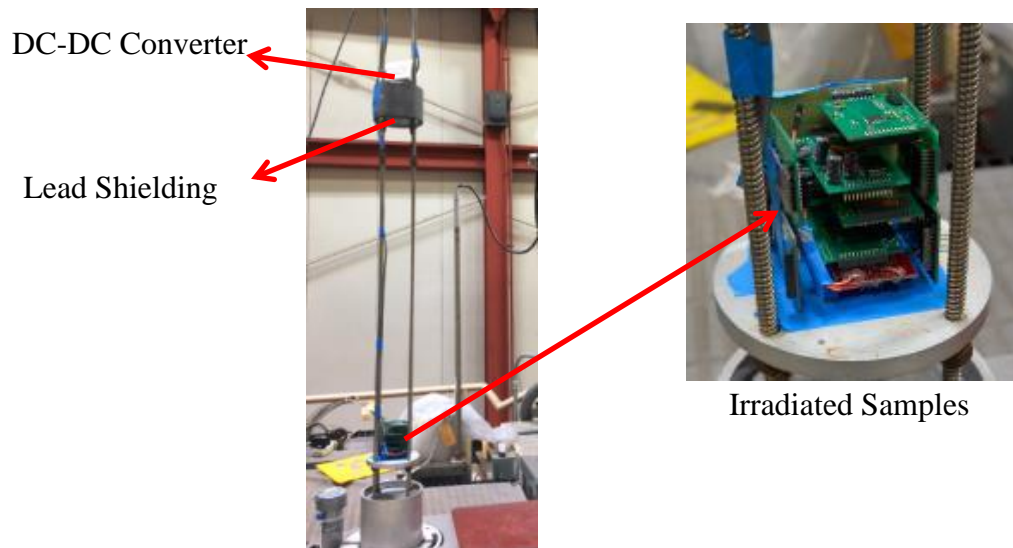


Figure 10-11: Picture of experimental setup in Experiment Part I

Several radiation levels are considered in this part of tests: 0 Rad, 10 K Rad, 30 K Rad, 50 K Rad, 100 K Rad, and 130 K Rad. The test is performed by first measuring electrical parameters of the device, then according to the selected radiation level, exposing it to ionizing radiation, after a fixed period of time (30 mins, 90 mins, 150 mins, 300 mins, and 390mins), re-measuring those parameters to obtain their responses. If a device permanently loses its function, it will not further be irradiated. According to measured parameters, radiation-tolerances of each module can be obtained and the radiation vulnerability in a wireless monitoring device using these modules can be also analyzed.

All irradiated samples and their information in Experiment PART I are summarized in Table 10-3.

Table 10-3: The summary of the irradiated devices in Experiment Part I

| Module Function | Semiconductor Device | Manufacture | Semiconductor Technology |
|----------------------------------|----------------------|--|--------------------------|
| Analog signal processing circuit | CLC502 LT1611 | National Semiconductor, Linear Technology | Bipolar, Bipolar |
| | LM108, MAX660 | Texas Instruments, Texas Instruments | CMOS, BiCMOS |
| | UA741, LM2662 | STMicroelectronics, Texas Instruments | BiFET, BiCMOS |
| Analog-to-digital converter | AD571 | Analog Devices | Bipolar |
| | AD674 | Analog Devices | CMOS |
| | AD1671 | Analog Devices | BiMOS |
| Microcontroller | P89V51RC2 | NXP | CMOS |
| | PIC16F77 | Microchip | CMOS |
| | C8051F581 | Silicon Labs | TTL Logic |
| Wireless transceiver | RF2905 | RF Micro Devices | Bipolar |
| | SX1278 | Silicon Labs | CMOS |
| | SI4463 | Semtech | TTL Logic |

10.2.3 Experimental Results

(1) Analog Signal Processing Circuits

The outputs of the analog signal processing circuits with the input signal with 4~20 mA during 390 minutes under the high dose rate (20 K Rad/h) are listed in Table 10-4 and are illustrated in Figure 10-12.

Table 10-4: Radiation responses of analog signal processing circuits during 390 minutes under a high dose rate condition

| Irradiated time (total dose) | Input signal (mA) | Output measurement (V) | | |
|---------------------------------|----------------------|------------------------|--------------|--------------|
| | | Sample-1 | Sample-2 | Sample-3 |
| 0 min (0 K Rad) | 4 | 0.251 | 0.470 | 0.466 |
| | 10 | 0.735 | 1.070 | 0.977 |
| | 20 | 1.515 | 2.070 | 1.890 |
| 30 mins (10 K Rad) | 4 | 0.252 | 0.470 | 0.465 |
| | 10 | 0.734 | 1.070 | 0.977 |
| | 20 | 1.530 | 2.080 | 1.890 |
| 90 mins (30 K Rad) | 4 | 0.250 | 0.470 | 0.468 |
| | 10 | 0.730 | 1.060 | 0.977 |
| | 20 | 1.470 | 2.070 | 1.890 |
| 150 mins (50 K Rad) | 4 | 0.250 | 0.484 | 0.451 |
| | 10 | 0.730 | 1.080 | 0.963 |
| | 20 | 1.460 | 2.080 | 1.850 |
| 300 mins (100 K Rad) | 4 | 0.646(incorrect) | 5.0 (Failed) | 5.0 (Failed) |
| | 10 | 0.984(incorrect) | 5.0 (Failed) | 5.0 (Failed) |
| | 20 | 1.780(incorrect) | 5.0 (Failed) | 5.0 (Failed) |
| 390 mins (130 K Rad) | 4 | 4.25 (Failed) | 5.0 (Failed) | 5.0 (Failed) |
| | 10 | 4.25 (Failed) | 5.0 (Failed) | 5.0 (Failed) |
| | 20 | 4.25 (Failed) | 5.0 (Failed) | 5.0 (Failed) |

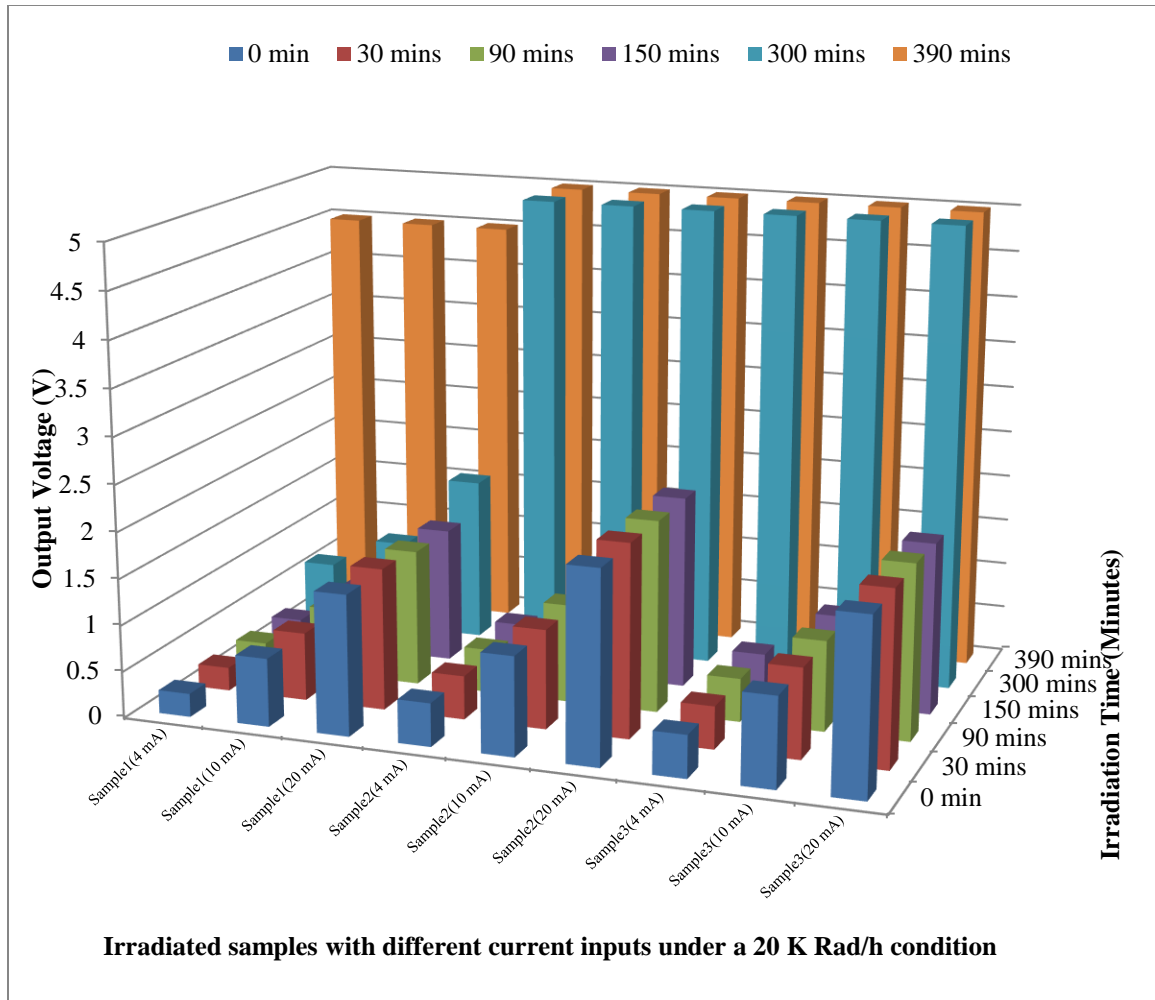


Figure 10-12: Radiation responses of analog signal processing circuits during 390 minutes under a high dose rate condition

Experimental results have shown that when total doses are less than 50 K Rad, each circuit works well with the complete function for different current inputs. At 50 K Rad, sample-2 and sample -3 (LM108 and UA741) still work well. However, when the total dose is 100 K Rad, the output of Sample-1 becomes incorrect and Sample-2 and Sample-3 have permanently failed. At 130 K Rad, all irradiated samples are permanently failed.

Function statuses of the failed analog processing circuits are listed in Table 10-5.

Table 10-5: Status of the failed analog signal processing circuits

| Irradiated Devices | Functions | Components | Output | Test Result |
|--------------------|-------------------|------------|---------|-------------|
| Sample-1 | -5V reference | LT1611 | 0.296 V | Failed |
| | Amplifier circuit | CLC502 | - | - |
| Sample-2 | -5V reference | MAX660 | -5V | Functional |
| | Amplifier circuit | LM108 | 0V | Failed |
| Sample-3 | -5V reference | LM2662 | 0.046V | Failed |
| | Amplifier circuit | UA741 | - | - |

(2) Analog-to-Digital Converter

The conversion outputs of ADC chips with the output of analog processing circuits during 390 minutes at high dose rate (20 K Rad/h) are listed in Table 10-5 and are illustrated in Figure 10-13. The ADC inputs are the outputs of signal processing circuits with 4~20 mA signals.

Table 10-6: Measurement conversion outputs of analog-to-digital converters during 390 minutes under a high dose rate condition

| Irradiated time (total dose) | Sample-1 | | Sample-2 | | Sample-3 | |
|---------------------------------|---------------|----------------------------|---------------|----------------------------|---------------|----------------------------|
| | Input voltage | Output code (Hex / Dec) | Input voltage | Output code (Hex / Dec) | Input voltage | Output code (Hex / Dec) |
| 0 min (0 K Rad(Si)) | 0.251 | 0020 / 32 | 0.470 | 0490 / 1168 | 0.466 | 00D0 / 208 |
| | 0.735 | 0050 / 80 | 1.070 | 0530 / 1328 | 0.977 | 0290 / 656 |
| | 1.515 | 00A0 / 160 | 2.070 | 0650 / 1616 | 1.890 | 0560 / 1392 |
| 30 mins (10 K Rad(Si)) | 0.252 | 0020 / 32 | 0.470 | 0490 / 1168 | 0.465 | 00D0 / 208 |
| | 0.734 | 0050 / 80 | 1.070 | 0530 / 1328 | 0.977 | 0290 / 656 |
| | 1.530 | 00A0 / 160 | 2.080 | 0650 / 1616 | 1.890 | 0560 / 1392 |
| 90 mins (30 K Rad(Si)) | 0.250 | 0020 / 32 | 0.470 | 0490 / 1168 | 0.468 | 00D0 / 208 |
| | 0.730 | 0050 / 80 | 1.060 | 0530 / 1328 | 0.977 | 0290 / 656 |
| | 1.470 | 00A0 / 160 | 2.070 | 0650 / 1616 | 1.890 | 0570 / 1392 |
| 150 mins (50 K Rad(Si)) | 0.250 | 0020 / 32 | 0.484 | 0490 / 1168 | 0.451 | 00D0 / 208 |
| | 0.730 | 0050 / 80 | 1.080 | 0530 / 1328 | 0.963 | 0280 / 640 |
| | 1.460 | 00A0 / 160 | 2.080 | 0650 / 1616 | 1.850 | 0560 / 1370 |
| 300 mins (100 K Rad(Si)) | 0.646 | 03FC (Failed) | 5.0 | 0FF0 (Failed) | 5.0 | 0FF0 (Failed) |
| | 0.984 | 03FC (Failed) | 5.0 | 0FF0 (Failed) | 5.0 | 0FF0 (Failed) |
| | 1.780 | 03FC (Failed) | 5.0 | 0FF0 (Failed) | 5.0 | 0FF0 (Failed) |
| 390 mins (130 K Rad(Si)) | 4.50 | 03FC (Failed) | 5.0 | 0FF0 (Failed) | 5.0 | 0FF0 (Failed) |
| | 4.50 | 03FC (Failed) | 5.0 | 0FF0 (Failed) | 5.0 | 0FF0 (Failed) |
| | 4.50 | 03FC (Failed) | 5.0 | 0FF0 (Failed) | 5.0 | 0FF0 (Failed) |

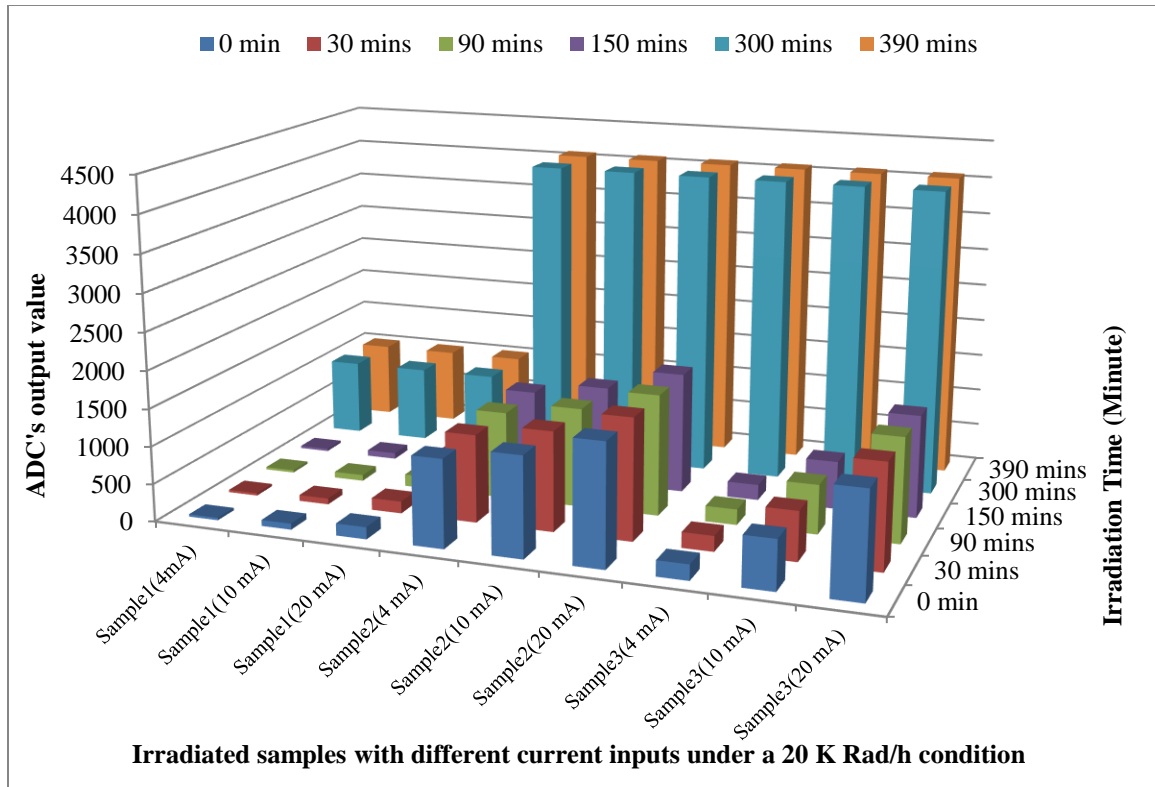


Figure 10-13: Radiation responses of analog-to-digital converter modules during 390 minutes under a high dose rate condition

The drive capability of ADC I/O port (output voltage) during 390 minutes under a high dose rate (20 K Rad/h) is shown in Table 10-7.

Table 10-7: the drive capability of ADC's output port during 390 minutes under a high dose rate condition

| Irradiated time (total dose) | Drive capability (V) | | |
|---------------------------------|----------------------|----------|----------|
| | Sample-1 | Sample-2 | Sample-3 |
| 0 min (0 K Rad) | 5.01 | 5.03 | 4.97 |
| 30 mins (10 K Rad) | 5.01 | 5.03 | 4.96 |
| 90 mins (30 K Rad) | 5.01 | 5.03 | 4.96 |
| 150 mins (50 K Rad) | 4.95 | 5.04 | 4.96 |
| 300 mins (100 K Rad) | Failed | Failed | Failed |
| 390 mins (130 K Rad) | Failed | Failed | Failed |

The experimental results have shown that all ADC circuits work well with full functions when total dose is less than or equal to 50 K Rad. Their drive capabilities and conversion outputs for different voltage inputs are same with those as before. However, all devices are permanently failed after irradiated 300 mins (100 K Rad). Hence, radiation-tolerances of all selected analog-to-digital conversion circuits seem to be between 50 K Rad and 100 K Rad.

(3) Microcontroller Module

The output voltages of GPIO during 390 minutes under a high dose rate (20 K Rad/h) condition for diversified microcontrollers are illustrated in Table 10-8.

Table 10-8: Output voltages of microcontroller's GPIOs during 390 minutes under a high dose rate condition

| Irradiated time (total dose) | Output voltage of GPIO (V) | | |
|---------------------------------|----------------------------|----------|----------|
| | Sample-4 | Sample-5 | Sample-6 |
| 0 min (0 K Rad) | 5.05 | 5.01 | 3.25 |
| 30 mins (10 K Rad) | 5.05 | 5.01 | 3.25 |
| 90 mins (30 K Rad) | 5.05 | 5.01 | 2.81 |
| 150 mins (50 K Rad) | 5.02 | Failed | Failed |
| 300 mins (100 K Rad) | 5.28 | Failed | Failed |
| 390 mins (130 K Rad) | Failed | Failed | Failed |

Several memory types of microcontroller are considered in this test: (1) Type-1, directly addressable internal data memory; (2) Type-2, indirectly addressable internal data memory; (3) Type-3, external data memory; and (4) Type-4, program memory. The performance of the memory on three samples during 390 minutes under a high dose rate (20 K Rad/h) condition is listed in Table 10-9.

Table 10-9: Performance of the memory in microcontrollers during 390 minutes under a high dose rate condition

| Irradiated time (total dose) | Memory type | Error units / total tested units | | |
|---------------------------------|----------------|----------------------------------|----------|----------|
| | | Sample-4 | Sample-5 | Sample-6 |
| 0 min (0 K Rad) | Type-1 | 0 / 32 | 0 / 32 | 0 / 32 |
| | Type-2 | 0 / 32 | 0 / 32 | 0 / 32 |
| | Type-3 | 0 / 32 | 0 / 32 | 0 / 32 |
| | Type-4 | 0 / 16 | 0 / 16 | 0 / 16 |
| 30 mins (10 K Rad) | Type-1 | 0 / 32 | 0 / 32 | 0 / 32 |
| | Type-2 | 0 / 32 | 0 / 32 | 0 / 32 |
| | Type-3 | 0 / 32 | 0 / 32 | 0 / 32 |
| | Type-4 | 0 / 16 | 0 / 16 | 0 / 16 |
| 90 mins (30 K Rad) | Type-1 | 0 / 32 | 0 / 32 | 0 / 32 |
| | Type-2 | 0 / 32 | 0 / 32 | 0 / 32 |
| | Type-3 | 0 / 32 | 0 / 32 | 0 / 32 |
| | Type-4 | 0 / 16 | 0 / 16 | 0 / 16 |
| 150 mins (50 K Rad) | Type-1 | 0 / 32 | Failed | Failed |
| | Type-2 | 0 / 32 | | |
| | Type-3 | 0 / 32 | | |
| | Type-4 | 0 / 16 | | |
| 300 mins (100 K Rad) | Type-1 | 0 / 32 | Failed | Failed |
| | Type-2 | 0 / 32 | | |
| | Type-3 | 0 / 32 | | |
| | Type-4 | 0 / 16 | | |
| 390 mins (130 K Rad) | Type-1 | Failed | Failed | Failed |
| | Type-2 | Failed | | |
| | Type-3 | Failed | | |
| | Type-4 | Failed | | |

The programming performance of diversified microcontrollers during 390 minutes under a high dose rate condition (20 K Rad/h) is illustrated in Table 10-10.

Table 10-10: Program performance of microcontroller during 390 minutes under a high dose rate condition

| Irradiated time (Total dose) | Sample-4 | Sample-5 | Sample-6 |
|---------------------------------|------------|------------|------------|
| 0 min (0 K Rad) | Program OK | Program OK | Program OK |
| 30 mins (10 K Rad) | Program OK | Program OK | Program OK |
| 90 mins (30 K Rad) | Program OK | Program OK | Program OK |
| 150 mins (50 K Rad) | Program OK | Failed | Failed |
| 300 mins (100 K Rad) | Program OK | Failed | Failed |
| 390 mins (130 K Rad) | Failed | Failed | Failed |

The accuracy of Pulse Width Modulation (PWM) frequency during 390 minutes under a high dose rate condition (20 K Rad/h) for diversified microcontrollers are illustrated in Table 10-11.

Table 10-11: PWM output of microcontrollers during 390 minutes under a high dose rate condition

| Irradiated time (Total dose) | PWM (Hz) | | |
|---------------------------------|----------|----------|----------|
| | Sample-4 | Sample-5 | Sample-6 |
| 0 min (0 K Rad) | 50.0 | 50.0 | 50.0 |
| 30 mins (10 K Rad) | 50.0 | 50.0 | 50.0 |
| 90 mins (30 K Rad) | 49.8 | 50.0 | 50.0 |
| 150 mins (50 K Rad) | 49.8 | Failed | Failed |
| 300 mins (100 K Rad) | 49.8 | Failed | Failed |
| 390 mins (130 K Rad) | Failed | Failed | Failed |

The functions of UARTs during 390 minutes under a high dose rate condition for diversified microcontrollers are illustrated in Table 10-12.

Table 10-12: UART function of microcontrollers during 390 minutes under a high dose rate condition

| Irradiated time (total dose) | UART Function | | |
|---------------------------------|---------------|----------|----------|
| | Sample-4 | Sample-5 | Sample-6 |
| 0 min (0 K Rad) | OK | OK | OK |
| 30 mins (10 K Rad) | OK | OK | OK |
| 90 mins (30 K Rad) | OK | OK | OK |
| 150 mins (50 K Rad) | OK | Failed | Failed |
| 300 mins (100 K Rad) | OK | Failed | Failed |
| 390 mins (130 K Rad) | Failed | Failed | Failed |

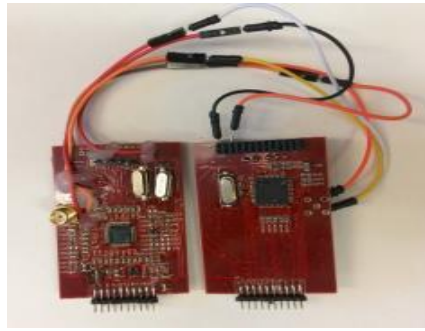
Experimental results have shown that all performance parameters (voltage output, memory testing, programming capability, PWM, and UART) are correct before the total dose reaches the limitation of the microcontroller. However, the total dose limitations of three microcontrollers are different. Sample-4 (P89V51RC2) can work well at 100 K Rad and it fails at 130 K Rad; both Sample-5 (PIC16F77) and Sample-6 (C8051F581) can work functionally when the total dose is less than or equal to 30 K Rad, but they fail at 50 K Rad. The status of typical functions in failed microcontroller is summarized in Table 10-13.

Table 10-13: The status of typical functions in failed microcontroller circuits

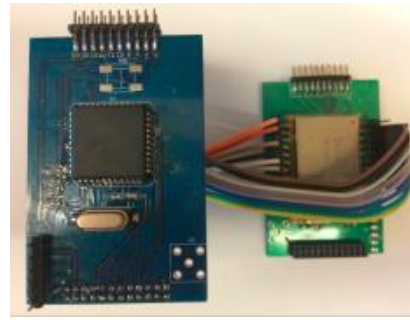
| Irradiated Device | Function | Output | Result |
|-------------------|----------|----------------|------------|
| Sample-4 | Crystal | 20 MHz | Functional |
| | GPIO | 5.05V | Functional |
| | UART | OK | Functional |
| | PWM | 49.8 Hz | Functional |
| | SRAM | OK | Functional |
| | EEPROM | Program failed | Failed |
| Sample-5 | Crystal | No responses | Failed |
| | GPIO | 0.0 V | Failed |
| | UART | No responses | Failed |
| | PWM | No responses | Failed |
| | SRAM | No responses | Failed |
| | EEPROM | Program OK | Functional |
| Sample-6 | Crystal | No responses | Failed |
| | GPIO | 1.7 V | Failed |
| | UART | No responses | Failed |
| | PWM | No responses | Failed |
| | SRAM | No responses | Failed |
| | FLASH | Program failed | Failed |

(4) Wireless Transceiver Module

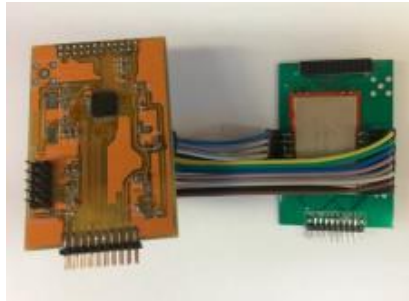
Several transceivers are involved to measure their communication performance, they are shown in Figure 10-14. Communication performance is evaluated through re-measuring the error rate and the loss rate during 2 minutes, frequency, and RSSI after wireless transceiver circuits expore in ionizing radiation for a specific period of time (30 mins, 90 mins, 150 mins, 300 mins, and 390 mins).



(a) Measurement unit for Sample-7



(b) Measurement unit for Sample-8



(c) Measurement unit for Sample-9

Figure 10-14: Pictures of the developed devices to measure the performance of irradiated wireless transceivers using in Experiment Part I

The output voltage of IO port (drive capability) during 390 minutes under high dose rate conditions of diversified wireless transceivers are illustrated in Table 10-14.

Table 10-14: The output voltage of IO port of wireless transceivers during 390 minutes under a high dose rate condition

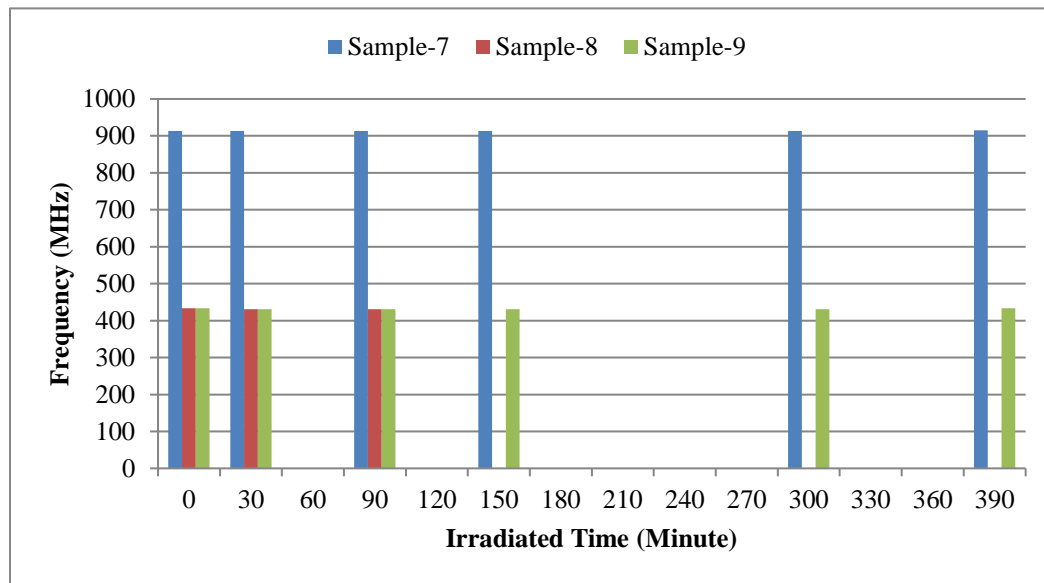
| Irradiated time (total dose) | Output voltage of GPIO (V) | | |
|---------------------------------|----------------------------|----------|----------|
| | Sample-7 | Sample-8 | Sample-9 |
| 0 min (0 K Rad) | 4.60 | 5.03 | 3.15 |
| 30 mins (10 K Rad) | 4.48 | 5.03 | 3.15 |
| 90 mins (30 K Rad) | 4.48 | 4.58 | 2.74 |
| 150 mins (50 K Rad) | 4.55 | Failed | 2.73 |
| 300 mins (100 K Rad) | 4.48 | Failed | 2.74 |
| 390 mins (130 K Rad) | 3.65 | Failed | 2.73 |

Communication performance parameters (packet error rate, packet loss rate, frequency, RSSI) of three wireless transmission circuits during 390 minutes under a high dose rate condition are illustrated in Table 10-15.

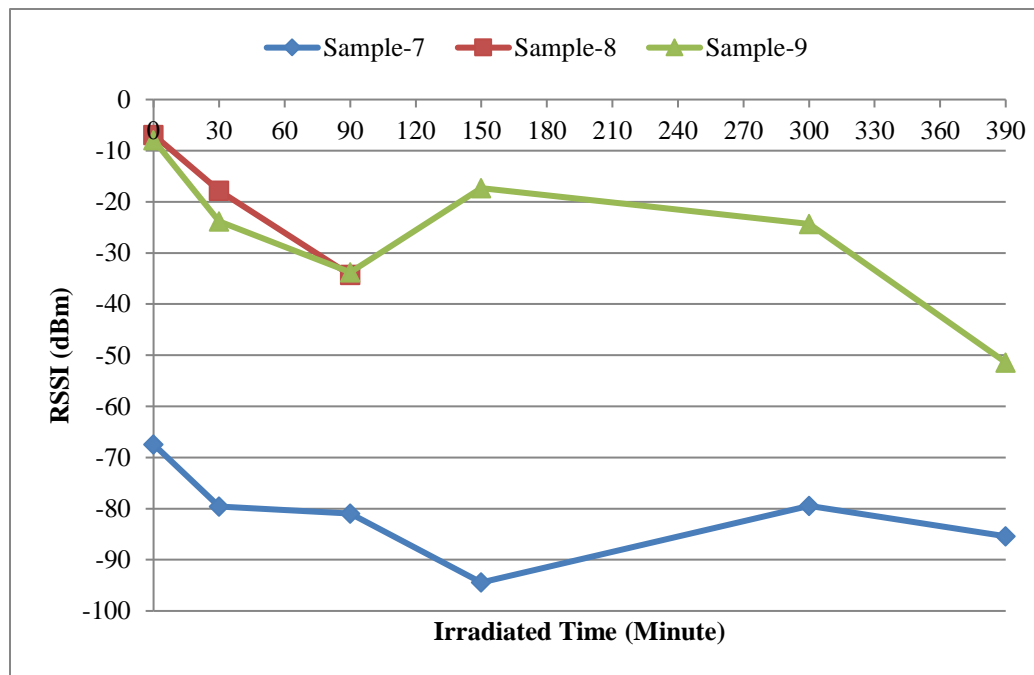
Table 10-15: Communication performance of wireless transceivers during 390 minutes under a high dose rate condition

| Irradiated duration (total dose) | Parameter | Sample-7 | Sample-8 | Sample-9 |
|-------------------------------------|---------------------|------------|------------|------------|
| 0 min (0 K Rad) | Total packets | 60 | 60 | 60 |
| | Packet error & rate | 0 (0%) | 0 (0%) | 0 (0%) |
| | Packet loss & rate | 0 (0%) | 0 (0%) | 0 (0%) |
| | Frequency | 913.243MHz | 433.225MHz | 433.225MHz |
| | RSSI | -67.43dBm | -6.90dBm | -7.90dBm |
| 30 mins (10 K Rad) | Total packets | 60 | 60 | 60 |
| | Packet error & rate | 0 (0%) | 0 (0%) | 0 (0%) |
| | Packet loss & rate | 0 (0%) | 0 (0%) | 0 (0%) |
| | Frequency | 912.973MHz | 431.261MHz | 431.261MHz |
| | RSSI | -79.56dBm | -17.8dBm | -23.80dBm |
| 90 mins (30 K Rad)) | Total packets | 60 | 60 | 60 |
| | Packet error & rate | 0 (0%) | 0 (0%) | 0 (0%) |
| | Packet loss & rate | 0 (0%) | 0 (0%) | 0 (0%) |
| | Frequency | 912.973MHz | 431.261MHz | 431.261MHz |
| | RSSI | -80.94dBm | -34.3dBm | -22.80dBm |
| 150 mins (50 K Rad (Si)) | Total packets | 60 | Failed | 60 |
| | Packet error & rate | 0 (0%) | Failed | 0 (0%) |
| | Packet loss & rate | 0 (0%) | Failed | 0 (0%) |
| | Frequency | 912.973MHz | Failed | 431.261MHz |
| | RSSI | -94.44dBm | Failed | -17.30dBm |
| 300 mins (100 K Rad (Si)) | Total packets | 60 | Failed | 60 |
| | Packet error & rate | 0 (0%) | | 0 (0%) |
| | Packet loss & rate | 0 (0%) | | 0 (0%) |
| | Frequency | 913.784MHz | | 431.261MHz |
| | RSSI | -79.43dBm | | -24.30dBm |
| 390 mins (130 K Rad (Si)) | Total packets | 60 | Failed | 60 |
| | Packet error & rate | 0 (0%) | | 0 (0%) |
| | Packet loss & rate | 0 (0%) | | 0 (0%) |
| | Frequency | 914.730MHz | | 433.090MHz |
| | RSSI | -85.42dBm | | -51.40dBm |

Comparison of wireless signal performance of three wireless devices used in Experiment Part I is shown in Figure 10-15.



(a) Frequency



(b) RSSI

Figure 10-15: Comparison of wireless signal performance of three wireless devices used in Experiment Part I

10.2.4 Discussions

Based on the experimental results and studies, the following summary can be drawn from Experiment Part I:

- (a) All irradiated circuits can work normally under the radiation condition with total dose as long as it is less than 30 K Rad.
- (b) When the total dose is more than 30 K Rad and less than 50 K Rad, for analog signal processing circuits, all irradiated samples remain working. For analog-to-digital converters, all irradiated circuits work well. For microcontrollers, Sample-5 and Sample-6 have failed for all tested functions. But Sample-4 still works well and it's all functions are normal. For wireless transceivers, Sample-7 and Sample-9 work well and their communication performance does not degrade, but Sample-8 has failed.
- (c) When the total dose is more than 50 K Rad but less than 100 K Rad, for analog processing circuits, the output sample-1 is incorrect, Sample-2 and Sample-3 failed permanently. For analog-to-digital converters, all irradiated circuits have permanently failed. For microcontrollers, Sample-4 still remains working. Wireless transceiver Sample-7 and Sample-9 also work well.
- (d) When the total dose is more than 100 K Rad but less than 130 K Rad, all analog signal processing circuits stop working. All analog-to-digital converters also failed. Microcontroller Sample-4 still works well with full functionalities. Wireless transceiver Sample-7 and Sample-9 also work well.
- (e) After testing samples are irradiated 390 minutes, the total dose reaches 130 K Rad (Si), Sample-4 stops working. Wireless transceiver Sample-7 and Sample-9 still work well. All communication parameters have no changes except RSSI.

Radiation resistances of all irradiated circuits in Experiment Part I are summarized in Table 10-16.

Table 10-16: Radiation resistances of irradiated circuits under a high dose rate condition in Experiment Part I

| Modules | Irradiated devices | Semiconductor technologies | Failed total doses | Estimated radiation resistances |
|---------------------------------------|--------------------|----------------------------|--------------------|---------------------------------|
| Analog signal processing circuits | Sample-1 | Bipolar | 100 K Rad | 50 K ~ 100 K Rad |
| | Sample-2 | CMOS, BiCMOS | 100 K Rad | 50 K ~ 100 K Rad |
| | Sample-3 | BiFET, BiCMOS | 100 K Rad | 50 K ~ 100 K Rad |
| Analog-to-digital conversion circuits | Sample-1 | Bipolar | 100 K Rad | 50 K ~ 100 K Rad |
| | Sample-2 | CMOS | 100 K Rad | 50 K ~ 100 K Rad |
| | Sample-3 | BiCMOS | 100 K Rad | 50 K ~ 100 K Rad |
| Microcontroller circuits | Sample-4 | CMOS | 130 K Rad | 100 K ~ 130 K Rad |
| | Sample-5 | CMOS | 50 K Rad | 30 K ~ 50 K Rad |
| | Sample-6 | TTL Logic | 50 K Rad | 30 K ~ 50 K Rad |
| Wireless transmission circuits | Sample-7 | Bipolar | - | > 130 K Rad |
| | Sample-8 | CMOS | 50 K Rad | 30 K ~ 50 K Rad |
| | Sample-9 | TTL Logic | - | > 130 K Rad |

Estimated radiation resistances of different modules are shown in Figure 10-16.

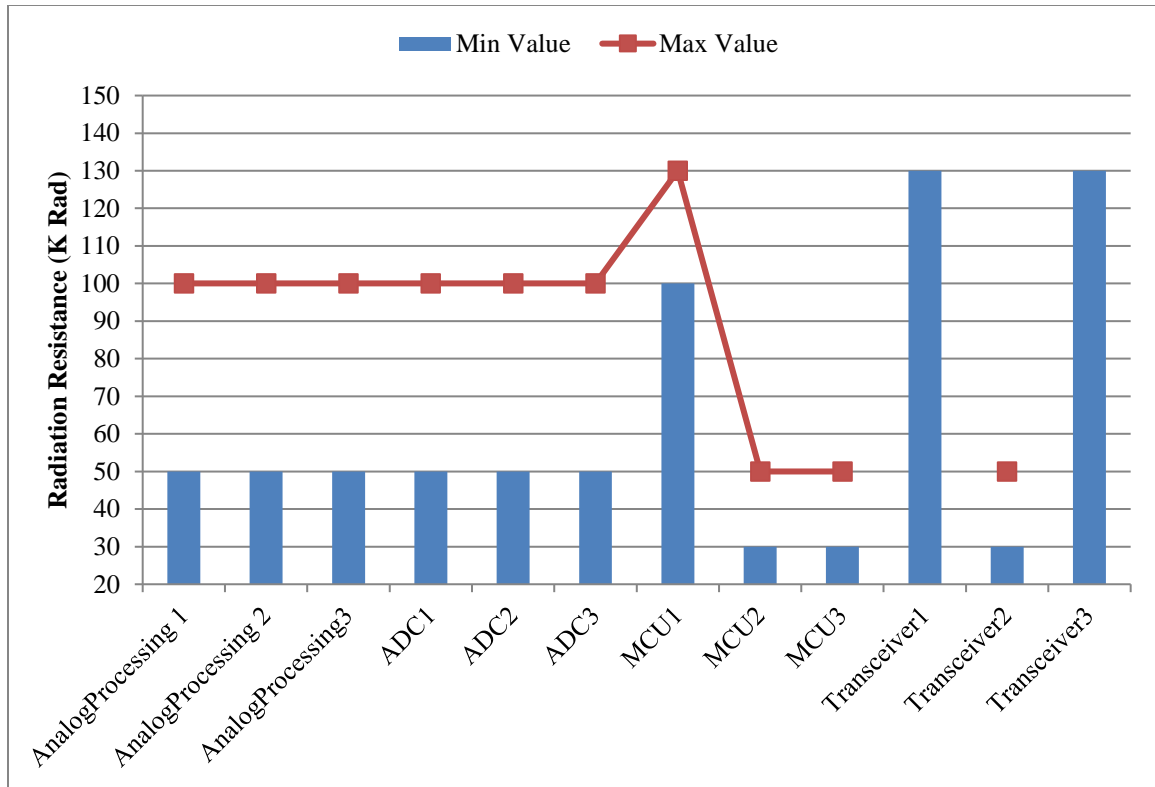


Figure 10-16: Estimated radiation resistances for irradiated simples testing used in Experiment Part I

The following conclusions apply to this total dose test:

- (a) Experimental results have shown that all irradiated devices have no the significant degradation of electrical parameters before they fail. All functions are correct until the total dose reaches the limitation. This discovery agrees well with the effects of total ionizing dose in Chapter 2.
- (b) According to the estimated radiation resistances shown in Figure 10-16, microcontroller modules may be more susceptible to high dose rate radiation than other modules.
- (c) Some selected COTS components can survive when the cumulative total dose is more than 100 K Rad, such as P89V51RC2, RF2905, and SI4463. They may have equivalent performances with some radiation-hardened components.

Total dose tests in this study are conducted to investigate the radiation vulnerability in a typical wireless monitoring system under a variety of operating conditions. However, there are some limitations that can be addressed in the future:

- (a) Online methods may be a better solution to obtain up-to-date responses of irradiated circuits and also to measure their limits of total dose in a more timely manner; and
- (b) More investigations for modern semiconductor devices and circuits need to be carried out in the future.

10.2.5 Summary

In this Section, total dose tests with ^{60}Co gamma source to investigate radiation vulnerability in the developed wireless monitoring devices have been performed. Those modules are conducted with diversified COTS semiconductor devices. Experimental results have shown that all the irradiated devices perform correctly before the total dose are more than their limits. According to the estimated radiation resistances, microcontroller modules are more susceptible to high level of radiation than other modules. Under a high dose rate condition, devices built with bipolar semiconductor technology have high level of radiation resistances than those with other semiconductor technologies.

Furthermore, experimental results have shown that all selected semiconductor devices can work normally at total dose 30 K Rad and radiation resistances of some modules and circuits are up to 130 K Rad. It has proved that the method of component selection in this work is correctness and effectiveness. It has also shown that the definition of total dose limits in this research (20 K Rad) is reasonably correct for electronic systems using in COTS components.

10.3 Part II: Evaluation of Six Industrial Wireless Transceivers and Networks in a Radiation Environment

Wireless monitoring techniques have been used in a wide variety of applications in past decades. A number of wireless transceivers and networks have been designed to acquire data from environment on physical processes. A design for a wireless monitoring system depends on the requirements of a specific application. To be used in a high level radiation environment, it will be benefited in the selecting of the wireless transceiver and network if radiation responses of those wireless transceivers and networks are known. However, so far, the investigation of this topic is very limited. In this Section, behaviors of six commonly used in industrial wireless transceivers and networks are investigated under a radiation environment with a high dose rate. The experimental results will provide a reference to design wireless monitoring systems to be used in high level radiation environments.

Six industrial wireless sensor nodes are chosen to undergo irradiation test in this Section, they are: CC2530 (2.4GHz ZigBee standard), CC2520 (2.4GHz WirelessHART standard), CC2530 (2.4GHz ISA100.11a standard), SX1278 (433MHz LoRa network), SI4463 (433MHz point-to-point network), and RF2905 (915MHz point-to-point network). Tests are conducted until each unit has a functional failure under a dose rate condition (20 K Rad/h). The behaviors of those devices and networks, e.g., communication performance (packet loss rate, packet error rate), wireless signal performance (frequency and RSSI), and survival time (lifespan), are continually online monitored throughout the tests.

This Section starts with an introduction to selected six industrial wireless sensor networks and nodes currently available on the market. Subsequently, the implementation of each wireless network and the related network configuration in this test is explained in detail. Then, the experimental setup and investigated parameters are presented. Finally, experimental results are also analyzed. Based on experimental results, several technical discussions are also provided, and potential limitations of those systems are also identified.

10.3.1 Introduction of Selected Industrial Wireless Systems

(1) Wireless Transceivers and Networks

In a typical wireless sensor network system, radio frequency (RF) signals are used to transfer the data from one node to another or a base station. Several distinct frequency bands have been assigned for wireless sensor networks in industrial applications, such as 433 MHz, 868 MHz, 915 MHz, and 2.4 GHz, etc. In the past few decades, a number of wireless transceivers have been developed to implement various communication functions. On the other hand, wireless sensor network standards define the functions and protocols for sensor nodes to integrate with a variety of networks. In recent years, many wireless sensor networks have also been developed to for various industrial applications, such as IEEE 802.15.4, ZigBee, WirelessHART, ISA100.11a, IETF 6LoW-PAN, IEEE 802.15.3, and Wibree (Yick *et al.*, 2008). Hence, a designer of industrial wireless systems faces many choices of wireless transceivers and network standards. However, if the application of these systems is within a high level radiation environment, further attentions have to be paid. Unfortunately, there are only limited resources available about radiation hardness of wireless transceivers and networks in the literature. Hence, the investigation of behaviors of wireless transceivers and networks is not only significant but also necessary.

In this Section, six industrial wireless devices and networks are selected as irradiated samples to investigate their behaviors under a high dose rate condition (20 K Rad/h). They are summarized in Table 10-17.

Table 10-17: Selected wireless transceivers and networks to be irradiated in Experiment Part II

| Sample | Network Protocol | Transceiver | Controller Unit | Frequency |
|----------|------------------|-------------|-----------------|-----------|
| Sample-1 | ZigBee | CC2530 | AVR ATMEGA 328 | 2.4 GHz |
| Sample-2 | WirelessHART | CC2520 | | 2.4 GHz |
| Sample-3 | ISA100.11a | CC2530 | STM32L486 | 2.4 GHz |
| Sample-4 | LoRa | SX1278 | PIC16F77 | 433 MHz |
| Sample-5 | Point-to-point | SI4463 | C8051F581 | 433 MHz |
| Sample-6 | Point-to-point | RF2905 | P89V51RC2 | 915 MHz |

Pictures of irradiated wireless devices used in Experiment Part II are shown in Figure 10-18.

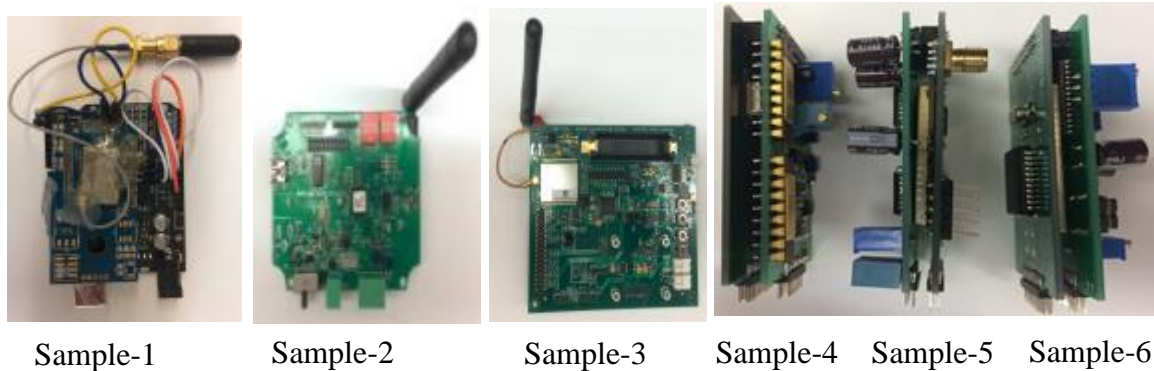


Figure 10-17: Irradiated wireless devices used in Experiment Part II

(2) Network Setup in Experiment PART II

This experiment is to be conducted in such a way that its performance is being monitored continually until the unit fails. Several wireless networks have been setup to online obtain radiation responses of wireless devices. The detailed information of each network and selected transceivers is introduced next.

➤ ZigBee network

ZigBee network supports Star, Tree, and Mesh topologies, and the star topology is often the best choice for industrial applications. Typical Star structure of ZigBee network for industrial application is illustrated in Figure 11-19 (Wang and Jiang, 2016). According to the role in network, devices are separated to three types: Coordinator, Router, and End Device. A Coordinator is used to initialize, maintain, and control the network, Router is responsible to route messages, and an End Device executes whatever actions associated the application (Wang and Jiang, 2016).

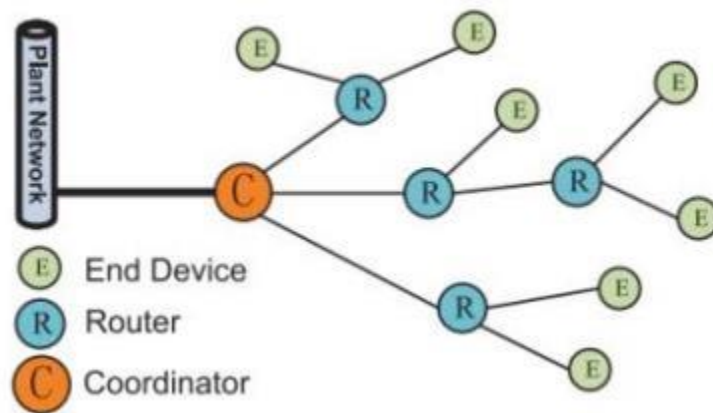
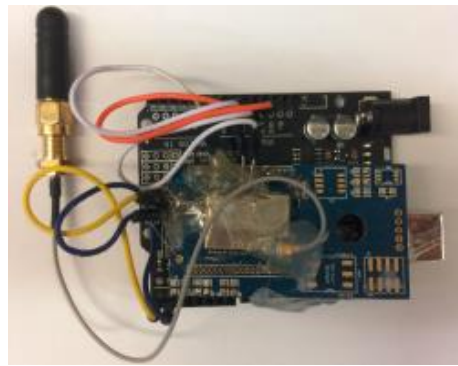


Figure 10-18: Typical Star topology of ZigBee network for industrial application (Wang and Jiang, 2016)

In this test, E800-DTU (Z2530-485-20) manufactured by Ebyte Electronic Company is used as Router and Coordinator, and E18-MS1PA1-IPX is considered as the transceiver of End Device, which is also manufactured by Ebyte Electronic Company. In addition, an AVR ATMEGA 328 is selected as the controller of End Device. Pictures of ZigBee devices using in Experiment Part II are shown in Figure 10-20. End Device sends one message to Router and Coordinator at a period of two seconds. The messages will then be transmitted to the Control Workstation through RS232 protocol.



(a) End device

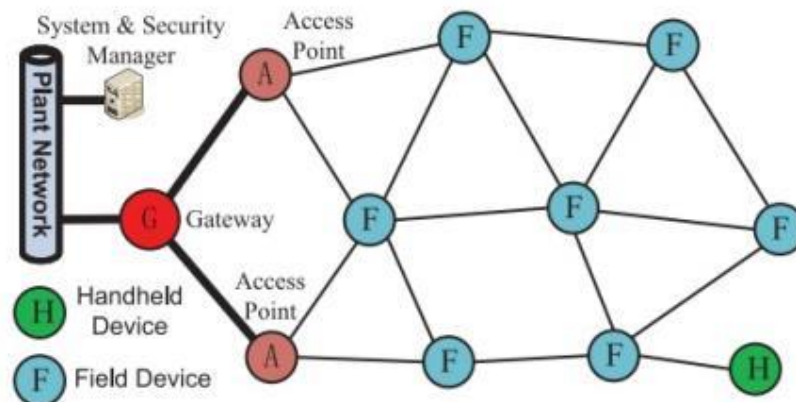


(b) Router & Coordinator

Figure 10-19: ZigBee devices used in Experiment Part II

➤ WirelessHART network

Basic elements in a WirelessHART network include: Field Devices, Gateway, Access Point, Network Manager, and Handheld Devices, which is shown in Figure 10-21 (Wang and Jiang, 2016). A Field Device is connected to the industrial process and also has the router function. An Access Point is used to connect Field Devices with Gateway. The network manager is used to configure the network, schedule and manage communications among WirelessHART devices (Wang and Jiang, 2016).

**Figure 10-20: WirelessHART network for industrial applications (Wang and Jiang, 2016)**

In this test, Awia Warrior 220 manufactured by AwiaTech Company is considered as a Field Device. WirelessHART device communicates with WirelessHART Gateway, which connects to a router. HART Server installed on the Control Workstation is selected to configure WirelessHART network. The communications are performed by WirelessHART network with proper standard protocols and HART IP between WirelessHART Gateway and the Control Workstation. Pictures of WirelessHART devices used in Experiment Part II are shown in Figure 10-22.

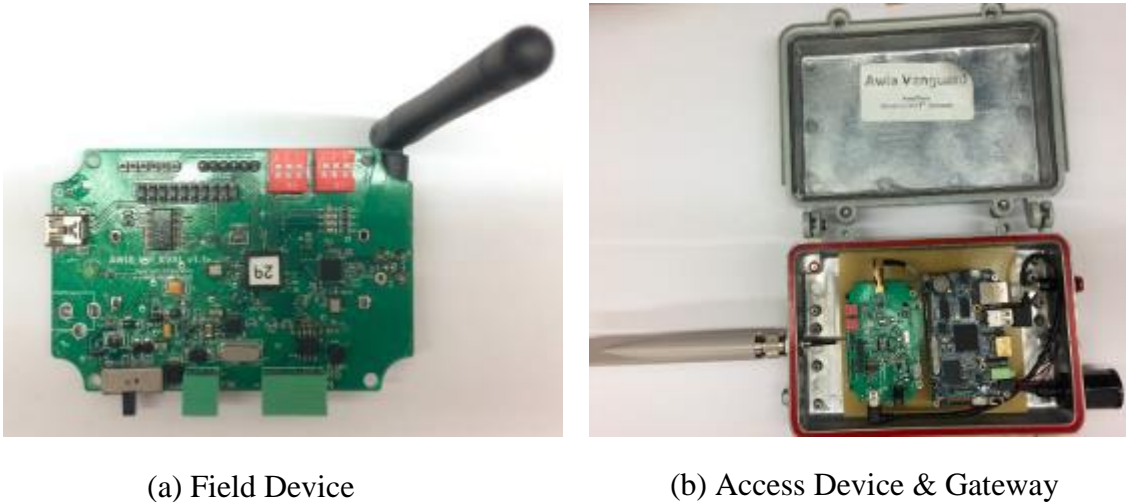


Figure 10-21: WirelessHART devices used in Experiment PART II

The menu of displaying value of chosen sensor in HART Server is shown in Figure 10-23. The connection will be disconnected when the irradiated Field Device is damaged by radiation. The tester needs to refresh this menu each a fixed period of time (5 minutes).

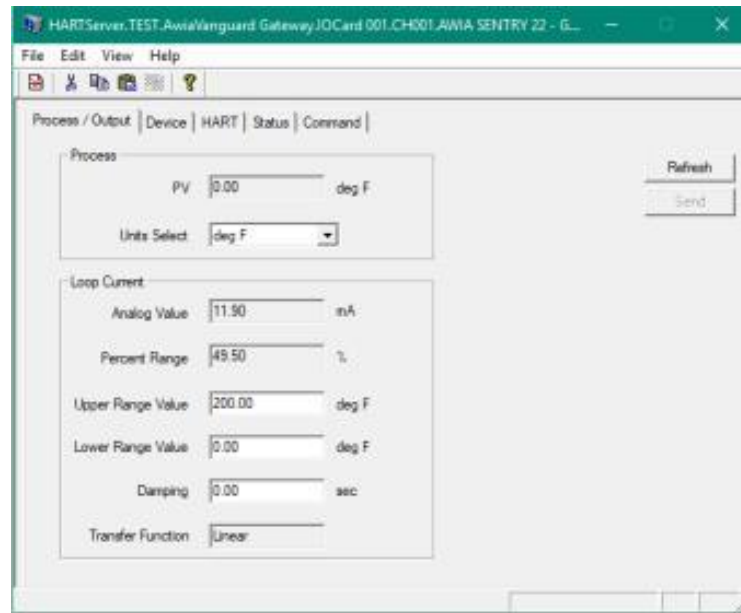


Figure 10-22: Menu of displaying value of chosen sensor in HART Server

➤ ISA100.11a network

A typical ISA100.11a network includes two type devices: Field Device and Infrastructure Devices. The former includes Routing Device, I/O Device, and Handheld Device. The latter includes Backbone Router, Gateway, and System and Security Manager (Wang and Jiang, 2016). The typical structure of ISA100.11a network for industrial applications is shown in Figure 10-24.

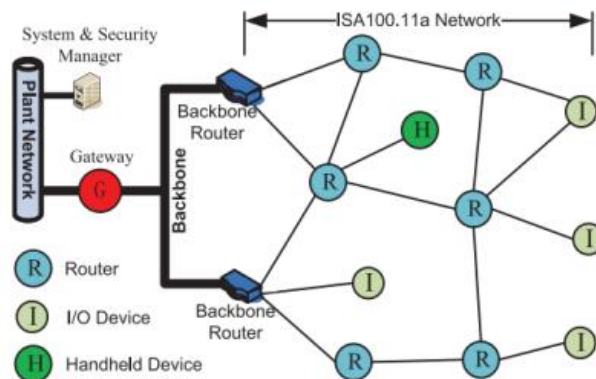


Figure 10-23: ISA100.11a network for industrial applications (Wang and Jiang, 2016).

In this test, VN210 manufactured by Company is considered as Field Router and IO Device. VersaRouter 900 is selected as Backbone Router and Gateway as hardware support for the infrastructure components, which also perform the functions of System Manager, Security Manager, and System Time Source. A web application called Monitoring Control System is developed to remotely check and configure ISA100.11a network, which is installed in VersaRouter 900 through Ethernet to communication with the Control Workstation. The user can use Internet Explorer to operator the web application at the Control Workstation. Pictures of ISA100.11a devices used in Experiment Part II are shown in Figure 10-25.



(a) I/O Device



(b) Router & Gateway

Figure 10-24: Pictures of ISA100.11a devices used in Experiment PART II

The web application installed in ISA100.11a Gateway is shown in Figure 10-26. The detailed device information is given in this application. Statistics of transmitted and received packets are also presented and analyzed in this web application. The Gateway cannot continually receive messages when irradiated ISA100.11a device is damaged by radiation. In the test, the tester needs to refresh this web application each a fixed period of time (5 minutes).

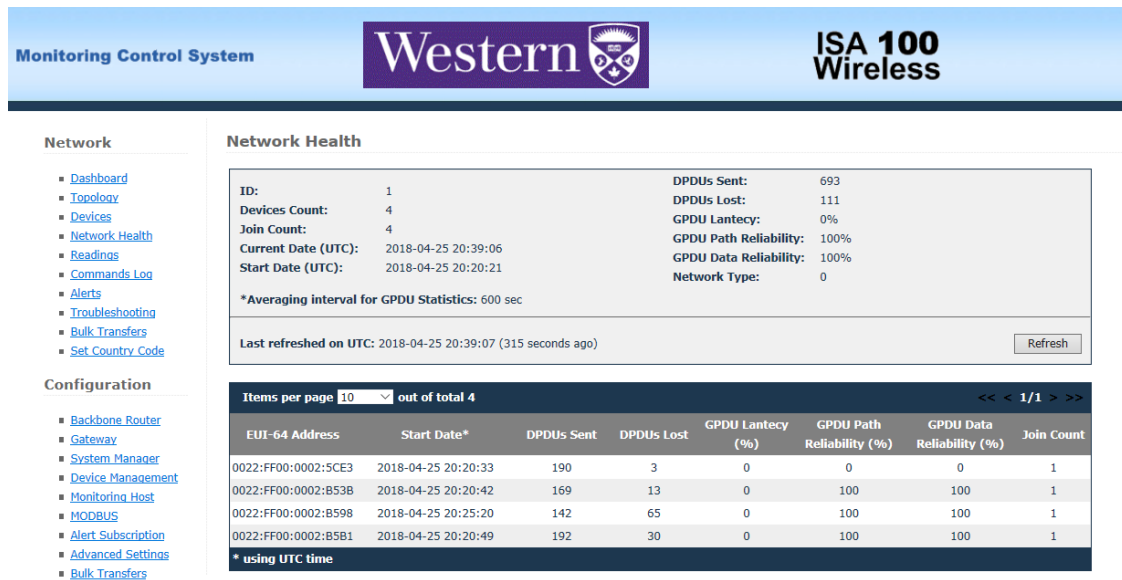


Figure 10-25: Web application installed in ISA100.11a Gateway

➤ LoRa network

LoRa devices and wireless radio frequency technology is developed proposed by Semtech, which is a long range, low power wireless platform for Internet of Things (IoT) applications (Georgiou and Raza, 2017). LoRa network includes three type devices: End Device, Gateway, and LoRa NetServer. The typical structure of LoRa network for industrial application is shown in Figure 10-27 (Centenaro *et al.*, 2016).

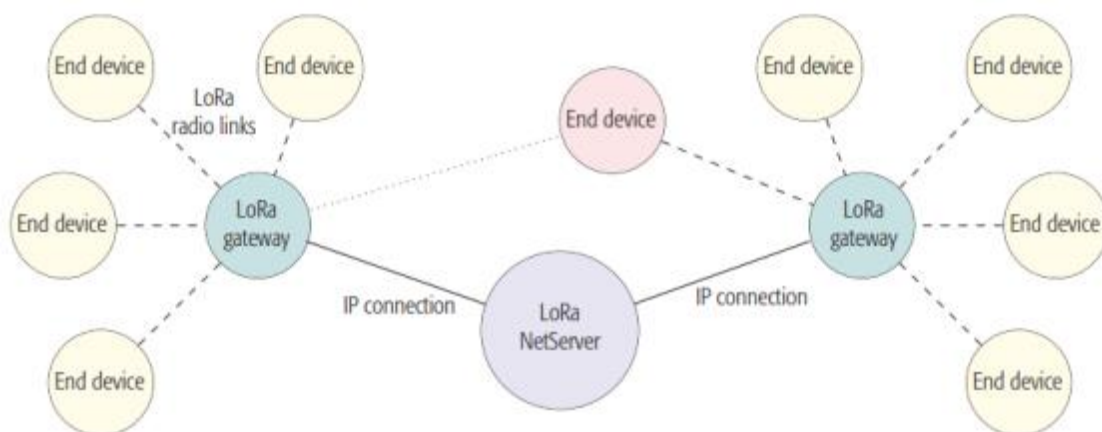


Figure 10-26: Typical structure of LoRa network in industrial application (Centenaro *et al.*, 2016)

In this test, E19-433MS1W (SX1278-based) manufactured by Ebyte Electronic Company is considered as LoRa device. A microcontroller PIC16F77 is selected to control and setup LoRa transceiver (SX1278). A gateway for LoRa, 433 MHz and 915 MHz networks shown in Figure 10-28 is also developed to obtain messages and then send them to the Control Workstation through RS232 protocol.



Figure 10-27: Pictures of gateway for LoRa, 433 MHz & 915MHz networks using in Experiment PART II

➤ 433MHz & 915MHz point-to-point network

A point-to-point network is the simplest arrangement in a communication system. It usually consists of two nodes. Typical structure of point-to-point network is shown in Figure 10-29.



Figure 10-28: Typical structure of point-to-point network

SI4463 manufactured by Silicon Labs Company is a high-performance and low-current transceiver. It is designed to be compliant with 802.15.4g and WMbus smart metering standards. In this test, SI4463 is considered as the transceiver of 433 MHz point-to-point

network and C8051F581 manufactured by Silicon Labs Company is selected as its controller.

RF2905 manufactured by is developed for linear or digital applications in different frequency bands. It is conducted with bipolar semiconductor technology. In this test, RF2905 is considered as the transceiver of 915 MHz point-to-point network and P89V51RC2 manufactured by NXP Company is selected as its controller.

10.3.2 Experimental Setup

In this part, samples are placed in the 6-inch diameter Co-60 irradiator tube. The gamma irradiator generates a dose rate of 20 K Rad/h on the samples. A potentiostat located outside the irradiator is connected to wireless measurement and transmission units as power supply with 30 ft wires. A DC-DC converter is used to generate +5 power supplies for all irradiated samples and installed at the top of the elevator. A lead shielding is used to mitigate radiation damages on the DC-DC converter. Picture of experimental setup for 2.4 GHz wireless networks used in Experiment Part II is shown in Figure 10-29.

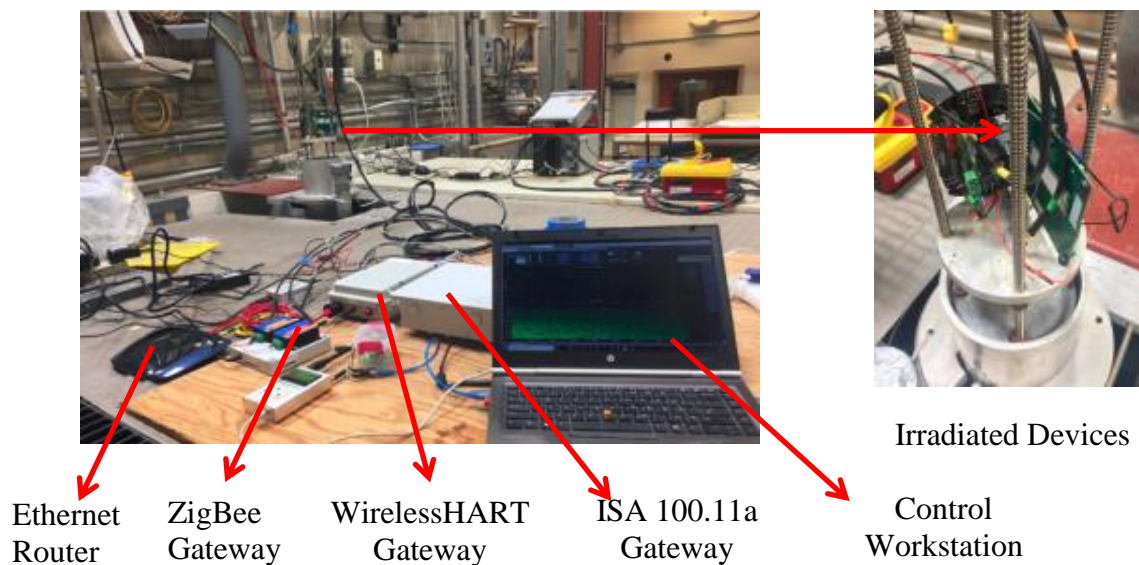


Figure 10-29: Experimental setup for 2.4 GHz wireless networks used in Experiment Part II

Picture of experimental setup for LoRa, 433 MHz, and 915 MHz wireless networks used in Experiment Part II is shown in Figure 10-30.

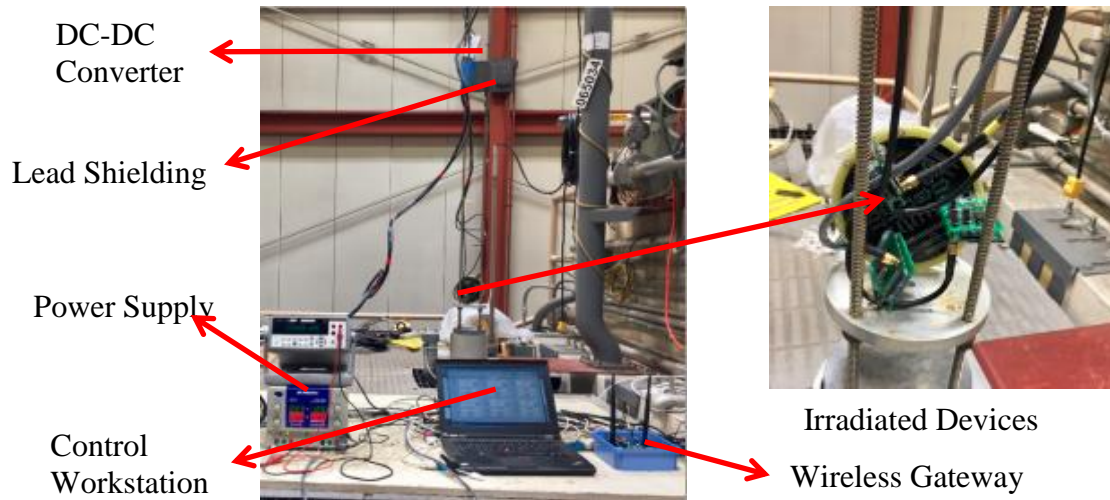


Figure 10-30: Experimental setup for LoRa, 433MHz, and 915MHz wireless devices and networks used in Experiment Part II

A software tool installed in the Control Workstation is developed to collect wireless messages of LoRa network, 433 MHz and 915 MHz network and to analyze their communication performances. Picture of the developed software tool used in Experiment Part II is shown in Figure 10-31.

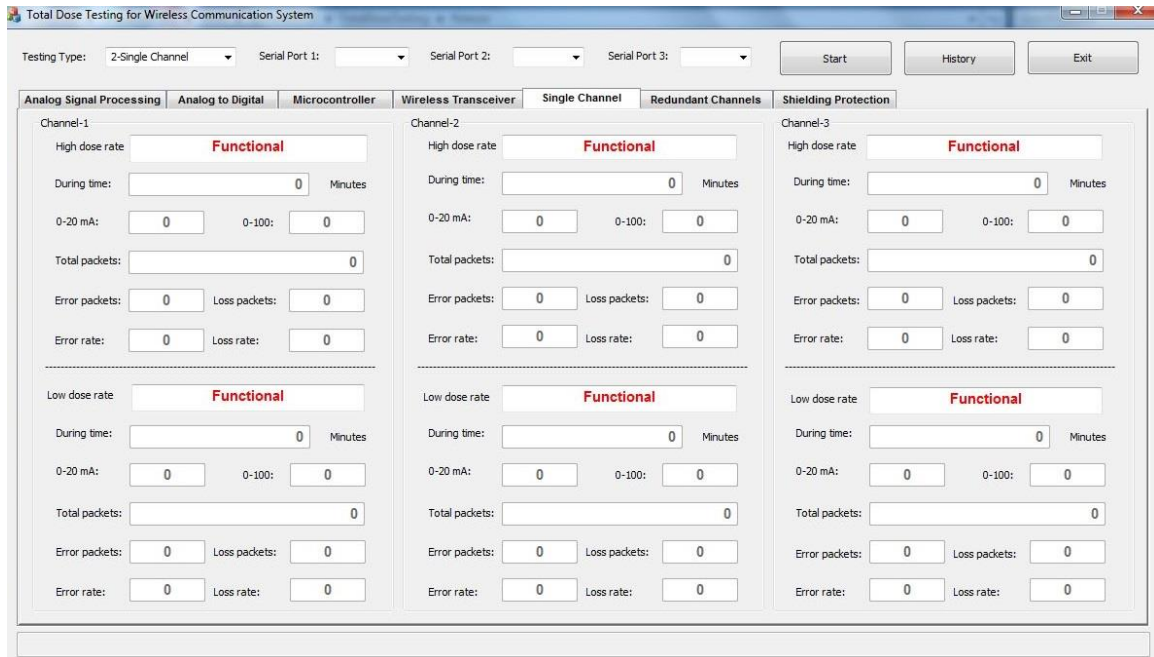


Figure 10-31: The developed software tool to collect wireless messages and analyze the communication performance used in Experiment PART II

10.3.3 Experimental Results

(1) Survival Time

According to Eq. (10-1), survival times and radiation resistances of irradiated wireless devices under a high dose rate condition (20 K Rad/h) are summarized in Table 10-18.

Table 10-18: Survival times and radiation resistances of irradiated wireless devices under a high dose rate condition in Experiment PART II

| Parameter | Sample-1 (ZigBee) | Sample-2 (Wireless HART) | Sample-3 (ISA100.11a) | Sample-4 (LoRa Network) | Sample-5 (433MHz Network) | Sample-6 (915 MHz Network) |
|------------------------------------|----------------------|--------------------------------|--------------------------|-------------------------------|---------------------------------|----------------------------------|
| Survival time (h) | 3h12m | 50m | 62m | 2h2m18s | 1h18m | 5h42m53s |
| Failed components | CPU & Transceiver | Transceiver | Transceiver | CPU & Transceiver | CPU | CPU |
| Radiation resistance (K Rad) | 64 | 16.7 | 20 | 40 | 26 | 114 |

Radiation resistances of six industrial wireless transceivers and networks used in Experiment Part II are shown in Figure 10-32.

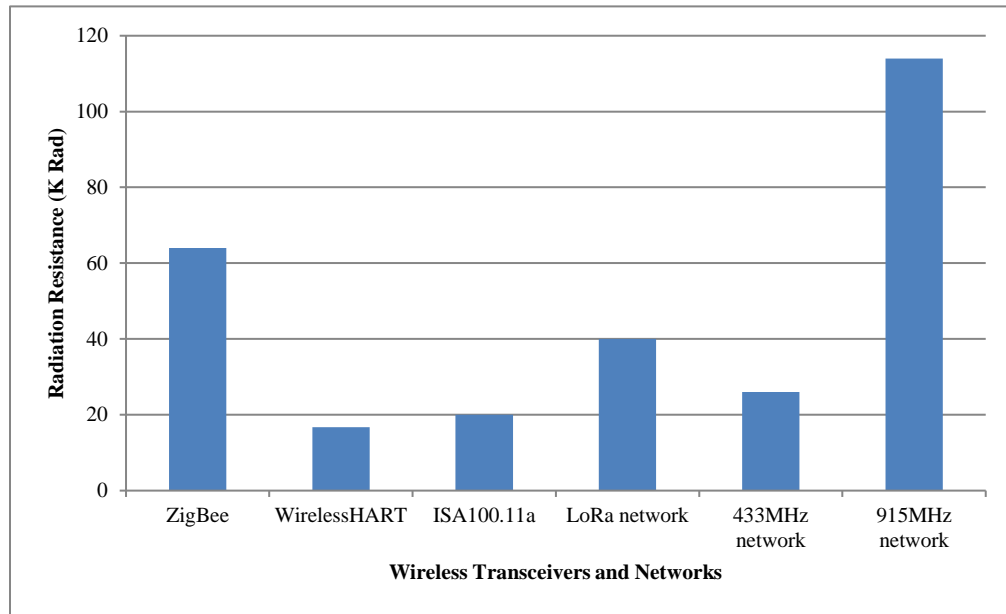


Figure 10-32: Radiation resistances of six industrial wireless transceivers and networks used in Experiment Part III

(2) Performance of Wireless Communication

Experimental results of communication performance of ZigBee device and network, as well as ISA100.11a device and network under both a normal condition and a high dose rate condition, are summarized in Table 10-19 and Table 10-20, respectively. The evaluation is performed through measuring its communication performance during a fixed period of time (5 minutes).

Table 10-19: Experimental results of communication performance of ZigBee devices and network used in Experiment Part II

| Radiation condition | Duration (minutes) | Total packets | Packet loss | Loss rate (%) | Packet error | Error rate (%) | Frequency (GHz) | RSSI (dBm) |
|---------------------|--------------------|---------------|-------------|---------------|--------------|----------------|-----------------|------------|
| Normal condition | 30 | 150 | 0 | 0.000 | 0 | 0.000 | 2.405 | -43.00 |
| | 60 | 150 | 0 | 0.000 | 0 | 0.000 | 2.406 | -32.00 |
| | 90 | 150 | 0 | 0.000 | 0 | 0.000 | 2.407 | -53.50 |
| | 150 | 150 | 0 | 0.000 | 0 | 0.000 | 2.404 | -35.00 |
| | 180 | 150 | 0 | 0.000 | 0 | 0.000 | 2.406 | -48.00 |
| 20 K Rad/h | 30 | 150 | 0 | 0.000 | 0 | 0.000 | 2.411 | -22.50 |
| | 60 | 150 | 0 | 0.000 | 0 | 0.000 | 2.411 | -53.50 |
| | 90 | 149 | 1 | 0.670 | 0 | 0.000 | 2.410 | -45.50 |
| | 150 | 150 | 0 | 0.000 | 0 | 0.000 | 2.409 | -35.50 |
| | 180 | 150 | 0 | 0.000 | 0 | 0.000 | 2.409 | -39.50 |
| | 192 | Failed | | | | | | |

Table 10-20: Summary of communication performance of ISA100.11a devices and network used in Experiment Part II

| Radiation condition | Duration (minutes) | Total packets | Packet loss | Loss rate (%) | Packet error | Error rate (%) | Frequency (GHz) | RSSI (dBm) |
|---------------------|--------------------|---------------|-------------|---------------|--------------|----------------|-----------------|------------|
| Normal condition | 30 | 119 | 0 | 0.000 | 0 | 0.000 | 2.406 | -33.50 |
| | 60 | 1375 | 0 | 0.000 | 0 | 0.000 | 2.403 | -50.50 |
| 20 K Rad/h | 30 | 117 | 2 | 1.709 | 0 | 0.000 | 2.403 | -45.00 |
| | 60 | 1368 | 9 | 0.658 | 0 | 0.000 | 2.403 | -51.00 |
| | 62 | Failed | | | | | | |

Experimental results of communication performance of WirelessHART device and network under both a normal condition and a high dose rate condition is listed in Table 10-21.

10.3.4 Discussions

Based on experimental results and studies, the following summaries can be drawn from the current study:

- (a) Radiation resistance: under a high dose rate condition (20 K Rad/h), all irradiated samples can only survive several hours. Survival time of Sample-6 (915 MHz device and network) is higher than that of other samples. Radiation resistance of Sample-6 is more than 100 K Rad. Hence, its radiation level can reached Class R in Radiation Hardness Assurance illustrated in Table 1-1. On the other hand, radiation resistances of WirelesHART and ISA100.11a devices are only 16.7 K Rad and 20 K Rad, respectively.
- (b) Communication performance: packet loss rates of four samples have a little increase and that of ZigBee device has no obvious increase under a gamma radiation environment. In addition, packet error rates of all samples have no significant changes under that condition.
- (c) Wireless signal performance: frequencies of all samples have no obvious changes under a gamma radiation environment. RSSIs of all samples have significant changes. However, due to many parameters can affect RSSIs, such as distance between the transmitter and the receiver, physical obstacles, antenna used, transmitted power, etc. Those changes of RSSIs may be caused by working condition instead of radiation. Moreover, those changes do not significant effects on communication performance.

The following conclusions apply to this total dose test:

- (a) The performance of wireless communication, e.g., packet loss rate and packet error rate, has no significant degradation under a high dose rate condition.
- (b) The parameters of wireless signal, e.g., frequency and RSSI, also have no significant effects by gamma radiation.

- (c) Wireless communication systems with a complicate hardware and software implementation, e.g., WirelessHART, ISA100.11a, may be not good solutions to be used in high level radiation environments.

10.3.5 Summary

In this Section, total dose tests with ^{60}Co gamma source to investigate radiation tolerances of six industrial wireless devices and networks have been performed. The experimental results have shown that both the performance of wireless communication and the quality of wireless signal have no significant degradation before the device stops working under a high dose rate condition.

On the other hand, the experimental results have shown that wireless system with a complicate hardware and software implementation, e.g., WirelessHART, ISA100.11a, may have no higher radiation resistances in a high dose rate condition. In addition, one solution of wireless communication system (RF2905 915MHz network) with the high radiation resistance (at least 100 K Rad) has been reported in this total dose test.

10.4 Part III: Evaluation of Diversified Wireless Monitoring Devices in Radiation Environments at both High and Low Dose Rates

Unlike other industrial accidents, in the event of a severe nuclear accident, a significant amount of radiation can be released due to failure of protection layers. Moreover, radiation levels of distinct stages in an accident and radiation condition of various areas in the plant are different. However, modern monitoring instruments are usually built with semiconductor-based electronic components, which are susceptible to distinct levels of radiation. These monitoring instruments have to work well in both high and low dose rate conditions. The objective of the experiment part III is to investigate behaviors of diversified non-redundant wireless monitoring devices in both high and low dose rate conditions. A total dose test has been performed to real-time continually measure the responses of three non-redundant wireless monitoring devices while they are being directly irradiated under gamma radiation environments at both high and also low dose rates separately. Specially, those three devices can independently complete the functions of both measurement and transmission and are conducted with diversified semiconductor-technologies. Four type parameters are reported in this study to reflect behaviors of developed wireless monitoring devices under both low and high dose rate conditions: (1) survival time; (2) measurement accuracy for 4~20 mA current signal; (3) communication performance, such as loss packets rate, and error packet rate; and (4) wireless signal parameters, such as frequency shift, received signal strength indicator (RSSI). The results of those tests will provide guideline to design wireless monitoring systems to be used in complicate radiation environments, as well as to validate the effectiveness of the diversified design.

This Section starts with an introduction of irradiated wireless devices used in this test. Subsequently, an experimental setup is developed to continually evaluate the behavior of three non-redundant wireless devices under two dose rates: a high dose rate (20 K Rad/h) and a low dose rate (200 Rad/h). These tests are performed through monitoring of measurement accuracy for a 4~20 mA signal and analyzing the wireless communication

performance. Experimental results are presented, and several technical discussions are carried out. Some potential limitations are identified.

10.4.1 Introduction of Irradiated Devices

As previously discussed, to implement a typical measurement and transmission unit, even though there can be many different components and circuits, the common building blocks are: signal processing circuit, analog-to-digital converter, microcontroller, and transceiver. However, those subsystems can be still built with different semiconductor technologies, different components from different manufactures. The understanding of radiation responses of these devices under different radiation conditions is not only important but also necessary to design a wireless monitoring system to be used in nuclear power plants under severe accident conditions.

Referring to radiation test data published by the NASA Goddard Space Flight Center, a number of semiconductor components listed in Chapter 4 are selected to build those functional blocks. Three non-redundant wireless measurement and transmission units are involved in the test, which are built with diversified semiconductor technologies. The specifics of three circuit compositions are illustrated in Figure 10-33.

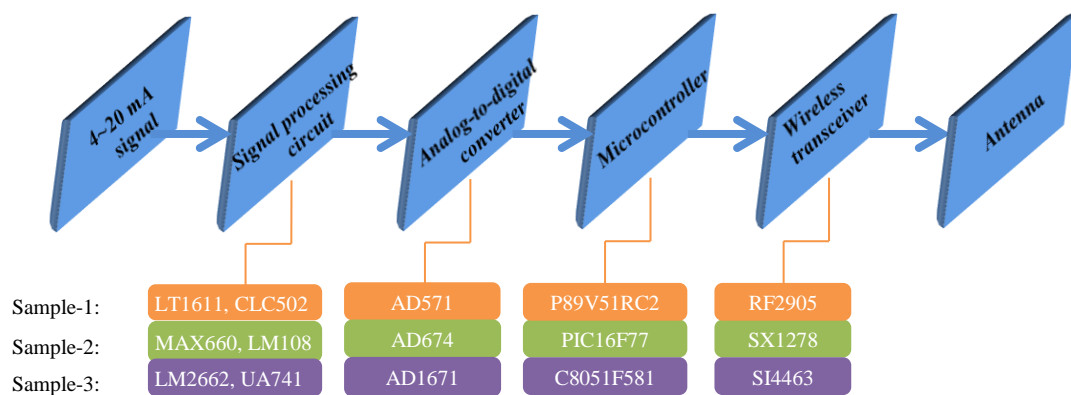


Figure 10-33: Block diagram of three diversified single-channel wireless monitoring units

In this test, through the comparing of parameters of three non-redundant wireless devices under different radiation conditions, e.g., normal condition, a low dose rate radiation, and

a high dose rate radiation, the behavior of those irradiated wireless devices can be analyzed. The parameters include the accuracy of measurement unit, performance of wireless communication, and survival time. Based on the experimental results, a designer can choose the most suitable semiconductor technology and system for a specific radiation environment. The three non-redundant wireless monitoring devices used in Experiment Part III are summarized in Table 10-25.

Table 10-25: Summary of irradiated monitoring devices used in Experiment Part III

| Type | Parameter | Sample-1 | Sample-2 | Sample-3 |
|--------------------------|----------------------------------|----------|--------------|---------------|
| Wireless parameter | Frequency | 915 MHz | 433 MHz | 433 MHz |
| Semiconductor technology | Analog signal processing circuit | Bipolar | CMOS, BiCMOS | BiFET, BiCMOS |
| | Analog-to-digit converter | Bipolar | CMOS | BiCMOS |
| | Microcontroller | CMOS | CMOS | TTL Logic |
| | Wireless transceiver | Bipolar | CMOS | TTL Logic |

10.4.2 Experimental Setup

In this test, wireless measurement and transmission devices have been placed in a 6-inch diameter Co-60 irradiator tube. They have been separated into two parts: measuring radiation responses while the device is being irradiated with 20 K Rad/h dose rate until all irradiated devices loss their functions; and measuring radiation responses of the device under a low dose rate condition (200 Rad/h) for a period of 14 hours. A potentiostat located outside the irradiator is used as power supply to wireless units using 30 ft wires. A DC-DC converter is installed over a lead shielding to provide +5V power for the irradiated devices. A current source is used as sensor input to generate 4~20 mA signal. A multi-meter is used to measure the generated 4~20mA current signal on-line. A wireless receiver and a laptop, also located outside the irradiator is used to receive data

through antennas connected to the irradiated units. A picture of the experimental setup used in Experiment Part III is shown in Figure 10-34.

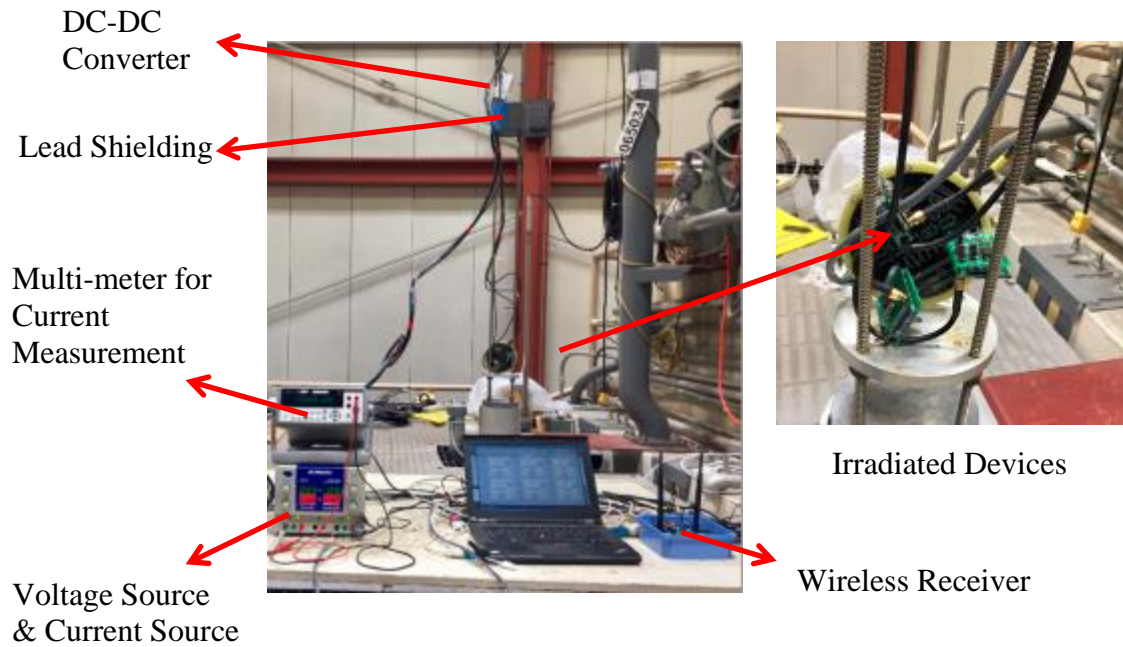


Figure 10-34: Picture of experimental setup used in Experimental Part III

An overview of the test setup used in Experimental Part III is shown in Figure 10-35.

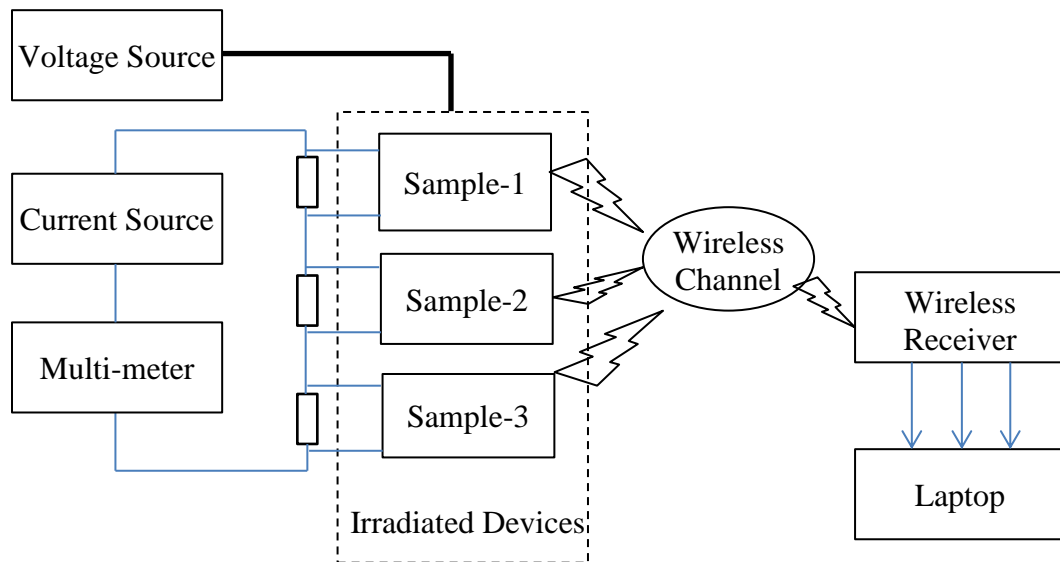


Figure 10-35: An overview of experimental setup used in Experimental Part III

A wireless receiver is developed to collect data from irradiated devices online and also to transmit to those data to the laptop as the Control Workstation through RS232 protocol. The developed wireless receiver is built with three wireless channels and three serial ports. The picture of the developed wireless receiver used in Experiment Part III is shown in Figure 10-36.



Figure 10-36: Picture of the developed wireless receiver used in Experiment Part III

A software tool developed in Visual Studio C++ shown in Figure 10-37, which is used to receive wireless data online and to record history data. The tool is installed at the Control Workstation. It receives wireless data from the wireless receiver through three RS232 serial ports.

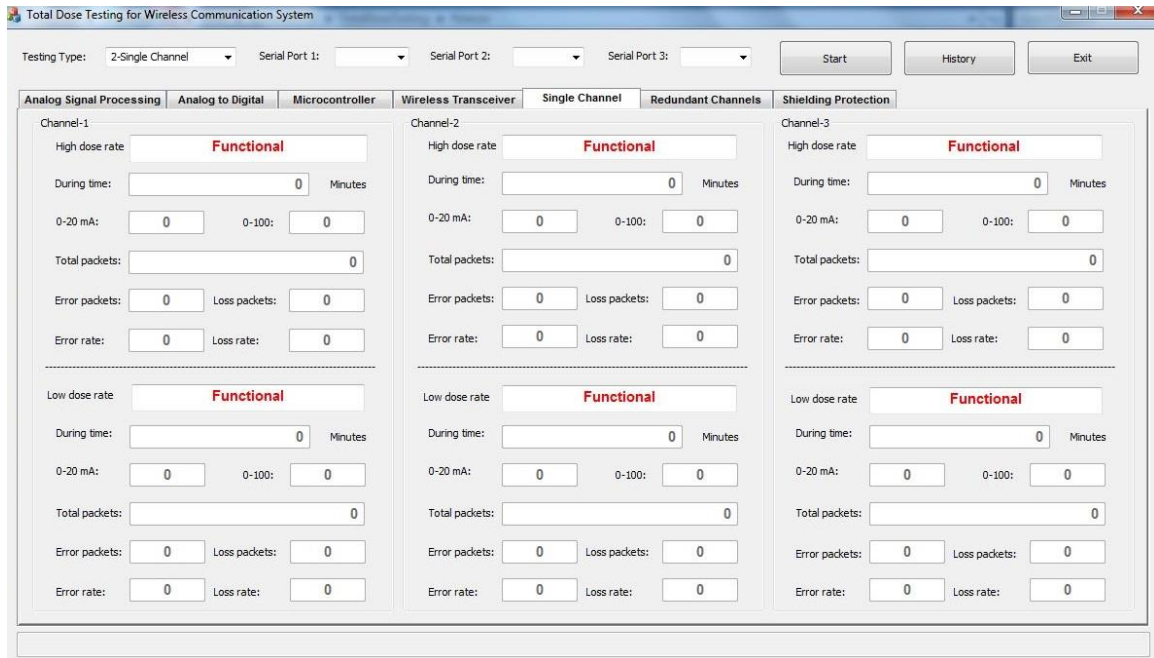


Figure 10-37: Interface of the developed software tool to receive and to record wireless data used in Experiment Part III.

Pictures of those three non-redundant wireless devices of before-irradiated and after-irradiated 20 hours under a high dose rate condition (20 K Rad/h) are shown in Figure 10-38.

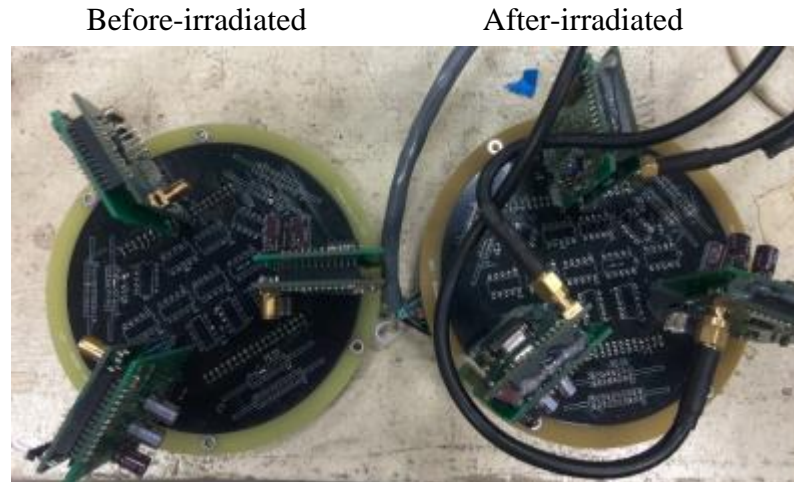


Figure 10-38: Pictures of the device before-irradiated and after-irradiated

10.4.3 Experimental Results

(1) Normal condition

The results of experimental evaluation of parameter measurement for non-redundant wireless devices under normal conditions are listed in Table 10-26.

Table 10-26: Results of experimental evaluation of parameter measurement for non-redundant wireless devices under a normal condition

| Channel | Parameters | 0 ~ 60 mins | 61 ~ 120 mins | 121 ~ 180 mins | 181 ~ 240 mins |
|----------|--------------------|-------------|---------------|----------------|----------------|
| Sample-1 | Input signal | 11.50 mA | 11.50 mA | 11.50 mA | 11.50 mA |
| | Value-1 /Count | 006C/262 | 006C/252 | 006C/244 | 006C/236 |
| | Value-2 /Count | 0070/1474 | 0070/1670 | 0070/1496 | 0070/1501 |
| | Value-3 /Count | 0074/55 | 0074/45 | 0074/46 | 0074/40 |
| | Standard Deviation | 1.618539 | 1.496598 | 1.550059 | 1.513845 |
| Sample-2 | Input signal | 11.50 mA | 11.50 mA | 11.50 mA | 11.50 mA |
| | Value-1 /Count | 0560/1381 | 0560/1507 | 0560/1478 | 0560/1491 |
| | Value-2 /Count | 0570/424 | 0570/295 | 0570/325 | 0570/308 |
| | Standard Deviation | 6.784891 | 5.921795 | 6.152103 | 6.028701 |
| Sample-3 | Input signal | 11.50 mA | 11.50 mA | 11.50 mA | 11.50 mA |
| | Value-1 /Count | 02E0/1298 | 02E0/1344 | 02E0/1394 | 02E0/1416 |
| | Value-2 /Count | 02F0/463 | 02F0/428 | 02F0/364 | 02F0/356 |
| | Value-3 /Count | 0300/10 | 0300/9 | 0300/10 | 0300/10 |
| | Standard Deviation | 7.327906 | 7.118259 | 6.815247 | 6.746642 |

The results of experiment evaluation of communication performance for non-redundant wireless devices under a normal condition are listed in Table 10-27.

Table 10-27: Results of experimental evaluation of communication performance for non-redundant wireless devices under a normal condition

| Channel | Parameters | 30 mins | 60 mins | 90 mins | 150mins | 240mins | 300mins |
|----------|-----------------|---------|---------|---------|---------|---------|---------|
| Sample-1 | Total packets | 896 | 1801 | 2689 | 4481 | 6970 | 7866 |
| | Packet loss | 0 | 0 | 0 | 0 | 0 | 0 |
| | Loss rate (%) | 0.000 | 0.000 | 0.000 | 0.000 | 0.000 | 0.000 |
| | Packet error | 2 | 3 | 3 | 6 | 11 | 13 |
| | Error rate (%) | 0.223 | 0.166 | 0.112 | 0.134 | 0.158 | 0.165 |
| | Frequency (MHz) | 915.946 | 916.486 | 915.756 | 915.069 | 916.168 | 916.305 |
| | RSSI (dBm) | -80.41 | -78.90 | -82.41 | -82.91 | -82.40 | -81.90 |
| Sample-2 | Total packets | 902 | 1804 | 2704 | 4508 | 7209 | 8109 |
| | Packet loss | 0 | 0 | 0 | 0 | 1 | 1 |
| | Loss rate (%) | 0.000 | 0.000 | 0.000 | 0.000 | 0.014 | 0.012 |
| | Packet error | 0 | 0 | 0 | 0 | 0 | 0 |
| | Error rate (%) | 0.000 | 0.000 | 0.000 | 0.000 | 0.000 | 0.000 |
| | Frequency (MHz) | 433.135 | 433.135 | 433.204 | 433.204 | 433.204 | 433.204 |
| | RSSI (dBm) | -10.90 | -18.40 | -10.40 | -18.40 | -11.90 | -10.40 |
| Sample-3 | Total packets | 902 | 1802 | 2702 | 4499 | 6985 | 8992 |
| | Packet loss | 0 | 2 | 3 | 7 | 14 | 18 |
| | Loss rate (%) | 0.000 | 0.111 | 0.111 | 0.155 | 0.200 | 0.199 |
| | Packet error | 0 | 0 | 0 | 0 | 0 | 0 |
| | Error rate (%) | 0.000 | 0.000 | 0.000 | 0.000 | 0.000 | 0.000 |
| | Frequency (MHz) | 433.135 | 433.135 | 433.204 | 433.204 | 433.204 | 433.204 |
| | RSSI (dBm) | -21.90 | -12.40 | -10.90 | -18.90 | -19.90 | -20.90 |

(2) High dose rate

The results of experimental evaluation of parameter measurement for non-redundant wireless devices under the condition with a high dose rate (20 K Rad/h) are listed in Table 10-28.

Table 10-28: Results of experimental evaluation of parameter measurement for non-redundant wireless devices under a high dose rate condition

| Channel | Parameters | 0 ~ 60 mins | 61 ~ 120 mins | 121 ~ 180 mins | 181~ 240 mins | 241 ~ 360 mins |
|----------|--------------------|-------------|----------------------------|------------------------------|---------------|----------------|
| Sample-1 | Input signal | 9.365mA | 10mA | 10mA | Failed | Failed |
| | Value-1 /Count | 0058/144 | - | 0060/235 | | |
| | Value-2 /Count | 005C/1644 | 0060/1307 | 0064/62 | | |
| | Value-3 /Count | 0060/5 | 0064/481 | Failed at 130mins | | |
| | Standard Deviation | 1.110921 | 1.774289 | 1.628417 | | |
| Sample-2 | Input signal | 9.365mA | 10mA | 10mA | Failed | Failed |
| | Value-1 /Count | 0530/1801 | 0540/1795 | 0540/71 Failed at 128mins | | |
| | Standard Deviation | 0.000000 | 0.000000 | 0.000000 | | |
| Sample-3 | Input signal | 9.365mA | 10mA | Failed | Failed | Failed |
| | Value-1 /Count | 0240/13 | 0270/11 | | | |
| | Value-2 /Count | 0250/1758 | 0280/413 | | | |
| | Value-3 /Count | 0260/27 | 0290/4 Failed at 78mins | | | |
| | Standard Deviation | 2.383874 | 2.987363 | | | |

The results of experimental evaluation of communication performance for non-redundant wireless devices under the condition with a high dose rate are listed in Table 10-29.

Table 10-29: Results of experimental evaluation of communication performance for non-redundant wireless devices under a high dose rate condition

| Channel | Parameters | 30 mins (30 K Rad) | 60 mins (60 K Rad) | 90 mins (90 K Rad) | 150 mins (150 K Rad) | 240 mins (240 K Rad) | 300 mins (100 K Rad) |
|----------|-----------------|--------------------------|--------------------------|--------------------------|----------------------------|----------------------------|----------------------------|
| Sample-1 | Total packets | 897 | 1793 | 2686 | 4477 | 7080 | 8610 |
| | Packet loss | 0 | 0 | 2 | 4 | 11 | 24 |
| | Loss rate | 0.00% | 0.00% | 0.07% | 0.09% | 0.16% | 0.28% |
| | Packet error | 3 | 19 | 19 | 19 | 19 | 19 |
| | Error rate | 0.33% | 1.06% | 0.70% | 0.42% | 0.26% | 0.22% |
| | Frequency (MHz) | 912.973 | 912.973 | 912.973 | 912.973 | 913.784 | 914.730 |
| | RSSI | -82.40 | -82.40 | -80.94 | -94.40 | -79.43 | -85.42 |
| Sample-2 | Total packets | 900 | 1802 | 2698 | 3602 | Failed | Failed |
| | Packet loss | 1 | 2 | 4 | 4 | | |
| | Loss rate | 0.11% | 0.11% | 0.15% | 0.11% | | |
| | Packet error | 0 | 0 | 0 | 0 | | |
| | Error rate | 0.00% | 0.00% | 0.00% | 0.00% | | |
| | Frequency (MHz) | 431.261 | 431.261 | 431.261 | - | | |
| | RSSI | -17.80 | -18.40 | -34.80 | - | | |
| Sample-3 | Total packets | 902 | 1798 | 2332 Failed at 78 | Failed | Failed | Failed |
| | Packet loss | 0 | 1 | 6 | | | |
| | Loss rate | 0.00% | 0.06% | 0.26% | | | |
| | Packet error | 0 | 0 | 0 | | | |
| | Error rate | 0.00% | 0.00% | 0.00% | | | |
| | Frequency (MHz) | 431.261 | 431.261 | - | | | |
| | RSSI | -23.80 | -22.80 | - | | | |

(3) Low dose rate

The results of experimental evaluation of parameter measurement for non-redundant wireless devices under the condition with a low dose rate are listed in Table 10-30.

Table 10-30: Results of experimental evaluation of parameter measurement for non-redundant wireless devices under a low dose rate condition

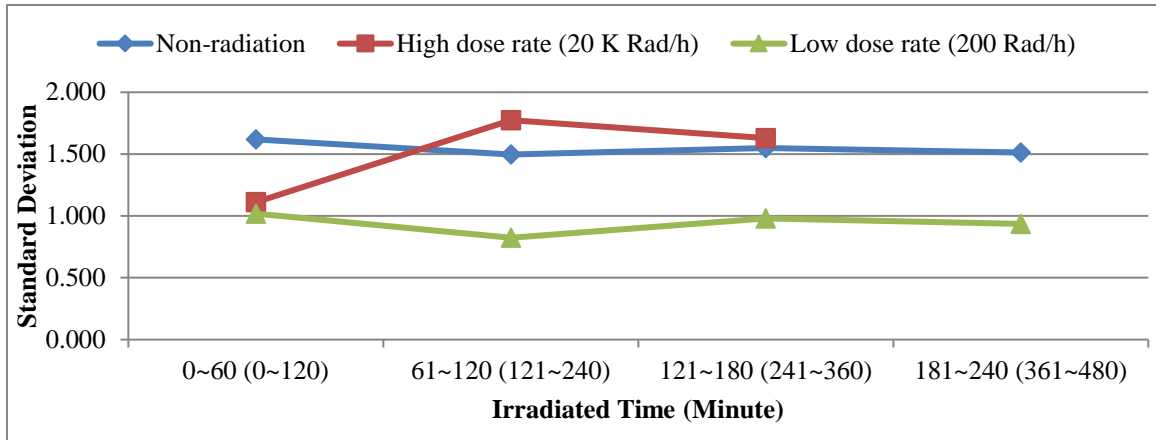
| Channel | Parameters | 0 ~ 120 mins | 121 ~ 240 mins | 241 ~ 360 mins | 361 ~ 480 mins | 481 ~ 600 mins | 601 ~ 720 mins | 721 ~ 840 mins |
|----------|--------------------|--------------|----------------|----------------|----------------|----------------|----------------|----------------|
| Sample-1 | Input signal | 10 mA | 10 mA | 10 mA | 10 mA | 10 mA | 10 mA | 10 mA |
| | Value-1 /Count | 004C /141 | 004C /96 | 004C /147 | 004C /80 | Failed | Failed | Failed |
| | Value-2 /Count | 0050 /3352 | 0050 /3412 | 0050 /3366 | 0050 /2331 | | | |
| | Value-3 /Count | 0054 /92 | 0054 /75 | 0054 /69 | 0054 /55 | | | |
| | Standard Deviation | 1.0184 25 | 0.8235 71 | 0.9785 22 | 0.9352 13 | | | |
| Sample-2 | Input signal | 10 mA | 10 mA | 10 mA | 10 mA | 10 mA | 10 mA | 10 mA |
| | Value-1 /Count | - | - | - | - | - | - | - |
| | Value-2 /Count | 0530 /3559 | 0530 /3559 | 0530 /3559 | 0530 /3561 | 0530 /3561 | 0530 /3561 | 0530 /3562 |
| | Value-3 /Count | 0540 /1 | - | - | - | - | - | - |
| | Standard Deviation | 0.2681 61 | 0.0000 00 | 0.0000 00 | 0.0000 00 | 0.0000 00 | 0.0000 00 | 0.0000 00 |
| Sample-3 | Input signal | 10 mA | 10 mA | 10 mA | 10 mA | 10 mA | 10 mA | 10 mA |
| | Value-1 /Count | - | 0240 /42 | 0240 /24 | 0240 /30 | 0240 /28 | 0240 /32 | 0240 /28 |
| | Value-2 /Count | 0250 /3014 | 0250 /2850 | 0250 /2928 | 0250 /2880 | 0250 /2906 | 0250 /2912 | 0250 /2895 |
| | Value-3 /Count | 0260 /590 | 0260 /712 | 0260 /651 | 0260 /694 | 0260 /671 | 0260 /659 | 0260 /681 |
| | Standard Deviation | 5.9209 73 | 6.6875 40 | 6.3418 14 | 6.5383 05 | 6.4424 36 | 6.4308 44 | 6.4783 68 |

The results of experimental evaluation of communication performance for non-redundant wireless devices under the condition with a low dose rate are listed in Table 10-31.

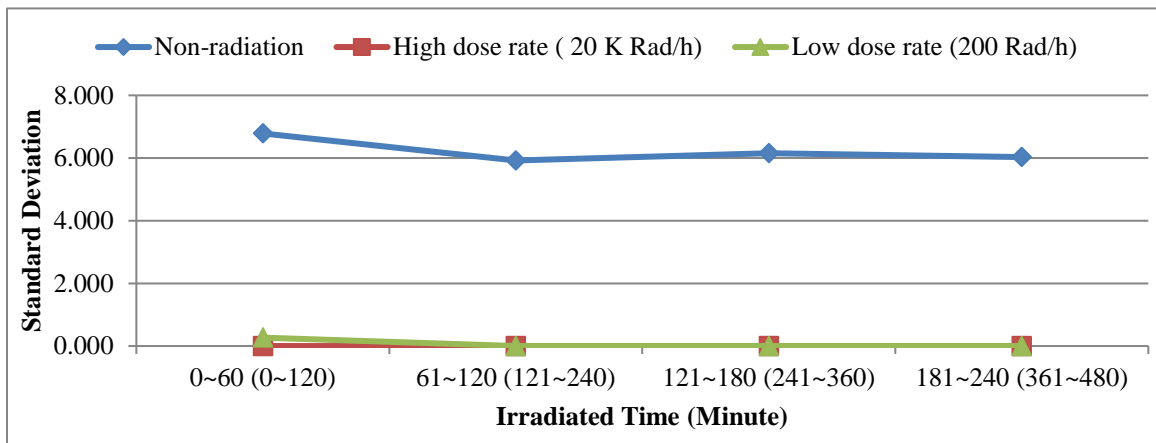
Table 10-31: Results of experimental evaluation of communication performance for non-redundant wireless devices under a low dose rate condition

| Channel | Parameters | 120 mins | 240 mins | 360 mins | 480 mins | 600 mins | 720 mins | 840 mins |
|----------|----------------|----------|----------|----------|----------|----------|----------|----------|
| Sample-1 | Total packets | 3580 | 7201 | 10801 | 13228 | Failed | Failed | Failed |
| | Packet loss | 0 | 0 | 0 | 0 | | | |
| | Loss rate (%) | 0.000 | 0.000 | 0.000 | 0.000 | | | |
| | Packet error | 0 | 0 | 0 | 0 | | | |
| | Error rate (%) | 0.00% | 0.00% | 0.00% | 0.00% | | | |
| Sample-2 | Total packets | 3560 | 7119 | 10681 | 14242 | 17803 | 21364 | 24926 |
| | Packet loss | 0 | 1 | 2 | 2 | 2 | 2 | 2 |
| | Loss rate (%) | 0.000 | 0.014 | 0.019 | 0.014 | 0.011 | 0.009 | 0.008 |
| | Packet error | 0 | 0 | 0 | 0 | 0 | 0 | 0 |
| | Error rate (%) | 0.000 | 0.000 | 0.000 | 0.000 | 0.000 | 0.000 | 0.000 |
| Sample-3 | Total packets | 3600 | 7196 | 10791 | 14392 | 18005 | 21605 | 25174 |
| | Packet loss | 5 | 14 | 21 | 26 | 34 | 42 | 49 |
| | Loss rate (%) | 0.138 | 0.194 | 0.194 | 0.180 | 0.188 | 0.194 | 0.194 |
| | Packet error | 0 | 0 | 0 | 0 | 0 | 0 | 0 |
| | Error rate (%) | 0.000 | 0.000 | 0.000 | 0.000 | 0.000 | 0.000 | 0.000 |

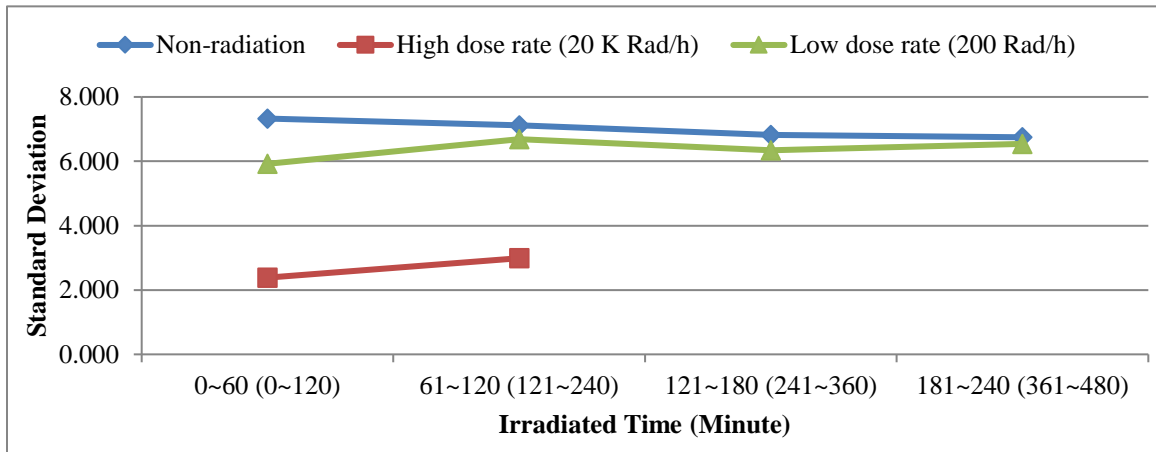
Based on experiment results listed in Table 10-26 to Table 10-31, comparison of the measurement accuracy, communication performance, and signal performance of each wireless device (Sample-1, Sample-2, and Sample-3) under three different radiation conditions is shown in Figure 10-39 (a), (b), (c), Figure 10-40 (a), (b), (c), Figure 10-41 (a), (b), (c), respectively.



(a) Sample-1

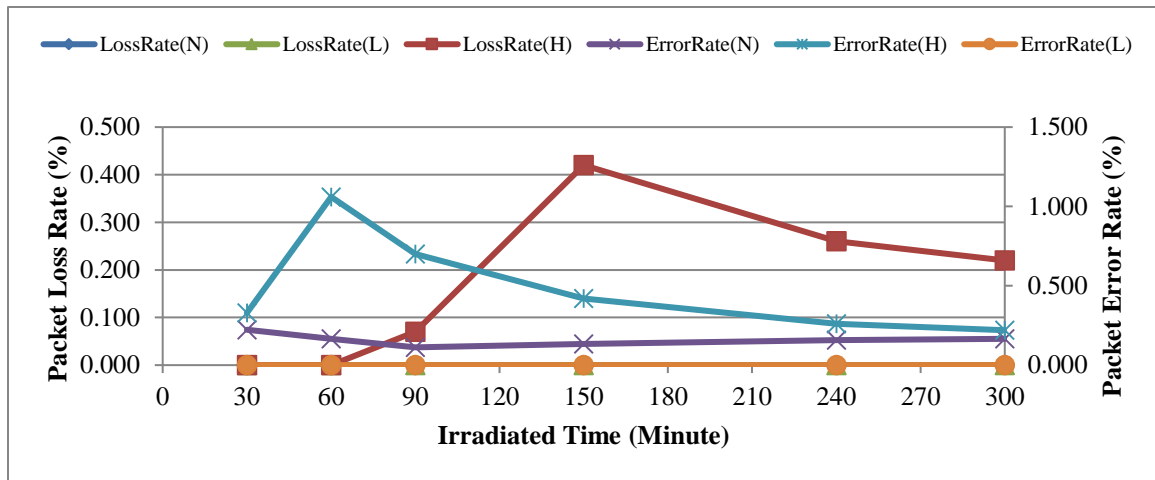


(b) Sample-2

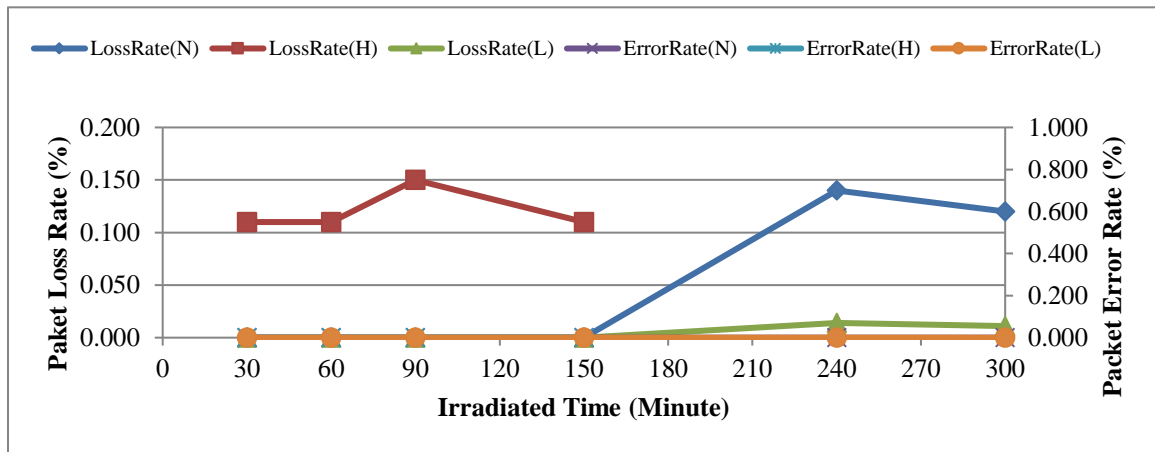


(c) Sample-3

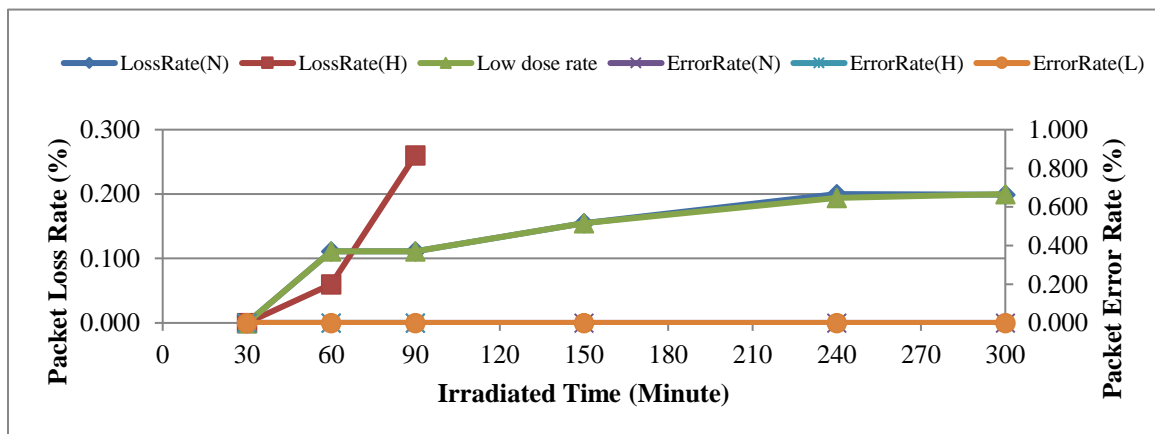
Figure 10-39: Comparison of measurement accuracy of non-redundant wireless devices under three different radiation conditions



(a) Sample-1

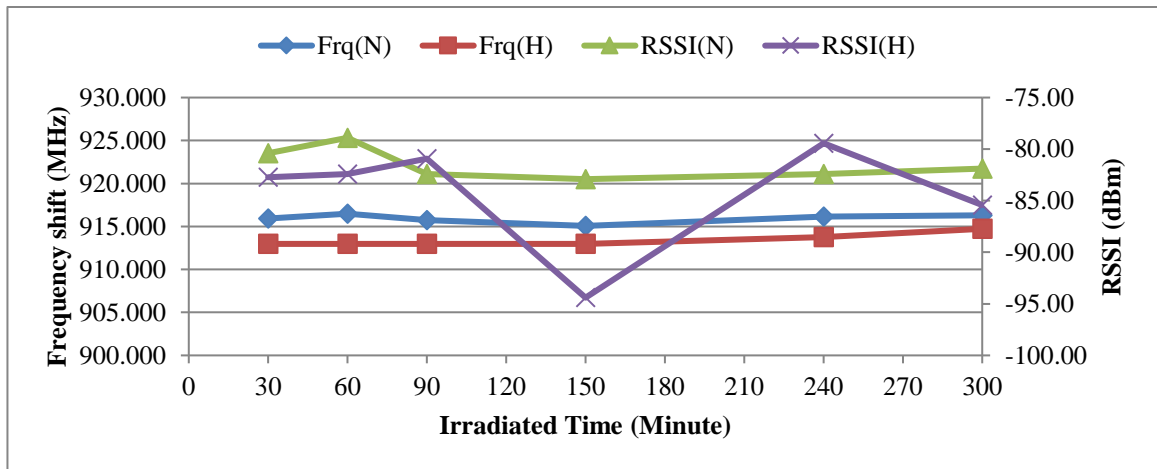


(b) Sample-2

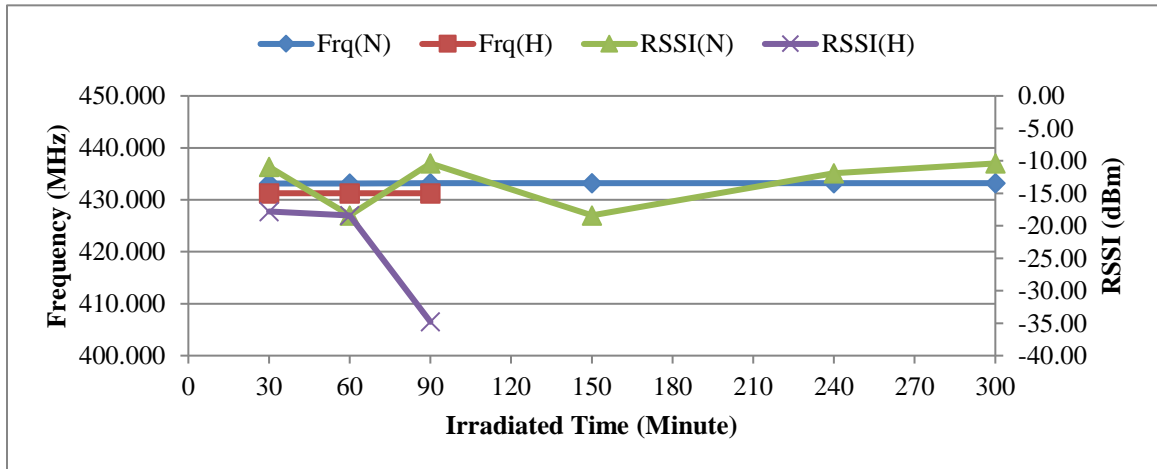


(c) Sample-3

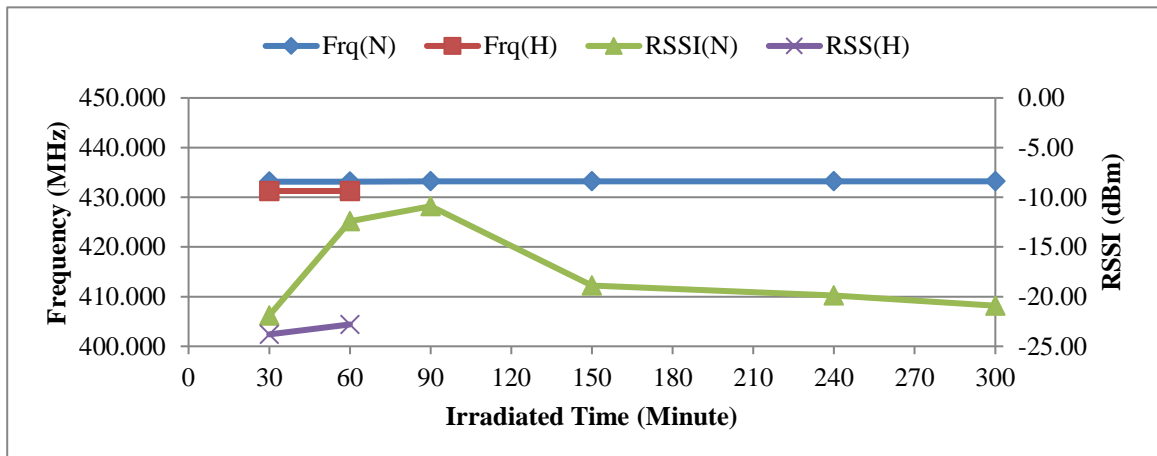
Figure 10-40: Comparison of communication performance of non-redundant wireless devices under three different radiation conditions



(a) Sample-1



(b) Sample-2



(c) Sample-3

Figure 10-41: Comparison of wireless signal performance of non-redundant wireless devices under different radiation conditions

10.4.4 Discussions

Under radiation conditions with different dose rates, radiation resistances of all irradiated devices are summarized in Table 10-32.

Table 10-32: Survival times of non-redundant wireless monitoring devices under both high and low dose rate conditions

| Dose Rates | Irradiated Device | Parameter Measurement | Wireless Communication |
|--------------------------------|-------------------|---|---|
| High dose rate (20 K Rad/h) | Sample-1 | 2h37m28s | 5h42m53s |
| | Sample-2 | Not available when it fails | 2h2m18s |
| | Sample-3 | Not available when it fails | 1h18m |
| Low dose rate (200 Rad/h) | Sample-1 | 7h20m58s | 7h20m58s |
| | Sample-2 | Still working after irradiated 14 hours | Still working after irradiated 14 hours |
| | Sample-3 | Still working after irradiated 14 hours | Still working after irradiated 14 hours |

The following observations can be made:

- (a) For Sample-1, under a high dose rate condition, after irradiated 2 hours 37 minutes 28 seconds, the function of parameter measurement has failed. The function of wireless communication has failed at 4 hours 12 minutes 20 seconds. Removing its power and waiting 2-3 minutes, the function of communication will recover. It then permanently failed after irradiated 5 hours 42 minutes 53 seconds. On the other hand, under a low dose rate condition, the function of wireless communication has failed only after irradiated for 7 hours 20 hours 58 seconds.
- (b) For Sample-2, under a high dose rate condition, after irradiated 2 hours 2 minutes 18 seconds, the function of wireless communication has failed and the function of parameter measurement still works. Interesting, under a low dose rate condition, after irradiated 14 hours 11 minutes 8 seconds, all functions still work as normal.

- (c) For Sample-3, under a high dose rate condition, after irradiated for 1 hour 18 minutes, the function of wireless communication stops working and the function of parameter measurement still works. Further, under a low dose rate condition, after irradiated for 14 hours 11 minutes 8 seconds, all functions still work as expected.

Based on the experimental results under three different radiation conditions: normal condition, high dose rate condition, and low dose rate condition, the following conclusions can be drawn about accuracy of parameter measurement and performance of wireless communication:

- (a) For Sample-1, before it fails, the accuracy of parameter measurement does not suffer from significant degradation. Furthermore, the performance of wireless communication also has no significant degradation. Under three different radiation conditions, packet loss rate is and packet error rate is 0.000%, 0.280%, 0.000%, and 0.165%, 0.220%, 0.000% separately.
- (b) For Sample-2, before it fails, the accuracy of parameter measurement has no significant degradation. On the other hand, the performance of wireless communication also has no significant degradation. Under three different radiation conditions, packet loss rate is and packet error rate is 0.012%, 0.110%, 0.008%, and 0.000%, 0.000%, 0.000%, separately.
- (c) For Sample-3, before it fails, the accuracy of parameter measurement has no significant degradation. On the other hand, the performance of wireless communication also has no significant degradation. Under different radiation conditions, packet loss rate is and packet error rate is 0.199%, 0.260%, 0.194%, and 0.000%, 0.000%, 0.000% separately.

Based on the results of these total dose tests, the following conclusions are in order:

- (a) The experimental results have shown that all irradiated devices will fail without significant degradation of electrical parameters. All functions are correct when eventually the total dose is less than the limit. They fail when the accumulated

total dose reaches their limitations. This observation matches well with the effects of total ionizing dose.

(b) Sample-1 has the higher radiation-resistance than that of other two samples.

Hence, for a high dose rate condition, the design and component selection are most appropriate. However, this design is more susceptible to a low dose rate condition.

(c) For a low dose rate condition, Sample-2 and Sample-3 are the more suitable solutions. However, they cannot survive for too long under a high dose rate condition.

(d) According to the experimental results, all wireless devices can only work several hours under the dose rate 20 K Rad/h. Radiation shielding protection has to be used to increase their radiation resistances.

(e) Wireless devices built with different semiconductor technologies can be sensitive to different dose rate conditions. Hence, for a complicate radiation environment, the method of using diversified hardware can be useful to increase their ultimate radiation-tolerance.

10.4.5 Summary

In this Section, total dose tests with ^{60}Co gamma source have been performed to investigate behaviors of diversified non-redundant wireless monitoring devices under different dose rate conditions. The experimental results have shown that the developed wireless devices can work for at least 2 hours under the radiation condition with 20 K Rad/h. It has proved that the method of component selection and the method of radiation-tolerance assessment are correct.

On the other hand, the experimental results have shown that both the performance of wireless communication and the accuracy of parameter measurement have no significant degradation before the device stops working. The experimental results have also shown that electronic devices built with different semiconductor technologies can be susceptible

to different radiation dose rates. For example, under a high dose rate condition, electronic devices built with bipolar semiconductor technology have the higher radiation resistance than that of devices built with CMOS technology. However, under a low dose rate condition with 200 Rad/h, the former is more susceptible than the latter. Hence, diversified hardware should be necessary for using a complicate radiation environment.

In addition, all wireless devices can only survive several hours under the radiation condition with 20 K Rad/h. Radiation shielding protection has to be used to extend their lifespan.

10.5 Part IV: Evaluation of the Developed Radiation-Tolerant Wireless Device in a Radiation Environment

In the design for a radiation-hardened electronic system, it is critical to evaluate the effectiveness of the proposed methods and techniques. This is usually performed by exposing the device and/or system to a radiation environment and measuring its performance parameters. In the previous work, several emulation experiments and calculation based radiation-tolerance assessment have been completed. However, these methods just focus on the correctness of those proposed techniques in a perceived radiation damage scenario.

This Section focuses on the validation of the radiation-tolerant design proposed in this research experimentally. The investigation is done by exposing the designed wireless devices to an ionizing radiation environment and measuring their performance parameters. The validation is achieved through comparison of radiation responses of non-redundant devices with that of the redundant device. Specially, this validation focuses on the system-level performance instead of component-level. Component damages are therefore not tested in depth in this part of experiment. Several distinct wireless measurement and transmission units built with off-the-shelf commercial electronic components are used: (1) three single-channel wireless devices, which are implemented by using diversified semiconductor components (bipolar, CMOS, and hybrid); and (2) a redundant wireless device protected with a radiation shielding layer.

This Section starts with description of experimental approach, irradiated devices, and investigated parameters. Subsequently, experimental setup is presented in detail. Then, experimental results of radiation responses of all irradiated devices are presented and compared. Finally, based on those experimental results, some technical discussions are provided and potential limitations of the designed experiments are identified.

10.5.1 Introduction of Irradiated Devices

(1) Samples chosen of irradiated tests

Several wireless devices with different designs are summarized in Table 10-33. They are used in this experiment.

Table 10-33: Wireless devices used in Experiment Part IV

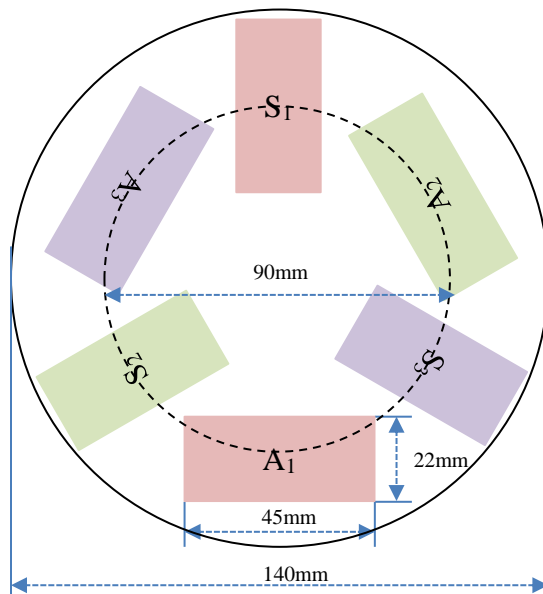
| Irradiated Sample | Description |
|-------------------|---|
| Sample-1 | Without using radiation-tolerant design and without any shielding protection, constructed with Bipolar semiconductor technology |
| Sample-2 | Without using radiation-tolerant design and without any shielding protection, constructed with CMOS semiconductor technology |
| Sample-3 | Without using radiation-tolerant design and without any shielding protection, constructed with hybrid semiconductor technology |
| Sample-4 | Using radiation-tolerant design and with a designed shielding protection, constructed with diversified semiconductor technologies |

Sample-1 is made with bipolar components except the microcontroller, Sample-2 is built with CMOS components, and Sample-3 mainly consists of hybrid components. All three samples can complete the required functions of parameter measurement and wireless communication. Semiconductor components used in samples are summarized in Table 10-34.

Table 10-34: Summary of semiconductor components used in irradiated devices in Experiment Part IV.

| Channel | Devices | Semiconductor technology | Manufacture |
|----------|-----------|--------------------------|------------------------|
| Sample-1 | LT1611 | Bipolar | Linear Technology |
| | CLC502 | | National Semiconductor |
| | AD571 | | Analog Devices |
| | RF2905 | | RF Micro Devices |
| | P89V51RC2 | CMOS | NXP |
| Sample-2 | REF03 | Bipolar | Analog Devices |
| | MAX660 | CMOS | Texas Instruments |
| | AD674 | | Analog Devices |
| | PIC16F77 | | Microchip |
| | SX1278 | | SEMTECH |
| Sample-3 | LM2662 | BiCMOS | Texas Instruments |
| | UA741 | Bipolar | STMicroelectronics |
| | AD1671 | BiCMOS | Analog Devices |
| | C8051F581 | TTL Logic | Silicon Labs |
| | SI4463 | | Silicon Labs |

Sample-1, Sample-2, and Sample-3 are selected as A_1/S_1 , A_2/S_2 , A_3/S_3 , separately. Sample-4 is an implementation of the radiation-tolerant architecture proposed in Chapter 6. In addition, considering gamma radiation source and the limitation of the size of dry tube, the shielding protection is a single layer of Lead, whose layout and size are illustrated in Figure 10-42. The radiation source is enclosure around the irradiated samples, the thickness of shielding for A_1, A_2, A_3 is about 12.5 mm and that of S_1, S_2, S_3 is about 2 mm.



(a) Top view



(b) Picture

Figure 10-42: Top view of the shielding protection in Experiment Part IV

Picture of those irradiated samples in experiment part IV is shown in Figure 10-43.

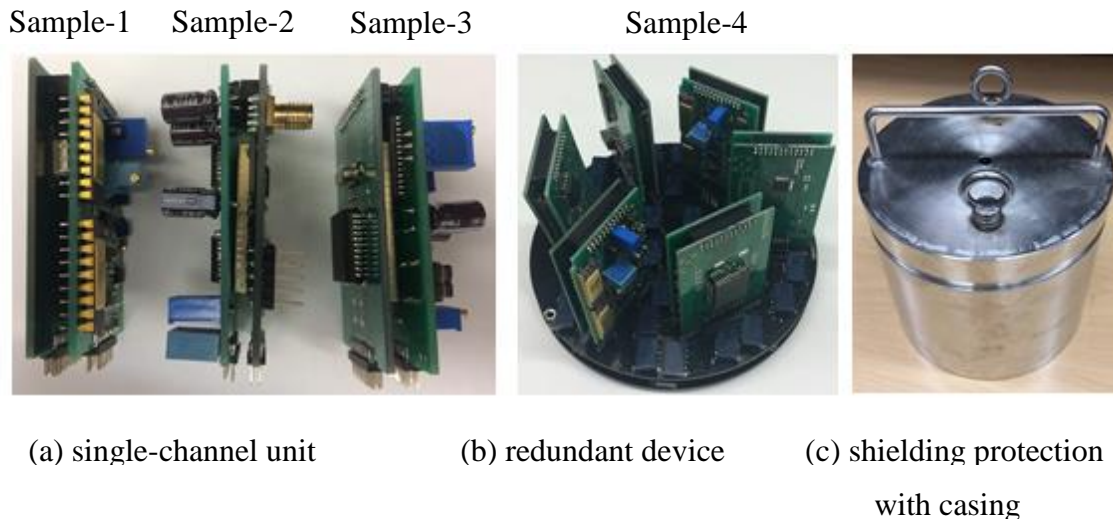


Figure 10-43: Irradiated samples used in experiment part IV

(2) Parameters Considered

As previously mentioned, this experiment focuses on system-level instead of component level. Therefore, the main parameters of interest are the lifespan of the units and the performance of wireless communication systems. The former refers to as the survival time. The latter involves of packet loss rate, packet error rate, and shift in wireless frequency and RSSI. Based on the comparison of those test results for non-redundant wireless devices and that of the redundant device, radiation tolerance of each device can be obtained, the effectiveness of the developed defense techniques can also be analyzed, and any potential limitations are identified.

10.5.2 Experimental Setup

In this study, the gamma irradiator generates a dose rate of 20 K Rad/h on the samples. A potentiostat located outside the irradiator is used as power supply to the wireless measurement and transmission units by using a 30 ft wire. A wireless receiver and a laptop, also located outside the irradiator, are used to capture the data through antennas connected to the irradiated units. A picture of this experimental setup for non-redundant devices is shown in Figure 10-44.

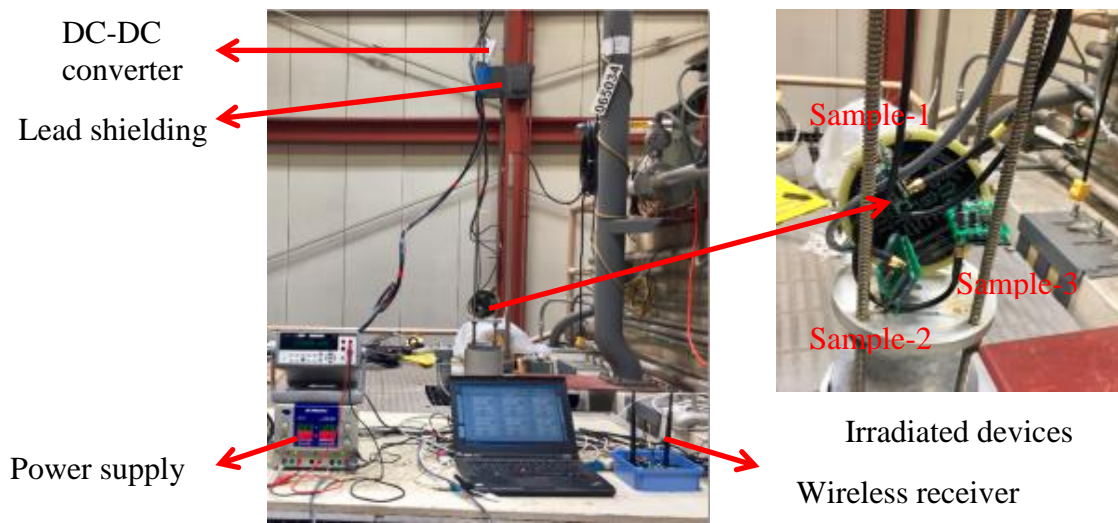


Figure 10-44: Experimental setup for the non-redundant wireless devices used in Experiment Part IV

Pictures of this experimental setup for redundant device with a shielding protection are shown in Figure 10-45.

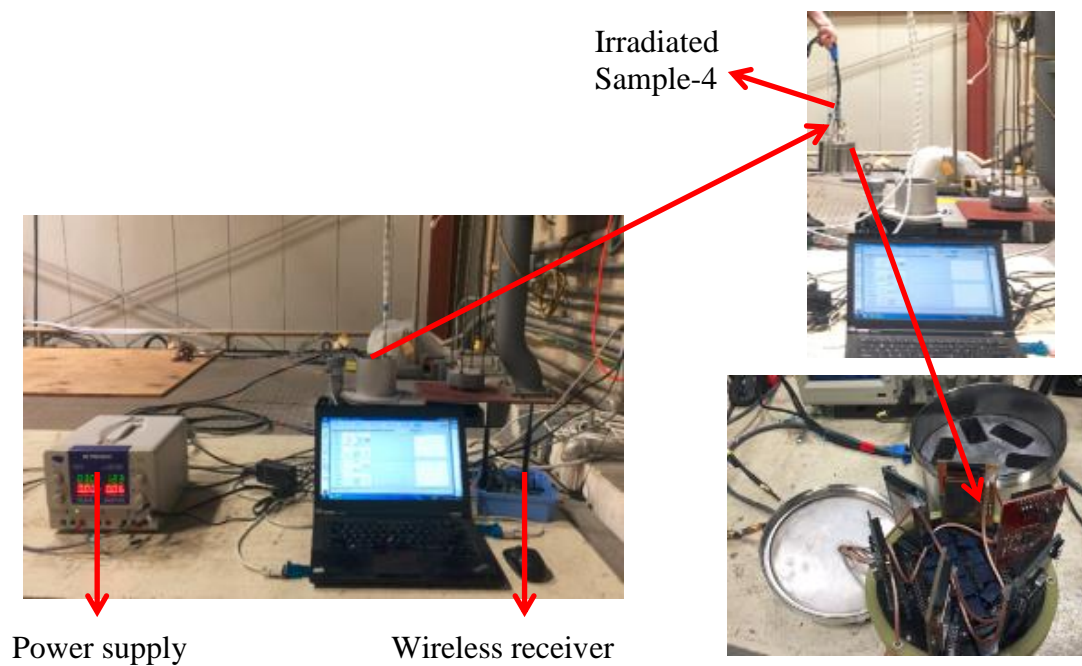


Figure 10-45: Experimental setup for the redundant wireless device used in Experiment Part IV

10.5.3 Experimental Results

(1) Survival time

According to the experimental results, survival time and radiation hardness of distinct irradiated samples are listed in Table 10-35.

Table 10-35: Survival time and radiation hardness of the irradiated wireless devices

| Parameters | Sample-1 | Sample-2 | Sample-3 | Sample-4 |
|----------------------------|------------|-----------|----------|--------------------|
| Survival time (h) | 5h 42m 53s | 2h 2m 18s | 1h 18m | 21 without failure |
| Radiation hardness (K Rad) | 114 | 40 | 26 | > 400 |

Comparison of radiation resistances of irradiated wireless devices used in Experiment Part IV is shown in Figure 10-46.

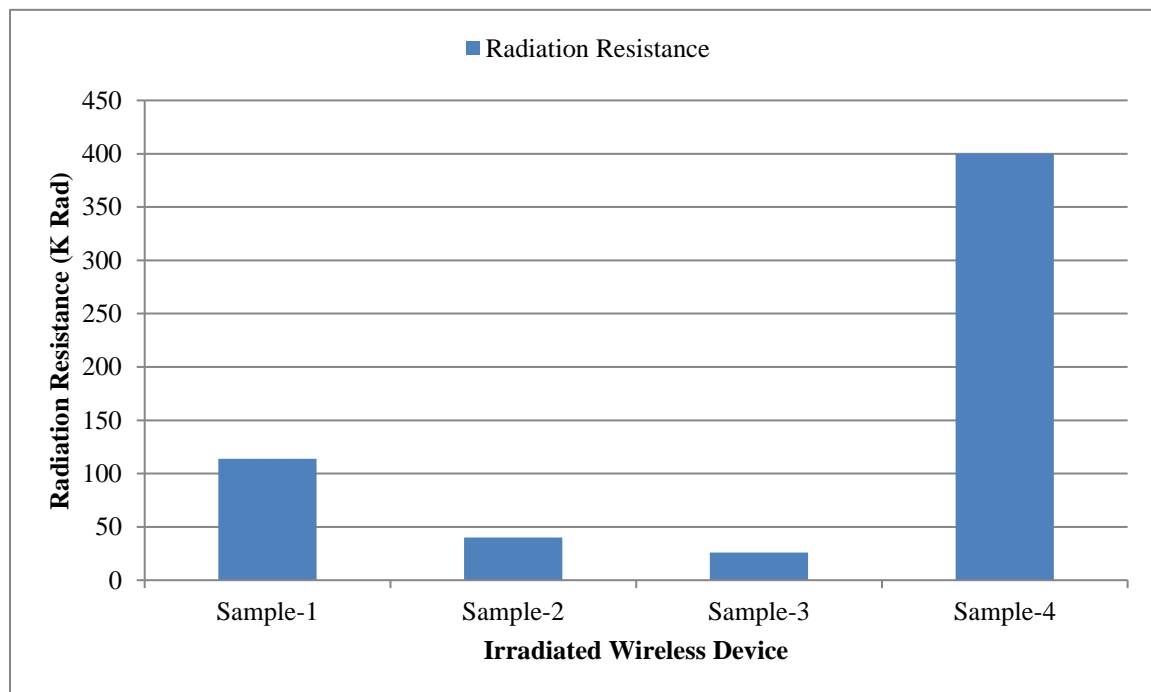


Figure 10-46: Radiation resistances of irradiated wireless devices used in Experiment Part IV

After irradiated for 21 hours under a high dose rate condition (20 K Rad/h), the status of each channel in the developed redundant device is listed in Table-36.

Table 10-36: The status of each channel in the developed redundant device after irradiated 21 hours under a high dose rate condition

| Channel | A1 | S1 | A2 | S2 | A3 | S3 |
|---------|------------|------------|--------|--------|--------|--------|
| Status | Functional | Functional | Failed | Failed | Failed | Failed |

(2) Performance of wireless communication

The comparison of wireless communication performance of Sample-1 under different radiation conditions (normal, high dose rate) is listed in Table-37.

Table 10-37: Comparison of wireless communication performance of Sample-1 under different exposure and radiation conditions

[illegible]

The comparison of wireless communication performance of Sampe-2 under different conditions (normal condition, high dose rate condition) is listed in Table-38.

Table 10-38: Comparison of wireless communication performance of Sample-2 under different exposure and radiation conditions

| Condition | Test Duration | Total Packets | Packet Loss | Loss Rate (%) | Packet Error | Error Rate (%) | Frequency (MHz) | RSSI (dBm) |
|---|---------------|---------------|-------------|---------------|--------------|----------------|-----------------|------------|
| Normal condition | 30mins | 902 | 0 | 0.000 | 0 | 0.000 | 433.135 | -10.90 |
| | 60mins | 1804 | 0 | 0.000 | 0 | 0.000 | 433.135 | -18.40 |
| | 90mins | 2704 | 0 | 0.000 | 0 | 0.000 | 433.204 | -10.40 |
| | 150mins | 4508 | 0 | 0.000 | 0 | 0.000 | 433.204 | -18.40 |
| | 240mins | 7209 | 1 | 0.014 | 0 | 0.000 | 433.204 | -11.90 |
| | 300mins | 8109 | 1 | 0.012 | 0 | 0.000 | 433.204 | -10.40 |
| High level radiation without the protection | 30mins | 900 | 1 | 0.111 | 0 | 0.000 | 431.261 | -17.80 |
| | 60mins | 1802 | 2 | 0.111 | 0 | 0.000 | 431.261 | -18.40 |
| | 90mins | 2698 | 4 | 0.148 | 0 | 0.000 | 431.261 | -34.80 |
| | 120mins | 3602 | 4 | 0.111 | 0 | 0.000 | - | - |
| | 122mins | Failed | | | | | | |

The comparison of wireless communication performance of Sample-3 under different conditions (normal condition, high dose rate condition) is listed in Table-39.

Table 10-39: Comparison of wireless communication performance of Sample-3 under different exposure and radiation conditions

| Condition | Test Duration | Total Packets | Packet Loss | Loss Rate (%) | Packet Error | Error Rate (%) | Frequency (MHz) | RSSI (dBm) |
|---|---------------|---------------|-------------|---------------|--------------|----------------|-----------------|------------|
| Normal condition | 30mins | 902 | 0 | 0.000 | 0 | 0.000 | 433.135 | -21.90 |
| | 60mins | 1802 | 2 | 0.111 | 0 | 0.000 | 433.135 | -12.40 |
| | 90mins | 2702 | 3 | 0.111 | 0 | 0.000 | 433.204 | -10.90 |
| | 150mins | 4499 | 7 | 0.155 | 0 | 0.000 | 433.204 | -18.90 |
| | 240mins | 6985 | 14 | 0.200 | 0 | 0.000 | 433.204 | -19.90 |
| | 300mins | 8992 | 18 | 0.199 | 0 | 0.000 | 433.204 | -20.90 |
| High level radiation without the protection | 30mins | 902 | 0 | 0.000 | 0 | 0.000 | 431.261 | -23.80 |
| | 60mins | 1798 | 1 | 0.056 | 0 | 0.000 | 431.261 | -22.80 |
| | 78mins | 2332 | 6 | 0.257 | 0 | 0.000 | - | - |
| | 79mins | Failed | | | | | | |

The comparison of wireless communication performance of Sample-4 under different conditions is listed in Table-40.

| Condition | Test Duration | Total Packets | Packet Loss | Loss Rate (%) | Packet Error | Error Rate (%) | Frequency (MHz) | RSSI (dBm) |
|--|---------------|---------------|-------------|---------------|--------------|----------------|-----------------|------------|
| High dose rate condition at the first 287 mins (A ₂ is primary channel) | 30mins | 885 | 0 | 0.000 | 1 | 0.113 | 432.955 | -15.60 |
| | 60mins | 1773 | 0 | 0.000 | 1 | 0.056 | 432.775 | -17.10 |
| | 90mins | 2662 | 0 | 0.000 | 1 | 0.036 | 433.045 | -14.90 |
| | 150mins | 4437 | 1 | 0.023 | 3 | 0.068 | 432.865 | -20.10 |
| | 240mins | 7100 | 1 | 0.014 | 3 | 0.042 | 432.865 | -25.60 |
| | 287mins | 8491 | 1 | 0.012 | 3 | 0.035 | 433.125 | -15.90 |
| High dose rate condition after irradiated 21hours(A ₁ is primary channel) | 30mins | 901 | 0 | 0.000 | 9 | 0.999 | 914.414 | -71.42 |
| | 60mins | 1801 | 0 | 0.000 | 16 | 0.888 | 913.243 | -85.93 |
| | 90mins | 2701 | 0 | 0.000 | 23 | 0.852 | 916.126 | -88.40 |
| | 150mins | 4501 | 0 | 0.000 | 38 | 0.844 | 914.865 | -87.42 |
| | 240mins | 7201 | 0 | 0.000 | 63 | 0.875 | 914.775 | -88.42 |
| | 300mins | 9001 | 0 | 0.000 | 93 | 1.033 | 915.766 | -87.91 |

Comparison of communication performance of Sample-1(S1) and Sample-4(S4) under a high dose rate (20 K Rad/h) condition is shown in Figure 10-47.

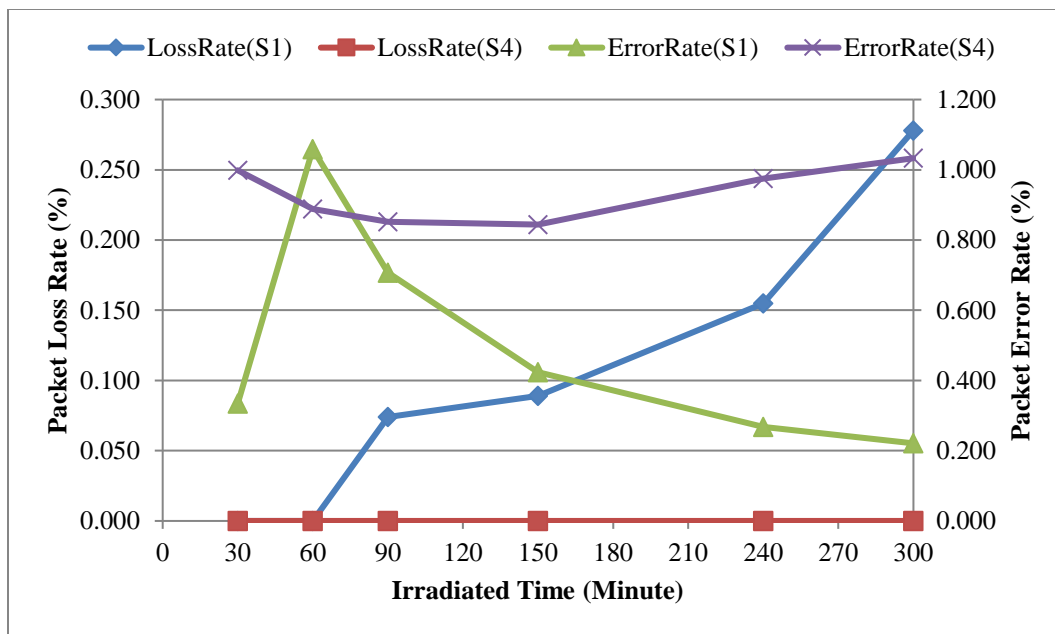


Figure 10-47: Comparison of communication performance of Sample-1(S1) and Sample-4(S4) under a high dose rate condition

Comparison of communication performance of Sample-2(S2) and Sample-4(S4) under a high dose rate (20 K Rad/h) condition is shown in Figure 10-48.

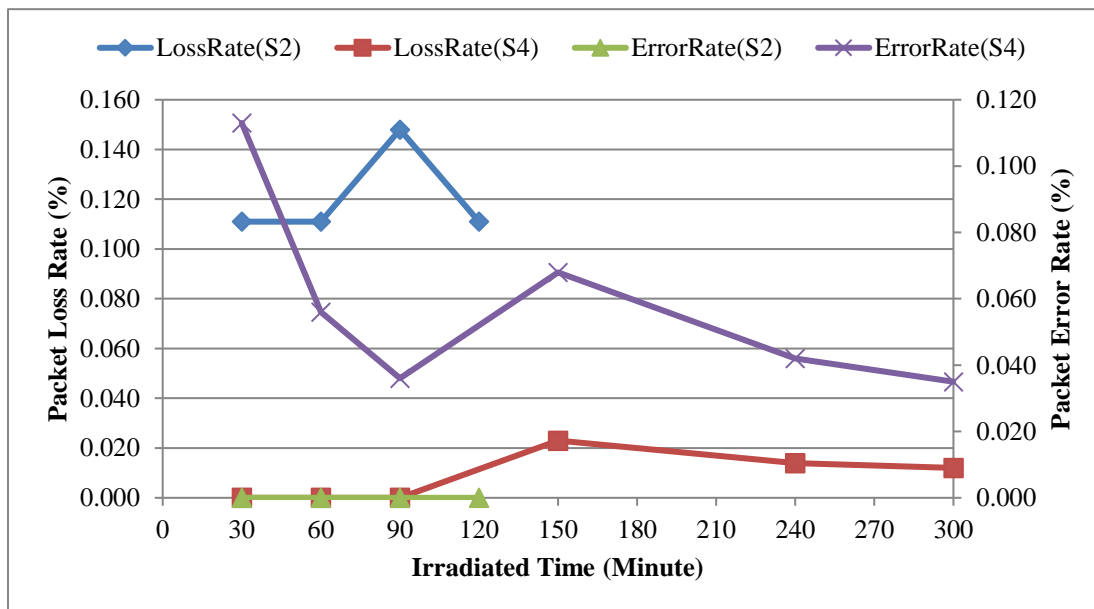


Figure 10-48: Comparison of communication of Sample-2(S2) and Sample-4(S4) under a high dose rate condition

10.5.4 Discussions

Based on experimental results, with respect to the effectiveness of the developed defense techniques, the following discussions apply to this total dose test:

- (a) For radiation resistance, under the same radiation condition with a high dose rate (20 K Rad/h), the lifespan of Sample-2 is increased from 122 minutes to 287 minutes by using the proposed defense techniques. Sample-4 can survive at least 21 hours but Sample-1 only works 342 minutes.
- (b) For communication performance, packet loss rate has a significant improvement by using the proposed defense techniques. On the other hand, packet error rate of the redundant wireless device has not been improved.
- (c) For the performance of wireless signal, both frequency and RSSI have no obvious improvement by using the proposed defense techniques. However, its performance is satisfied to the function of the wireless communication.

The proposed total dose test is to identify the performance of the developed wireless devices for a variety of operating conditions. However, there are a number of limitations that must be addressed in the future. There limitations include:

- (1) Single particle effects test does not involve in this test, the effectiveness of the developed fault-tolerant techniques has not been identified;
- (2) The test does not measure the exact radiation resistance of the developed redundant wireless device. After irradiated 21 hours, the test is stopped.

10.5.5 Summary

In this Section, total dose tests with ^{60}Co gamma source have been performed to investigate the effectiveness of the proposed defense techniques. Experimental results have proved that the system can work effectively under a high dose rate condition. Radiation resistance has been significantly improved by using the radiation shielding protection. Moreover, it can be more improved by increasing the thickness of shielding

protection. It shows that the developed shielding protection can be used to mitigate the effects of total dose.

On the other side, single event effect test is not involved in this test. Hence, the effectiveness of fault-tolerant design has not been investigated. It needs to be performed in the future.

10.6 Conclusions

In this Chapter, a number of total dose tests for the developed distinct wireless devices with ^{60}Co gamma source is presented to investigate their radiation tolerances and to validate the effectiveness of the proposed methods and systems. The following conclusions can be drawn:

- (1) The experimental results have concluded that the proposed method of the component selection is correct and effective. All selected semiconductor devices can survive at least 1 hour under the radiation condition with dose rate at 20 K Rad/h.
- (2) The experimental results have proved that the developed wireless monitoring device can work in a radiation environment with accumulated total dose at least 400 K Rad.
- (3) The experimental results have confirmed that the wireless device built with bipolar semiconductor components has higher radiation resistance than those devices built with CMOS components. However, they are susceptible to radiation with low dose rate.
- (4) The experimental results have indicated that the complicate solutions for wireless communication systems may not be suitable for high level radiation environments.
- (5) The experimental results have shown that microcontroller/microprocessor module may be the most weakness part in a wireless monitoring system for using in high level of radiation environments.
- (6) The experimental results have indicated that RF2905 wireless device has the highest radiation resistance among all tested wireless devices.

- (7) The experimental results have demonstrated the proposed defense techniques and methods are effectively to prolong the life of the COTS-based electronic system in high level radiation environments.

The results of these tests will provide guidelines to design wireless monitoring systems to be used in high level radiation environments. These results are significant and important references to analyze radiation-induced responses of irradiated wireless devices and circuits. They can also help other researchers and engineers to design and produce more radiation-hardened monitoring systems using regular commercial off-the-shelf components.

Chapter 11

11 Summary, Conclusion, and Future Work

11.1 Summary

In this research, based on the literature survey, the conventional approach to design electronic systems with high radiation tolerance is to use rad-hardened components, which are prohibitively expensive and are not available for many new data processing algorithms and communication technologies. In this research, several methods and systems have been investigated to deal with different aspects for allowing COTS-based electronic systems in high level radiation environments. In this research, the investigation can be divided into five primary components:

- (1) A method has been presented to analyze radiation responses of circuits and electronic systems. The circuit analysis method for post-irradiation developed in this research can be used to obtain the responses of electronic systems for post-irradiation. This method can be also applied to analyze and to design radiation-hardened circuits with the robustness of radiation effects.
- (2) Several radiation-tolerant techniques have been developed to mitigate radiation effects on electronic system and to prolong its lifetime. They are:
 - A method of component selection and a multi-layer are developed to allow COTS-based electronic systems using in high level radiation environments.
 - A radiation-tolerant architecture developed in this research is very useful to involve all functions in a complete communication system, such as measurement, source decoder, modulation, transmission, etc. The developed architecture and the reconfigurator mechanism can be also applied in the fault-tolerant system without additional detectors and/or hardware voters. The diversified architecture and techniques proposed in this research can be used to avoid the common-damage in the redundant system.

- An online detection mechanism developed in this research can be used timely to detect and to locate the damages in redundant channels.
- (3) A wireless monitoring system has been implemented in this research. The developed wireless monitoring system can be a potential solution for high level radiation environments in NPP applications. Related methods and techniques developed in this research can be used to implement similar monitoring systems for high level radiation environments. It also validates the correctness of the proposed methods and techniques.
- (4) A method has been proposed to evaluate the performance of the developed methods and systems without repeated destructive physical tests in the design phase. The emulation method developed in this research through external circuits to mimic radiation responses can be used to validate the proposed algorithm and systems. The hardware emulation bench built in this research is very useful to debug and to validate the proposed methods and systems in the design phase. The assessment method developed in this research can also be applied to select COTS components and to evaluate the radiation-tolerance of the whole system in the design phase.
- (5) Several total dose tests have been performed to validate the developed devices and system.
- The irradiation experimental scheme proposed in this research can be used to validate the radiation-tolerance and to evaluate the performance of the developed system.
 - The experimental results provide the fundament to judge whether the developed system satisfies the design requirements.
 - The investigation of radiation vulnerable of each module is critical to improve the radiation-tolerance of the developed wireless device.

- The results of radiation responses of different type measurement units and wireless transceivers can be used in the component selection for applications with different radiation conditions.
- The experimental results can be is a reference for other researches in the design of wireless monitoring applications using in radiation environments.

11.2 Conclusions

The conclusions of this research are listed as follows:

(1) Investigated alternative ways to analyze, to design, and to evaluate rad-hardened electronic systems.

A method is presented in this research to obtain radiation responses of devices and circuits and to accurately analyze their behavior under the high level of radiation.

Validation results show that the following objectives have been achieved:

- Several mathematical models of semiconductor device for post-irradiation can be investigated from the proposed technique. Those models can be applied to analyze circuit responses of post-irradiation.
- The proposed technique can be used to design circuit robust ionizing radiation effects without repeated physical radiation tests.

A multi-layer radiation protection is developed in this research to mitigate radiation damages of total ionizing dose and to avoid the common-mode damage in redundant systems, as well as an evaluation method of radiation shielding protection. Simulation study results show that the following objectives have been achieved:

- The developed multi-layer radiation protection can be applied to effectively mitigate damages of total ionizing dose for redundant systems using in high level radiation environments.

- The evaluation method of radiation protection can be used to calculate the required shielding thickness.

A radiation-tolerant architecture is proposed in this research to allow COTS-based electronic system using in high level radiation environments. The following properties of the architecture are demonstrated by the experimental studies.

- The proposed scheme can be applied to design redundant systems without additional detection units and/or hardware voters.
- The developed diversified protections and enforcing differences can be used to avoid the common-fault in redundant system.
- The proposed decision algorithm can effectively generate reconfigurator suggestions when radiation damages occur in redundant system.
- The developed reconfigurator scheme is effectively to power-off the device if it encounters radiation damages.

An online scheme based on build-in-test (BIT) technique is studied in this research to timely detect radiation faults in redundant systems. The numerical studies support conclusions that:

- The proposed fault analysis model can be used to identify radiation damages in electronic systems.
- The developed online detection mechanism is effectively to detect radiation faults in redundant systems.
- The developed diagnosis mechanism can be used to locate radiation faults in redundant systems.

The hardware emulation bench has successfully supported the research in several methods and systems. It is observed that:

- The test bench allows independent access to process the tolerant logic, to implement detection mechanism, and to construct analysis algorithm.
- Single fault and multiple faults can be effectively simulated and injected by logical emulation and external circuit emulation.
- Emulation methods through external circuits to mimic radiation responses can be used to validate the proposed detection mechanism and algorithm.

An assessment method based on reliability analysis is studied in this research. The numerical studies support conclusions that:

- Assessment model developed in this research can be used to analyze the reliability of redundant systems for post-irradiation.
- Radiation degradation factor proposed in this research is effectively to describe the radiation response of an item under the given radiation dose.
- The developed assessment method can be applied to evaluate the radiation-tolerance of the whole electronic system without repeated destructive physical tests.

(2) Investigated the developed methodologies to design, to implement, and to validate a wireless monitoring system for post-accident environments in NPPs.

A wireless monitoring system for high level radiation environments in NPPs has successfully been implemented and constructed. It is observed that:

- The developed monitoring system can be effectively used to collect the up-to-date information and to transmit them to remote monitoring station.
- The developed monitoring system satisfies the design requirements and can be used in nuclear applications.

Irradiation experimental validation shows that the investigated scheme has several desirable features.

- The proposed irradiation experimental scheme can be used to validate the investigated methods and systems.
- The developed monitoring system can work in high level radiation environment (at least 400 K Rad (Si)).
- The experimental results have proved that the investigated methods and systems in this research can be effectively used to increase radiation resistance of electronic systems.
- A number of observes in total dose tests provide significant references for other researches in the design of wireless monitoring applications using in radiation environments

In other words, the objective of this research is to design rad-hardened systems without using rad-hardened components for high level radiation environments. The investigated methods and systems in this research have achieved those objectives.

11.3 Future Work

This research encompassed multiple areas related to radiation-tolerant design without rad-hardened components. Even though the principles and effectiveness of the several proposed methods and systems have been demonstrated within the scope, there are interesting issues that can be further investigated. Some possible topics include:

- To investigate radiation-hardened design from network-level, such as wireless frequency, network protocol, etc., to build a diversified wireless network for high level radiation environments.
- To investigate radiation-hardened techniques from circuit-level, for example, to design diversified self-healing circuits to accomplish communication functions of

wireless monitoring systems, and to analyze radiation responses on more devices and related circuits.

- To investigate more radiation shielding protection for neutron radiation, as well as simulation studies for various radiation particles with high level energy by using various simulator.
- To investigate radiation sensors to accurately measure critical parameters in high level radiation range, such as neutron sensor, gamma sensor, etc.
- To investigate radiation resistances of more semiconductor devices and circuits in the modern digital communication system through physical radiation tests.
- To investigate other communication techniques for high level of radiation environments, for example, using optical fiber as the sensor and/or the transceiver and to build an optical fiber monitoring system for high level radiation environments.

Bibliography

- Abate, F., Sterpone, L., and Violante, M., 2008. A new mitigation approach for soft errors in embedded processors. *IEEE Transactions on Nuclear Science* 55, 2063-2069.
- Abdao, A. E. S., 2002. Calculation of the cross-sections for fast neutrons and gamma-rays in concrete shields. *Annals of Nuclear Energy* 29, 1977-1988.
- Adalja, A. A., Toner, E. S., Cicero, A., Fitzgerald, J., and Inglesby, T. V., 2011. Radiation at Fukushima: basic issues and concepts. *Clinicians' Biosecurity News, Analysis of Advances and Challenges in Clinical Biosecurity*.
- Adell, P. C., Esqueda, I. S., Barnaby, H. J., Rax, B., and Johnston, A. H., 2012. Impact of low temperatures (<125 K) on the total ionizing dose response and ELDRS in gated lateral PNP BJTs. *IEEE Transactions on Nuclear Science* 59, 3081-3086.
- Adell, P. C., and Scheick L. Z., 2013. Radiation effects in power systems: a review. *IEEE Transactions on Nuclear Science* 60, 1929-1952.
- Adell, P. C., Schrimpf, R. D., Holman, W. T., Todd, J. L., Caveriviere, T. S., Cizmarik, R. R., and Galloway, K. F., 2004. Total dose effects in a linear voltage regulator. *IEEE Transactions on Nuclear Science* 51, 3816-3821.
- Aguirre, C., and Wirth, G., 2013. Simulation of TID effect on floating gate cells. 28th Symposium on Microelectronics Technology and Devices, Curitiba, Brazil.
- Aguirre, M. A., Baena, V., Tombs, J., and Violante, M., 2007. A new approach to estimate the effect of single event transients in complex circuits. *IEEE Transactions on Nuclear Science* 54, 1018-1024.
- Akhmetov, A. O., Boychenko, D. V., Bobrovskiy, D. V., Chumakov, A. I., Kalashnikov, O. A., Nikiforov, A. Y., and Nekrasov, P. V., 2014. System on module total ionizing dose distribution modeling. *Microelectronics Proceedings, Proc. 29th International Conference on Microelectronics, Belgrade & Serbia*, 329-331.

- Akkurt, I., Akyildirim, H., Mavi, B., Kilincarslan, S., and Basyigit, C., 2010. Gamma-ray shielding properties of concrete including barite at different energies. *Progress in Nuclear Energy* 52, 620-623.
- Alexander, D. R., 2003. Transient ionizing radiation effects in devices and circuits. *IEEE Transactions on Nuclear Science* 50, 565-582.
- Allenspach, M., Dachs, C., Johnson, G. H., Schrimpf, R. D., Lorfevre, E., Palau, J. M., Brews, J. R., Galloway, K. F., Titus, J. L., and Wheatley, C. F., 1996. SEGR and SEB in n-channel power MOSFETs. *IEEE Transactions on Nuclear Science* 43, 2927-2931.
- Alles, M. L., Hughes, H. L., Ball, D. R., McMarr, P. J., and Schrimpf, R. D., 2014. Total-ionizing-dose response of narrow, long channel 45 nm PDSOI transistors. *IEEE Transaction on Nuclear Science* 61, 2945-2950.
- Allison, J., 2006. Geant4 developments and applications. *IEEE Transactions on Nuclear Science* 53, 270-278.
- American National Standard for Gamma-Ray Attenuation Coefficients and Buildup Factors for Engineering Materials, (1991). ANSI/ANS-6.4.3-1991.
- Andreeva, M., Pavlova, M. P., and Groudev, P. P., 2008. Overview of plant specific severe accident management strategies for Kozloduy nuclear power plant, WWER-1000/320. *Annals of Nuclear Energy* 35, 555-564.
- ANSI/ANS-4.5-1980, 1980. Criteria for accident monitoring functions in light-water-cooled reactors. The American National Standards Institute.
- ANSI/IEEE. Std. 497-1981, 1981. IEEE standard criteria for accident monitoring instrumentation for nuclear power generating stations.
- Artola, L., Gaillardin, M., Hubert, G., Raine, M., and Paillet, P., 2015, Modeling single event transients in advanced devices and ICs, *IEEE Transactions on Nuclear Science* 62, 1528-1539.
- Artola, L., Roche, N. J. H., Hubert, G., Youssef, A. Al., Khachatryan, A., McMarr, P., and Hughes, H., 2015. Analysis of angular dependence of single-event latchup sensitivity

- for heavy-ion irradiations of 0.18-um CMOS technology. *IEEE Transactions on Nuclear Science* 62, 2539-2546.
- Arutt, C. N., Warren, K. M., Schrimpf, R. D., Weller, R. A., Kauppila, J. S., Rowe, J. D., Sternberg, A. L., Reed, R. A., Ball, D. R., and Fleetwood, D. M., 2015. Proton irradiation as a screen for displacement-damage sensitivity in bipolar junction transistors. *IEEE Transactions on Nuclear Science* 62, 2498-2504.
- Atkinson, N. M., Blaine, R. W., Kauppila, J. S., Armstrong, S. E., Loveless, T. D., Hotten, N. C., Holman, W. T., Massengill, L. W., and Warner, J. H., 2013. RHBD technique for single-event charge cancellation in folded-cascode amplifiers. *IEEE Transactions on Nuclear Science* 60, 2756-2761.
- Aydos, G., and Fey, G., 2017. Empirical results on parity-based soft error detection with software-based retry. *Microprocessors and Microsystems* 48, 62-68.
- Avizienis, A., 1985. The N-version approach to fault-tolerant software. *IEEE Transactions on Software Engineering* 11, 1491-1501.
- Bagatin, M., and Gerardin S., 2015. Ionizing radiation effects in electronics: from memories to imagers. CRC Press, Taylor & Francis Group.
- Bagatin, M., Gerardin, S., Paccagnella, A., Visconti, A., Beltrami, S., Bertuccio, M., and Czeppel, L. T., 2011. Effects of total ionizing dose on the retention of 41-nm NAND flash cells. *IEEE Transactions on Nuclear Science* 58, 2824-2829.
- Balasubramanian, A., Bhuva, B. L., Black, J. D., and Massengill, L. W., 2005. RHBD techniques for mitigating effects of single-event hits using guard-gates. *IEEE Transactions on Nuclear Science* 52, 2531-2535.
- Ballarini, F., Battistoni, G., Brugger, M., Campanella, M., Carboni, M., Cerutti, F., Empl, A., Fasso, A., Ferrari, A., Gadioli, E., Garzelli, M. V., Lantz, M., Mairani, A., Mostacci, A., Muraro, S., Ottolenghi, A., Patera, V., Pelliccioni, M., Pinsky, L., Ranft, J., Roesler, S., Sala, P. R., Scannicchio, D., Smirnov, G., Sommerer, F., Trovati, S., Villari, R., Vlachoudis, V., Wilson, T., and Zapp, N., 2007. The physics of the FLUKA code: recent developments. *Advances in Space Research* 40, 1339-1349.

- Bak, S. I., Park, T. S., and Hong, S. W., 2010. GEANT4 simulation of the shielding of neutron from ^{252}Cf source. *Journal of the Korean Physical Society* 59, 2071-2074.
- Barbottin, G., and Vapaille, A., 1999. *Instabilities in silicon devices, new insulators, devices and radiation effects*. North-Holland.
- Barnaby, H. J., 2006. Total-ionizing-dose effects in modern CMOS technologies. *IEEE Transactions on Nuclear Science* 53, 3103-3121.
- Barnaby, H. J., Schrimpf, R. D., Galloway, K. F., Li, X., Yang, J., and Liu, C., 2017. Displacement damage in bipolar junction transistors: beyond Messenger-Spratt. *IEEE Transactions on Nuclear Science* 64, 149-155.
- Barros, M., Guilherme, J., and Horta, N., 2010. Analog circuits optimization based on evolutionary computation techniques. *Integration* 43, 136-155.
- Baumann, R. C., 2005. Radiation-induced soft errors in advanced semiconductor technologies. *IEEE Transactions on Nuclear Science* 5, 305-316.
- Beaucour, J., Carriere, T., Gach, A., and Laxague, D., 1994. Total dose effects on negative voltage regulator. *IEEE Transactions on Nuclear Science* 41, 2420-2426.
- Becker, H. N., Miyahira, J. F., and Johnston, A. H., 2002. Latent damage in CMOS devices from single-event latchup. *IEEE Transactions on Nuclear Science* 49, 3009-3015.
- Bernacki, S. Hunt, K., Tyson, S., Hudgens, S., Pashmakov, B., and Czubytyj, W., 2000. Total dose radiation response and high temperature imprint characteristics of chalcogenide based RAM resistor elements. *IEEE Transactions on Nuclear Science* 47, 2528-2533.
- Beskrovnaia, L., Florko, B., Paraipan, M., Sobolevsky, N., and Timoshenko, G., 2008. Verification of Monte Carlo transport codes FLUKA, GEANT4 and SHIELD for radiation protection purposes at relativistic heavy ion accelerators. *Nuclear Instruments and Methods in Physics Research B*, 4058-4060.
- Blaine, R. W., Atkinson, N. M., Kauppila, J. S., Armstrong, S. E., Hotten, N. C., Loveless, T. D., Warner, J. H., Holman, W. T., and Massengill, L. W., 2012.

- Differential charge cancellation (DCC) layout as an RHBD technique for bulk CMOS differential circuit design. *IEEE Transactions on Nuclear Science* 59, 2867-2871.
- Blum, D. R., and Delgado-Frias, J., 2006. Schemes for eliminating transient width clock overhead from set-tolerant memory-based systems. *IEEE Transactions on Nuclear Science* 53, 1564-1573.
- Boch, J., Saigne, F., Schrimpf, R. D., Fleetwood, D. M., Ducret, S., Dusseau, L., David, J. P., Fesquet, J., Gasiot, J., and Ecoffet, R., 2004. Effect of switching from high to low dose rate on linear bipolar technology radiation response. *IEEE Transactions on Nuclear Science* 51, 2896-2902.
- Borulta, N., Lum, G. K., O'Donnell, H., Tobinette, L., Shaneyfelt, M. R., and Schwank, J. R., 2001. A new physics-based model for understanding single-event gate rupture in linear devices. *IEEE Transactions on Nuclear Science* 48, 1917-1924.
- Boutte, A. J., Cochran, D.J., Chen, D., Campola, M.J., Pellish, J.A., Ladbury, R.L., Wilcox, E. P., Lauenstein, J., Gigliuto, R.A., LaBel, K.A., and O'Bryan, M.V., 2013. Compendium of recent total ionizing dose and displacement damage for candidate spacecraft electronics for NASA, 2013 IEEE Radiation Effects Data Workshop (REDW), San Francisco, CA, USA
- Brews, J. R., Allenspach, M., Schrimpf, R. D., and Galloway, K. F., 1993. A conceptual model of single-event gate-rupture in power MOSFETs. *IEEE Transactions on Nuclear Science* 40, 1959-1966.
- Brinkley, P., Carmichael, A., and Carmichael, C., 2000. SEU mitigation design techniques for the XQR400XL. Technical report, Xilinx.
- Brisset, C., Ferlet-Cavrois, V., Flament, O., Musseau, O., Leray, J. L., Pelloie, J. L., Escoffier, R., Michez, A., Cirba, C., and Bordure, G., 1996. Two-dimensional simulation of total dose effects on NMOSFET with lateral parasitic transistor. *IEEE Transactions on Nuclear Science* 43, 2651-2658.
- Brugger, M., Carbonez, P., Pozzi, F., Silari, M., and Vincke, H., 2014. New radiation protection calibration facility at CERN. *Radiation Protection Dosimetry* 161, 181-184.

- Buchner, S., and McMorrow, D., 2006. Single-event transients in bipolar linear integrated circuits. *IEEE Transactions on Nuclear Science* 53, 3079-3102.
- Calin, T., Nicolaidis, M., and Velazco, R., 1996. Upset hardened memory design for submicron CMOS technology. *IEEE Transactions on Nuclear Science* 43, 2874-2878.
- Calzada, E., Grunauer, F., Schillinger, B., and Turck, H., 2011. Reusable shielding material for neutron- and gamma-radiation. *Nuclear Instruments and Methods in Physics Research A: Accelerators, Spectrometers, Detectors and Associated Equipment* 1, 77-80.
- Camplani, A., Shojaii, S., Shrimali, H., Stabile, A., and Liberali, V., 2014. CMOS IC radiation hardening by design. *Electronics and Energetics* 27, 251-258.
- Cardoso, A. S., Chakraborty, P. S., Karaulac, N., Fleischhauer, D. M., Lourenco, N. E., Fleetwood, Z. E., Omprakash, A. P., England, T. D., Jung, S., Najafizadeh, L., Roche, N. J. -H., Khachatryan, A., Warner, J. H., McMorrow, D., Buchner, S. P., Zhang, E. X., Zhang, C. X., McCurdy, M. W., Reed, R. A., Fleetwood, D. M., Paki-Amouzou, P., and Cressler, J. D., 2014. Single-event transient and total dose response of precision voltage reference circuits designed in a 90-nm SiGe BiCMOS technology. *IEEE Transactions on Nuclear Science* 61, 3210-3217.
- Cardoso, A. S., Chakraborty, P. S., Lourenco, N. E., Song, P., England, T. D., Kenyon, E. W., Karaulac, N., Cressler, J. D., 2013. Total ionizing dose response of triple-well FET-based wideband, high-isolation RF switches in a 130 nm SiGe BiCMOS technology. *IEEE Transactions on Nuclear Science* 60, 2567-2573.
- Carter, L. L., and Cashwell, E. D., 1975. Particle-transport simulation with the Monte Carlo method. ERDA Critical Review Series, report number: TID-26607.
- Cellere, G., Paccagnella, A., Visconti, A., Bonanomi, M., Schwank, J. R., Shaneyfelt, M. R., and Paillet, P., 2007. Total ionizing dose effects in NOR and NAND flash memories. *IEEE Transactions on Nuclear Science* 54, 1066-1070.
- Cellere, G., and Paccagnella, A., 2004. A review of ionizing radiation effects in floating gate memories. *IEEE Transactions on Device and Materials Reliability* 4, 359-370.

- Centenaro, M., Vangelista, L., Zanella, A., and Zorzi, M., 2016. Long-range communications in unlicensed bands: the rising stars in the IoT and smart city scenarios. *IEEE Wireless Communications* 23, 60-67.
- Chabi, D., Zhao, W., Klein, J., and Chappert, C., 2014. Design and analysis of radiation hardened sensing circuits for spin transfer torque magnetic memory and logic. *IEEE Transactions on Nuclear Science* 61, 3258-3264.
- Chang, J., Cho, J. Y., Gil, C. S., and Lee, W. J., 2014. A simple method to calculate the displacement damage cross section of silicon carbide. *Nuclear Engineering and Technology* 46, 475-480.
- Chen, R. M., Diggins, Z. J., Mahatme, N. N., Wang, L., Zhang, E. X., Chen, Y. P., Liu, Y. N., Narasimham, B., Witulski, A. F., Bhuva, B. L., and Fleetwood, D. M., 2017. Effects of total-ionizing-dose irradiation on SEU- and SET-induced soft errors in bulk 40-nm sequential circuits. *IEEE Transactions on Nuclear Science* 64, 471-476.
- Chen, W., Fang, R., Barnaby, H. J., Balaban, M. B., Gonzalez-Velo, Y., Taggart, J. L., Mahmud, A., Holbert, K., Edwards, A. H., and Kozicki, M. N., 2017. Total-ionizing-dose effects on resistance stability of programmable metallization cell based memory and selectors. *IEEE Transactions on Nuclear Science* 64, 269-276.
- Choi, S. Y., Yoo, S. J., Lee, K. J., and Rim, C. T., 2012. Wireless power system design for mobile robots used in nuclear power plants. *Transactions of the Korean Nuclear Society Spring Meeting, Jeju & Korea*.
- Ciani, L., and Catelani, M., 2014. A fault tolerant architecture to avoid the effects of single event upset in avionics applications, *Measurement* 54, 256-263.
- Citterio, M., Camplani, A., Cannon, M., Chen, H., Chan, K., Deng, B., Liu, C., Meroni, C., Kierstead, J., Takai, H., Wirthlin, M., and Ye, J., 2016. Radiation testing campaign results for understanding the suitability of FPGAs in detector electronics. *Nuclear Instruments and Methods in Physics Research A* 824, 270-271.
- Claeys, C., and Simoen, E., 2013. *Radiation effects in advanced semiconductor materials and devices*. Springer-Verlag Barlin Heidelberg.
- Clara, S., 2004. *Athena/Atlas user's manual*. CA: Silvaco Inc.

- Clark, L. T., Patterson, D. W., Hindman, N. D., Holbert, K. E., Maurya, S., and Guertin, S. M., 2011. A dual mode redundant approach for microprocessor soft error hardness. *IEEE Transactions on Nuclear Science* 58, 3018-3025.
- Clark, T. L., Patterson, D. W., Remamurthy C., and Holbert, K. E., 2015. An embedded microprocessor radiation hardened by microarchitecture and circuits. *IEEE Transactions on Computers* 65, 1-14.
- Cochran, D. J., Buchner, S. P., Sanders, A. B., LaBel, K. A., Carts, M. A., Poivey, C. F., Oldham, T. R., Ladbury, R. L., O'Bryan, M. V., and Mackey, S., 2008. Compendium of recent total ionizing dose result for candidate spacecraft electronics for NASA. 2008 IEEE Radiation Effects Data Workshop (REDW), Tucson, AZ, USA.
- Cochran, D. J., Kniffin, S. D., Buchner, S. P., LaBel, K. A., O'Bryan, M. V., Ladbury, R. L., Sanders, A. B., Hawkins, D. K., Cox, S. R., Poivey, C. F., Oldham, T. R., Kim, H., Irwin, T. L., Friendlinch, M. R., Dung-Phan, A. M., Carts, M. A., Berg, M. D., Seidleck, C. M., and Forney, J. D., 2006. Compendium of total ionizing dose results and displacement damage results for candidate spacecraft electronics for NASA. 2006 IEEE Radiation Effects Data Workshop (REDW), Ponte Vedra, FL, USA.
- Cock, W. D., Versmissen, H., Leroux, P., and Uffelen, M. V., 2009. Modeling of γ -radiation effects in bipolar transistors with VHDL-AMS. 2009 European Conference on Radiation and Its Effects on Components and Systems, Bruges, Belgium.
- Cressler, J. D., 2013. Radiation effects in SiGe technology. *IEEE Transactions on Nuclear Science* 60, 1992-2014.
- Cuenca-Asensi, S., Martinez-Alvarez, A., Restrepo-Calle, F., Palomo, F. R., Guzman-Miranda, H., and Aguirre, M. A., 2011. A novel co-design approach for soft errors mitigation in embedded systems. *IEEE Transactions on Nuclear Science* 58, 1059-1165.
- Damla, N., Cevik, U., Kobya, A. I., Celik, A., Celik, N., and Grieken, R. V., 2010. Radiation dose estimation and mass attenuation coefficients of cement samples used in Turkey. *Journal of Hazardous Materials* 176, 644-649.

- Das, S., Tokunaga, C., Pant, S., Ma, W., Kalaiselvan, S., Lai, K., Bull, D. M., and Blaauw, D. T., 2009. Razor II: in situ error detection and correction for PVT and SER tolerance. *IEEE Journal of Solid-State Circuits* 44, 32-48.
- Davinci, 2003. Three-dimensional device simulation program manual. Mountain View, CA, Synopsys, Inc.
- Dementyev, A. V., and Sobolevsky, N. M., 1999. SHIELD universal Monte-Carlo hadron transport code: scope and applications. *Radiation Measurements* 30, 553-557.
- Deng, Y., Fjeldly, T. A., Ytterdal, T., and Shur, M. S., 2003. SPICE modeling of Neutron displacement damage and annealing effects in bipolar junction transistors. *IEEE Transactions on Nuclear Science* 50, 1873-1877.
- Dierking, W. H., Katz, G. E., and Steele, E. L., 1969. Transient radiation current generator model for semiconductor devices. *IEEE Transaction on Nuclear Science* 16, 144-152.
- Ding, L., Guo, H., Chen, W., Yao, Z., Yan, Y., Chen, D., Paccagnella, A., Gerardin, S., Bagatin, M., Chen, L., Sun, H., and Fan, R., 2014. Analysis of TID failure modes in SRAM-based FPGA under Gamma-ray and focused synchrotron X-ray irradiation. *IEEE Transactions on Nuclear Science* 61, 1777-1784.
- Dodd, P. E., 1996. Device simulation of charge collection and single-event upset. *IEEE Transactions on Nuclear Science* 43, 561-575.
- Dodd, P. E., 2005. Physics-based Simulation of single-event effects. *IEEE Transactions on Device Materials Reliability* 5, 343-357.
- Dodd, P. E., and Massengill, L. W., 2003. Basic mechanisms and modeling of single-event upset in digital microelectronics. *IEEE Transactions on Nuclear Science* 50, 583-602.
- Dodd, P. E., Schwank, J. R., Shaneyfelt, M. R., Felix, J. A., Paillet, P., Ferlet-Cavrois, V., Baggio, J., Reed, R. A., Warren, K. M., Weller, R. A., Schrimpf, R. D., Hash, G. L., Dalton, S. M., Hirose, K., and Saito, H., 2007. Impact of heavy ion energy and nuclear interactions on single-event upset and latchup in integrated circuits. *IEEE Transactions on Nuclear Science* 54, 2303-2311.

- Dodd, P. E., Shaneyfelt, M. R., Felix, J. A., and Schwank J. R., 2004. Production and propagation of single-event transients in high-speed digital logic ICs. *IEEE Transactions on Nuclear Science* 51, 3278-3284.
- Dodd, P. E., Shaneyfelt, M. R., Walsh, D. S., Schwank, J. R., Hash, G. L., Loemker, R. A., Draper, B. L., and Winokur, P. S., 2000. Single-event upset and snapback in silicon-on-insulator devices and integrated circuits. *IEEE Transactions on Nuclear Science* 47, 2165-2174.
- Dodds, N. A., Hooten, N. C., Reed, R. A., Schrimpf, R. D., Warner, J. H., Roche, N. J. - H., McMorro, D., Wen, S. -J., Wong, R., Salzman, J. F., Jordan, S., Pellish, J. A., Marshall, C. J., Gaspard, N. J., Bennett, W. G., Zhang, E. X., and Bhuva, B. L., 2012. Effectiveness of SEL hardening strategies and the latchup domino effect. *IEEE Transactions on Nuclear Science* 59, 2642-2650.
- Duan, G. X., Zhang, C. X., Zhang, E. X., Hachtel, J., Fleetwood, D. M., Schrimpf, R. D., Reed, R. A., Alles, M. L., Pantelides, S. T., Bersuker, G., and Yong, C. D., 2014. Bias dependence of total ionizing dose effects in SiGe-SiO₂/HfO₂ pMOS FinFETs. *IEEE Transactions on Nuclear Science* 61, 2834-2838.
- Eckhardt, D. E., Caglayan, A. K., Knight, J. C., Lee, L. D., McAllister, D. F., Vouk, M. A., and Kelly, J. P. J., 1991. An experimental evaluation of software redundancy as a strategy for improving reliability. *IEEE Transactions on software engineering* 17, 692-702.
- Eftaxiopoulos, N., Axelos, N., and Pekmestzi, K., 2016. Low latency radiation tolerant self-repair reconfigurable SRAM architecture. *Microelectronics Reliability* 56, 202-211.
- Eisler, R., 2012. The Fukushima 2011 disaster. U.S. Geological Survey.
- Ejlali A., Al-Hashimi B. M., Schmitz M. T., Rosinger P., and Miremadi S. G., 2006. Combined time and information redundancy for SEU-tolerance in energy-efficient real-time systems. *IEEE Transactions on Very Large Scale Integration (VLSI) Systems* 14, 323-335.

- Enlow, E. W., and Alexander, D. R., 1988. Photocurrent modeling of modern microcircuit PN junctions. *IEEE Transactions on Nuclear Science* 35, 1467-1474.
- Esqueda, I. S., 2007. Modeling of total ionizing dose effects in advanced complementary metal-oxide-semiconductor technologies. PhD thesis, Arizona State University.
- Esqueda, I. S., Barnaby, H. J., and King, M. P., 2015. Compact modeling of total ionizing dose and aging effects in MOS technologies, *IEEE Transactions on Nuclear Science* 62, 1501-1515.
- Fasso, A., Ferrari, A., Roesler, S., Sala, P. R., Ballarini, F., Ottolenghi, A., Battistoni, G., Cerutti, F., Gadioli, E., Garzelli, M. V., Empl, A., and Randt, J., 2003. The physics models of FLUKA: status and recent developments. *Computing in High Energy and Nuclear Physics 2003 Conference (CHEP2003)*, La Jolla & CA, USA.
- Fasso, A., Ferrari, A., Ranft, J., and Sala, P. R., 2005. FLUKA: a multi-particle transport code. CERN-2005-10, INFN/TC_05/11, SLAC-R-773.
- Fenton, W. G., McGinnity, T. M., and Maguire, L. P., 2001. Fault diagnosis of electronic systems using intelligent techniques: a review. *IEEE Transactions on Systems, Man, and Cybernetics – Part C: Applications and Reviews* 31, 269-281.
- Ferlet-Cavrois, V., Colladant, T., Paillet, P., Leray, J. L., Musseau, O., Schwank, J. R., Shaneyfelt, M. R., Pelloie, J. L., and Poncharra, J. du Port de, 2000. Worst-case bias during total dose irradiation of SOI transistors. *IEEE Transactions on Nuclear Science* 47, 2183-2188.
- Ferlet-Cavrois, V., Massengill, L. W., and Gouker, P., 2013. Single event transients in digital CMOS – a review. *IEEE Transactions on Nuclear Science* 60, 1767-1790.
- Fernandez-Hernando, J. L., Barlow, R. J., Bungau, A., Keller, L., and Watson, N. K., 2006. Shower simulations, comparison of Fluka, Geant4 and EGS4. *Proceedings of EPAC 2006*, Edinburgh & Scotland.
- Fernandez-Martinez, P., Palomo, F. R., Hidalgo, S., Fleta, C., Campabadal, F., and Flores, D., 2013. Analysis of displacement damage effects on MOS capacitors. *Nuclear Instruments and Methods in Physics Research A* 730, 91-94.

- Fjeldly, T. A., Deng, Y., Shur, M. S., Hjalmarson, H. P., Muyschondt, A., and Ytterdal, T., 2001. Modeling of high-dose-rate transient ionizing radiation effects in bipolar devices. *IEEE Transactions on Nuclear Science* 48, 1721-1730.
- Flament, O., Autran, J. L., Roche, P., Leray, J. L., Musseau, O., Truche, R., and Orsier, E., 1996. Enhanced total dose damage in junction field effect transistors and related linear integrated circuits. *IEEE Transactions on Nuclear Science* 43, 3060-3067.
- Fleetwood, D. M., 2013. Total ionizing dose effects in MOS and low-dose-rate-sensitive linear-bipolar devices. *IEEE Transactions on Nuclear Science* 60, 1706-1730.
- Foster, C. C., 2003. Total ionizing dose and displacement damage effects in microelectronics. *MRS Bulletin* 28, 136-140.
- Gadlage, M. J., Schrimpf, R. D., Benedetto, J. M., Eaton, P. H., Mavis, D. G., Sibley, M., Avery, K., and Turflinger, T. L., 2004. Single event transient pulsewidths in digital microcircuits. *IEEE Transactions on Nuclear Science* 51, 3285-3290.
- Gaillardin, M., Paillet, P., Ferlet-Cavrois, V., Faynot, O., Jahan, C., and Cristoloveanu, S., 2006. Total ionizing dose effects on triple-gate FETs. *IEEE Transactions on Nuclear Science* 53, 3158-3165.
- Gaillardin, M., Marcandella, C., Martinez, M., Raine, M., Paillet, P., Duhamel, O., and Richard, N., 2017. Total ionizing dose effects in multiple-gate field-effect transistor. *Semiconductor Science and Technology* 32, number 8.
- Galloway, K. F., and Schrimpf, R. D., 1990. MOS device degradation due to total dose ionizing radiation in the natural space environment: a review. *Microelectronics Journal* 21, 67-81.
- Gao, Z., Cecati, C., and Ding, S. X., 2015. A survey of fault diagnosis and fault-tolerant techniques – part I: fault diagnosis with model-based and signal-based approaches. *IEEE Transactions on Industrial Electronics* 62, 3768-3774.
- Garg, R., Jayakumar, N., Khatri, S. P., and Choi, G. S., 2009. Circuit-level design approaches for radiation-hard digital electronics. *IEEE Transactions on Very Large Scale Integration (VLSI) Systems* 17, 781-792.

- Gencil, O., Bozkurt, A., Kam, E., and Korkut, T., 2011. Determination and calculation of gamma and neutron shielding characteristics of concretes containing different hematite proportions. *Annals of Nuclear Energy* 38, 2719-2723.
- George, C. M., 1992. A summary review of displacement damage from high energy radiation in semiconductors and semiconductor devices. *Radiation and its Effects on Devices and Systems*, 35-40.
- Georigiou, O., and Raza, U., 2017. Low power wide area network analysis: Can LoRa scale? *IEEE Wireless Communications Letters* 6, 162-165.
- Gerardin, S., Bagatin, M., Paccagnella, A., Grurmann, K., Gliem, F., Oldham, T. R., Irom, F., and Nguyen, D. N., 2013. Radiation effects in flash memories. *IEEE Transactions on Nuclear Science* 60, 1953-1969.
- Ghali, K., Dorie, L., and Hammami, O., 2005. Dynamically reconfigurable analog circuit design automation through multiobjective optimization and direct execution, in *Proc. 12th IEEE ICECS*, Dec. 2015, 1-4.
- Gittus, J., 1978. *Irradiation effects in crystalline solids*. Applied Science Publishers LTD, London.
- Gleason, J. D., Baranaby, H. J., Alles, M. L., and Schlenvogt, G. J., 2013. An examination of high-injection physics of silicon p-n junctions with applications in photocurrent modeling. *IEEE Transaction on Nuclear Science* 60, 4570-4575.
- Goncalves, O., Prenat, G., and Dieny, B., 2013. Radiation hardened MRAM-based FPGA. *IEEE Transactions on Magnetics* 49, 4355-4358.
- Gorbunov, M. S., Danilov, I. A., Zebrev, G. I., and Osipenko, P. N., 2011. Verilog-A modeling of radiation-induced mismatch enhancement. *IEEE Transactions on Nuclear Science* 58, 785-792.
- Gorbunov, M. S., Dolotov, P. S., Antonov, A. A., Zebrev, G. I., Emeliyanov, V. V., Boruzdina, A. B., Petrov, A. G., and Ulanova, A. V., 2014. Design of 65 nm CMOS SRAM for space applications: a comparative study. *IEEE Transactions on Nuclear Science* 61, 1575-1582.

- Gorbunov, M. S., Zebrev, G. I., and Osipenko, P. N., 2009. Radiation-hardening-by-design with circuit-level modeling of total ionizing dose effects in modern CMOS technologies. Processing of SPIE – The International Society for Optical Engineering 7521.
- Gover, J. E., 1984. Basic radiation effects in electronic technology 1984. IEEE NSREC Short Course, Colorado Springs & CO.
- Greenwood, L. R., and Smither, P. K., 1985. SPECTER: Neutron Damage Calculations for Materials Irradiations. ANL/FPP/TM-197.
- Gregory, B. L., and Gwyn, C.W., 1974. Radiation effects on semiconductor devices. Proceedings of the IEEE 62, 1264-1273.
- Gregory, B. L., and Shafer, B. D., 1973. Latch-up in CMOS integrated circuits. IEEE Transactions on Nuclear Science 19, 293-299.
- Guizzo, E., 2011. Can Japan send in robots to fix troubled nuclear reactors. IEEE Spectrum, 22 March, 2011.
- Guizzo, E., 2011. Robotic aerial vehicle captures dramatic footage of Fukushima Reactors. IEEE Spectrum, 20 April, 2011.
- Gwyn, C. W., Scharfetter, D. L., and Wirth, J. L., 1967. The analysis of radiation effects in semiconductor junction devices. IEEE Transactions on Nuclear Science NS-14, 153-169.
- Hao, M., Hu, H., Wang, B., Liao, C., Kang, H., and Su, H., 2017. Study on influence of γ -ray total dose radiation effect on the electrical properties of the uniaxial strained Si nanometer NMOSFET. Solid-State Electronics 133, 45-52.
- Hash, G. L., Shaneyfelt, M. R., Sexton, F. W., and Winokur, P. S., 1997. Radiation hardness assurance categories for COTS technologies. Radiation Effects Data Workshop, 1997 IEEE, Snowmass Village, CO, USA.
- Hashemian, H. M., 2011. On-line monitoring applications in nuclear power plants. Progress in Nuclear Energy 53, 167-181.

- Hazucha, P., Karnik, T., Walstra, S., Bloechel, B. A., Tschanz, J. W., Maiz, J., Soumyannth, K., Dermer, G. E., Narendra, S., De, V., and Borka, S., 2004. Measurements and analysis of SER-tolerant latch in a 90-nm dual- V_T CMOS process. *IEEE Journal of Solid-State Circuits* 39, 1536-1543.
- He, J., Zou, K., and Liu, M., 2010. Section-representation scheme for evolutionary analog filter synthesis and fault tolerance design. in *Proc. 3rd IWACI*, pp. 265-270.
- Herrera-Alzu, I., and Lopez-Vallejo, M., 2013. Design techniques for xilinx virtex fpga configuration memory scrubbers. *IEEE Transactions on Nuclear Science* 60, 376-385.
- Hohl, J. H., and Johnson, G. H., 1989. Features of the triggering mechanism for single event burnout of power MOSFETS. *IEEE Transactions on Nuclear Science* 36, 2260-2266.
- Hohl, J. H., and Galloway, K. F., 1987. Analytical model for single event burnout of power MOSFETs. *IEEE Transactions on Nuclear Science* 34, 2260-2266.
- Hollinger, G. A., and Gwaltney, D. A., 2006. Evolutionary design of fault-tolerant analog control for a piezoelectric pipe-crawling robot. in *Proc. 8th Annu. Conf. GECCO*, 761-768.
- Holmes-Siedle, A., and Adams, L., 2002, *Handbook of radiation effects*. Second ed., Oxford University press Inc., New York.
- Houssay, L. P., 2000. Robotics and radiation hardening in the nuclear industry. Master thesis, University of Florid.
- Howard, D. C., Saha, P. K., Shankar, S., Diestelhorst, R., Engladn, T. D., Lourenco, N. E., Kenyon, E., and Cressler, J. D., 2012. An 8-16 GHz SiGe low noise amplifier with performance tuning capability for mitigation of radiation-induced performance loss. *IEEE Transactions on Nuclear Science* 59, 2837-2846.
- Hu, X., Choi, B. K., Barnaby, H. J., Fleetwood, D. M., Schrimpf, R. D., Lee, S., Shojah-Ardala, S., Wilkins, R., Mishra, U. K., and Dettmer, R. W., 2004. The energy dependence of Proton-induced degradation in AlGaIn/GaN high electron mobility transistors. *IEEE Transactions on Nuclear Science* 51, 293-297.

- Hu, J., Zhong, X., and Goodman, E. D., 2005. Open-ended robust design of analog filters using genetic programming. in *Proc. Conf. Genet. Evol. Comput.*, pp. 1619-1626.
- Huang, H. X., Bi, D. W., Zhang, and Z. X., 2014. Investigation of the total dose response of partially depleted SOI nMOSFETs using TCAD simulation and experiment. *Microelectronics Journal* 45, 759-766.
- Huang, P., Chen, S., Chen, J., Bin, L., and Wu, Z., 2017. Simulation study of large-scale charge sharing mitigation using seamless guard band. *IEEE Transactions on Device and Materials Reliability* 17, 176-183.
- Huang, R. H. -M., Hsu, D. K.-H., and Wen, C. H. -P., 2015. A determinate radiation hardened technique for safety-critical CMOS designs. *J Electron Test* 31, 181-192.
- Hubert, G., Bourdarie, S., Artola, L., Duzellier, S., and Roussel, J. F., 2011. Multi-scale modeling to investigate the single event effects for space missions. *Acta Astronautica* 69, 526-536.
- Hubert, G., Truyen, D., Artola, L., Briet, M., Heng, C., Lakys, Y., and Leduc, E., 2014. SET and SEU analysis based on experiments and multi-physics modeling applied to the ATMEL CMOS library in 180 and 90-nm technology nodes. *IEEE Transactions on Nuclear Science* 61, 3178-3186.
- Hughes, H. L., and Benedetto, J. M., 2003. Radiation effects and hardening of MOS technology: devices and circuits. *IEEE Transactions on Nuclear Science* 50, 500-521.
- Hui, X., Yun, Z., and Bin, L., 2015. DICE-based test structure to measure the strength of charge sharing effect. *IEICE Electronics Express* 12, 1-6.
- IAEA, 2009. Severe accident management programmes for nuclear power plants. IAEA Safety Standards. No. NS-G-2.15.
- IEEE. Std. 497-1981, 1981. IEEE standard criteria for accident monitoring instrumentation for nuclear power generating stations.
- IEEE Std. 487, 2002. Standard criteria for accident monitoring instrumentation for nuclear power generating stations.

- IEEE Std. 487, 2010. Standard criteria for accident monitoring instrumentation for nuclear power generating stations.
- IEEE Std. 487-2016, 2016. Standard criteria for accident monitoring instrumentation for nuclear power generating stations.
- Inanlou, F., Kenyon, E., and Cressler, J., 2013. An investigation of total ionizing dose damage on a pulse generator intended for space-based impulse. *IEEE Transactions on Nuclear Science* 60, 2605-2610.
- Inanlou, F., Lourenco, N. E., Fleetwood, Z. E., Song, I., Howard, D. C., Cardoso, A., Zeinolabedinzadeh, S., Zhang, E., Zhang, C. X., Paki-Amouzou, P., and Cressler, J. D., 2014. Impact of total ionizing dose on a 4th generation, 90nm SiGe HBT Gaussian pulse generator. *IEEE Transactions on Nuclear Science* 61, 3050-3054.
- Inguibert, C., and Duzellier, S., 2004. SEU rate calculation with GEANT4 (comparison with CREME86). *IEEE Transactions on Nuclear Science* 51, 2805-2810.
- Iniewski, K., 2010. Radiation effects in semiconductors. Boca Raton, Taylor & Francis.
- Irani, K. H., Pil-Ali, A., and Karami, M. A., 2017. A new guard ring for radiation induced noise reduction in photodiodes implemented in 0.18 um CMOS technology. *Optical and Quantum Electronics* 49 (9).
- Ishaque, A. N., Howard, J. W., Becker, M., and Block, R. C., 1991. An extended ambipolar model: formulation, analytical investigations, and application to photocurrent modeling. *Journal of Applied Physics* 69, 307.
- Ishaque, A. N., Howard, J. W., Becker, M., and Block, R. C., 1989. Photocurrent modeling at high dose rates. *IEEE Transactions on Nuclear Science* 36, 2092-2098.
- Iwase, H., Niita, K., and Nakamura, T., 2002. Development of general-purpose particle and heavy ion transport code. *Journal of Nuclear Science and Technology* 39, 1142-1151.
- Ives, N. E., Chen, J., Witulski, A. F., Schrimpf, R. D., Fleetwood, D. M., Bruce, R. W., McCurdy, M. W., Zhang, E. X., and Massengill, L. W., 2015. Effects of proton-

- induced displacement damage on gallium nitride HEMTs in RF power amplifier applications. *IEEE Transactions on Nuclear Science* 62, 2417-2422.
- Jagannathan, S., Herbison, D. R., Holman, W. T., and Massengill, L. W., 2010. Behavioral modeling techniques for TID degradation of complex analog circuits. *IEEE Transactions on Nuclear Science* 57, 3708-3715.
- Jayakumar, G. D., and Srinivasan, R., 2017. SET analysis of silicon nanotube FET. *Journal of Computational Electronics* 16, 307-315.
- Ji, Q., Wang, Y., Xie, M., and Cui J., 2007. Research on fault-tolerance of analog circuits based on evolvable hardware. in *Proc. 7th Int. Conf. ICES*, 100-108.
- Johnston, A. H., and Hughlock B. W., 1990. Latchup in CMOS from single particles. *IEEE Transactions on Nuclear Science* 37, 1886-1893.
- Johnston, A.H., Swift, G.M., and Rax, B.G., 1994. Total dose effects in conventional bipolar transistor and linear integrated circuits. *IEEE Transactions on Nuclear Science* 41, 2427-2436.
- Johnston, A. H., Swift, G. M., and Edmonds, L. D., 1997. Latchup in integrated circuits from energetic protons. *IEEE Transactions on Nuclear Science* 44, 2367-2377.
- Johnston, A. H., Swift G. M., Miyahira, T., and Edmonds, L. D., 1998. Breakdown of gate oxides during irradiation with heavy ions. *IEEE Transactions on Nuclear Science* 45, 2500-2508.
- Johnston, A. H., Swift, G. M., and Rax, B. G., 1994. Total dose effects in conventional bipolar transistors and linear integrated circuits. *IEEE Transactions on Nuclear Science*, vol. 41, 2427-2436.
- Johnston, A. H., Schrimpf, R. D., Galloway, K. F., and Koga, R., 1992. Temperature dependence of single-event burnout in n-channel power MOSFETs. *IEEE Transactions on Nuclear Science* 39, 1605-1612.
- Jung, S., Lourenco, N. E., Song, I., Oakley, M. A., England, T. D., Arora, R., Cardoso, A. S., Roche, N. J. -H., Khachatryan, A., McMorro, D., Buchner, S. P., Melinger, J. S., Warner, J. H., Paki-Amouzou, P., Babcock, J. A., and Cressler, J. D., 2014. An

- investigation of single-event transients in C-SiGe HBT on SOI current mirror circuits. *IEEE Transactions on Nuclear Science* 61, 3193-3200.
- Kalavagunta, A., Touboul, A., Shen, L., Schrimpf, R. D., Reed, R. A., Fleetwood, D. M., Jain, R. K., and Mishra, U. K., 2008. Electrostatic mechanisms responsible for device degradation in Proton irradiated AlGaIn/AlN/GaN HEMTs. *IEEE Transactions on Nuclear Science* 55, 2106-2122.
- Kaldenbach, B. J., Moore, M. R., Ewing, P. D., Manges, W. W., Dillard, C. L., Korsah, K., and Kisner, R. A., 2005. Assessment of wireless technologies and their application at nuclear facilities. NUREG/CR-6882.
- Kalshnikov, O. A., Dernidov, A. A., Figuero, V. S., Nikiforov, A. Y., Polevich, S. A., Telets, V. A., Maljudin, S. A., and Artamonov, A. S., 1998. Integrating analog-to-digital converter radiation hardness technique and results. *IEEE Transactions on Nuclear Science*, 45, 2611-2615.
- Karnik, T., Hazucha, P., and Patel, J., 2004. Characterization of soft errors caused by single event upsets in CMOS processes. *IEEE Transactions on Dependable and Secure Computing* 1, 128-143.
- Kaushal, G., Rathod, S. S., Maheshwaram, S., Manhas, S. K., Saxena, A. K., and Dasgupta, S., 2012. Radiation effects in Si-NW GAA FET and CMOS inverter: a TCAD simulation study. *IEEE Transactions on Electron Devices* 59, 1563-1566.
- Kay, M. J., Gadlage, M. J., Duncan, A. R., Ingalls, D., Howard, A., and Oldham, T. R., 2012. Effect of accumulated charge on the total ionizing dose response of a NAND flash memory. *IEEE Transactions on Nuclear Science* 59, 2945-2951.
- Kelly, A. T., Adell, P. C., Witulski, A. F., Holman, W. T., Schrimpf, R. D., and Pouget, V., 2007. Total dose and single event transients in linear voltage regulators. *IEEE Transactions on Nuclear science* 54, 1327-1334.
- Kern, W., and Smeltzer, R. K., 1986. Borophosphosilicate glasses for integrated circuits. *Microelectronics Reliability* 26, 792-792.
- Kerr, B., Axness, C. L., Verley, J. C., Hembree, C. E., and Keiter, E. R., 2012. A new time-dependent analytic model for radiation-induced photocurrent in finite 1D

- epitaxial diodes. Technical report SAND2012-2161, Sandia National Laboratories, Albuquerque, NM.
- Keymeulen, D., Zebulum, R. S., Jin, Y., and Stoica, A., 2000. Fault-tolerant evolvable hardware using field programmable transistor arrays. *IEEE Transactions on Reliability* 49, 305-316.
- Kharita, M. H., Takeyeddin, M., Alnassar, M., and Yousef, S., 2008. Development of special radiation shielding concretes using natural local materials and evaluation of their shielding characteristics. *Progress in Nuclear Energy* 50, 33-36.
- Kharita, M. H., Yousef, S., and AlNassar, M., 2011. Review on the addition of boron compounds to radiation shielding concrete. *Progress in Nuclear Energy* 53, 207-211.
- Khorsandi, B., 2007. Modeling of displacement damage in silicon carbide detectors resulting from neutron irradiation. PhD dissertation, The Ohio State University.
- Kim, K., and Cho, S., 2012. Automated synthesis of multiple analog circuits using evolutionary computation for redundancy-based fault-tolerance. *Applied Soft Computing* 12, 1309-1321.
- Kim, K. J., and Cho, S. B., 2009. Combining multiple evolved analog circuits for robust evolvable hardware. *Intell. Data Eng. Automated Learning* 5788, 359-367.
- Kim, K. J., Wang, A., and Lipson, H., 2010. Automated synthesis of resilient and tamper-evident analog circuits without a single point of failure. *Genet. Programming Evolvable Mach.* 11, 35-59.
- Kim, M. H., Lee, S., and Lee, K. C., 2010. Kalman predictive redundancy system for fault tolerance of safety-critical systems. *IEEE Transactions on Industrial Informatics* 6, 46-53.
- Kim, S. J., Seong, P. H., Lee, J. S., Kim, M. C., Kang, H. G., and Jang, S. C., 2006. A method for evaluating fault coverage using simulated fault injection for digitalized systems in nuclear power plants. *Reliability Engineering and System Safety* 91, 614-623.

- Kleiner, C. T. and Messenger, G. C., 1982. An improved bipolar junction transistor model for electrical and radiation effects. *IEEE Transactions on Nuclear Science* 29, 1569-1579.
- Ko, D. Y., and Lee, S. I., 2013. Applicable approach of the wireless technology for Korean nuclear power plants. *Nuclear Engineering and Design* 265, 519-525.
- Koga, R., and Kolasinski, W. A., 1989. Heavy ion induced snapback in CMOS devices. *IEEE Transactions on Nuclear Science* 36, 4127-4130.
- Koga, R., Penzin, S. H., Crawford, K. B., Crain, and W. R., 1997. Single event functional interrupt (SEFI) sensitivity in microcircuits. *RADECS 97. Fourth European Conference on Radiation and Its Effects on Components and Systems, Cannes, France.*
- Koga, R., Yu, P., Crawford, K. B., Crain, S. H., and Tran, V. T., 2001. Permanent single event functional interrupts (SEFIs) in 128- and 256-Megabit synchronous dynamic random access memories (SDRAMs). 2001 IEEE Radiation Effects Data Workshop REDW.2001.
- Kolasinsky, W. A., Blake, J. B., Anthony, J. K., Price, W. E., and Smith, E. C., 1979. Simulation of cosmic-ray induced soft errors and latchup in integrated-circuit computer memories. *IEEE Transactions on Nuclear Science* 26, 5087-5091.
- Korkut, T., Karabulut, A., Budak, G., Aygun, B., Gencel, O., and Hancerliogullari, A., 2012. Investigation of neutron shielding properties depending on number of boron atoms for colemanite, ulexite and tincal ores by experiments and FLUKA Monte Carlo simulations. *Applied Radiation and Isotopes* 70, 341-345.
- Korkut, T., Un, A., Demir, F., Karabulut, A., Budak G., Sahin, R., and Oltulu, M., 2010. Neutron dose transmission measurements for several new concrete samples including colemanite. *Annals of Nuclear Energy* 37, 996-998.
- Kortou, V., and Ustyantsev, Y., 2013. Chernobyl accident: causes, consequences and problems of radiation measurements. *Radiation Measurements* 55, 12-16.
- Kosier, S. L., Wei, A., Schrimpf, R. D., Fleetwood, D. M., DeLaus, M. D., Pease, R. L., and Combs, W. E., 1995. Physically based comparison of hot-carrier-induced and

- ionizing-radiation-induced degradation in BJT's. *IEEE Transactions on Nuclear Science* 42, 436-444.
- Kuboyama, S., Matsuda, S., Kanno, T., and Ishii, T., 1992. Mechanism for single-event burnout of power MOSFET's and its characterization technique. *IEEE Transactions on Nuclear Science* 39, 1698-1703.
- Kulkarni, R. D., and Agarwal, V., 2003. Reliability analysis of a modern power supply under nuclear radiation effects. *Power Electronics and Drive Systems, PEDS 2003*.
- Kurudirek, M., 2014. Radiation shielding and effective atomic number studies in different types of shielding concretes, lead base and non-lead base glass systems for total electron interaction: a comparative study. *Nuclear Engineering and Design* 280, 440-448.
- Kurudirek, M., Turkmen, I., and Ozdemir, Y., 2009. A study of photon interaction in some building materials: high-volume admixture of blast furnace slag into Portland cement. *Radiation Physics and Chemistry* 78, 751-759.
- LaBel, K. A., and Gates, M. M., 1996. Single-event-effect mitigation from a system perspective. *IEEE Transactions on Nuclear Science* 43, 654-660.
- LaBel, K. A., Stassinopoulos, E. G., Brucker, G. J., and Stauffer, C. A., 1992. SEU tests of a 80386 based flight-computer/data-handling system and discrete PROM and EEPROM devices, and SEL tests of discrete 80386, 80387, PROM, EEPROM and ASICS. *Workshop Record., Radiation Effects Data Workshop 1992, New Orleans, LA, USA*.
- Lacoe, R.C., 2008. Improving integrated circuit performance through the application of hardness-by-design methodology. *IEEE Transactions on Nuclear Science* 55, 1903-1925.
- Lauridsen, K., Christensen, P., and Kongso, H. E., 1996. Assessment of the reliability of robotic systems for use in radiation environments. *Reliability Engineering and System Safety* 53, 265-276.

- Lauridsen, K., Decreton, M., Seifert, C. C., and Sharp, R. E., 1996. Reliability and radiation tolerance of robots for nuclear applications. The final report of CEC/TELEMAN project, No. FI2T-CT90-0011, ENTOREL.
- Lawrence, T. C., Patterson, D. W., Ramamurthy, C., and Holbert, E. H., 2015. An embedded microprocessor radiation hardened by microarchitecture and circuits. *IEEE Transactions on Computers* 65, 382-395.
- Layzell, P., and Thompson, A., 2000. Understanding inherent qualities of evolved circuits: evolutionary history as a predictor of fault tolerance. in *Proc. Evol. Syst.: From Biology to Hardware*, LNCS 1801. 133-144.
- Leavy, J. F., and Poll, R. A., 1969. Radiation-induced integrated circuit latchup. *IEEE Transactions Nuclear Science* 6, 96-103.
- Lee, C. I., Rax, B. G., and Johnston, A. H., 1994. Total ionizing dose effects on high resolution (12-/14-bit) analog-to-digital converters. *IEEE Transactions on Nuclear Science* 41, 2459-2466.
- Lee, C. I., and Johnston, A. H., 1998. Comparison of total dose responses on high resolution analog-to-digital converter technologies. *IEEE Transactions on Nuclear Science* 45, 1444-1449.
- Lee, C. I., Rax, B. G., and Johnston, A. H., 1994. Total ionizing dose effects on high resolution (12/14-bit) analog-to-digital converters. *IEEE Transactions on Nuclear Science* 41, 2459-2466.
- Lee, C. I., Rax, B. G., and Johnston, A. H., 1995. Hardness assurance and testing techniques for high resolution (12- to 16-bit) analog-to-digital converters. *IEEE Transactions on Nuclear Science* 42, 1681-1688.
- Lee, J. K., Jeong, S.C., Jeong, K.H., Oh, D.Y., and Kim, J. H., 2009. Wireless technology application to nuclear power plants. *Transactions of the Korean Nuclear Society Autumn Meeting*, Gyeongju & Korea.
- Lee, M.B., and Farnum, E.H., 1995. The effect of neutron energy on defect production in alumina. *Nuclear Instruments and Methods in Physics Research B*, 113-118.

- Lei, F., Truscott, P.R., Dyer, C.S., Quaghebeur, B., Heynderickx, D., Nieminen, P., Evans, H., and Daly, E., 2002. MULASSIS: A Geant4-based multilayered shielding simulation tool. *IEEE Transactions on Nuclear Science* 49, 2788-2793.
- Lho, Y. H. and Kim, K. Y., 2005. Radiation effects on the power MOSFETs for space applications. *ETRI Journal* 27, 449-452.
- Li, T., Yang, H., Cai, G., Zhi, T., and Li, Y., 2014. A CMOS triple inter-locked latch for SEU insensitivity design. *IEEE Transactions on Nuclear Science* 61, 3265-3273.
- Li, Y., Li, D., and Wang, Z., 2000. A new approach to detect-mitigate-correct radiation-induced faults for SRAM-based FPGAs in aerospace application. In *National Aerospace and Electronics Conference*, 588-594.
- Lin, Y., Zwolinski, M., and Halak, B., 2016. A low-cost, radiation-hardened method for pipeline protection in microprocessors. *IEEE Transactions on Very Large Scale Integration (VLSI) Systems* 24, 1688-1701.
- Lindoso, A., Entrena, L., Millan, E.S., Cuenca-Asensi, S., Martinez-Alvarez, A., and Restrepo-Calle, F., 2012. A co-design approach for SET mitigation in embedded systems. *IEEE Transactions on Nuclear Science* 59, 1034-1039.
- Liu, B., Wang, Y., Yu, Z., Liu, L., Li, M., Wang, Z., Lu, J., and Fernandez, F. V., 2009. Analog circuit optimization system based on hybrid evolutionary algorithms. *INTEGRATION, the VLSI J.* 42, 137-148.
- Liu, J., Zhou, J., Luo, H., Kong, X., En, Y., Shi, Q., and He, Y., 2010. Total-dose-induced edge effect in SOI NMOS transistors with different layouts. *Microelectronics Reliability* 50, 45-47.
- Liu, M., and He, J., 2013. An evolutionary negative-correlation framework for robust analog-circuit design under uncertain faults. *IEEE Transactions on Nuclear Science* 17, 640-665.
- Liu, S., Boden, M., Girdhar, D.A., and Titus, J.L., 2006. Single-event burnout and avalanche characteristics of power DMOSFETs. *IEEE Transactions on Nuclear Science* 53, 3379-3385.

- Lopez-Morillo, E., Palomo, F. R., Marquez, F., and Munoz, F., 2018. Design of a radiation hardened power-on-reset. *IEEE Transactions on Nuclear Science* 65, 1943-1950.
- Lu, Y., Lombardi, F., Pontarelli, S., and Ottavi, M., 2014. Design and analysis of single-event tolerant slave latches for enhanced scan delay testing. *IEEE Transactions on Device and Materials Reliability* 14, 333-343.
- Lv, L., Li, P., Ma, X., Liu, L., Yang, L., Zhou, X., Zhang, J., Cao, Y., Bi, Z., Jiang, T., Zhu, Q., and Hao, Y., 2017. Fast and thermal neutron radiation effects on GaN PIN devices. *IEEE Transactions on Nuclear Science* 64, 643-647.
- Mahmood, A., and McCluskey, E., 1988. Concurrent error-detection using watchdog processors – a survey. *IEEE Transactions on Computers* 37, 160-174.
- Makowski, D., 2006. The impact of radiation on electronic devices with the special consider of neutron and gamma radiation monitoring. PhD dissertation, Technical University of Lodz.
- Mangeret, R., Carriere, T., and Beaucour, J., 1996. Effects of material and/or structure on shielding of electronic devices. *IEEE Transactions on Nuclear Science* 43, 2665-2670.
- Marcelot, O., Goiffon, V., Raine, M., Duhamel, O., Gaillardin, M., Molina, R., and Magnan, P., 2015. Radiation effects in CCD and CMOS devices: first analysis of TID and DDD effects. *IEEE Transactions on Nuclear Science* 62, 2965-2970.
- Marquez, F., Munoz, F., Palomo, F. R., Sanz, L., Lopez-Morillo, E., Aguirre, M. A., and Jimenez, A., 2015. Automatic single event effects sensitivity analysis of a 13-bit successive approximation ADC. *IEEE Transactions on Nuclear Science* 62, 1609-1616.
- Massengill, L. W., Diehl, S. E., and Browning, J. S., 1986. Dose-rate upset patterns in a 16K CMOS SRAM. *IEEE Transactions on Nuclear Science* 33, 1541-1545.
- Mayer, D. C., Lacoe, R. C., King, E. E., and Osborn, J. V., 2004. Reliability enhancement in high-performance MOSFETs by annular transistor design. *IEEE Transactions on Nuclear Science* 51, 3615-3620.

- Mavis, D. G., and Eaton, P. H., 2002. Soft error rate mitigation techniques for modern microcircuits. Reliability Physics Symposium Proceedings, Dallas, TX.
- McCaffrey, J.P., Shen, H., Downton, B., and Mainegra-Hing, E., 2007. Radiation attenuation by lead and nonlead materials used in radiation shielding garments. *Medical Physics* 34, 530-537.
- McGarrity, J. M., McLean, F. B., DeLancey, W. M., Palmour, J., Carter, C., and Edmond, J., 1992. Silicon carbide JFET radiation response. *IEEE Transactions on Nuclear Science* 39, 1974-1981.
- McLean, F. B., and Oldham, T. R., 1987. Basic mechanisms of radiation effects in electronic materials and devices. Defense Nuclear Agency Technical Report.
- Messenger, G. C., and Ash, M. S., 1991. The effects of radiation electronic systems. Van Nostrand Reinhold, New York, 2nd edition.
- Messenger, G. C., and Spratt, J. P., 1958. The effects of neutron irradiation on germanium and silicon. *Proceedings of the IRE*, 46, 1038-1044.
- Michez, A., Dhombres, S., and Boch, J., 2015. ECORCE: a TCAD tool for total ionizing dose and single event effect modeling. *IEEE Transactions on Nuclear Science* 62, 1516-1527.
- Michez, A., Boch, J., Dhombres, S., Saigne, F., Touboul, A. D., Vaille, J. -R., Dusseau, L., Lorfevre, E., and Ecoffet, R., 2013. Modeling dose effects in electronics devices: dose and temperature dependence of power MOSFET. *Microelectronics Reliability* 53, 1306-1310.
- Mikkola, E., 2008. Hierarchical simulation method for total ionizing dose radiation effects on CMOS mixed-signal circuits. PhD dissertation, The University of Arizona.
- Mikkola, E., Vermeire, B., Chiu, T., Barnaby, H., and Parks, H. G., 2007. Total dose radiation effect simulations on a high-precision data acquisition system. *Radiation and Its Effects on Components and Systems*, 1-6.

- Mikkola, E. O., Vermeire, B., Parks, H. G., and Graves, R., 2007. VHDL-AMS modeling of total ionizing dose radiation effects on CMOS mixed signal circuits. *IEEE Transactions on Nuclear Science* 54, 929-934.
- Montagner, X., Briand, R., Fouillat, P., Schrimpf, R. D., Touboui, A., Galloway, K. F., Calvet, M. C., and Calvel, P., 1998. Dose-rate and irradiation temperature dependence of BJT SPICE model rad-parameters. *IEEE Transactions on Nuclear Science* 45, 1431-1437.
- Morelos-Zaragoza, R. H., 2002. The art of error correcting and coding. Wiley.
- Mukherjee, S., Kontz, and M., Reinhardt, S., 2002. Detailed design and evaluation of redundant multithreading alternatives. *Proceeding 29th Annual International Symposium on Computer Architecture*, Anchorage, AK, USA.
- Munteanu, D., Autran, J. L., 2008. Modeling and simulation of single-event effects in digital devices and ICs. *IEEE Transactions on Nuclear Science* 55, 1854-1878.
- Najm, F. N., 2010. Circuit simulation. Wiley-IEEE Press, ISBN: 978-0-470-53871-5.
- Nasr-Storey, S. S. E., Boeuf, F., Baudot, C., Detraz, S., Fedeli, J. M., Marris-Morini, D., Olantera, L., Pezzullo, G., Sigaud, C., Soos, C., Troska, J., Vasey, F., Vivien, L., Zeiler, M., and Ziebell, M., 2015. Modeling TID effects in Mach-Zehnder interferometer silicon modulator for HL-LHC data transmission applications, *IEEE Transactions on Nuclear Science* 62, 2971-2978.
- Neamen, D. A., 1984. Modeling of MOS radiation and post irradiation effects. *IEEE Transactions on Nuclear Science* 31, 1439-1443.
- Neuberger, G., Kastensmidt, F. G. L., and Reis, R., 2005. An automatic technique for optimizing Reed-Solomon codes to improve fault tolerance in memories. *IEEE Design & Test of Computers* 22, 50-58.
- Nguyen, D. N., Guertin, S. M., Swift, G. M., and Johnston, A. H., 1999. Radiation effects on advanced flash memories. *IEEE Transactions on Nuclear Science* 46, 1744-1750.
- Nicolaidis, M., 1999. Time redundancy based soft-error tolerance to rescue nanometer technologies. *VLSI Test Symposium*, 86-94.

- Nicolaidis, M. and Zorian, Y., 1998. On-line testing for VLSI – a compendium of approaches. *Journal of Electronic Testing* 12, 7-20.
- Nicosia, G., Rinaudo, S., and Sciacca, E., 2008. An evolutionary algorithm-based approach to robust analog circuit design using constrained multiobjective optimization. *Knowledge-Based Syst.* 21, 175-183.
- Nidhin, T. S., Bhattacharyya, A., Behera, R. P., and Jayanthi, T., 2017. A review on SEU mitigation techniques for FPGA configuration memory. *IETE Technical Review*, 1-12.
- Nilamani, S., and Ramakrishnan, V. N., 2017. Gate and drain SEU sensitivity of sub-20-nm FinFET- and junctionless F inFET-based 6T-SRAM circuits by 3D TCAD simulation. *Journal of Computational Electronics* 16, 74-82.
- Norgett, M. J., Robinson M. T., and Torrens, I. M., 1975. A proposed method of calculating displacement dose rates. *Nuclear Engineering and Design* 33, 50-54.
- Nsengiyumva, P., Ball, D. R., Kauppila, J. S., Tam, N., McCurdy, M., Holman, W. T., Alles, M. L., Bhuva, B. L., and Massengill, L. W., 2016. A comparison of the SEU response of planar and FinFET D flip-flops at advanced technology nodes. *IEEE Transactions on nuclear science* 63, 266-272.
- O'Loughlin, M. J., 1987. Radiation effects in high electron mobility transistors: total dose gamma irradiation. *IEEE Transactions on Nuclear Science* 34, 1808-1811.
- Oberg, D. L., and Wert, J. L., 1987. First nondestructive measurements of power MOSFET single event burnout cross sections. *IEEE Transactions on Nuclear Science* 34, 1736-1741.
- Ochoa, A., Sexton, F. W., Wrobel, T. F., Hash, G. L., and Sokel, R. J., 1984. Snap-back: a stable regenerative breakdown mode of MOS devices. *IEEE Transactions on Nuclear Science* 30, 4127-4130.
- Okuno, K., 2005. Neutron shielding material based on colemanite and epoxy resin. *Radiation Protection Dosimetry* 115, 258-261.

- Oldham, T. R., 2011. Basic mechanisms of TID and DDD response in MOS and bipolar microelectronics. Proc. NSREC Tutorial Short 2011.
- Oldham, T. R., Labury, R. L., Friendlich, M., Kim, H. S., Berg, M. D., Irwin, T. L., Seidleck, C., and LaBel, K. A., 2006. SEE and TID characterization of an advanced commercial 2Gbit NAND flash nonvolatile memory. *IEEE Transactions on Nuclear Science* 53, 3217-3222.
- Oldham, T. R., and McLean, F. B., 2003. Total ionizing dose effects in MOS oxides and devices. *IEEE Transactions on Nuclear Science* 50.
- Pacheco, M. A. C., and Vellasco, M. M. R., 2002. Automatic repair techniques for analog circuits. in *Proc. IEEE Int. Conf. Ind. Technol.*, vol. 2, pp. 804-809.
- Park, H., Dixit, S. K., Choi, Y. S., Schrimpf, R. D., Fleetwood, D. M., Nishida, T., and Thompson, S. E., 2008. Total ionizing dose effects on strained HfO₂-based nMOSFETs. *IEEE Transactions on Nuclear Science* 55, 2981-2985.
- Passeri, D., Moscatelli, F., Morozzi, A., and Bilei, G. M., 2016. Modeling of radiation damage effects in silicon detectors at high fluences HL-LHC with sentaurus TCAD. *Nuclear Instruments and Methods in Physics Research A: Accelerators, Spectrometers, Detectors and Associated Equipment* 824, 443-445.
- Patel, A. M., and Hong, S. J., 1974. Optimal rectangular code for high density magnetic tapes. *IBM Journal of Research and Development* 18, 579-588.
- Patrick, E., Rowsey, N., Law, M. E., 2015. Total dose radiation damage: a simulation framework. *IEEE Transactions on Nuclear Science* 62, 1650-1657.
- Pearton, S. J., Ren, F., Patrick, E., Law, M. E., and Polyakov, A. Y., 2016. Review-ionizing radiation damage effects on GaN devices. *ECS Journal of Solid State Science and Technology* 5, 35-60.
- Pease, R. L., 2003. Total ionizing dose effects in bipolar devices and circuits. *IEEE Transactions on Nuclear Science* 50, 539-551.
- Pease, R. L., Cohn, L. M., Fleetwood, D. M., Gehlhausen, M. A., Turflinger, T. L., Brown, D. B., and Johnston, A. H., 1997. A proposed hardness assurance test

- methodology for bipolar linear circuits and devices in a space ionizing radiation environment. *IEEE Transactions on Nuclear Science* 44, 1981-1988.
- Pease, R. L., Dunham, G. W., Seiler, J. E., Platteter, D. G., and McClure, S. S., 2007. Total dose and dose rate response of an AD590 temperature transducer. *IEEE Transactions on Nuclear Science* 54, 1049-1054.
- Pease, R. L., Gehlhausen, M., Krieg, J., Titus, J., Turflinger, T., Emily, D., and Cohn, L., 1998. Evaluation of proposed hardness assurance method for bipolar linear circuits with enhanced low dose rate sensitivity (ELDRS). *IEEE Transactions on Nuclear Science* 45, 2665-2672.
- Pease, R. L., McClure, S., Gorelick, J., and Witczak, S. C., 1998. Enhanced low-dose-rate sensitivity of a low-dropout voltage regulator. *IEEE Transactions on Nuclear Science* 45, 2571-2576.
- Penfield, P., 2004. Information and entropy. Technical report, Massachusetts Institute of Technology.
- Petrosjanc, K. O., Kharitonov, I. A., and Orekhov, E. V., 2009. TCAD technique to simulate total dose effects in SOI MOSFETs. *Proc. Int. Conf. on Micro- and Nanoelectronics*.
- Pizanoa, J. E., Maa, T. H., Attiab, J. O., Schrimpf, R. D., Galloway, K. F., and Witulskia, A. F., 1998. Total dose effects on power-MOSFET switching converts. *Microelectronics Reliability* 38, 1935-1939.
- Policy Elements Post-accident management in the event of nuclear accident. the Steering Committee for the Management of the Post-Accident Phase of a Nuclear Accident (CODIRPA), 2012.
- Polyakov, A. Y., Pearton, S. J., Frenzer, P., Ren, F., Liu, L., and Kim, J., 2013. Radiation effects in GaN materials and devices. *Journal of Materials Chemistry C* 1, 877-887.
- Praveen, K. C., Pushpa, N., Naik, P. S., Cressler, J. D., Tripathi, A., Prakash, A. P. G., 2012. Application of a Pelletron accelerator to study total dose radiation effects on 50 GHz SiGe HBTs. *Nuclear Instruments and Methods in Physics* 273, 43-46.

- Prelas, M., Boraas, M., Aguilar, F. T., Seeling, J., Tchouaso, M. T., 2016. Interactions of ionizing radiation with matter and direct energy conversion, *Nuclear Batteries and Radioisotopes*, 81-175.
- Proakis J.G., and Salehi M., 2008. *Digital communications*, Fifth edition. McGraw-Hill Higher Education.
- Purser, M., 1995. *Introduction to error-correcting codes*. Artech House.
- Qi, C., Xiao, L., Guo, J., and Wang, T., 2015. Low cost and highly reliable radiation hardened latch design in 65 nm CMOS technology. *Microelectronics Reliability* 55, 863-872.
- Quinn, H. M., Black, D. A., Robinson, W. H., and Buchner, S. P., 2013. Fault simulation and emulation tools to augment radiation-hardness assurance testing. *IEEE Transactions on Nuclear Science* 60, 2119-2142.
- Rad Pro Calculator, [Online]. Available: www.radprocalculator.com/Gamma.aspx. Accessed on June 10, 2017.
- Rajaei, R., 2016. Radiation-hardened design of nonvolatile MRAM-based FPGA. *IEEE Transactions on Magnetics* 52, 3402010.
- Rajaei, R., Fazeli, M., and Tabandeh, M., 2015. Soft error-tolerant design of MRAM-based nonvolatile latches for sequential logics. *IEEE Transactions on Magnetics* 51, 4400414.
- Rajaei, R., and Mamaghani, S. B., 2017. Ultra-low power, highly reliable, and nonvolatile hybrid MTJ/CMOS based full-adder for future VLSI design. *IEEE Transactions on device and materials reliability* 17, 213-220.
- Rajaei, R., Tabandeh, M., and Fazeli, M., 2013. Low cost soft error hardened latch designs for nano-scale CMOS technology in presence of process variation. *Microelectronics Reliability* 53, 912-924.
- Ramachandran, V., Narasimham, B., Fleetwood, D. M., Schrimpf, R. D., Holman, W. T., Witulski, A. F., Pease, R. L., Dunham, G. W., Seiler, J. E., and Platter, D. G., 2006.

- Modeling total-dose effects for a low-dropout voltage regulator. *IEEE Transactions on Nuclear Science* 53, 3223-3231.
- Randell, B., 1975. System structure for software fault tolerance. *IEEE Transactions on Software Engineering* 1, 220-232.
- Raoul, V., 2007. Radiation effects on embedded systems. Springer Netherlands.
- Rathod, S. S., Saxena, A. K., and Dasgupta, S., 2011. Radiation effects in MOS-based devices and circuits: a review. *IETE Technical Review* 28, 451-469.
- Ratnakumar, B. V., Smart, M. C., Whitcanack, L. D., Davies, E. D., Chin, K. B., Deligiannis, F., and Surampudi, S., 2005. Behavior of Li-Ion cells in high-intensity radiation environments. *Journal of the Electrochemical Society* 152, 357-363.
- Ravi, V., Reddy, P. J., and Zimmermann, H. J., 2000. Fuzzy global optimization of complex system reliability. *IEEE Transactions on Fuzzy Systems* 8, 241-248.
- Raymond, J. P., and Willis, J., 1965. Generalized model analysis of ionizing radiation effects in semiconductor devices. *IEEE Transactions on Nuclear Science* 12, 55-68.
- Re, V., Manghisoni, M., Ratti, L., Speziali, V., and Traversi, G., 2006. Total ionizing dose effects on the noise performances of a 0.13 μm CMOS technology. *IEEE Transactions on Nuclear Science* 53, 1599-1606.
- Re, V., Gaioni, L., Manghisoni, M., Ratti, L., and Traversi, G., 2008. Comprehensive study of total ionizing dose damage mechanisms and their effects on noise source in a 90nm CMOS technology. *IEEE Transactions on Nuclear Science* 55, 3272-3279.
- Rebaudengo, M., Reorda, M., and Violante, M., 2004. A new approach to software implemented fault tolerance. *J. Electronic Testing-Theory and Applications* 20, 433-437.
- Reed R. A., Weller, R. A., Mendenhall, M. H., Fleetwood, D. M., Warren, K. M., Sierawski, B. D., King, M. P., Schrimpf, R. D., and Auden, E. C., 2015. Physical processes and applications of the Monte Carlo radiative energy deposition (MRED) code. *IEEE Transactions on Nuclear Science* 62, 1441-1461.

- Reed R. A., Weller, R. A., Akkerman, A., Barak, J., Culpepper, W., Duzellier, S., Foster, C., Gaillardin, M., Hubert, G., Jordan, T., Jun, I., Koontz, S., Lei, F., McNulty, P., Mendenhall, M. H., Murat, M., Nieminen, P., O'Neil, P., Raine, M., Reddell, B., Saigne, F., Santin, G., Sihver, L., Tang, H. H. K., Truscott, P. R., and Wrobel, F., 2013. Anthology of the development of radiation transport tools as applied to single event effects. *IEEE Transactions on Nuclear Science* 60, 1876-1911.
- Regulatory Guide 1.97, Rev. 03, 1983. Instrumentation for light-water-cooled nuclear power plants to assess plant and environs conditions during and following an accident. U. S. Nuclear Regulatory Commission.
- Regulatory Guide 1.97, Rev. 04, 2005. Criteria for accident monitoring instrumentation for nuclear power plants. U. S. Nuclear Regulatory Commission.
- Regulatory Guide 1.180 (Rev. 1), 2003. Guideline for evaluating electromagnetic and radio-frequency interference in safety-related instrumentation and control system. U. S. Nuclear Regulatory Commission.
- Ren, S., Bhuiyan, M. A., Wu, H., Jiang, R., Ni, Kai, Zhang, E. X., Reed, R. A., Fleetwood, D. M., Ye, P. and Ma, T. P., 2017. Total ionizing dose (TID) effects in ultra-thin body Ge-on-Insulator (GOI) junctionless CMOSFETs with recessed source/drain and channel. *IEEE Transactions on Nuclear Science* 64, 176-180.
- Rezzak, N., Wang, J., 2015. Single event latch-up hardening using TCAD simulations in 130 nm and 65 nm embedded SRAM in flash-based FPGAs. *IEEE Transactions on Nuclear Science* 62, 1599-1608.
- Robinson, M. T., 1994. Basic physics of radiation damage production. *Journal of Nuclear Materials* 216, 1-28.
- Roche P., Gasiot, G., Autran, J. L., Munteanu, D., Reed, R. A., and Weller, R. A., 2014. Application of the TIARA radiation transport tool to single event effects simulation. *IEEE Transactions on Nuclear Science* 61, 1498-1500.
- Roig, F., Dusseau, L., Ribeiro, P., Auriel, G., Roche, N. J-H., Privat, A., Vaille, J. -R., Boch, J., Saigne, F., Marec, R., Calvel, P., Bezerra, F., Ecoffet, R., and Azais, B.,

2014. Impact of neutron-induced displacement damage on the ATREE response in LM124 operational amplifier. *IEEE Transactions on Nuclear Science* 61, 3043-3049.
- Roig, F., Dusseau, L., Ribeiro, P., Auriel, G., Roche, N. J-H., Privat, A., Vaille, J.-R., Boch, J., Saigne, F., Marec, R., Calvel, P., Bezerra, F., Ecoffet, R., and Azais, B. 2014. Study and modeling of impact of TID on the ATREE response in LM124 operational amplifier. *IEEE Transactions on Nuclear Science* 61, 1603-1610.
- Ronald, P. L., Johnston, A. H., and Azarewicz, J. L., 1988. Radiation testing of semiconductor devices for space electronics. *Proceeding of IEEE* 76, 1510-1526.
- Ruano, O., Maestro, J. A., Reyes, P., and Reviriego, P., 2007. A simulation platform for study of soft errors on signal processing circuit thorough software fault injection. *IEEE International Symposium on Industrial Electronics*, 3316-3321.
- Saenko, V., Ivanov, V., Tsyb, A., Bogdanova, T., Tronko, M., Demidchik, Y., and Yamashita, S., 2011. The Chernobyl accident and its consequences. *Clinical Oncology* 23, 234-243.
- Sajid, M., Chechenin, N. G., Torres, F. S., Hanif, M. N., Gulzari, U. A., Arslan, S., and Khan, E. U., 2018. Analysis of total ionizing dose effects for highly scaled CMOS devices in low earth orbit. *Nuclear Instruments and Methods in Physics Research B* 428, 30-37.
- Samson, J. R., Torre, L. D., Wiley P., Stottlar, T., and Ring, J., 2001. A comparison of algorithm-based fault tolerance and traditional redundant self-checking for SEU mitigation. *Digital Avionics Systems* 2, 8E4/1-8E4/11.
- Santin, G., Nieminen, P., Evansa, H., Daly, E., Lei, F., Truscott, P. R., Dyer, C. S., Quaghebeur, B., and Heynderickx, D., 2003. New Geant4 based simulation tools for space radiation shielding and effects analysis. *Nuclear Physics B – Proceedings Supplements* 125, 69-74.
- Schlenvagt, G. J., Barnaby, H. J., Wilkinson, J., Morrison, S., and Tyler, L., 2013. Simulation of TID effects in a high voltage ring oscillator. *IEEE Transactions on Nuclear Science* 60, 4547-4554.

- Schmidt, D. M., Fleetwood, D. M., Schrimpf, R. D., Pease, R. L., Graves, R. J., Johnson, G. H., Galloway, K. F., and Combs, W. E., 1995. Comparison of ionizing-radiation-induced gain degradation in lateral, substrate, and vertical PNP BJTs. *IEEE Transactions on Nuclear Science* 42, 1541-1549.
- Schmidt, D. M., Wu, A., Schrimpf, R. D., Fleetwood, D. M., and Please, R. L., 1996. Modeling ionizing radiation induced gain degradation of the lateral PNP bipolar junction transistor. *IEEE Transactions on Nuclear Science* 43, 3032-3039.
- Schrimpf, R. D., Wahle, P. J., Andrews, R. C., Cooper, D. B., and Galloway, K. F., 1988. Dose-rate effects on the total-dose threshold-voltage shift of power MOSFETs. *IEEE Transactions on Nuclear Science* 35, 1536-1540.
- Schrimpf, R. D., and Fleetwood, D. M., 2004. Radiation effects and soft errors in integrated circuits and electronic devices. World Scientific Publishing Co. Pte. Ltd.
- Schwank, J., Ferlet-Cavrois, V., Shaneyfelt, M. R., Paillet, P., and Dodd, P., 2003. Radiation effects in SOI technologies. *IEEE Transactions on Nuclear Science* 50, 522-538.
- Schwank, J. R., 1994. Basic mechanisms of radiation effects in the natural space environment. *Proc. NSREC Short Course*.
- Schwank, J., Ferlet-Cavrois, V., Shaneyfelt, M. R., Paillet, P., and Dodd, P., 2003. Radiation effects in SOI technologies. *IEEE Transactions on Nuclear Science* 50, 522-538.
- Schwank, J. R., Shaneyfelt, M. R., Fleetwood, D. M., Felix, J. A., Dodd, P. E., Paillet, P., and Ferlet-Cavrois, V., 2008. Radiation effects in MOS oxides. *IEEE Transactions on Nuclear Science* 55, 1833-1853.
- Schwank, J. R., Shaneyfelt, M. R., and Dodd, P. E., 2013. Radiation hardness assurance testing of microelectronic devices and integrated circuits: radiation environments, physical mechanisms, and foundations for hardness assurance. *IEEE Transactions on Nuclear Science* 60, 2074-2100.
- Seifert, N., Jahinuzzaman, S., Velamala, J., Ascazubi, R., Patel, N., Gill, B., Basile, J., and Hicks, J., 2015. Soft error rate improvements in 14-nm technology featuring

- second-generation 3D tri-gate transistors. *IEEE Transactions on Nuclear Science* 62, 2570-2577.
- Seixas, L. E., Goncalvez, O. L., Souza, R., Finco, S., Vaz, R. G., Silva, G. A., and Gimenez, S. P., 2017. Improving MOSFETs' TID tolerance through diamond layout style. *IEEE Transactions on Device and Materials Reliability* 17, 593-595.
- Sexton, F. W., 1996. Microbeam studies of single-event effects. *IEEE Transactions on Nuclear Science* 43, 687-695.
- Sexton, F.W., 2003. Destructive single-event effects in semiconductor devices and ICs. *IEEE Transactions on Nuclear Science* 50, 603-621.
- Sexton, F. W., Fleetwood, D. M., Shaneyfelt, M. R., Dodd, P. E., and Hash, G. L., 1997. Single event gate rupture in thin gate oxides. *IEEE Transactions on Nuclear Science* 44, 2345-2352.
- Sexton, F. W., Fleetwood, D. M., Shaneyfelt, M. R., Dodd, P. E., Hash, G. L., Krisch, K. S., Green, M. L., Weir, B. E., and Silverman, P. J., 1998. Precursor ion damage and angular dependence of single event gate rupture in thin oxides. *IEEE Transactions on Nuclear Science* 45, 2509-2518.
- Shaneyfelt, M. R., Schwank, J. R., Dodd, P. E., and Felix, J. A., 2008. Total ionizing dose and single event effects hardness assurance qualification issues for microelectronics. *IEEE Transactions on Nuclear Science* 55, 1926-1946.
- Sharp, R., and Decretton, M., 1996. Radiation tolerance of components and materials in nuclear robot applications. *Reliability Engineering and System Safety* 53, 291-299.
- Shetler, K. J., Atkinson, N. M., Holman, W. T., Kauppia, J. S., Loveless, T. D., Witulski, A. F., Bhuva, B. L., Zhang, E. X., and Massengill, L. W., 2015. Radiation hardening of voltage references using chopper stabilization. *IEEE Transactions on Nuclear Science* 62, 3064-3071.
- Shirvani, P. P., and McCluskey, E. J., 2000. Software-implemented EDAC protection against SEUs. *IEEE Transactions on Reliability* 49, 273-284.

- Shooman, M. L., 2003. Reliability of computer systems and networks: fault tolerance, analysis, and design. John Wiley and Sons, Inc.
- Shultis, J. K., and Faw, R. E., 2005. Radiation shielding technology. *Health Physics* 88, 587-612.
- Siegle, F., Vladimirova, T., Ilstad, J. and Emam, O., 2015. Mitigation of radiation effects in SRAM-based FPGAs for space applications. *ACM Computing Surveys* 47, 1-34.
- Simoen, E., Rafi, J. M., Mercha, A., and Claeys, C., 2004. Total ionizing dose damage in deep submicron partially depleted SOI MOSFETs induced by proton irradiation. *Solid-State Electronics* 48, 1045-1054.
- Simoen, E., Gaillardin, M., Paillet, P., Reed, R. A., Schrimpf, R. D., Alles, M. L., El-Mamouni, F., Fleetwood, D. M., Griffoni, A., and Claeys, C., 2013. Radiation effects in advanced multiple gate and silicon-on-insulator transistors. *IEEE Transactions on Nuclear Science* 60, 1970-1991.
- Singh, V. P., and Badiger, N. M., 2014. The gamma-ray and neutron shielding factors of fly-ash brick materials. *Journal of Radiological Protection* 34, 89-101.
- Smith, F., and Mostert, S., 2007. Total ionizing dose mitigation by means of reconfigurable FPGA computing. *IEEE Transactions on Nuclear Science* 54, 1343-1349.
- Snow, E. H., Grove, A. S., and Fitzgerald, D. J., 1967. Effects of ionizing radiation on oxidized silicon surfaces and planar devices. *Proceedings of the IEEE* 55, 1168-1185.
- Soliman, K., and Nichols, D. K., 1983. Latchup in CMOS devices from heavy ions. *IEEE Transactions on Nuclear Science* 30, 4514-4519.
- Song, I., Jung, S., Lourenco, N. E., Raghunathan, U. S., Fleetwood, Z. E., Zeinolabedinzadeh, S., Gebremariam, T., Roche, N. J. -H., Khachatrian, A., McMorro, D., Buchner, S. P., Melinger, J. S., Warner, J. H., Paki-Amouzou, P., and Cressler, J. D., 2014. Design of radiation-hardened RF low-noise amplifiers using inverse-mode SiGe HBTs. *IEEE Transactions on Nuclear Science* 61, 3218-3225.

- Song, Y., Vu, K. N., Cable, J. S., Witteles, A. A., Kolasinski, W. A., Koga, R., Elder, J. H., Osborn, J. V., Martin, R. C., and Ghoniem, N. M., 1988. Experimental and analytical investigation of single event, multiple bit upsets in poly-Silicon load, 64 K x NMOS SRAMs. *IEEE Transactions on Nuclear Science* 35, 1673-1677.
- Song, Y., and Wang, B., 2013. Survey on reliability of power electronic systems. *IEEE Transactions on Power Electronics* 28, 591-604.
- Sonmez, O. S., and Dunder, G., 2011. Simulation-based analog and RF circuit synthesis using a modified evolutionary strategies algorithm. *Integration, the VLSI J.* 44, 144-154.
- Srour, J. R., 1982. Basic mechanisms of radiation effects on electronic materials, devices, and integrated circuits. Defense Nuclear Agency Technical Report.
- Srour, J. R., 1983. Basic mechanisms of radiation effects on electronic materials, devices, and integrated circuits. 1983 IEEE NSREC Short Course, Gatlinburg & TN.
- Srour, J. R., Marshall, C. J., and Marshall, P. W., 2003. Review of displacement damage effects in silicon devices. *IEEE Transactions on Nuclear Science* 50, 653-670.
- Srour J. R., and McGarrity J. M., 1988. Radiation effects on microelectronics in space. *Proceedings of the IEEE* 76, 1443-1469.
- Srour J. R., and Palko, J. W., 2013. Displacement damage effects in irradiated semiconductor devices. *IEEE Transactions on Nuclear Science* 60, 1740-1766.
- Stassinopoulos, E. G., Brucker, G. J., Calvel, P., Baiget, A., Peyrotte, C., and Gaillard, R., 1992. Charge generation by heavy ions in power MOSFET's, burnout space predictions, and dynamic SEB sensitivity. *IEEE Transactions on Nuclear Science* 39, 1704-1711.
- Sterpone, L., Porrmann, M., and Hagemeyer, J., 2013. A novel fault tolerant and runtime reconfigurable platform for satellite payload processing. *IEEE Transactions on Computers* 62, 1508-1525.

- Sterpone, L., Violante, M., and Rezgui, S., 2006. An analysis based on fault injection of hardening techniques for SRAM-based FPGAs. *IEEE Transactions on Nuclear Science* 53, 2054-2059.
- Straka, M., Kastil, J., Kotasek, Z., and Miculka, L., 2013. Fault tolerant system design and SEU injection based testing. *Microprocessors and Microsystems* 37, 155-173.
- Strnberg, A. L., Massengill, L. W., Hale, M., and Blalock, B., 2006. Single-event sensitivity and hardening of a pipelined analog-to-digital converter. *IEEE Transactions on Nuclear Science* 53, 3532-3538.
- Summers, G. P., Burke, E. A., Xapsos, M. A., Dale, C. J., Marshall, P. W., and Petersen, E. L., 1998. Displacement damage in GaAs structures. *IEEE Transactions on Nuclear Science* 35, 1221-1226.
- Sun, X., Saadat, O. I., Chen, J., Zhang, E. X., Cui, S., Palacios, T., Fleetwood, D. M., and Ma, T. P., 2013. Total-ionizing-dose radiation effects in AlGaIn/GaN HEMTs and MOS-HEMTs. *IEEE Transactions on Nuclear Science* 60, 4074-4079.
- Suteau, C. and Chiron, M., 2005. An iterative method for calculating Gammy-ray build-up factors in multi-layer shields. *Radiation Protection Dosimetry* 116, 489-492.
- Sutton, A. K., Prakash, A. P. G., Jun, B., Zhao, E., Bellini, M., Pellish, J., Diestelhorst, R. M., Carts, M. A., Phan, A., Ladbury, R., Cressler, J., Marshall, P. W., Mashall, C. J., Reed, R. A., Schrimpf, R. D., and Fleetwood, D. M., 2006. An investigation of dose rate and source dependent effects in 200 GHz SiGe HBTs. *IEEE Transactions on Nuclear Science* 53, 3166-3174.
- Tang, H. H. K., and Cannon, E. H., 2004. SEMM-2: A modeling system for single event upset analysis. *IEEE Transactions on Nuclear Science* 51, 3342-3348.
- Takahashi, S., 2014. Radiation monitoring and dose estimation of the Fukushima nuclear accident. Springer Tokyo Heidelberg New York Dordrecht London.
- Tam, S., 2004. Multiple bit error correction. Technical report, Xilinx.
- Tessa. C. L., Fino, L. D., Larosa, M., Lee, K., Mancusi, D., Matthia, D., Narici, L., and Zacont, V., 2009. Simulation of ALTEA calibration data with PHITS, FLUKA and

- GEANT4. Nuclear Instruments and Methods in Physics Research B: Beam Interactions with Materials and Atoms 267, 3549-3557.
- Titt, U., and Newhaser, W. D., 2005. Neutron shielding calculations in proton therapy facility based on Monte Carlo simulations and analytical models: criterion for selecting the method of choice. *Radiation Protection Dosimetry* 115, 144-148.
- Titus, J. L., 2013. An updated perspective of single event gate rupture and single event burnout in power MOSFETS. *IEEE Transactions on Nuclear Science* 60, 1912-1928.
- Titus, J. L., Johnson, G. H., Schrimpf, R. D., and Galloway, K. F., 1991. Single-event burnout of power bipolar junction transistors. *IEEE Transactions on Nuclear Science* 38, 1315-1322.
- Tiwari, A., and Tomko, K. A., 2005. Enhanced reliability of finite-state machines in FPGA through efficient fault detection and correction. *IEEE Transactions on Reliability* 54, 459-467.
- Troutman, R. R., 1986. Latchup in CMOS technology, the problem and its cure. Norwell, MA: Kluwer.
- Truscott, P., Lei, F., Dyer, C. S., Frydland, A., Clucas, S., Trousse, B., Hunter, K., Comber, C., Chugg, A., and Moutrie, M., 2004. Assessment of neutron- and proton-induced nuclear interaction and ionization models in Geant4 for simulation single event effects. *IEEE Transactions on Nuclear Science* 51, 3369-3374.
- Tsiligiannis, G., Dilillo, L., Gupta, V., Bosio, A., Girard, P., Virazel, A., Puchner, H., Bosser, A., Javanainen, A., Virtanen, A., Frost, C., Wrobel, F., Dusseau, L., and Saigne, F., 2014. Dynamic test methods for COTS SRAMs, *IEEE Transactions on Nuclear Science* 61, 3095-3102.
- Turowsky, M., Raman, A., and Schrimpf, R. D., 2004. Nonuniform total-dose-induced charge distribution in shallow-trench isolation oxides. *IEEE Transactions on Nuclear Science* 51, 3166-3171.
- Uznanski, S., Todd, B., Dinius, A., King, Q., and Brugger, M., 2014. Radiation hardness assurance methodology of radiation tolerant power converter controls for large hadron collider, *IEEE Transactions on Nuclear Science* 61, 3694-3700.

- Velazco, R., Clemente, J. A., Hubert, G., Mansour, W., Palomar, C., Franco, F. J., Baylac, M., Rey, S., Rosetto, O., and Vila, F., 2014. Evidence of the robustness of a COTS soft-error free SRAM to neutron radiation. *IEEE Transactions on Nuclear Science* 61, 3103-3108.
- Veronique, F. C., Lloyd, W. M., and Pascale, G., 2013. Single event transients in digital CMOS – a review. *IEEE Transactions on Nuclear Science* 60, 1767-1790.
- Vijaykumar, T., Pomeranz, I., and Cheng, K., 2002. Transient-fault recovery using simultaneous multithreading. *Proceeding 29th Annual International Symposium on Computer Architecture*, Anchorage, AK, USA.
- Violante, M., Meinhardt, C., Reis, R., and Reorda, M. S., 2011. A low-cost solution for deploying processor cores in harsh environments. *IEEE Transactions on Industrial Electronics* 58, 2617-2626.
- Vizkelethy, G., Doyle, B. L., Brice, D. K., Dodd, P. E., Shaneyfelt, M. R., and Schwank, J. R., 2005. Radiation effects microscopy for failure analysis of microelectronic devices. *Nuclear Instruments and Methods in Physics Research B: Beam Interactions with Materials and Atoms* 231, 467-475.
- Wahle, P. J., Schrimpf, R. D., and Galloway, K. F., 1990. Simulated space radiation effects on power MOSFET's in switching power supplies. *IEEE Transactions on Industry Applications* 26, 798-802.
- Wallden, Johan, 2014. Radiation induced effects in electronic devices and radiation hardening by design techniques. Thesis, Department of Electrical Engineering, Linköping University.
- Wang, B., Wang, Z., Hu, C., Zhao, Y., Zhang, Y., and Zhao W., 2018. Radiation-hardening techniques for spin orbit torque-MRAM peripheral circuitry. *IEEE Transactions on Magnetics* 54, 1-5.
- Wang, C., Bai, X., Chen, W., Yang, S., Liu, Y., Jin, X., and Ding, L., 2015. Simulation of synergistic effects on lateral PNP bipolar transistors induced by neutron and gamma irradiation. *Nuclear Instruments and Methods in Physics Research A: Accelerators, Spectrometers, Detectors and Associated Equipment* 796, 108-113.

- Wang, H. -B., Li, Y., -Q., Chen, L., Li, L. -X., Liu, R., Baeg, S., Mahatme, N., Bhuva, B. L., Wen, S. -J., Wong, R., and Fung, R., 2015. An SEU-tolerant DICE latch design with feedback transistors. *IEEE Transactions on Nuclear Science* 62, 548-554.
- Wang, Q, and Jiang, J., 2016. Comparative examination on architecture and protocol of industrial wireless sensor network standards. *IEEE Communications Surveys & Tutorials* 18, 2197-2219.
- Wang, T., 2011. Study of single-event transient effects on analog circuits. Ph.D. dissertation, University of Saskatchewan.
- Wang, X., Holbert, K. E., and Clark, L. T., 2011. Single event upset mitigation techniques for FPGAs utilized in nuclear power plant digital instrumentation and control. *Nuclear Engineering and Design* 241, 3317-3324.
- Warren, K. M., Sternberg, A. L., Weller, R. A., Baze, M. P., Massengill, L. W., Reed, R. A., Mendenhall, M. H., and Schrimpf, R. D., 2008. Integrating circuit level simulation and Monte-Carlo radiation transport code for single event upset analysis in SEU hardened circuitry. *IEEE Transactions on Nuclear Science* 55, 2886-2894.
- Weller, R. A., Mendenhall, M. H., and Fleetwood, D. M., 2004. A screened coulomb scattering module for displacement damage computations in Geant4. *IEEE Transactions on Nuclear Science* 51, 3669-3678.
- Weller, R. A., Mendenhall, M. H., Reed, R. A., Schrimpf, R. D., Warren, K. M., Sierawski, B. D., and Massengill, L. W., 2010. Monte Carlo simulation of single event effects. *IEEE Transactions on Nuclear Science* 57, 1726-1746.
- Wheatley, C. F., Titus, J. L., and Burton, D. I., 1994. Single-event gate rupture in vertical power MOSFETs; an original empirical expression. *IEEE Transactions on Nuclear Science* 41, 2152-2159.
- Wigner, E. P., 1946. Theoretical physics in the metallurgical laboratory of Chicago. *Journal of Applied Physics* 17, 857-863.
- Wirth, G. I., Vieira, M. G., Neto, E. H., and Kastensmidt, F. L., 2008. Modeling the sensitivity of CMOS circuits to radiation induced single event transients. *Microelectronics Reliability* 48, 29-36.

- Wirth, J. L., and Rogers, S. C., 1964. The transient response of transistors and diodes to ionizing radiation. *IEEE Transactions on Nuclear Science* 11, 24-38.
- Witczak, S. C., Laco, R. C., Osborn, J. V., Hutson, J. M., and Moss, S. C., 2005. Dose-rate sensitivity of modern nMOSFETs. *IEEE Transactions on Nuclear Science* 52, 2602-2608.
- Wunsch, T. F., and Axness, C. L., 1992. Modeling the time-dependent transient radiation response of semiconductor junctions. *IEEE Transactions on Nuclear Science* 39, 2158-2169.
- Yan, A., Huang, Z., Fang, X., Ouyang, Y., and Liang, H., 2017. Single event double-upset fully immune and transient pulse filterable latch design for nanoscale CMOS. *Microelectronics Journal* 61, 43-50.
- Yick, J., Mukherjee, B., and Ghosal, D., 2008. Wireless sensor network survey. *Computer Networks* 52, 2292-2330.
- Yilmaz, E., Baltas, H., Kiris, E., Ustabas, I., Cevik, U., and El-Khayatt A. M., 2011. Gamma ray and neutron shielding properties of some concrete materials. *Annals of Nuclear Energy* 38, 2204-2012.
- Yu, F. X., Liu, J. R., Huang, Z. L., Luo, H., and Lu, Z. M., 2011. Overview of radiation hardening techniques for IC design. *Information Technology Journal* 9, 1068-1080.
- Yu, H., Nicolaidis, M., and Anghel, L., 2009. An effective approach to detect logic soft errors in digital circuits based on GRAAL. *Quality Electronic Design (ISQED)*, 236-240.
- Yue, K., Luo, W., Dong, X., Wang, C., Wu, G., Jiang, M., and Zha, Y., 2009. A new lead-free radiation shielding material for radiotherapy. *Radiation Protection Dosimetry* 133, 256-260.
- Zand, R., and DeMara, R. F., 2017. Radiation-hardened MRAM-based LUT for non-volatile FPGA soft error mitigation with multi-node upset tolerance. *Journal of Physics D: Applied Physics* 50.

- Zeb, J., Arshed, W., Rashid, A., and Akhter, P., 2010. Gamma shielding by Aluminum. PINSTECH-219.
- Zebrev, G. I., and Gorbunov, M. S., 2009. Modeling of radiation-induced leakage and low dose-rate effects in thick edge isolation of modern MOSFETs. *IEEE Transactions on Nuclear Science* 56, 2230-2236.
- Zebrev, G. I., Vatiev, A. S., Useinov, R. G., Emeliyanov, V. V., Anashin, V. S., Gorbunov, M. S., Turin, V. O., and Yesenkov, K. A., 2014. Microdose induced drain leakage effects in power trench MOSFETs: experiment and modeling, *IEEE Transactions on Nuclear Science* 61, 1531-1536.
- Zebrev, G. I., and Gorbunov, M. S., 2009. Modeling of radiation-induced leakage and low dose-rate effects in thick edge isolation of modern MOSFETs,” *IEEE Transactions on Nuclear Science* 56, 2230-2236.
- Zeynali, O., Masti, D., and Gandomkar, S., 2012. Shielding protection of electronic circuits against radiation effects of space high energy particles. *Advances in Applied Science Research* 3, 446-451.
- Zebrev, G. I., and Gorbunov, M. S., 2009. Modeling of radiation-induced leakage and low dose-rate effects in thick edge isolation of modern MOSFETs. *IEEE Transactions on Nuclear Science* 56, 2230-2236.
- Zebulum, R. S., Pacheco, M. A., Vellasco, M., and Sinohara, H. T., 2000. Evolvable hardware: on the automatic synthesis of analog control systems. in *Proc. IEEE Aerospace Conf.* 5, 451-463.
- Zebulum, R. S., Stoica, A., Keymeulen, D., Sekaninna, L., Ramesham, R., and Guo, X., 2005. Evolvable hardware system at extreme low temperature. in *Proc. Int. Conf. Evolvable Syst.*, 37-45.
- Zeynali, O., Masti, D., and Gandomkar, S., 2012. Shielding protection of electronic circuits against radiation effects of space high energy particles. *Advances in Applied Science Research* 3, 446-451.
- Zhang, E. X., Fleetwood, D. M., El-Mamouni, F., Alles, M. L., Schrimpf, R. D., Xiong, W., Hobbs, C., Akarvardar, K., and Cristoloveanu, S., 2010. Total ionizing dose

- effects on FinFET-based capacitor-less 1T-DRAMs. *IEEE Transactions on Nuclear Science* 57, 3298-3304.
- Zhang, E. X., Fleetwood, D. M., Pate, N. D., Reed, R. A., Witulski, A. F., and Schrimpf, R. D., 2013. Time-domain reflectometry measurements of total-ionizing-dose degradation of nMOSFETs. *IEEE Transactions on Nuclear Science* 60, 4470-4475.
- Zhang, E. X., Fleetwood, D. M., Hachtel, J. A., Liang, C., Reed, R. A., Alles, M. L., Schrimpf, R. D., Linten, D., Mitard, J., Chisholm, M. F., and Pantelides, S. T., 2017. Total ionizing dose effects on strained Ge pMOS FinFETs on bulk Si. *IEEE Transactions on Nuclear Science* 64, 226-232.
- Zhao, Q., Zhuang, Y., Bao, J., and Hu, W., 2015. Model of radiation-induced gain degradation of NPN bipolar junction transistor at different dose rates. *Journal of Semiconductors* 36.
- Zhao, Y., Wang, L., Yue, S., Wang, D., Zhao, X., Sun, Y., Li, D., Wang, F., Yang, X., Zheng, H., Ma, J., and Fan, L., 2015. SEU and SET of 65 bulk CMOS flip-flops and their implications for RHBD. *IEEE Transactions on Nuclear Science* 62, 2666-2672.
- Zheng, J., Tagami, K., Watanabe, Y., Uchida, S., Aono, T., Ishii, N., Yoshida, S., Kubota, Y., Fuma, S., and Ihara, S., 2012. Isotopic evidence of plutonium release into the environment from the Fukushima NPP accident. *Scientific Reports* 2.
- Zhou, Q., and Mohanram, K., 2004. Transistor sizing for radiation hardening. *Reliability Physics Symposium Proceedings*, 310-315.
- Zhou, Q., and Mohanram, K., 2006. Gate sizing to radiation harden combinational logic. *IEEE Transactions on Computer-Aided Design of Integrated Circuits and Systems* 25, 155-166.
- Ziegler, F. J., 2004. SRIM-2003. *Nuclear instruments and methods in physics research B*, 113-118.
- Zuleeg, R., Notthoff, J. K., and Lehovc, K., 1977. Radiation effects in enhancement mode GaAs junction field effect transistors. *IEEE Transactions on Nuclear Science* 24, 2305-2308.

Zuleeg, R., and Lehovec, K., 1980. Radiation effects in GaAs junction field-effect transistors. IEEE Transactions on Nuclear Science 27, 1343-1354.

[Online] available: <https://www.theguardian.com/environment/2017/feb/03/fukushima-daiichi-radiation-levels-highest-since-2011-meltdown>, accessed date: Aug. 20, 2018.

Appendix

Appendix A: Hardware Emulation Bench

In this research, a hardware emulation bench, as illustrated in Figure A-1, is developed to evaluate the correctness and effectiveness of the proposed methods and systems. The bench houses a combination of fault injection techniques, which consist of two emulation methods: logic emulation and circuit emulation. Logic emulation is used to mimic radiation effects on semiconductor devices. It is based on software-implemented fault injection, and uses injection commands to forcibly control and/or stop system functions. Circuit emulation is based on hardware-implemented fault injection, using external circuits to mimic circuit responses under radioactive conditions.

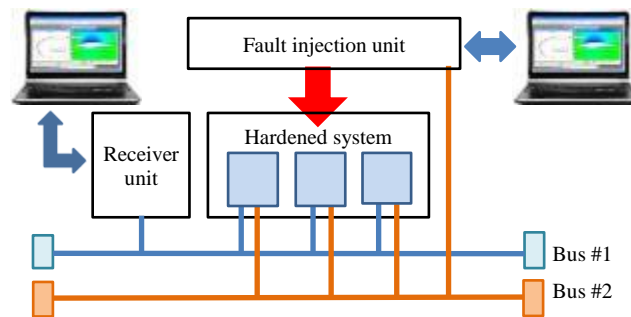


Figure A-1: The architecture of the developed hardware emulation bench.

The developed hardware emulation bench includes four parts: a redundant wireless device, a wireless gateway, emulation circuits, and a control tool. The emulation bench is built with two communication buses: bus #1 (915MHz network) is used to transmit/receive the normal communication data; and bus #2 (RS485) is used to transmit/receive commands/reports for fault injection. In addition, the fault injection unit is connected to the control computer by an Ethernet network. A software tool for fault injection is installed on the control computer to control, to collect, and to display the diagnostic information, which is developed in Microsoft Visual C++.

The picture of the hardware emulation bench is illustrated in Figure A-2.

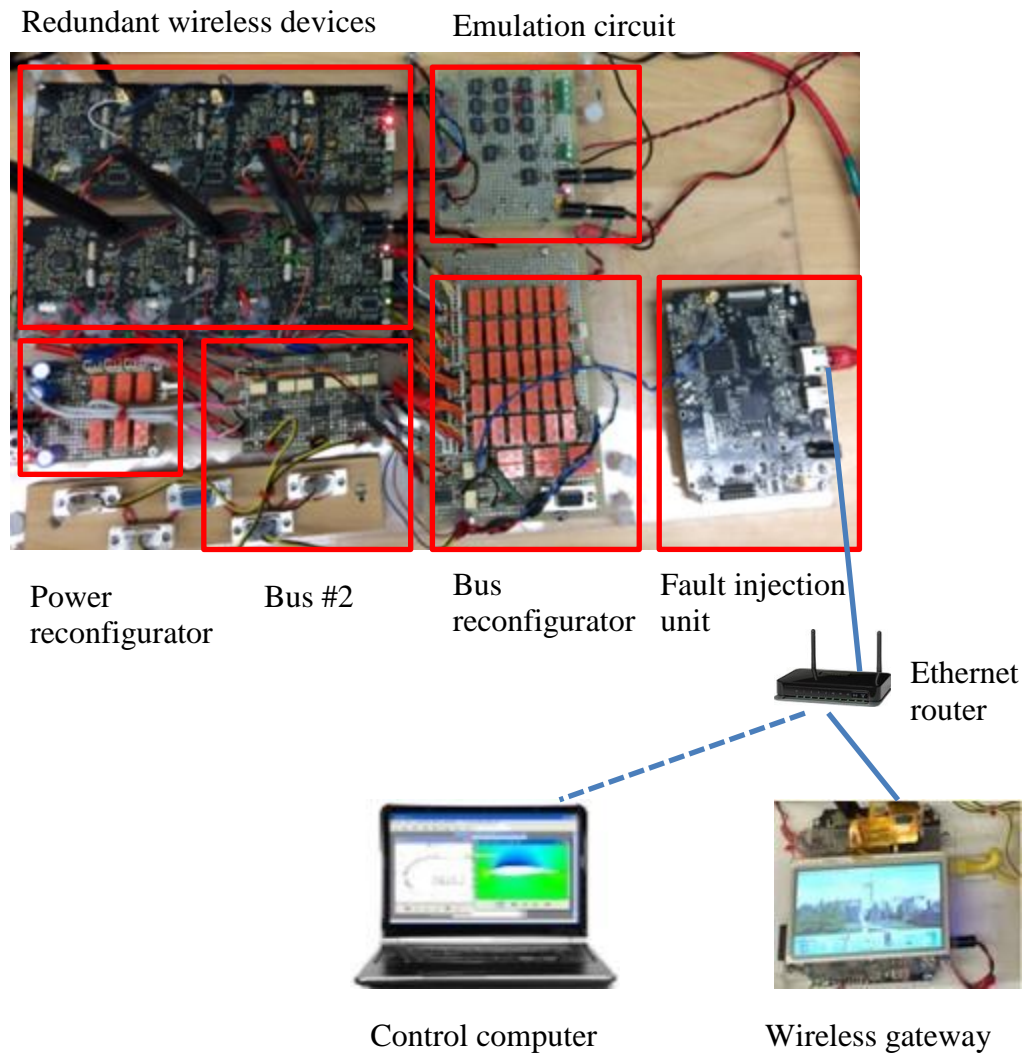


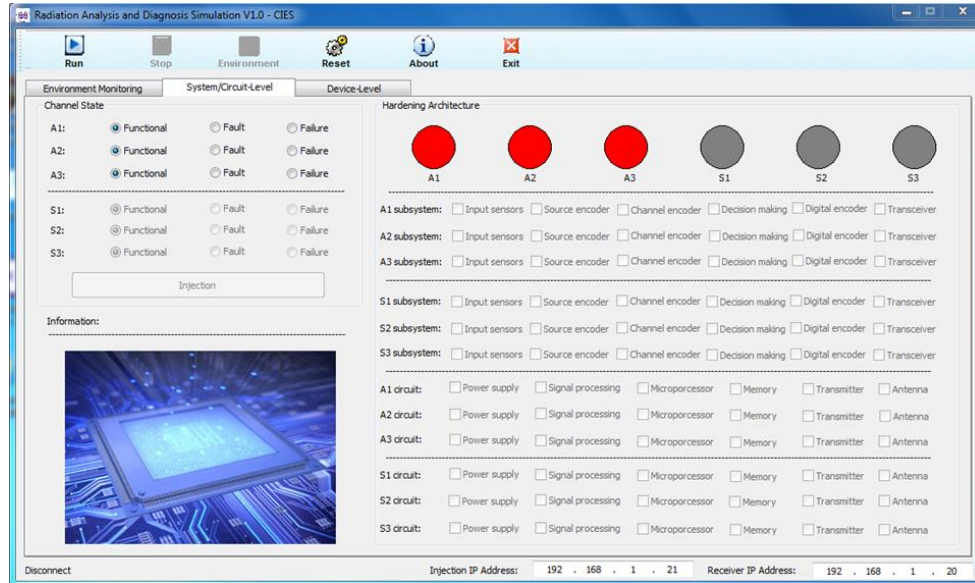
Figure A-2: Picture of the developed hardware emulation bench

The detailed hardware implementation is listed in Table A-1.

Table A-1: The implementation of the hardware emulation platform

| Function | Sub-function | Component | Manufacture |
|----------------------|-----------------------------|-----------|-------------------|
| Redundant system | Analog signal processing | LM741 | Texas Instruments |
| | Analog-to-digital converter | AD7689 | Analog Devices |
| | Microcontroller | P89C51RC2 | NXP |
| | Wireless transceiver | RF2905 | RF Micro Devices |
| Receiver | Microprocessor | i.max 285 | NXP |
| | Ethernet | LAN8720A | Microchip |
| | Wireless transceiver | RF2905 | RF Micro Devices |
| Fault injection unit | Microprocessor | i.max 285 | NXP |
| | Ethernet | LAN8720A | Microchip |
| | RS485 | MAX487 | MAXIM |
| | Emulation circuits | EU2-5NU | KEMET |
| | | LM741 | Texas Instruments |

The screen shot of the software tool in the control computer is shown in Figure A-3.

**Figure A-3: Screen shot of the software tool in the control computer**

Curriculum Vitae

Name: Qiang Huang

Post-secondary Education and Degrees: Hubei University of Technology
Wuhan, Hubei, China
1998-2002 B.A.

Wuhan University of Technology
Wuhan, Hubei, China
2004-2007 M.A.

The University of Western Ontario
London, Ontario, Canada
2013-2018 Ph.D.

Related Work Experience Research Assistant & Teaching Assistant
The University of Western Ontario
2013-2018

Research Assistant
Wayne State University
2011-2013

Lecturer
Wuhan Sports University
2009-2011

Embedded System Engineer
TECOM Inc.
2006-2009

Publications:

Qiang Huang, and Jin Jiang, 2018. A radiation-tolerant wireless monitoring system using a redundant architecture and diversified commercial off-the-shelf (COTS) components. *IEEE Transactions on Nuclear Science* 65, 2582-2592.

Qiang Huang, and Jin Jiang, 2019. An overview of radiation effects on electronic devices under severe accident conditions in NPPs, rad-hardened design techniques and simulation tools. *Progress in Nuclear Energy* (Accepted on Feb. 28, 2019 in press).

Qiang Huang, and Jin Jiang, 2017. Radiation-tolerance assessment of a redundant wireless device,” *International Conference on Advancements in Nuclear Instrumentation Measurement Methods and their Applications*, Liege, Belgium, June 19-23, 2017 (Presented)

Qiang Huang, and Jin Jiang, 2015. A literature review of radiation effects on wireless post-accident monitoring systems and rad-hardened design techniques. *The 9th International Conference on Nuclear Plant Instrumentation, Control & Human-Machine Interface Technologies*, Charlotte, North Carolina, USA, Feb. 23-26, 2015 (Presented)

Qiang Huang, Yongqiang Deng, and Jin Jiang, 2019. Comparative evaluation of three wireless sensor transceivers in a high radiation environment. *International Conference on Advancements in Nuclear Instrumentation Measurement Methods and their Applications*, Portoroz, Slovenia, June 17-21, 2019 (Accepted on Feb. 19, 2019). (To be presented)

Qiang Huang, and Jin Jiang, 2019. Prototype design, construction and experimental evaluation of a design methodology for radiation-tolerant electronic systems without relying on rad-hardened components. *IEEE Transactions on Nuclear Science* (Submitted on March 8, 2019, under review).

Yixin Su, and Qiang Huang, 2007. Design of Vxworks BSP based on S3C44B0x. *Electronic Component & Device Application*, vol. 9, no.7, 2007.

Qiang Huang, 2010. Design and implementation of video monitoring system based on S3C2440. *China Water Transport*, vol. 10, no.2, 2010.

Qiang Huang, 2010. Design of rating system for Free Combat based on ARM. *China Conference of Sports Engineering*, Wuhan, China, Sept. 2010 (Presented).

Manuscripts to be submitted:

Qiang Huang, and Jin Jiang, 2019. A redundant architecture for single event effects mitigation in electronic systems. *Microelectronics Journal* (To be submitted on March 2019).

Qiang Huang, and Jin Jiang, 2019. Design and evaluation of diversified wireless monitoring devices for using in distinct radiation environments. *IEEE Transactions on Instrumentation and Measurement* (To be submitted on April 2019).

Qiang Huang, Yongqiang Deng, and Jin Jiang, 2019. Investigation of radiation vulnerability in a wireless monitoring system using diversified COTS components. *IEEE Transactions on Computer-Aided Design of Integrated Circuits and Systems* (To be submitted on May 2019).

Patents:

United States Provisional Patent Application No.: 62/810,237

Inventors: Qiang Huang, and Jin Jiang

Title: System and method for facilitating use of commercial off-the-shelf (COTS) components in radiation-tolerant electronic systems

Status: Filed on February 25, 2019

United States Patent Application

Inventors: Qiang Huang, and Jin Jiang

Title: System and method for facilitating use of commercial off-the-shelf (COTS) components in radiation-tolerant electronic systems

Status: Under preparation and to be submitted in May, 2019.